

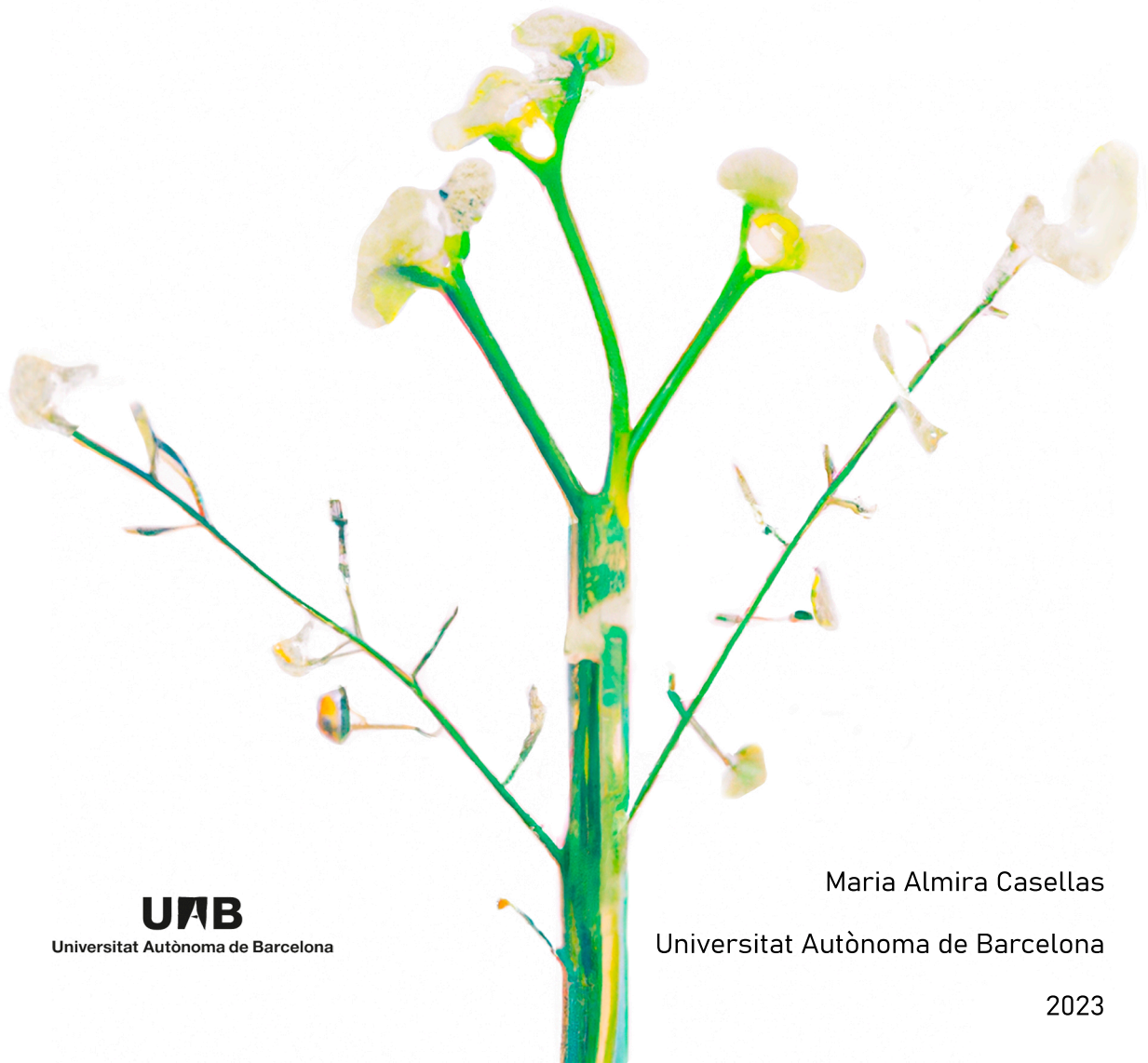
ADVERTIMENT. L'accés als continguts d'aquesta tesi queda condicionat a l'acceptació de les condicions d'ús establertes per la següent llicència Creative Commons:  <https://creativecommons.org/licenses/?lang=ca>

ADVERTENCIA. El acceso a los contenidos de esta tesis queda condicionado a la aceptación de las condiciones de uso establecidas por la siguiente licencia Creative Commons:  <https://creativecommons.org/licenses/?lang=es>

WARNING. The access to the contents of this doctoral thesis it is limited to the acceptance of the use conditions set by the following Creative Commons license:  <https://creativecommons.org/licenses/?lang=en>

PhD Thesis

Integrated studies on the natural variation in *Arabidopsis thaliana* responses to alkaline salinity



UAB

Universitat Autònoma de Barcelona

Maria Almira Casellas

Universitat Autònoma de Barcelona

2023

Integrated study on the natural variation in *Arabidopsis thaliana* responses to alkaline salinity

Doctoral Thesis

by

Maria Almira Casellas

Doctoral Program in Plant Biology and Biotechnology

Universitat Autònoma de Barcelona

Codirected by

Dr. Charlotte Poschenrieder,

Dr. Mercè Llugany,

Firmado por
POSCHENRIEDER WIENS,
CARLOTA (FIRMA) el
día 25/04/2023 con

MERCE
LLUGANY OLLE
- DNI
46337803W

Digitally signed by
MERCE LLUGANY OLLE
- DNI 46337803W
Date: 2023.04.26
09:12:38 +02'00'

MARIA-JOSÉ
ALMIRA CASELLAS
- DNI 47994197M

Firmado digitalmente por
MARIA-JOSÉ ALMIRA
CASELLAS - DNI 47994197M
Fecha: 2023.04.25 14:55:09
+02'00'

Maria Almira Casellas

Environmental Biologist by Universitat Autònoma de Barcelona

Master in Plant Biology & Biotechnology by Universitat Autònoma de Barcelona

Title of Thesis:

Integrated study on the natural variation in *Arabidopsis thaliana* responses to alkaline salinity

For the degree of:

Doctor in Plant Biology and Biotechnology

Declaration of Research Integrity:

I certify that this thesis has been done and composed by me and has not been accepted in any previous application for a degree. I certify that this work is free of plagiarism and all materials appearing in this thesis have been distinguished by quotation marks and the sources of information specifically acknowledged. I confirm that the work submitted is my own, except where work which has formed part of jointly-authored publications has been included. My contribution and those of the other authors to this work have been explicitly indicated in the manuscript. I confirm that appropriate credit has been given within this thesis where reference has been made to the work of others.

Maria J. Almira Casellas,

April 2023

MARIA-JOSÉ
ALMIRA
CASELLAS - DNI
47994197M

Firmado
digitalmente por
MARIA-JOSÉ
ALMIRA CASELLAS
- DNI 47994197M
Fecha: 2023.04.25
14:55:37 +02'00'

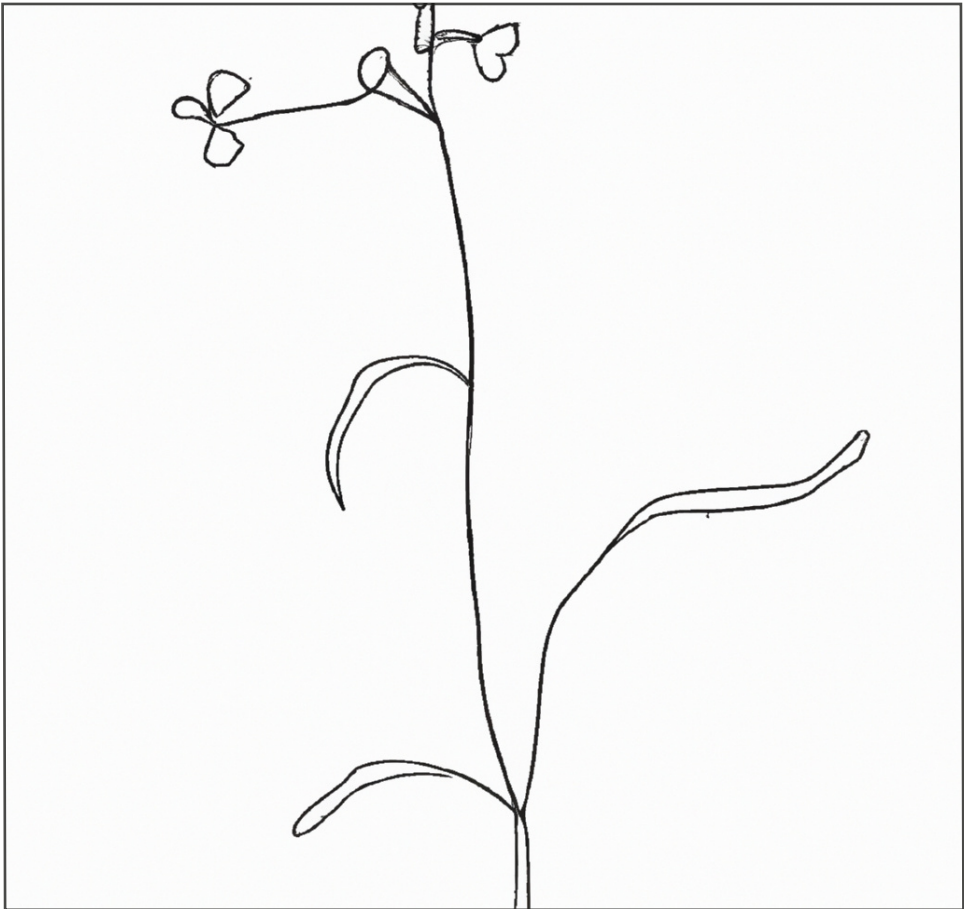
“Why should we tolerate a diet of weak poisons, a home in insipid surroundings, a circle of acquaintances who are not quite our enemies, the noise of motors with just enough relief to prevent insanity? Who would want to live in a world which is just not quite fatal?”

— **Rachel Carson, *Silent Spring***

“¿Por qué deberíamos tolerar una dieta de venenos débiles, un hogar en un entorno insípido, un círculo de conocidos que no son del todo nuestros enemigos, el ruido de los motores con el alivio justo para evitar la locura? ¿Quién querría vivir en un mundo que no es del todo fatal?”

— **Rachel Carson, *Primavera silenciosa***

Acknowledgements



Acknowledgements

Voldria agrair, en primer lloc, a les meves directores, Charlotte Poschenrieder i Mercè Llugany, per donar-me l'oportunitat de realitzar la tesi en aquest projecte i pel seu suport i consells. Gràcies, Charlotte, per ser un referent per a mí des que vaig començar a estudiar a la UAB i per l'exemple que has donat al llarg d'aquests anys - i que segueixes donant cada dia. Mercè, gràcies per la teva ajuda i tota la supervisió en aquesta tesi.

Molt agraïda a tot el personal investigador de la Unitat de Fisiologia Vegetal per aquests quatre anys de companyia (i companyonia). Gràcies als estudiants de grau – June, Margalida, Pau - i màster – Laura – per la feina ben feta, a les ja doctores Daniela i Nithya, per la vostra empatia i amistat, al ya doctor López-Valiñas i la Glo, por esos preciados análisis bioinformáticos y vuestro saber estar, i a en Toni Garcia, pels gabinets de crisi ben resolts. Gràcies a Rosa Padilla, per la immensa quantitat de mostres extretes i analitzades i pels seus consells, a Salvador Bartolomé, pel bon tracte, i al personal administratiu del departament, per la feinada i bona disposició. ¡Gracias, Anita, Ale, Manolo, Jose y compañía, por vuestra alegría y cariño! I, especialment, gràcies a aquest *FV-FemCore* que tants bons i mals moments ha presenciats: Sole, per la teva dedicació constant, optimisme i passió pel que fas. Eli, por ese huracán de energía que trajiste a nosotras y por estar siempre pendiente. Lau, por haber tomado las riendas de todo, estando sola, y haber sido un ancla para las siguientes (y, sobretodo, por haber montado conmigo esta tesis sobre 1 papel de filtro). Nic, por tantos años de coco-aventuras, BBQs, animales, risas a pierna suelta y huertos compartidos. A Marina, por la empatía y por ser ejemplo viviente de que los kg perdidos se recuperan. Als meus minions, Glòria i Carlos, per haver convertit l'etapa més dura al lab en la més bonica per a mi. I a tu més que a ningú, Sílvia, per ser la mentora que qualsevol voldria tenir i ajudar-me des d'abans de conèixer-me (Sílvia C*****!). Gràcies a totes!

I would also like to acknowledge the Yant's Lab people at the University of Nottingham, Levi, Razi, Emma and Ana, for their collaboration in carrying out the genomics of this thesis with our thaliana project. I owe great thanks to Professor Mark Aarts and all lab members of the Plant Genetics Laboratory at WUR, for giving me the chance to work in such a great research group. Endlessly indebted to you, René Boesten, for being my partner in crime (call it science...) ever since we were MSc students and for all your support over these years. Finally, we did it.

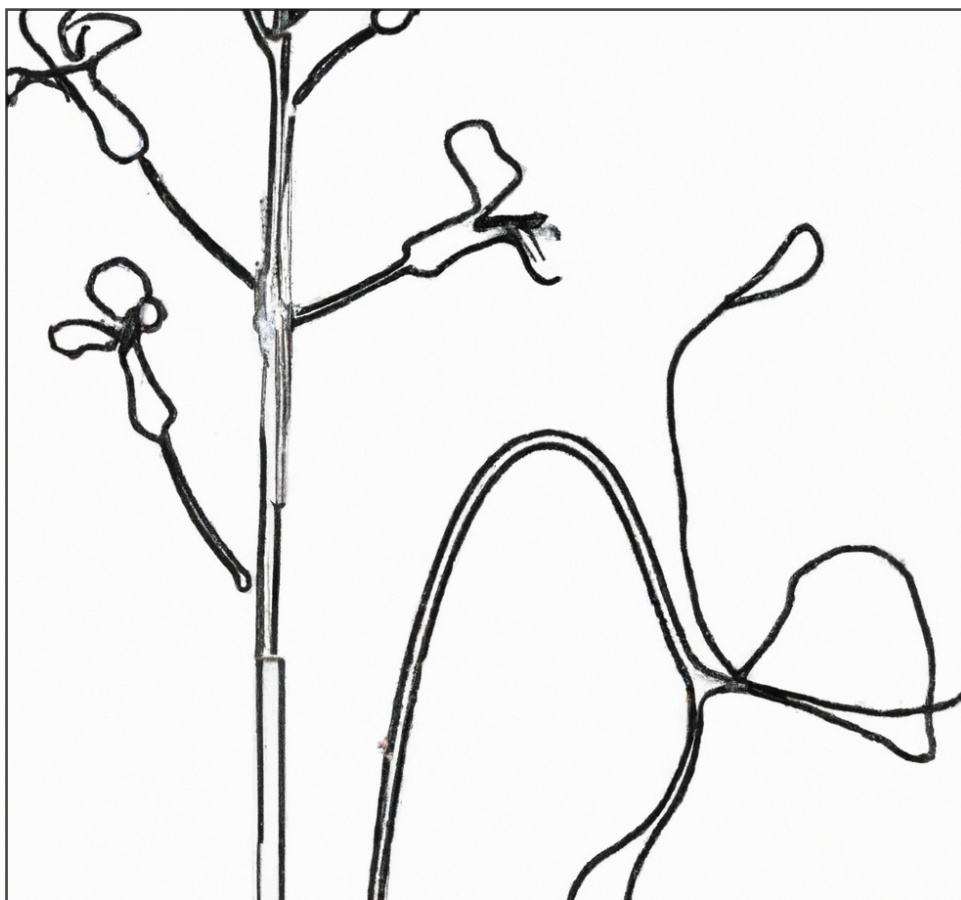
Sempre agraïda a les amigues, que m'han acompanyat aquests anys (i tota una vida), per ser la família escollida; Nur, Nina, Dali, Laia, Sacha i Moon; David i Marta; Berta i Giulio; Glòria, Neus i Marc, Tom, Jan, Pol i tothom qui em deixo i que s'ha preocupat per mi; sabeu qui sou. Y a mi Anni, por tus visitas furtivas al lab, voluntariado en siembras de 2 días enteros y tareas de secretaria bibliográfica. Al Moi, que ja ha passat per això i ha empatitzat. A la gent del nostre Versailles, escenari d'aquests 4 anys de tesi; Álex, Debs i Aleix, sou casa. Eternal thanks to my second home, Droevendaalsesteeg 107, and the old and recent droevies – mi Vickymiles, Debs, Claire, Matika, Marco, Yanni... - for being part of such a beautiful bubble and teaching me different ways to see life. Y gracias, Angelito, por haber sido el punto de partida de todo ello sin darte ni cuenta.

Mama i papá, gràcies per saber preguntar el just i necessari, preocupar-vos en silenci i acompanyar-me sempre sense haver-vos-ho de demanar (y por los tupperes, claro...); aquesta tesi és per a vosaltres. A la iaïona i l'abuelita - que, si hi fossin per a veure-ho, tindrien la sensatesa de no entendre pas res – i a la resta de la meua família (el d'aquí y los de allá!).

Σε ευχαριστώ, μωράκι, που ξέρεις να με βρίσκεις στη χειρότερη φάση και να τη μετατρέπεις στο καλύτερο ταξίδι μου. Σ' αγαπώ.

Aquests estudis han estat finançats pel Ministeri de Ciència i Innovació, dins dels projectes **BFU2016-75176-R i PID2019-104000RP-100**.

Abstract



Abstract

More than 20 % of world's cultivated area is affected by alkaline salinity stress, but 98% of plants are glycophytes – unable to successfully grow under salinity. In a scenario of decreased availability of irrigation water and temperature increase, soil salinity poses a major agricultural threat. The focus of this research was to better understand natural variation existing in the responses of *Arabidopsis thaliana* to salinity on siliceous and calcareous soils. The transition to flowering is a key adaptive developmental trait, and crop improvement techniques are irrevocably tied to it. For the detection of adaptation processes in genes regulating flowering time, genotyping of major flowering regulators, and analyses of whole genome sequence variation between groups of local *Arabidopsis thaliana* populations with contrasted flowering time were conducted. These analyses revealed genomic divergence between early and late flowering individuals at the *FRI* locus and at 3 other loci reported as *FLC* regulators, which provides evidence of different potential selective patterns within the studied collection. To seek for alkaline salinity characteristic traits shaping genomic diversity in the studied demes, divergence scans were complemented with Environmental and Phenotypic Genome Wide Association analyses, which provided promising candidates for enhanced tolerance to alkaline salinity encoding phytohormone (NPF6.2, SUE4), K⁺ (KAT1 and KEA5) and Fe (YSL2) transporters, and regulators of the cellular Ca²⁺ pool (ACA2) and the acidification of intracellular compartments (VAB2 and VHA-c1). Based on the differential growth and nutrient profiles observed between genotypes when submitted to different salinity types, a subset of 4 contrasted demes was used for transcriptomic analyses after exposure to neutral and alkaline salinity conditions. The combination of physiological indicators, nutrient traits, profiling of endogenous secondary metabolites, and RNA-Sequencing allowed for the description of the convergent and divergent response pathways between neutral

and alkaline salinity, and also stressed the importance of focusing on the plant Fe status for the maintenance of photosynthetic efficiency and carbon balance under alkaline salinity. Finally, genomic regions involved in alkaline salinity responses were assessed in a broader *Arabidopsis thaliana* natural diversity panel by means of Genome-Wide Association Studies (GWAS) on leaf nutrient profiles from plants grown on a natural saline calcareous soil from the region of study. Significant natural variation in leaf Na⁺ was reported, in line with the observations on the local deme collection. Allelic variations at *NINJA* and *YUC8* loci were shown to be involved in plant differential growth performance under alkaline salinity. Besides, differential leaf Fe accumulation was revealed and associated to *ALA3* variation. Overall, the present study provides useful insights into key targets for breeding in alkaline saline soils by means of integrating genomics, transcriptomics, physiological measurements, and association analyses.

Resumen

Más del 20% del área mundial cultivable está afectada por estrés por salinidad alcalina, mientras que el 98% de las plantas se definen como glicófitas –incapaces de desarrollarse bajo condiciones de salinidad. En el actual contexto de cambio climático, donde la creciente escasez de agua para el riego y el constante aumento de las temperaturas son dos grandes condicionantes, la salinidad del suelo supone una fuerte amenaza para la agricultura. El principal objetivo del presente trabajo de investigación ha sido el de definir y caracterizar la variación natural existente en la respuesta a la salinidad, tanto en suelo silíceo como calcáreo, de diferentes poblaciones naturales de la planta modelo *Arabidopsis thaliana*. Por tratarse de un carácter clave dentro del desarrollo vegetal, se analizó la base genética de la variación en el tiempo de floración presente en un grupo de poblaciones locales de *A. thaliana* mediante el genotipado de los dos principales reguladores de la floración (*FRI* y *FLC*) y la realización de escáneres de divergencia genómica. Mediante dichos análisis, se detectaron regiones genómicas divergentes entre ambos grupos, mapeando a *FRI* y a otros 3 genes descritos por su papel regulador de *FLC*, lo que apoya la presencia de distintos patrones de presión selectiva dentro de la colección de estudio. Con el propósito de detectar qué factor ambiental resulta en cada proceso selectivo, los escáneres genómicos se complementaron con análisis de asociación genoma-ambiente y genoma-fenotipo. Para ello, se usaron datos del perfil ionómico de cada suelo de origen, junto con datos del perfil nutricional foliar de todas las poblaciones de estudio, tras su tratamiento con estrés por salinidad alcalina. Se identificaron candidatos potencialmente involucrados en el desarrollo de mecanismos de tolerancia a estrés por salinidad alcalina fueron identificados, que codifican a transportadores fitohormonales (NPF6.2 y SUE4), de potasio (KAT1 y KEA5) y de hierro (YSL2), así como reguladores de la reserva celular de calcio (ACA2) y de la acidificación de compartimentos intracelulares (VAB2 and VHA-c1). La variación obtenida en la respuesta nutricional y de crecimiento de las poblaciones de estudio al

tratamiento por salinidad neutra y alcalina llevó a la selección de una muestra de 4 poblaciones contrastadas para su análisis transcriptómico. Mediante la combinación de datos fisiológicos, perfiles nutricionales y de metabolitos secundarios, y secuenciación de RNA, se describieron las convergencias y divergencias en las vías de respuesta a la salinidad neutra y alcalina de cada población. Además, se enfatizó la importancia de los mecanismos reguladores del estado nutricional de hierro para el mantenimiento de la eficiencia fotosintética y el balance de carbono bajo salinidad alcalina. Finalmente, el papel de la salinidad alcalina como agente selectivo para la adaptación local se evaluó en un mayor rango geográfico mediante Estudios de Asociación del Genoma Completo (GWAS) en una colección de 270 poblaciones naturales de *A. thaliana* crecidas en un suelo calcáreo salino. Los resultados obtenidos de la asociación entre la variación genómica y la variación en los perfiles nutricionales en hoja revelaron la presencia de variantes alélicas de *NINJA* y *YUC8* causantes de la acumulación diferencial de sodio, y de *ALA3* con efectos en la acumulación diferencial de hierro en hoja. En conjunto, mediante la integración de análisis genómicos, transcriptómicos, fisiológicos y de asociación ambiental, el presente estudio proporciona información de utilidad para un mejor conocimiento de los mecanismos de tolerancia a salinidad alcalina, así como de dianas clave para la mejora de cultivos sobre suelos calcáreos y salinos.

Abbreviations

ABA: Absciscic acid

ACC: 1-Aminocyclopropane-1-carboxylic acid

alkSAL: Alkaline Salinity

ATP: Adenosine triphosphate

BAP: 6-benzylaminopurine

BT: Bolting Time

CCCs: Chloride-Cation Co-transporters

CatDeme: the collection of Catalanian demes of *Arabidopsis thaliana*

Chr: Chromosome

CN: Calcareous Non-Saline soil

CKs: Cytokinins

CO: Constans

coreSAL: DEGs set shared among salinity types

CS: Calcareous Saline soil

DEGs: Differentially Expressed Genes

FDR: False Discovery Rate

FRI: FRIGIDA

FLC: Flowering Locus C

F_{ST}: Fixation index

FT: Flowering Locus T

GA: Gibberellic Acid

GEA: Genotype-Environment Association

GO: Gene Ontology

GPA: Genotype-Phenotype Association

IAA: Indole acetic Acid

InDel: Insertion/Deletion

JA: Jasmonic Acid

JA-Ile: Jasmonoyl-Isoleucine

KA: Kinetin
KEGG: Kyoto Encyclopedia of Genes and Genomes
LFMM: Latent Factor Mixed Model
neuSAL: Neutral Salinity
NGS: Next Generation Sequencing
NSCC: Non-Selective Cation Channels
onlyalkSAL: DEGs set exclusive from alkaline salinity
onlyneuSAL: DEGs set exclusive from neutral salinity
PAA: 2-phenylacetic acid
PCA: Principal Component Analysis
ROS: Reactive oxygen species
SA: Salicylic Acid
SNP: Single Nucleotide Polymorphism
SS: Siliceous Saline soil
SMVs: Single nucleotide Methylation Variants
UTM: Universal Transverse Mercator
WGCNA: Weighted Gene Co-expression Network Analysis
WGS: Whole-Genome Sequencing

Table of Contents

ACKNOWLEDGEMENTS.....	IX
ABSTRACT.....	XIII
RESUMEN	XV
ABBREVIATIONS.....	XVII
GENERAL INTRODUCTION	27
The big picture: abiotic stress as a driver of fine-scale variation in plants.....	27
The target: local adaptation and implications for tolerance to abiotic stress	28
The means: methods of study of selection and local adaptation in natural populations	29
The challenge: soil alkaline salinity as a global threat	31
Definition and characteristics	31
Sources of origin	32
Effects on plant-soil interactions	32
Alkaline salinity threads for agricultural productivity, food security and ecosystem services	33
Overview on plant salinity response mechanisms.....	34
Current knowledge on plant response mechanisms to alkaline salinity	36
The resource: <i>Arabidopsis thaliana</i> as model system and natural populations as a source of variation	37
The plant	37

Taxonomy	38
Distribution and habitat.....	38
Origin as a model system	39
The <i>Arabidopsis thaliana</i> Catalan collection	39
 OBJECTIVES	 43
SUMMARY OF CONTENTS	45
 CHAPTER 1	 49
INTRODUCTION	49
Floral timing: implications for abiotic stress responses.....	49
Genomic diversity involved in flowering time variation of <i>A. thaliana</i> natural populations.....	50
<i>A. thaliana</i> diversity patterns at local scales	52
Salinity-mediated selection in the local collection of <i>A. thaliana</i> wild populations of this study	52
 RESULTS & DISCUSSION	 54
Genetic structure.....	55
<i>FRI</i> and <i>FLC</i> genotyping.....	61
Window - based genome scans	70
Assessing genotype-environment associations (GEA) and genotype-phenotype associations (GPA) in CatDeme under alkaline salinity.....	75
Addressing soil variables as potential selective pressures at the candidate adaptive loci regulating CatDeme nutrition and flowering responses	89

METHODS	95
Studied populations	96
Native soils	96
Whole-Genome Sequencing	96
Analysis of genetic diversity and population structure	97
FLC alignment and PCA	98
Selection scans	98
Experimental setup	99
Elemental analysis of soil and leaf samples	101
GPA and GEA analyses	102
GO enrichment analysis	103
 CHAPTER 2	 107
INTRODUCTION	107
Differential effects of neutral and alkaline salinity on plant performance	 107
Plant transcriptomic responses to alkaline salinity	108
 RESULTS & DISCUSSION	 111
Physiological responses of <i>A. thaliana</i> demes under neutral and alkaline salinity	 111
Demes from coastal siliceous soils display reduced growth and photosynthesis under alkaline salinity	 112
K ⁺ and Fe uptake efficiency are indicators of plant tolerance to salinity	 113
Differential auxin, ABA and CKs alkaline-elicitation is origin-dependent	 117

Multivariate analysis reveal new players defining the alkalinity component of salinity	121
Transcriptome profiling of <i>A. thaliana</i> under neutral and alkaline salinity	125
Exclusive and shared molecular components of neutral and alkaline salinity.....	126
KEGG enrichment analysis of onlyNEUSAL and only ALKSAL DEGs.....	129
Upregulated transcripts in only NEUSAL and only ALKSAL reveal higher demand for antioxidant protection under alkaline salinity	132
Convergence and divergence of endogenous phytohormonal pathways under neutral and alkaline salinity.....	133
KEGG enrichment analysis of coreSAL DEGs	140
coreSAL transcript activation reflects shared salinity stress responses.....	140
coreSAL transcript inhibition reveals differential sensitivities to alkSAL in the studied demes.....	141
A reduced coreSAL DEG subset orchestrates contrasted plant responses to neuSAL and alkSAL....	146
WGCNA Network	149
METHODS.....	157
Plant material.....	157

Irrigation experiment.....	157
Leaf nutrition	158
PSII efficiency	158
Endogenous phytohormones	158
Transcriptome profiling.....	159
Total RNA Exaction and RNA-Seq library preparation .	160
RNA-Seq analysis	160
Gene functional annotation.....	161
Protein-Protein Interaction (PPI) network analysis	162
WGCNA Network	162
Statistical analysis.....	162
 CHAPTER 3	 167
INTRODUCTION.....	167
RESULTS	171
<i>A. thaliana</i> HapMap performance on saline calcareous soil .	171
Detection of SNPs associated with differential leaf elemental profile on saline calcareous soil	179
Mutant phenotyping.....	184
Effects of natural allelic variation of the locus of interest in gene expression and plant growth performance under alkaline salinity	187
Causal polymorphisms at the <i>NINJA</i> , <i>YUC8</i> and <i>ALA3</i> loci	192
Identified novel loci are not masked by effects of known major players in Na and Fe homeostasis	193
DISCUSSION	196

Natural variation in the response of <i>A. thaliana</i> HapMap accessions to alkaline salinity.....	196
Footprint of eco-geographical adaptation in the ionic profiles of <i>A. thaliana</i> natural populations.....	196
Detection of SNPs associated with differential leaf elemental profile on Saline Calcareous Soil.....	200
METHODS.....	204
HapMap phenotyping and GIS data extrapolation.....	204
Elemental composition of soils and plants.....	205
GWA Studies and candidate genes selection	206
Candidate genes validation.....	207
Potted soil culture	207
Hydroponic culture.....	208
Plate culture	208
Gene expression analysis	209
Statistical analysis.....	210
CONCLUSIONS.....	213
REFERENCES	219
SUPPLEMENTARY MATERIAL.....	255
SUPPLEMENTARY FIGURES	257
SUPPLEMENTARY TABLES.....	285
SUPPLEMENTARY DATABASES.....	333

General Introduction



General Introduction

The big picture: abiotic stress as a driver of fine-scale variation in plants

An abiotic stress is defined as a non-living environmental factor potentially causing a negative impact on living organisms for being beyond its normal range of variation (Pereira, 2016). As land plants are rooted, they grow under the multiple variable environmental factors occurring in their habitat. Native plants are adapted to such usual changes in environmental conditions; however, extreme levels elicit abiotic stress responses (Qi et al., 2020). The condition for an environmental change to be considered an abiotic stress is that it must adversely affect plant physiology, development and/or fitness (Chaudhry et al., 2022) and reduce crop yield and fruit quality (Zhang et al., 2022). In this context, differences in the way that plants cope with environmental challenges through a variety of physiological and morphological changes lead to differential stress tolerance (Bonhert et al., 1995). This has significant impact on plant survival and reproductive success, ultimately leading to natural selection for traits that are beneficial in a particular environment (Haak et al., 2017). Such differences, inherent within a population, subpopulation, or variety, result of the interplay between genetic, environmental, and random factors and are referred to as natural variation (Alonso-Blanco et al., 2009). The analysis of natural variation can help to unravel the genetic and molecular bases determining how plants cope with their unfavorable surroundings, providing information on the evolutionary processes driving the integrated regulation of adaptation and tolerance and how this regulation is influenced by natural selection (Mitchell-Olds et al., 2006; Haak et al., 2017). Therefore, it is of great utility in the field of plant abiotic stress research, which encompasses all studies on environmental

abiotic factors that can impose stress on a variety of species (Sulmon et al., 2015).

The target: local adaptation and implications for tolerance to abiotic stress

Adaptation refers to the process by which a species evolves over time in response to changes in its environment to become better suited - more successful at surviving and reproducing - to the conditions in a particular location. Natural variation across a geographic range of a species is maintained partly by local adaptation, as the environmental conditions in a particular location can shape the characteristics of a population through directional selection, which favors different alleles under different environmental conditions (Kawecki & Ebert 2004; Hereford, 2009). Local adaptation requires environment-dependent variation in fitness, that is, the expression of an organism's genotype is influenced by the environment in which it lives (genotype-by-environment interaction) (Ågren et al., 2013; Des Marais et al., 2013). Therefore, genotype-by-environment interaction influences directly on the selective pressures acting on a population and is a crucial topic of investigation when studying local adaptation. A key aspect of genotype-environment interaction is phenotypic plasticity, i.e., the ability of an organism to change its observable characteristics or traits in response to environmental cues. Plasticity contributes to natural variation and, at the same time, can promote adaptive divergence and thus play an important role in local adaptation, evolution, and speciation (West-Eberhard, 2003). Furthermore, as local adaptation may involve the evolution of new traits or the loss of existing traits that are no longer beneficial, its contribution to the development of plant tolerance to abiotic stress - ability of an organism to withstand environmental stress without suffering negative effects - is evident. The study of plant tolerance mechanisms to abiotic stresses is indispensable

for the development of strategies of crop performance improvement in challenging environments.

The means: methods of study of selection and local adaptation in natural populations

Agronomy-based research faces the challenge of identifying the mechanisms leading to the evolution within a species of responses that differ in signals and regulatory mechanisms, constituting genotypes adapted to specific stressful environments (Pereira, 2016). The establishment of a correlation between genetic variation and a particular trait under certain abiotic stressor can be carried out by exploiting natural variation, either by seeking general stress signatures (pointing out common response mechanisms among collections of plant specimens) or by determining differential plant responses to the same stress (Lefebvre et al., 2009). Either way, the detection of common and differential stress response mechanisms can be addressed by comparing tolerant and sensitive individuals within a species to a defined stress (Pereira, 2016). Common garden experiments and reciprocal transplants are important approaches to study local adaptation in plants, as they allow to unravel the relative contributions of genetics and the environment in shaping plant traits and performance. Common garden experiments involve growing plants from multiple populations in a standardized environment, such as a greenhouse or a field plot, to compare their differential performance – growth, reproduction, or survival, among others – in a common environment under controlled conditions. Complementarily, reciprocal transplants consist in comparing the performance of plants from different populations in their native and non-native environments to detect the presence of the geographic footprint of the population and local adaptation. The limitations in common gardens and reciprocal transplant experiments to examine the genetic basis of phenotypes

has been overcome in the era of genomic information, which adds value to these traditional methods, rather than replacing them (Sork, 2018). Having a large number of accessions characterized along with high-density molecular marker maps are useful tools for genotype-phenotype associations. Such dense marker panels across the genome are provided by high-throughput genotyping, and the simplest high-throughput genotyping method is whole-genome sequencing (WGS) or, for non-model species, genome representation sequencing (Sork, 2018). Examples of successful combination of common garden and Next Generation Sequencing (NGS) technologies in studying local adaptation are reported in *Arabidopsis thaliana* (Fournier et al., 2011), maize (Wang et al., 2016), or rice (Liu et al., 2021), among others. In them, identification of loci associated with distinct climatic factors, frost tolerance, drought tolerance and soil nitrogen, respectively, was possible through phenotyping and Genome Wide Association Study (GWAS) in native populations from different environments. On the other hand, the generation of segregant populations, derived from crosses between two accessions with distinct genetic characteristics, allow the study of trait inheritance and the role of specific genes on trait expression (Mackay et al., 2001). The integration of common garden experiments and genetic information obtained from crosses of interest is an approach that is still being applied in novel studies with non-model species like white clover (Wright et al., 2022). In this species, local adaptation to native sites through effects of selection in flowering time was detected through genetic mapping of fitness and reproductive traits in two biparental F2 mapping populations. Alternatively – or complementarily –, linking reciprocal transplant experiments and gene expression data allows the elucidation of how ecotypes adjust to the environment transcriptionally (Johnson et al., 2022). This is the case of the recent RNA-sequencing study in *Brassica rapa* (Hamann et al., 2021), in which it was found that changes in gene expression that influence traits under selection like flowering time are related to fluctuating precipitations. In *Mimulus guttatus*, a reciprocal

transplant experiment and RNA-sequencing analysis performed on locally adapted accessions found that allelic variation in specific genes was associated with differences in gene expression among coastal and inland locations (Gould et al., 2021). The study of changes in gene expression that do not involve a variation in the underlying DNA sequence – referred to as epigenetics – provides valuable information about plant responses to new environmental stressors because they are rapid and reversible changes (Bräutigam et al., 2013) but can also reveal genes that contribute to the evolution of a species, since epigenetic changes can be inherited (Schmitz et al., 2011). Tree population longevity provides more chances for individuals facing the need of using fast response mechanisms to changing environmental conditions and thus for epigenetic modifications to accumulate over time (Bräutigam et al., 2013). Studies on common garden experiment of adult *Quercus lobata* progeny sampled over a broad environmental gradient (Gugger et al., 2016; Sork et al., 2022) revealed single nucleotide methylation variants (SMVs) associated with maximum temperatures and identified a dehydrin-response gene as the top candidate SMV gene body. Overall, next generation sequencing, gene expression profiling and epigenetics, when combined with experimental gardens and natural population sampling, constitute a thorough approach in current research to explore the evolution of local adaptation in plant populations and create helpful applications for climate change and conservation biology studies (Sork, 2018).

The challenge: soil alkaline salinity as a global threat

Definition and characteristics. According to the US Salinity Laboratory (1947), a saline soil is defined as “a soil containing sufficient exchangeable sodium to interfere with the growth of most crop plants and containing

appreciable quantities of soluble salts". Soluble salts contributing to salinity are reported to originate mainly from NaCl and Na₂SO₄, and saline soils are defined by an electrical conductivity of the saturation extract (EC_e) of 4 dS/m or greater, which is equivalent to approximately 40 mM of sodium chloride (NaCl) exerting an osmotic pressure of 0.2 MPa (Al-Busaidi et al., 2003). On the other hand, alkaline saline stress is induced by presence of other salts in the soil like NaHCO₃ and Na₂CO₃, which further increase soil pH by releasing hydroxyl ions (Fang et al., 2021). In alkaline saline soils, the percentage of exchangeable-sodium (the degree of saturation of the soil exchange complex with sodium, defined as [(exchangeable sodium / cation exchange capacity) x 100]) is established to be above 15, EC_e criterion is maintained to be above 4 dS/m and the pH of the saturated soil usually raises up to 8.5. Contrarily, non-saline-alkali soils do not contain appreciable soluble salts and usually show a pH in the range of 8.5 to 10 (Hayward et al., 1949). Posterior classifications, however, determined that salt-alkali conditions in soils, according to salt content and pH, range from mild (salt content up to 3‰, and pH between 7.1 and 8.5), to moderate (salt content between 3 and 6‰, and pH between 8.5 and 9.5), or severe (salt content exceeding 6‰, and pH value over 9.5) (Oster et al., 1999).

Sources of origin. Saline-alkali soils are typically found in arid and semi-arid regions, where there is little precipitation and high evaporation that lead to incomplete leaching and transport of soluble salts to the ocean and their accumulation on the soil surface (Li et al., 2020). Changes in climate, changes in the chemical properties of major rock-forming materials and geologic changes such as erosion, weathering, and deposition are primary contributors to the occurrence of saline-alkali soils over time (Harris, 1920; de Sigmond, 1938). However, saline alkalinization is accelerated by anthropogenic sources, mainly due to irrigation mismanagement, since irrigation waters frequently carry significant amounts of dissolved salts (Hayward et al., 1949).

Effects on plant-soil interactions. Plants are often simultaneously exposed to concurrent stressors that cause profound effects on overall plant performance (Rasmussen et al., 2013). Effects of complex or combined stresses have been reviewed mainly for drought and heat (Rizhsky et al., 2004) and abiotic-biotic interactions (Atkinson et al., 2012). Similarly, the effects of saline-alkali soils (referred to as alkaline salinity stress hereafter) have been reported to involve a combination of both NaCl and NaHCO₃ stress: salinity ions from soluble salts will cause both ion toxicity (by entering the cell through membrane channels and carriers) and osmotic potential reduction (due to extracellular ion increase), leading to physiological drought (osmotic stress), whereas high pH has severe effects on cell pH stability, cell membrane integrity and photosynthetic function (Zhang et al., 2017; Kaiwen et al., 2020). Moreover, recent studies on alkalinity by presence of bicarbonates when compared to high pH alone concluded that bicarbonate stress exerts stronger transcriptome alteration (Pérez-Martín, 2021). Therefore, alkaline salinity from saline calcareous soils can cause plant metabolic disorders in a major degree than NaCl stress in terms of plant growth, ion imbalance, reduced ability of osmotic adjustment, and inhibition of the antioxidant system (Amirinejad et al., 2017; Chen et al., 2017; Wang et al., 2017; Wang et al., 2020).

Alkaline salinity threads for agricultural productivity, food security and ecosystem services. Soil alkaline salinization has become a concern on a global scale as it has become a major limiting factor for crop production (Shabala, 2013). This represents a major constraint for agriculture, which faces the challenge of feeding a growing population, expected to reach around 9.7 billion by 2050 (Arora, 2019). According to statistics, more than one million hectares are affected by alkaline salinity worldwide, consisting of 14,9% - 20% of the planet's land area (estimates vary by source). Alkaline saline soils can be found in many parts of Asia, Africa, South America, and

Australia, and also in Mediterranean regions (Pérez-Martín et al., 2022), due to the movement of soluble ions like Na^+ , Ca^{2+} , Mg^{2+} , K^+ , CO_3^{2-} and HCO_3^- to the superficial soil layers produced by the increase in evapotranspiration rates (Singh, 2021). The development of land use strategies is crucial to address the problem of cropland scarcity (Yang et al., 2022). This must necessarily be addressed from the perspective of enhancing crop tolerance to abiotic stresses and framed in the context of climate-smart agriculture, which aims to increase the resilience of agricultural systems to the impacts of climate change (Lipper et al., 2014).

Overview on plant salinity response mechanisms. During plant exposure to salinity, two distinct phases of response can be observed: the osmotic phase and the ion-specific phase. The osmotic phase occurs immediately upon exposure to salt and is characterized by the presence of salt outside of the roots, which impacts growth. The ion-specific phase develops over time and is characterized by the accumulation of ions in the shoot above tolerance threshold levels, which causes leaf death and ultimately reduction in photosynthesis inhibition of growth (Munns & Tester, 2008). Competitive exclusion of K^+ leads to Na^+ uptake into the plant root cells due to their similar chemical properties (Schachtman & Liu, 1999). Na^+ (i) uptake, (ii) restriction, (iii) translocation and (iv) compartmentalization systems are pivotal components of plant salinity tolerance mechanisms. They govern ion homeostasis regulation processes: (i) Na^+ uptake is mediated by uniporters or ion channels, including weakly voltage-dependent non-selective cation channels (NSCC) (Britto et al., 2010), high affinity K^+ transporters (HKT), high-affinity K^+ uptake transporters (HAK) (Assaha et al., 2017) and low-affinity cation transporters (LCT) (Maathuis et al., 2014). HKTs are crucial Na^+ -selective uniporters and Na^+/K^+ symporters (Platten et al., 2006), and HKT1 has been extensively studied and reviewed as a regulator of Na^+ transport to shoots (Rus et al., 2006; Baxter et al., 2010; Venkataraman et al., 2021). (ii) Na

influx restriction is facilitated by apoplastic barriers (which act as physical barriers) comprising of Casparian strip (CS) and suberin lamellae (SL) (Geldner, 2013), and Na^+ extrusion occurs through members of the Na^+/H^+ antiporter family. The SALT OVERLY SENSITIVE 1 (SOS1) is the most characterized member of Na^+/H^+ antiporters regulating long distance transport of Na^+ in plants (Mahi et al., 2019). (iii) Root-to-shoot Na^+ movement is mediated by the bypass flow of Na^+ through the apoplastic route or through NSCC and Na^+/H^+ antiporters at the membrane of xylem-parenchyma (Maathuis et al., 2014), like members of CHX cation antiporter family (Hall et al., 2006), but also through chloride-cation co-transporters (CCCs) like $\text{K}^+:\text{Cl}^-$ transporters (KCCs), $\text{Na}^+:\text{Cl}^-$ transporters (NCCs) and $\text{Na}^+:\text{K}^+:\text{Cl}^-$ co-transporters (NKCCs), characterized by their absolute requirement of Cl^- and Na^+/K^+ for its symport activity (Gupta et al., 2021). (iv) The remaining Na^+ can be sequestered in vacuoles by tonoplast Na^+/H^+ antiporters, such as the Na^+/H^+ exchanger (NHX) family in *Arabidopsis*, in coordination with vacuolar H^+ -ATPases, like AVP1 (Basu et al., 2021). Prevention of cellular K^+ efflux is also involved in the regulation of plant ion homeostasis under salt stress. On one side, as for Na^+ , high affinity K^+ transporters (HKT) and high-affinity K^+ uptake transporters (HAK) mediate K^+ uptake in plant cells (Basu et al., 2021) and, on the other side, H^+ -ATPase activity contributes to conserving high K^+ concentrations in plant cells by maintenance of negative membrane potential (Assaha et al., 2017). For some species like soybean, citrus or grapevine, Cl^- is considered more toxic than Na^+ because plants have a better Na^+ transport capacity than Cl^- . Cl^- is passively loaded into the xylem through anion channels (AtNPF2.4 and SLAH1) (Li et al., 2016; Cubero-Font et al., 2016), reported to be downregulated by ABA, which may serve to limit Cl^- transfer to the shoot under saline conditions (Li et al., 2017). Besides ion transport regulation, other plant response mechanisms to salinity thoroughly studied include (i) growth reduction via changed water relations, a process which involves ABA regulation of stomatal conductance, hormonal balance, or

carbon supply (Munns, 2002), (ii) the increased cytosolic and organelle accumulation of compatible solutes like sucrose, proline, and glycine betaine, that are compatible with metabolic activity even at high concentrations and are synthesized to balance the osmotic pressure of the ions in the vacuole, (iii) activation of oxidative stress signaling by ROS (reactive oxygen species) signaling through upregulation of key enzymes such as superoxide dismutase (SOD), ascorbate peroxidase (APX) or catalase (CAT), and (iv) changes in plasma membrane permeability and lipid peroxidation, traditionally identified by an increase in malondialdehyde (MDA) (Ma et al., 2015).

Current knowledge on plant alkaline salinity response mechanisms.

Despite extensive research over the past decades has contributed to unravel the mechanisms of plant response to salt stress, studies focusing on alkaline salinity are still scarce, and most findings logically overlap with the response mechanisms and genes responsive to neutral salinity described above (growth inhibition, ion homeostasis regulation, reduction in photosynthesis, synthesis of compatible solutes, ROS signaling, and antioxidants). However, effects of alkaline salinity on the mentioned biological processes are commonly reported to be aggravated when compared to neutral salinity (Guo et al., 2017; Cao et al., 2020) and tolerance to neutral salinity has been observed to be insufficient – even detrimental – for plant fitness under alkaline salinity (Pérez-Martín et al., 2022). The most described plant response to alkaline salinity is the reduction of rhizospheric pH by PM H⁺-ATPase-mediated root H⁺ efflux, a process tightly linked to SOS1 signaling (Yang et al., 2018) and thus potentially being a central regulatory switch of the salinity and alkalinity components. Precisely, PM H⁺-ATPase activity is triggered by cytosolic Ca increase, which is induced both under neutral and alkaline salinity (Yang et al., 2019). Efficient supply of Fe is likely related to plant saline-alkali tolerance: Fe concentration was higher and Fe-deficiency-responsive genes were significantly upregulated

in an saline-alkali tolerant rice variety than in a sensitive one under alkaline salinity (Li et al., 2016).

The resource: Arabidopsis thaliana as model system and natural populations as a source of variation

The plant. *Arabidopsis thaliana* (mouse ear-cress or thale-cress) is a small flowering plant that belongs to the mustard family (Brassicaceae). It is characterized by a rosette of small leaves at the base, a main stem (branched in older plants), with possible secondary stems, topped by an inflorescence, and roots forming a taproot system, only exceptionally adventitious. The plant's height can range from 30-40 cm depending on various factors such as nutrition - in soil with poor nutrient content, the plants can still produce seeds with a height of only a few centimeters. The inflorescence is a raceme bearing several four sepal- and four white petal-flowers, approximately 3 mm in length and 1 mm in diameter, with the youngest flower located at the top. Petals safeguard six stamens consisting of 2 shorter and 4 longer filaments with a pollen-bearing anther. The center of the flower contains an ovary with two carpels. Although typically self-fertilize, plants can also be cross-fertilized relatively easily in a laboratory setting. After fertilization, ovary elongation leads into a silique, which matures approximately two weeks later (at 25 °C) and contains 30-60 seeds. The seeds are small, weighing less than 20 mg on average, and a few hundred micrometers in length at their longest point. As plants potentially produce flowers for months, it is possible to collect above 10.000 seeds from a single plant (Meyerovitz, 1987).

Taxonomy. The classification of the Brassicaceae family (338 genera and 3,709 species) has been a subject of debate due to poor definition of the boundaries between genera and artificial demarcation of tribes recognized prior to 2006 (Guindon & Gascuel, 2003). Based on analyses of rDNA seq, the

genus *Arabidopsis* was reported to include nine species and five subspecies (O'Kane Jr & Al-Shehbaz, 1997). A recent thorough study sequencing 27 taxa representing the entire genus *Arabidopsis* (Novikova et al., 2016) confirmed that it can be grouped into four common species (*A. thaliana*, *A. halleri*, *A. lyrata* and *A. arenosa*), three species with limited geographic distribution (*A. croatica*, *A. cebennensis* and *A. pedemontana*) and two allotetraploid species (*A. suecica* and *A. kamchatica*).

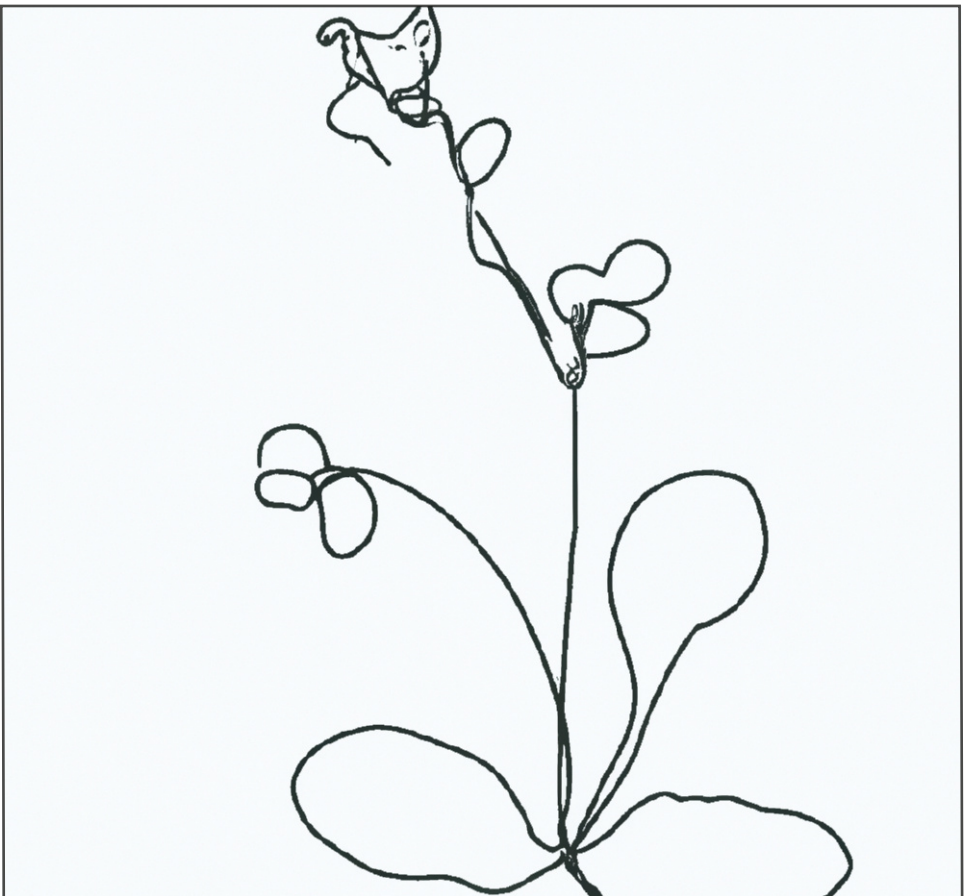
Distribution and habitat. The nine species that currently comprise the *Arabidopsis* genus are all indigenous to Europe, with two species extending into northern and eastern Asia and North America to the central United States (Al-Shehbaz & O'Kane Jr, 2002). *Arabidopsis* is believed to be native to the Old World, although its exact geographic origin is unknown. It has been reported in many different regions and climates, ranging from high elevations in the tropics to the cold climate of northern Scandinavia, and including locations in Europe, Asia, Africa, Australia, and North America (Redei, 1970; Kirchheim & Kranz, 1981). There is evidence of *Arabidopsis thaliana* Pleistocene migrations across Europe and Asia, and post-Pleistocene colonization of Europe from glacial refugia near the Mediterranean and in Asia. Only a few ecotypes of *A. thaliana* are available in central Asia, and these show tantalizing patterns of genetic diversity for molecular and phenotypic traits (Sharbel et al., 2000). Generally, *Arabidopsis* can be found in a variety of habitats including open or disturbed areas, sandy soil, riverbanks, roadsides, rocky slopes, waste places, cultivated ground, meadows, slightly alkaline flats, under shrubs, and open areas at altitudes ranging from sea level to 4250 meters (Al-Shehbaz & O'Kane Jr, 2002)

Origin as a model system. *Arabidopsis* crops up again as a subject for laboratory investigation in 1943 when Friedrich Laibach described its short generation time, fecundity, ease of crosses, and the possibility of mutagenesis (Laibach, 1943). In addition, its small size and small genome

avored its adoption as a genetic model organism (Meyerowitz, 2001) for controlled-environment studies of the genetic architecture of quantitative traits (Langridge, 1958; Langridge & Griffing, 1959). Today, the study of natural variation in *Arabidopsis* continues to reveal new biology (Koorneef et al., 2004; de Jong et al., 2019; Coolen et al., 2019; De Pessemier et al., 2022; Szymanska-Lejman et al., 2023). In addition, the entire genus is increasingly being used to address fundamental questions of evolution (Mitchell-Olds & Schmitt, 2006; Bergelson & Roux, 2010; Choi et al., 2021; Schultz et al., 2021).

The *A. thaliana* CatDeme collection. In March 2013, 2014, and 2015, natural stands of *A. thaliana* were identified in coastal and adjacent inland locations in the northeast of Catalonia, Spain (Busoms, 2015). The term “*A. thaliana* deme” was established referring to “a small group or stand of *A. thaliana* plants growing in relatively homogeneous ecological conditions and separated from other groups by at least 35 m” (Busoms, 2015). Whole Genome Sequencing was performed on 74 individuals from 19 demes. By using this well-characterized and geographically documented *A. thaliana* collection, local adaptation to coastal and inland habitats was detected. However, no genome-wide signature associated with coastal versus inland habitats was observed after population genetic analysis. Soil salinity (in terms of Na⁺ concentration) was identified as a driving factor for the observed local adaptation (Busoms, 2015). Further studies including de novo genome assembly characterized three allelic variants of the high-affinity K⁺ transporter (*HKT1;1*) locus and confirmed that *HKT1;1* is under fluctuating selection in response to highly variable seasonal levels of Na⁺ (Busoms et al., 2018). Same as with neutral salinity, contrasted sensitivity to soil carbonates was observed among the studied demes (Terés, 2019). However, when assessing plant responses to alkaline salinity (Pérez-Martín et al., 2021) a detrimental effect of deme adaptation to neutral salinity (siliceous soils) in the plant response to alkaline salinity (calcareous soils) was reported.

Objectives



General and specific objectives

The general aim of this thesis was to characterize the genetic, molecular, and physiological mechanisms orchestrating differential responses to alkaline salinity in *Arabidopsis thaliana*, by exploiting the existing genetic and phenotypic variation in natural populations at different geographical scales.

The specific objectives that arose from the proposed research and that were covered along this dissertation are:

1. To perform Whole-Genome Re-Sequencing of the *Arabidopsis thaliana* Catalan germplasm collection (CatDeme).

- 1.1. To detect footprints of selection on genes regulating CatDeme flowering variation by means of genotyping and landscape genomic approaches.

- 1.2. To assess significant associations between the variation in CatDeme genomic regions and variation in leaf and soil elements driving plant responses to alkaline salinity by means of Genotype-Phenotype (GPA) and Genotype-Environment (GEA) Association analyses.

2. To characterize the differential plant responses to neutral and alkaline salinity by integrating physiological, nutritional, phytohormonal and RNA-Sequencing data.

- 2.1. To describe plant differential responses to neutral and alkaline salinity by the phenotyping of growth, photosynthetic yield, leaf ionome and endogenous phytohormone profiles of a subset of contrasted *Arabidopsis thaliana* demes

- 2.2. To dissect, at the transcriptomic level, major biological pathways differentially regulated among deme subsets to identify candidate genes for tolerance to alkaline salinity.

3. To evaluate the genomic variation in a collection of *A. thaliana* accessions with a broader geographic distribution and to identify genomic variants statistically associated with specific alkaline salinity traits by means of GWAS.

Summary of contents

The first chapter of this dissertation presents the collection of *A. thaliana* Catalan demes (CatDeme), for which a total of 70 individuals from 20 demes are re-sequenced. The natural variation in the flowering time of the studied demes is described, and the CatDeme genomic data is used for the performance of demographic analyses, genotyping of major flowering regulators and landscape genomic approaches to seek for the detection of adaptive patterns in the CatDeme variation at loci regulating flowering. Next, natural variation in soils from the collection sites of all demes is used to classify individuals according to the properties of their native soil. Specifically, soil Na⁺ and CaCO₃ contents are shown to be the main drivers of such variation, and differential performance in terms of leaf nutrition is observed under alkaline salinity when demes are grouped according to each soil-type category. Data on soil elements differentiating saline-calcareous soils is exploited through Genotype-Environmental Association analysis (GEA) for the assessment of allelic variants potentially under selection driven by alkaline salinity. Likewise, a Genotype-Phenotypic Association analysis (GPA) is performed with leaf nutrition data from all demes grown on alkaline salinity conditions in order to detect genomic variation involved in differential plant responses to alkaline salinity. Finally, candidates obtained from the divergence scan and the two association analyses are combined to detect footprints of selection driven by soil composition in CatDeme flowering traits.

In the second chapter, a subset of 4 characterized *A. thaliana* demes with contrasted origin (2 belonging to coastal siliceous soils and 2 from moderately calcareous soils and intermediate distance from the coast) are grown under neutral and alkaline salinity irrigation regimes, and leaf samples are used for transcriptomic analysis. Data of relative growth, photosynthetic efficiency, leaf mineral nutrition, and endogenous leaf phytohormone concentration are

integrated with data from RNA-Seq analysis for the identification of shared and exclusive response pathways among the two salinity types in each genotype. Enriched biological pathways from each shared and exclusive responsive gene sets are dissected, and subsets of differentially expressed genes with contrasting expression among the studied demes or among treatments are presented as candidates for driving differential responses to neutral and alkaline salinity.

In the third chapter, 270 accessions from the HapMap collection are grown under a natural alkaline-saline soil from Catalonia (NE Spain), and growth and leaf nutrition traits are used as phenotypes to perform a Genome-Wide Association Study (GWAS). After detecting the possible presence of ecogeographical footprints in the performance of the studied accessions under alkaline salinity, significant natural variation in the leaf concentrations of Na (LNa) and Fe (LFe) is shown, and novel players in leaf sodium and iron homeostasis under alkaline salinity are suggested.

Chapter 1



Chapter 1

Population genomic approaches for the detection of loci contributing to adaptive variation in a local collection of *A. thaliana* natural stands

Introduction

Floral timing: implications for abiotic stress

Flowering is defined as the switch from vegetative to reproductive growth (Araki, 2001). The transition to flowering is a key adaptive developmental trait which impacts plant survival and fitness (Osnato et al., 2022). The proper timing of flowering is critical to plant development, as it ensures species continuity (Amasino & Michaels, 2010). Agriculture and genetic improvement of crops are irrevocably tied to flowering, as flowering is a prerequisite for seed and fruit yield and, at the same time, avoidance of flowering must be addressed when exploiting vegetative resources as tubers or roots (Jung et al., 2017).

Four major pathways of flowering regulation in *Arabidopsis* have been widely described and relay both on environmental or endogenous cues: photoperiod (day and night periods), vernalization (low temperatures near the freezing point), autonomous flowering (inhibition of the flowering repressor FLC) and gibberellin (regulation of gibberellin signaling pathway-related genes) (Conti, 2017; Andrés & Coupland, 2012; Amasino, 2010; Mutasa-Göttgens & Hedden, 2009). In the past 17 years age and ambient temperature pathways have been included in this framework (Samach & Wigge, 2005; Huijser & Schmid, 2011; Conti, 2017). Regardless of the classification criteria for the study of flowering time, it has become clear that plants have coordinated flowering time and reproduction with the prevailing environmental conditions (Jung et al., 2017). This implies that the wide range of environmental information present in a natural environment

can be recognized and integrated by plants (Brachi et al., 2013; Kooyers, 2015; Burghardt et al., 2016). Consequently, the modulation of the flowering process in front of adverse environmental conditions plays an important role in plant adaptation (Kazan & Lyons, 2016; Takeno, 2016).

Changes in flowering responses in front of extreme environmental conditions have pointed to stress (biotic and abiotic) as a common factor responsible for such responses, to the point that stress-induced flowering is considered one more category of flowering pathway and the ultimate stress adaptation (Blanvillain et al., 2011; Riboni et al., 2014; Kazan & Lyons, 2016; Takeno, 2016). To overcome the effects of any stress factor, the perception of environmental cues must be translated into internal signals and results into plant developmental responses (Santner et al., 2009).

Genomic diversity involved in flowering time variation of A. thaliana natural populations.

Flowering time variation and its role in adaptive evolution are topics of great interest in the study of plant responses to the environment. There is high natural genetic variation in the flowering time of *A. thaliana* wild populations (Lempe et al., 2005; Shindo et al., 2005). Such variation is reported to be key for adaptation to geographical and environmental factors present in the species' broad distribution range (Alonso-Blanco et al., 2009; Crimmins et al., 2010; Weigel, 2015). Vernalization is defined as the prolonged exposure to low temperature causing the induction of flowering initiation. It has been shown to be needed in some accessions from high latitudes and/or altitudes (Shindo et al., 2005; Mendez-Vigo et al., 2011), despite *A. thaliana* being initially described as a species with no obligate requirement for flowering induction (Martínez-Zapater et al., 1994). According to their vernalization requirements, wild accessions have been qualitatively classified into winter- (showing late flowering that

responds to vernalization) or summer-annuals (defined for an early flowering with low vernalization response) (Napp-Zinn, 1969; Rédei, 1970). The genetic analysis based on this classification allowed the identification of *FRI* and *FLC* genes (Michaels & Amasino, 1999; Johanson et al., 2000), which present null mutations, accounting for 50 to 70% of FT variation (Shindo et al., 2005), and rare variants, restricted to specific lines (Li et al., 2014).

The molecular function and phenotypic effects of multiple *A. thaliana* flowering-time genes have been identified besides *FRI* and *FLC*, such as the light-sensing protein PHYTOCHROME C (*PHYC*) (Balasubramanian et al., 2006; Samis et al., 2008) and the transcription factor MADS affecting flowering 2 (*MAF2*) (Caicedo et al., 2009; Rosloski et al., 2010), among others (Korves et al., 2007; Atwell et al., 2010; Bloomer & Dean, 2017; Wadgyman et al., 2018). However, studies simultaneously addressing flowering, genomic and environmental variation are crucial to understand the implications of genomic variation in flowering time for adaptation to abiotic stress factors (Tabas-Madrid et al., 2018). In this regard, phenotypic genome-wide association (PGWA) and environmental genome-wide association (EGWA) analysis are fundamental tools for the dissection of quantitative traits and the detection of environmental factors shaping genomic diversity (Tabas-Madrid et al., 2018), respectively. In the Iberian Peninsula collection of *A. thaliana* wild accessions, candidate genes for adaptation to temperature by altered flowering time were only detected through the combination of PGWA and EGWA (Tabas-Madrid et al., 2018).

Arabidopsis thaliana diversity patterns at local scales

It has been previously shown that regional instead of global GWA analyses allow to increase GWAS statistical power and to identify local selective agents modulating adaptive phenological variation (Brachi et al., 2013). Likewise,

genomic analyses in ecologically diverse but closely located natural *A. thaliana* stands provide data on the correlation between differences in diversity and specific habitats, which is vital to understand the fine-scale dynamics of wild populations (Bomblies et al., 2010).

Salinity-mediated selection in the local collection of A. thaliana wild populations of study

By using the well-characterized and geographically documented CatDeme collection (see General Introduction), local adaptation to coastal and inland habitats in terms of soil Na⁺ was detected (Busoms, 2015; Terés, 2017).

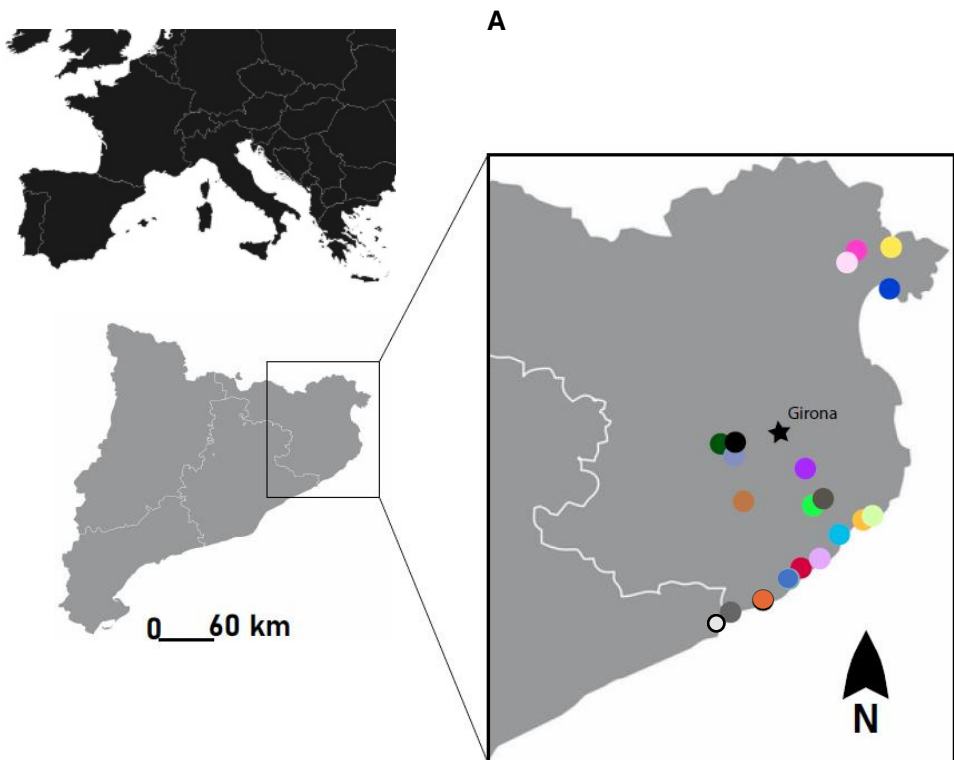
Although high variation in the bolting time of the 20 demes was observed both at laboratory and greenhouse and field reciprocal experiments, the environmental and molecular elements determining the flowering time of the CatDeme collection have not yet been identified. Both early and late flowering phenotypes were found in CatDeme, as expected for South-Western Europe, where summer and winter annuals are reported (Johanson et al., 2000; Le Corre et al., 2002). It has been previously suggested that the variation in flowering time of *A. thaliana* may be as high within regional samples as throughout the species range (Le Corre et al., 2002; Le Corre, unpublished), and that flowering time has evolved under selection for adaptation to local conditions (Pigliucci, 2003). Based on field and laboratory observations, a possible role of early flowering time in the coastal CatDeme subset was hypothesized to be a stress induced response to salinity on siliceous soils (Busoms et al., 2015, Terés et al., 2017). In CatDeme, recent studies report a detrimental effect of adaptation to neutral salinity (assessed as salinity present in siliceous soils and as NaCl irrigation treatments at pH 5.9) in the plant response to alkaline salinity (Pérez-Martín et

al., 2022). Besides, flowering time has not been established as an adaptive trait for the studied collection so far.

Here, 70 individuals from the 20 demes were re-sequenced and combined with a set of 74 previously sequenced samples. The combined genomic set of study was used to infer population structure of CatDeme. Next, nucleotide variation at major locus underlying flowering time differences (*FRI* and *FLC*) was assessed in all demes to see their contribution to a putative adaptive phenotypic variation in CatDeme flowering time, and the vernalization sensitivity of an early (Ro2) and a late (T6) flowering deme were compared. Complementarily, diversity-based scans comparing deme subsets with contrasting flowering time were performed for the identification of other potential regions of recent selection associated with flowering time variation (adaptive candidates). In addition, data on leaf nutrition and elemental profiles from CatDeme collection sites was used to perform environmental and phenotypic GWA analyses (LFMM candidates). Finally, the adaptive candidates and LFMM candidates' lists were combined to seek for genomic regions under selection specifically driven by soil composition and potentially regulating flowering traits.

Results & discussion

The CatDeme genomic set was used to assess the genetic architecture of flowering time and the role of soil alkaline salinity in generating local-scale diversity patterns. Figure 1.1 shows (A) the distribution map of the studied demes and lists (B) the deme symbol, location, and flowering time phenotype (E: early; I: intermediate; L: late). Flowering time (BT, *Bolting Days*) was measured after 4-week vernalization under 10h day light photoperiod conditions in a previous greenhouse reciprocal (Pérez-Martín et al., 2022) and a rockwool irrigation experiment. Datasets S1.1-1.3 show raw data on all BT and leaf nutrition phenotyping. Table S1.1 summarizes deme characteristics and experiments.



B

Deme	Source	UTM (x)	UTM (y)	BT
● A1	S. Busoms	46,91	46,45	I
● A5	S. Busoms	47,04	46,44	I
● CALA	S. Busoms	49,56	46,20	I
● JBB	K. Bomblies	48,39	46,14	I
● LG5	K. Bomblies	49,11	46,31	L
● LG7	K. Bomblies	49,08	46,31	I
○ LLO2	S. Busoms	48,63	46,17	E
● LM2	K. Bomblies	48,91	46,12	E
● O3	S. Busoms	46,77	46,45	E
● PA10	K. Bomblies	50,48	46,29	I
● PO1	Anthos	51,35	46,86	E
● Ro2	Anthos	51,60	46,80	E
● SCF	S. Busoms	47,72	46,35	I
● SFG	S. Busoms	50,21	46,26	I
● T6	K. Bomblies	49,39	46,20	L
● T9	S. Busoms	49,38	46,18	I
● T11	S. Busoms	49,22	46,19	I
● T13	S. Busoms	49,41	46,19	I
● V1	Anthos	51,25	46,86	L
● V3	S. Busoms	51,18	46,86	L

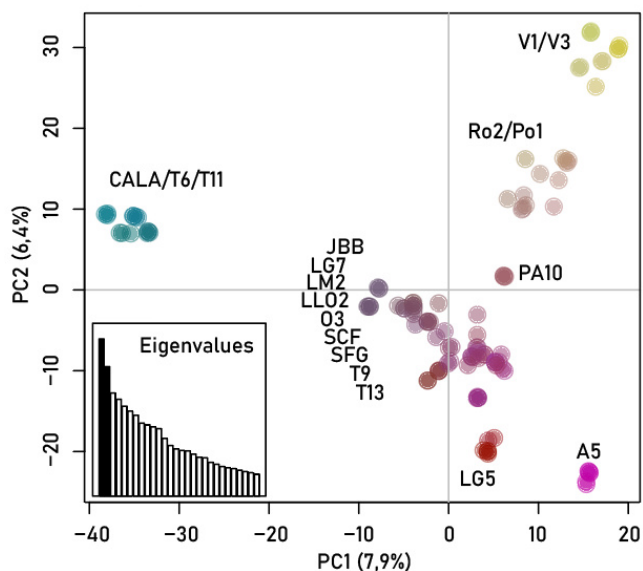
Figure 1.1. Study region. (A) Zoomed area shows the geographical distribution of the studied *Arabidopsis thaliana* CatDeme collection. (B) List of demes from CatDeme collection. Each colored dot represents 1 deme, indicated on the map. UTM coordinates of collection sites and flowering time category (BT; E: early, L: late, I: intermediate) are shown.

Genetic structure

We inferred relationships among the studied *A. thaliana* demes using the R package adegenet version 2.1.1 (Jombart, 2008) based on four-fold degenerate SNPs (4dgs VCF), considered as putatively neutral (see methods). First, we calculated principal component analysis (PCA) and a neighbor-joining (NJ) tree. PCA reduces data dimensionality and summarizes the genetic diversity present in the study data, whereas NJ Trees, applied to NGS data, summarize genetic similarity among populations.

Overall, the total variance in the data explained by retaining the two first PCs was low (8% for PC1 and 6% for PC2). This is not surprising when looking at the results in the context of the size of the data (thousands to millions of variants) and samples from the study (114 sequences). PCA exhibited 4 genetic clusters, three of them showing geographic structure (Figure 1.2A): along the first PC axis all replicates from three coastal demes (T6/T11 and CALA) clustered separately from all other individuals (cluster 1), whereas the second PC axis separated demes from the northeastern region of the study from all other samples, in a

A



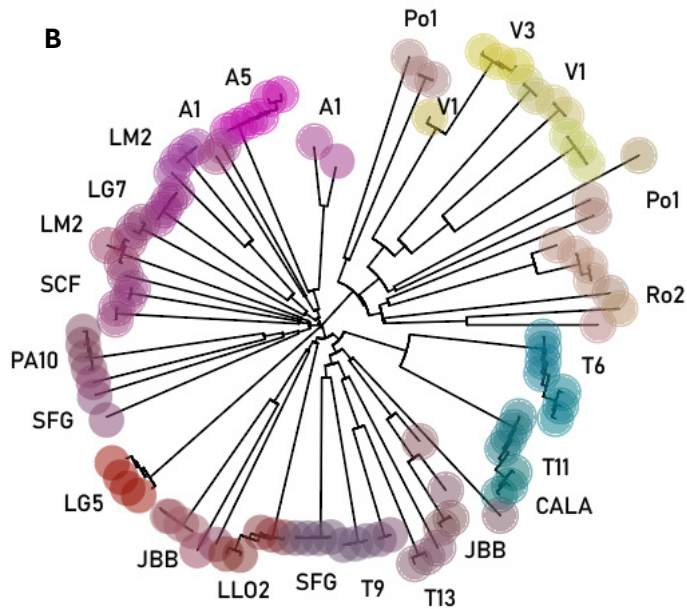


Figure 1.2. Population structure. (A) Principal component analysis (PCA). Scatter plot of the first two principal components. The horizontal and vertical axes represent PC1 and PC2. Each dot represents a deme. (B) Neighborhood Joining (NJ) phylogenetic tree construction of the 20 studied demes. The correspondence between both analyses is shown using colors based on PCs with the color plot function in adegenet (Jombart, 2018).

coastal (Ro2, PO1) to inland (V1, V3) cline (cluster 2). Finally, A5, from one of the two most inland collection sites, separated from cluster 1 along the PC1 axis and from cluster 2 along the PC2 axis. Contrastingly, cluster 4, which corresponded to all other samples, showed an aggregate of closely related demes which occurred scattered across the study area. This structure was broadly confirmed by the NJ tree (Figure 1.2B), which indicated a main subdivision of demes into three distinct groups, being the largest group further subdivided into three subgroups (LG5/T6, T11, CALA/ rest of demes). In both PCA and NJ Tree, genetic diversity is represented complementarily by the distances

(further away = more genetically different), and by the colors (contrasted colors = higher genetic difference). As seen, samples arrangement was generally based on genotype (replicates of each deme grouped together), while no grouping according to flowering time was shown.

Isolation by distance (IBD) was tested using Mantel test between a matrix of genetic distances based on Nei's estimate (Nei, 1972), and a matrix of geographic distances among all studied demes. In the IBD model, genetic differentiation within- and among- natural populations correlates positively with geographic distance (Wright, 1943). In CatDeme, the correlation value between

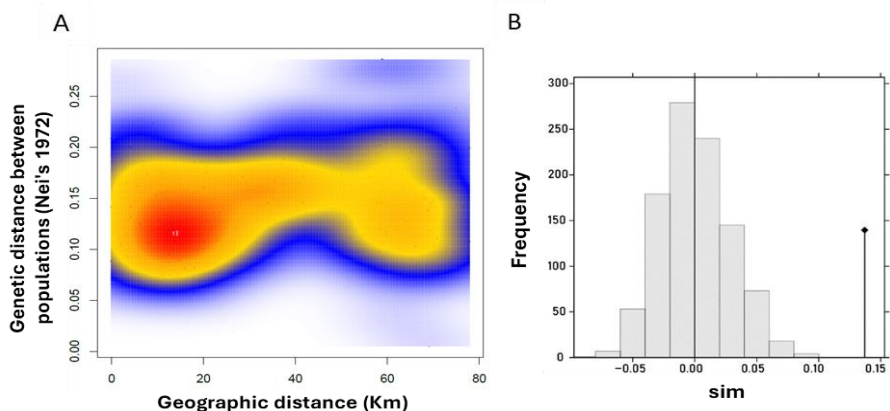


Figure 1.3. Isolation by distance (IBD). Kernel density plot of the correlation between pairwise genetic and geographic distances between demes. The color scale ranges from low (blue) to high (red) density of points.

the distance matrices (represented as a dot in the histogram from Figure 1.3) was out of the reference distribution of permuted values that would represent a random structure (histogram), therefore indicating significant spatial structure. IBD is the most important driver of genetic differentiation within and among *A. thaliana* natural populations (Castilla et al., 2020) and is also present among natural stands at a regional scale (Bomblies et al., 2010; Brennan et al., 2014). The significant IBD observed for CatDeme could be occurring under a classical

IBD scenario (a continuous cline of genetic differentiation causing the correlation between the genetic and geographic distances of the studied demes) but could also be caused by distant and differentiated populations resulting in distance patches. To see which of the two biological scenarios better reflected the CatDeme population structure, the genetic and geographic distances among demes were plotted against each other, and local density of the data was measured using a 2-dimensional kernel density estimation in the adegenet package. The resulting plot (Figure 1.3) displayed one single cloud of data points, with higher density at shorter km number (red-colored, representing the higher number of demes from geographically closer collection sites) and lower density at higher km number (yellow-colored, reinforcing the existence of higher genetic differentiation in the northeastern deme group of V1/V3/PO1/Ro2). Hence, the CatDeme genetic variation showed a continuous IBD pattern across the studied region, although these results must be adopted with caution: the northeastern cluster was the major (if not only) contributor to the significant positive correlation between genetic and geographic distance in the studied samples.

Next, admixture clustering analysis was implemented as a complementary clustering method by using the NGSadmix software (<http://www.popgen.dk/software>). Genetic admixture is the process in which two isolated populations interbreed, leading to a mixture of alleles from different ancestral populations in their offspring. NGSadmix uses the genotype likelihoods (i.e., probability of a specific genotype at a specific position) to infer admixture proportions (Skotte et al., 2013) and therefore the ancestry of each studied individual. NGSadmix was run with K values ranging from 2 to 10 to get an accurate estimate of the “best” K for our data. This was inferred by pulling out the log-likelihood values from each run (which measure the goodness of fit of each K number in the dataset) and then using an ad hoc statistic, DeltaK, based on the log-likelihood rate of change among the successive inferred K's. K

= 3 was obtained as the best number of inferred populations for CatDeme (Figure 1.4), supporting the T6/T11/CALA (cluster 1) and the northeastern (cluster 2) genetically differentiated groups.

In summary, our results suggest that the studied demes maintain high clonality regardless of their location within the sampled region (they group by genotype),

K=3

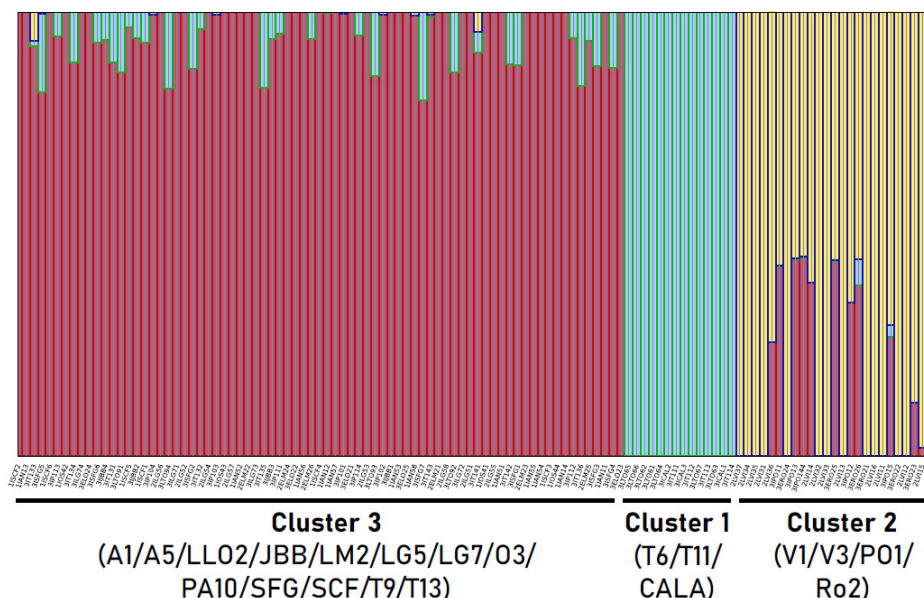


Figure 1.4. Admixture proportions using NGSadmix. Analyses were carried out under the assumption of various numbers of ancestral populations ($K = 2-10$). Admixture plot for $K = 3$, as best K according to Evanno's test, is shown. The 114 CatDeme sample sequences were used. Columns represent individuals and each color represents one inferred ancestral population. The length of each segment in each column depicts the proportion of ancestry in each population and samples group into colored clusters according to the proportion of their ancestry components.

although distant demes belonging to the identified northeastern cluster have higher genetic differentiation from those at the center of the range, probably due to geographic isolation. Likewise, according to PCA and NJ Tree results, coastal

demes from the northeastern cluster tend to differentiate from inland demes at the same latitude, and the same trend is observed for the coastal T6/T11/CALA cluster. This implies factors other than geographic distance (like environmental heterogeneity) are acting on the genetic structure of the CatDeme collection and suggests local adaptation events partially contributing to genome-wide differentiation among demes.

Although to a lesser extent than IBD, local adaptation to environmental gradients accounts for the distribution of genetic diversity within- and among-populations in *Arabidopsis* (Castilla et al., 2020). In the case of flowering time, Genotype x Environment interactions (GxE) are often the drivers of its regulation (Sasaki et al., 2015) and, therefore, the genetic basis of this trait changes across environments (Yan et al., 2021). In CatDeme demographic analyses, individuals were not grouped according to their flowering time. Thus, BT variation among demes did not reflect genetic differentiation. However, when working at the whole-genome level, it is likely that genomic variation outside loci responsible for variation in the trait of interest (in this case BT) dominates grouping. This has previously been observed when studying population genomic relationships between plants differentiating in specific adaptive traits (Busoms et al., 2018). Therefore, the analysis of the molecular basis of flowering time variation in CatDeme was further pursued.

FRI and FLC genotyping

FRI (*FRIGIDA*) and *FLC* (*FLOWERING LOCUS C*) allelic variation is a major determinant of flowering time in *Arabidopsis*. Briefly, *FLC* is a floral repressor regulated by *FRI*. Without vernalization, *FRI* promotes *FLC* expression, resulting in flowering repression. Under vernalization, *FLC* expression is reduced, counteracting *FRI* effects and promoting flowering. Several loss-of-function mutations at the *FRI* locus have led to flowering acceleration in accessions like

Col-0 and Ler-0, and extensive *FLC* allelic variation is also reported to contribute to rapid-cycle accessions deriving from late flowering ancestors (Koornneef et al., 1991; Michaels & Amasino, 1999; Johanson et al., 2000; Gazzani et al., 2003).

To see if the contribution of both loci accounted for the variation in the flowering habit of CatDeme, *FRI* and *FLC* genotyping was performed for all sequenced individuals (n = 114) against Col-0 reference genome.

For *FRI* sequence, a total of 10 SNPs and 1 insertion of 16 base pairs (bp) were detected across demes at different frequencies (top of Figure 1.5, Table S1.2) when compared to Col-0. From the 10 SNPs, 7 were non-coding (2 located at the putative-promoter region, 51 bp upstream the 5'UTR region and 82 bp upstream the start codon; 1 was intronic, and 4 located at the 3'UTR), whereas 3 were frameshift (1) and missense (2) variants at the first 1 Kb exon. The 2 missense variants were found in all demes and resulted in amino acid differences (Glu¹⁴⁶→Gly and Ile¹⁴⁸ → Met). These 2 variants and the 16 bp insertion are characteristic of accessions bearing the *FRI* dominant allele. In Col-0, Ler-0 and other rapid-cycle accessions, Gly¹⁴⁶ → Glu and Met¹⁴⁸ → Ile, together with the 16-bp deletion at the end of exon 1 (which changes the reading frame and terminates the ORF immediately at the beginning of the exon), characterize the recessive *FRI* (loss of function allele) (Johanson et al., 2000). Therefore, *FRI* allele in all studied demes was assumed to be fully functional and not accounting for the constitutive early flowering of Ro2, O3, LLO2 or LM2, as none had an obvious disruption of the *FRI* coding sequence, and no further mutation was exclusive to the early flowering individuals (Table S1.2). Whether this group of demes carry *FRI* alleles with an unidentified lesion (Werner et al., 2005) remains undetermined.

Another explanation for the earliness in demes with a functional *FRI* allele could be the presence of defects in *FLC*, since *FRI* acts solely through *FLC* to control

flowering (Michaels & Amasino, 2001). A total of 22 variants, including 2 deletions and 4 insertions, were detected among *FLC* sequenced demes, being 11 shared by all demes, and nonexclusive from early or late phenotypes (bottom of Figure 1.5; Table S1.3). Col-0 belongs to *FLC^A* haplogroup of rapid-cycle accessions (strong *FLC*), and precisely 22 SNPs and 6 indels are reported to distinguish *FLC^A* from *FLC^B* (weak *FLC*) haplogroups (Caicedo et al., 2004). However, we considered the total number of detected polymorphisms not consistent enough for classifying the CatDeme collection in the *FLC^B* major haplogroup, as none of the studied phenotypes was extremely late flowering and CatDeme is a southern-Europe collection, where dominance of *FLC^A* is expected (Caicedo et al., 2004).

Besides the above-mentioned SNP variants and small indels, a 30-bp deletion at the intron 1 of all sequenced individuals was detected in all demes. This region regulates *FLC* expression and *FLC* repression after vernalization (Sheldon et al., 2002). Col-0 is reported to bear this 30-bp insertion, contrasting with the CatDeme collection. However, this indel has been detected in both strong and weak *FLC* accessions and is considered not to interfere with *FLC* function (Gazzani et al., 2003).

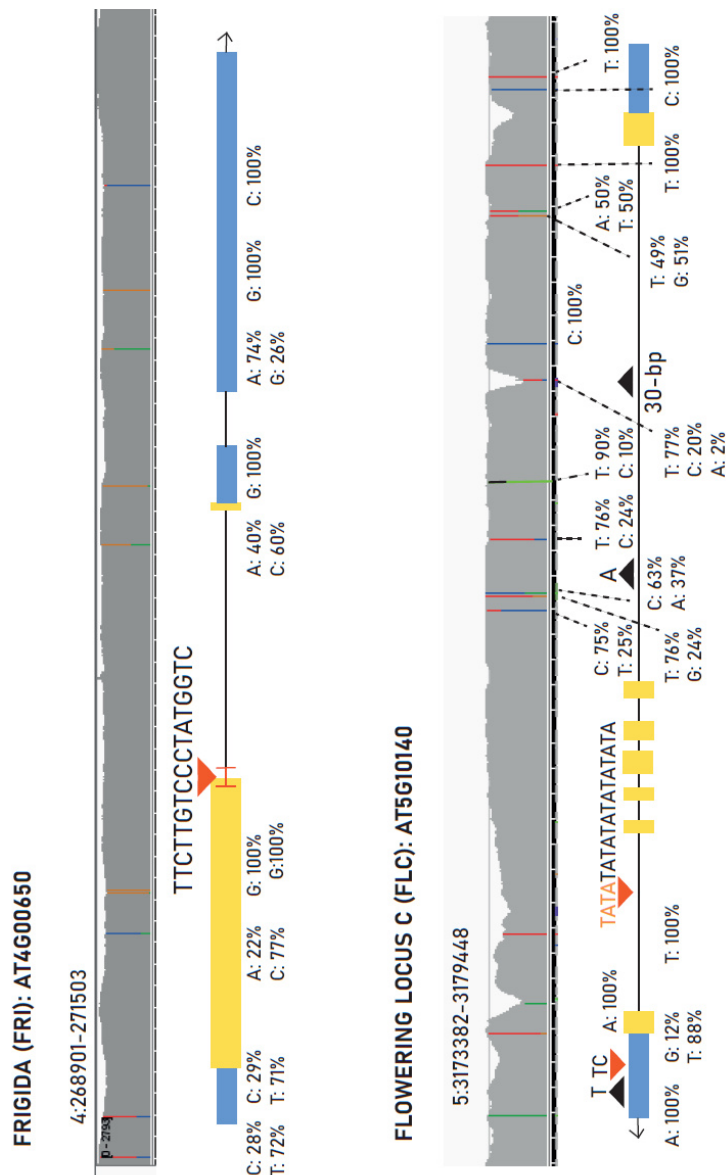


Figure 1.5. *FRI* and *FLC* genotyping. BAM files of the *FRI* and *FLC* region of all CatDeme samples were uploaded to the Integrative Genome Viewer (IGV) for multiple alignments. Each mutation site becomes a colored column inside the read coverage track (gray area). Detected variants and allele frequencies are pictured on each gene model. Gene orientation is indicated with an arrow on the right (*FRI*) and left (*FLC*). Exons: yellow boxes; UTR's: blue boxes; Introns: connecting lines. Insertions: orange triangles; Deletions: black inverted triangles.

Finally, two indels previously described, known as *Indel-1075* (Méndez-Vigo et al. 2011) and *Del-57* (Sánchez-Bermejo et al., 2012) were detected in CatDeme subsets (Table S1.3). *Indel-1075* is a haplotype of moderate frequency first identified in a collection of 182 Iberian populations by Mendez-Vigo and colleagues (Mendez-Vigo et al., 2011). It is reported as an Iberian-specific haplotype belonging to the major *FLC^A* haplogroup and spread around northeastern Spain (Caicedo et al., 2004). In agreement, the *Indel-1075* haplotype was present in all the studied demes except T2, T6, T11 and T13, all sampled at the same location (Tossa de Mar) but different collection sites (Figure 1.1B). *Del (-57)* is a 50-bp-deletion located 57 bp upstream from the start codon and affecting the *FLC* 5'-UTR. Accessions bearing *Del (-57)* are described as a subgroup inside the *Indel-1075* group and are reported to be significantly associated with increased vernalization sensitivity (i.e, lower number of cold days required for flowering initiation) and reduced *FLC* expression after vernalization. Moreover, its presence was found to be concentrated just in the eastern part of *Indel-1075* domain (Sánchez-Bermejo et al., 2012), which comprises the area of study (Figure 1.1A). In CatDeme, the *Del (-57)* haplotype was not exclusive from early flowering phenotypes either (Table S1.3). Thus, the CatDeme collection belongs to the *FLC^A* haplogroup, although the observed BT differences do not seem to rely (at least solely) in *FLC* polymorphisms.

Besides sequence variation, changes in flowering time and in relative *FLC* expression levels were assessed with and without 28-days of vernalization in a subsample of CatDeme samples: 3 Ro2 individuals as constitutive early-flowering deme, and 3 T6 individuals as a late-flowering deme. Three Col-0 individuals were also included as a known genotype with nonfunctional *FRI* and strong *FLC* from the *FLC^A* haplogroup. Vernalization resulted in a significant decrease in the flowering time (measured as number of days from sowing to BT) in Col-0 and T6 when compared to the non-vernalized plants (adj. *p*-value < 0.05), whereas the early flowering Ro2 showed a vernalization-unsensitive

phenotype (Figure 1.6A; Table S1.4). However, significant reduction in *FLC* expression was observed after 28 days of cold exposure in all individuals (adj. p -value < 0.05) (Figure 1.6B), and *FLC* levels before and after vernalization in CatDeme samples reflected those of Col-0, classified as a rapid vernalization haplogroup (Li et al., 2014).

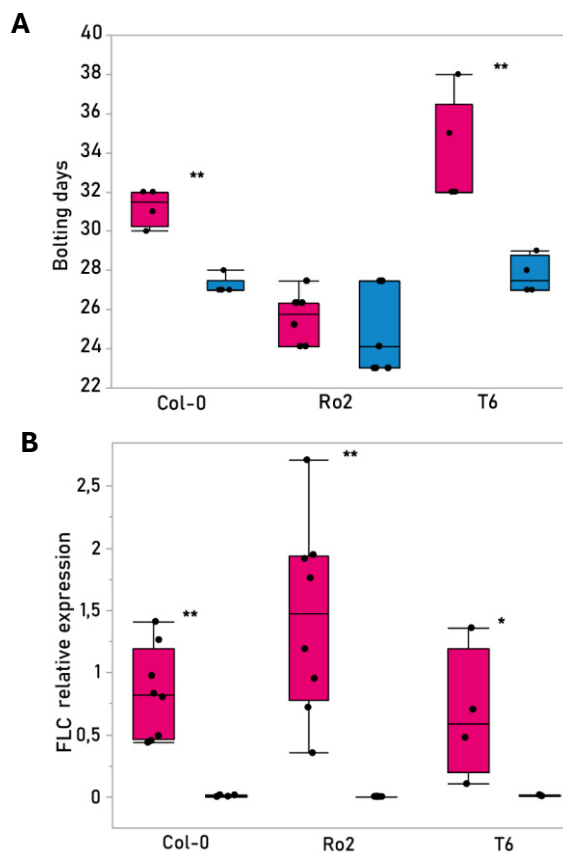


Figure 1.6. Vernalization response in early and late flowering demes. Col-0, Ro2 (early flowering) and T6 (late flowering) were cold-treated for 0 (pink) or 28 (blue) days and grown under an escalating 10-12-14-16h light photoperiod. (A) Flowering time expressed as number of days from sowing to the appearance of the first bud (bolting days). (B) *FLC* transcript levels. Each dot represents a biological replicate. Asterisks indicate significant differences between non-vernalized and vernalized plants ($p < 0.05$, Student t -Test).

To gain insights into the distribution of the identified *FLC* alleles, and to see if constitutive early flowering demes showed signs of bearing a distinctive *FLC* variant not detected in the CatDeme demography and genotyping analyses, the sequences of the *FLC* region from the 114 CatDeme samples were framed with the 1135 *A. thaliana* *FLC* sequences (<https://1001genomes.org>). A merged dataset of 1,212 sequences was created and a Principal Component Analysis (PCA) of the *FLC* locus (a 7-Kbp region comprising promoter + gene) from all samples was performed. Available sequences of accessions known to belong to *FLC^A* (11) and *FLC^B* (7) major haplotypes (Caicedo et al., 2004), as well as accessions carrying the six *FLC* haplotypes identified in 1307 worldwide *A. thaliana* accessions (bearing strong, weak, or nonfunctional *FLC* alleles) (Horton et al., 2012; Li et al., 2014) were used as a reference to contextualize the position of the CatDeme individuals on the PCA (Figure 1.7).

Overall, the two first PCs accounted for large amounts of the observed variation (42% and 14%, respectively) and *FLC* sequences from the 1135 accessions clustered into 3 main groups. Along PC1, accessions bearing *FLC^B* allele (Bs-1, Kas-1, Li-7) and accessions from the RV1 haplotype (Wt-1, Kondara, Nok-3 and Ct-1, showing rapid vernalization response) clustered separately from several identified *FLC* genotypes: Van-0, Da-(1)-(12) and Ler-0, which bear functional alleles of *FRI* but are early flowering because of weak alleles of *FLC*; LI-0, from the Iberian Indel-1075 *FLC* haplotype; and the Col-0 strong *FLC* allele. As all the above-mentioned variants belong to the *FLC^A* haplotype, we concluded that the two major *FLC^A* and *FLC^B* haplotypes clustered separately along the PC1 axis. Along the PC2 axis, individuals from the haplotype Hap5, comprised predominantly by accessions from the United Kingdom and with a relatively slow vernalization response (SV1) were separated from the rest of identified SV and RV haplotypes (Li et al., 2014). All CatDeme samples clustered closer to *FLC^A* than to *FLC^B* and only spread along the PC2 axis, in which LM2 and PO1 (with reported early flowering), together with single replicates from JBB, T13 and

V1 (intermediate and late flowering) clustered close to the Hap5 haplogroup. Considering the observed *FLC* expression levels from the vernalization experiments, the latitudinal distribution of the CatDeme collection sites, and the higher affinity of CatDeme sequences for the *FLC^A* haplotype on the PCA, we confirmed the classification of the CatDeme collection as a *FLC^A* allele in a *FRI* nondeletion background (Caicedo et al., 2004).

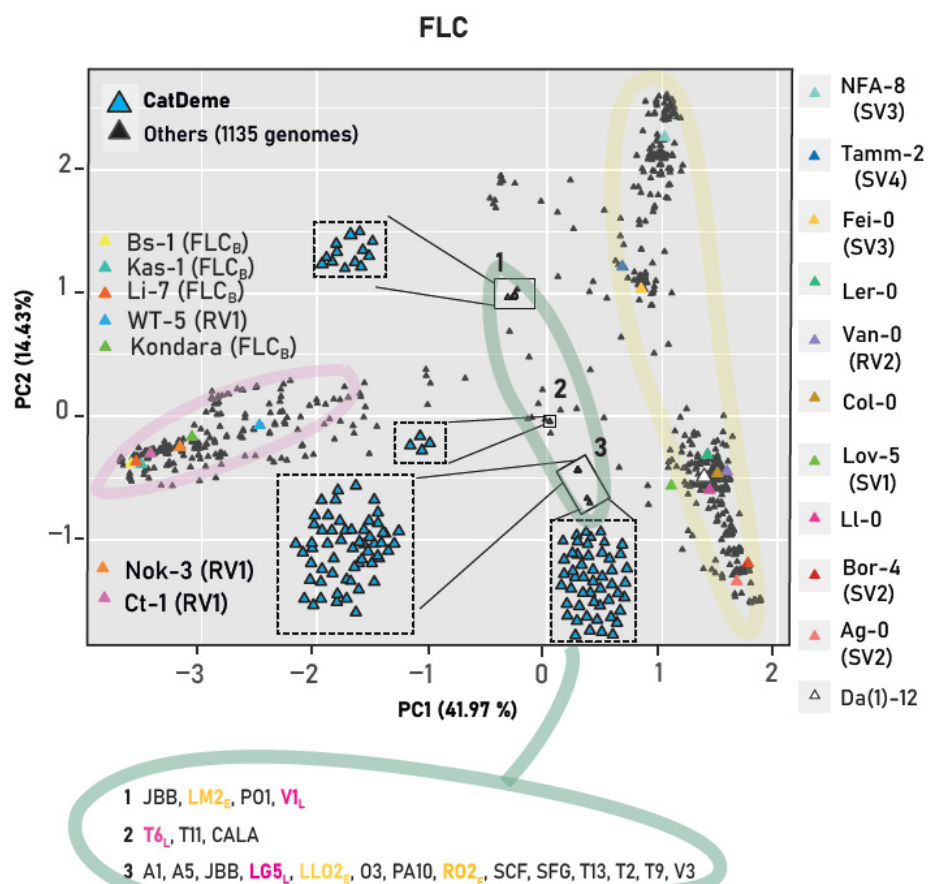


Figure 1.7. PCA of *FLC* locus data of all CatDeme sequences and 1,135 *A. thaliana* genomes (1001genomes.org/). CatDeme distribution is zoomed and CatDeme subgroups are listed below the PCA plot. Early (E) and late (L) flowering genotypes are color-coded in yellow and pink, respectively.

This could imply that demes with constitutive early flowering (like Ro2) bear *FLC* intronic mutations leading to normal-length *FLC* transcript but inactive FLC protein, as reported for the early flowering FRI-*FLC*^A accession Van-0 (Werner et al., 2005). Moreover, this would not be in conflict with the PCA results, as Van-0 clustered together with accessions differing in flowering time, like Ll-0 (Sánchez-Bermejo et al., 2012). Early flowering types with high *FLC* levels or late-flowering individuals with low *FLC* levels have been reported before, which proves the extensive variation in flowering-time genes and implies that genes other than *FLC* could repress flowering (Shindo et al., 2005). To get more information about possible variables accounting for the distribution of CatDeme *FLC* variants in the world-wide context, the accessions clustering more closely to the CatDeme cluster (i.e., individuals with similar load factors in the loading matrix) were identified. Excepting 1 UK genotype, all accessions clustering with CatDeme individuals are originally from France, Italy, Greece and Morocco, which agrees with a latitude dependent *FLC* polymorphism pattern (Calceido et al., 2004).

Overall, the presence of *FLC* variants differentiating early from late flowering demes was not supported in CatDeme, nor by the genotyping of the full *FLC* region, neither by the PCA of the *FLC* region from a world-wide distributed collection of *A. thaliana* accessions. As reported for ecotypes collected from geographically close regions or same localities, the variation observed in flowering time indicates the presence of microenvironments that can lead to complex selective forces. In this context, an absent or low vernalization requirement and an early flowering phenotype could be selectively advantageous to escape summer drought and soil Na⁺ increase in coastal areas, among others (Johanson et al., 2000; Busoms, 2015).

To increase our understanding of these processes, the genetic diversity and differentiation among populations with contrasted flowering times were quantified.

Window - based genome scans

To seek for an adaptive genomic footprint in the flowering time of CatDeme, a genomic divergence scan was performed between two CatDeme subsets exhibiting contrasting flowering times (indicated as E- *early*; L-*late* in Figure 1.1B). The divergence scans were performed by calculating pairwise F_{ST} and Tajima's D for each comparison group in non-overlapping 5-kb genome windows. F_{ST} , or fixation index, relates to the variance in allele frequency among populations (Wright, 1949). Loci under selection can be detected as regions with significantly high levels of differentiation between the compared subpopulations (i.e., high F_{ST} values), indicating different alleles being favored in each subpopulation (Beaumont and Nichols, 1996). In this case, F_{ST} values above the 99th percentile for the simulated distribution of F_{ST} (therefore, loci exhibiting outlier F_{ST} values between the compared groups) were considered as potential adaptive candidates, for showing more extreme differentiation than what would be expected under neutrality. Tajima's D is another statistical test applied to distinguish between neutral and non-random evolution processes. Positive selection will lead to an excess of rare variation, which be reflected by negative values of Tajima's D.

The F_{ST} average in the comparison was 0.16, and the Tajima's D averages for early and late flowering groups were 1.015 and 0.74, respectively. This points to a pattern of balancing selection in the two compared groups, especially in early flowering individuals, in which Tajima's D genome-wide distribution values were higher (Figure S1.1). It is plausible that an adaptive force sustains balanced polymorphisms affecting flowering time within CatDeme, due to fluctuating environmental conditions and small-scale spatial heterogeneity from the sampled region (Busoms, 2015; Wu et al., 2017). However, in addition to these global patterns, the sliding window scan revealed a total of 426 diverged variants between the early and the late flowering groups (Dataset S1.4). Gene ontology (GO) analysis of the 426 obtained candidates showed no significant

enrichment (Fisher's exact test, $p < 0.05$; FDR correction) for biological processes, molecular functions, or cellular components, but loci potentially contributing to adaptive differences between flowering phenotypes were obtained by gene annotation and description of all F_{ST} outliers.

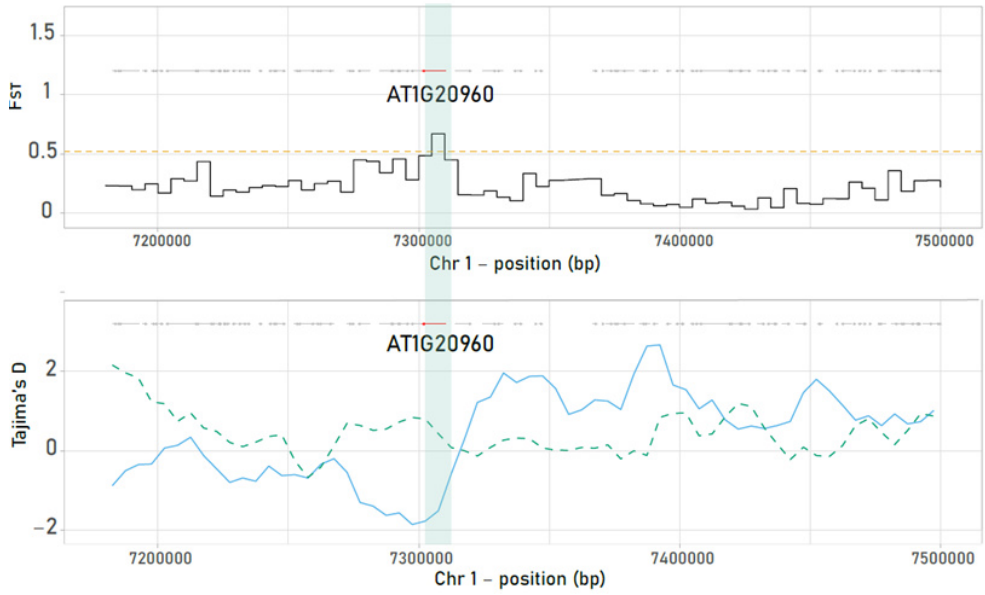
Allele frequency differences around 4 loci involved in flowering time variation were observed: *BRR2a* (AT1G20960), *FRI* (AT4G00650), *AGL19* (AT4G22950) and *AGL71* (AT5G51870) (Figure 1.8). *BRR2a* encodes an ATP-dependent RNA helicase protein involved in the processing of flowering time gene transcripts, specially *FLC*. In *Arabidopsis*, an early flowering *BRR2a* allele was reported to cause defects in *FLC* splicing, thus leading to reduced *FLC* expression (Mahrez et al., 2016). Here, the *BRR2a* outlier displayed contrasted trends in Tajima's D values among groups (Dataset S1.5): 0.5 for late flowering individuals, but a sharp decrease to -1.9 in the early flowering group. This is consistent with an advantageous variant of *BRR2a* replacing a major part of the variation in the region for early flowering demes. Although *FLC_{Ro2}* expression levels without vernalization did not differ from those of *FLC_{T6}* (Figure 1.6), an effect of *BRR2a* rare variant in *FLC* splicing, causing constitutive early flowering in demes with apparent *FRI-FLC^A* (like *Ro2*), should be further addressed. Extensive *FLC* expression analyses under short- and long-day conditions, and coimmunoprecipitation assays to test for differential interaction strength between *BRR2a_{EARLY} - FLC* and *BRR2a_{LATE} - FLC* in all demes will help elucidating the proposed *BRR2a - FLC* regulation mechanism.

Concerning *FRI*, the performed genome scans support the presence of a weak *FRI* allele in early flowering demes not identified in the previous CatDeme *FRI* genotyping. *FRI* polymorphism patterns in CatDeme did not exhibit *FRI_{Col-0}* or *FRI_{Ler-0}* indels (Figure 1.5, Table S1.2), but *FLC_{Col-0}* expression levels did not significantly differ from *FLC_{EARLY}* and *FLC_{LATE}* without vernalization (Figure 1.6). This supports the presence of a loss of function *FRI* allele in CatDeme. *FRI* loss-of-function mutations are abundant in *Arabidopsis* natural populations and are

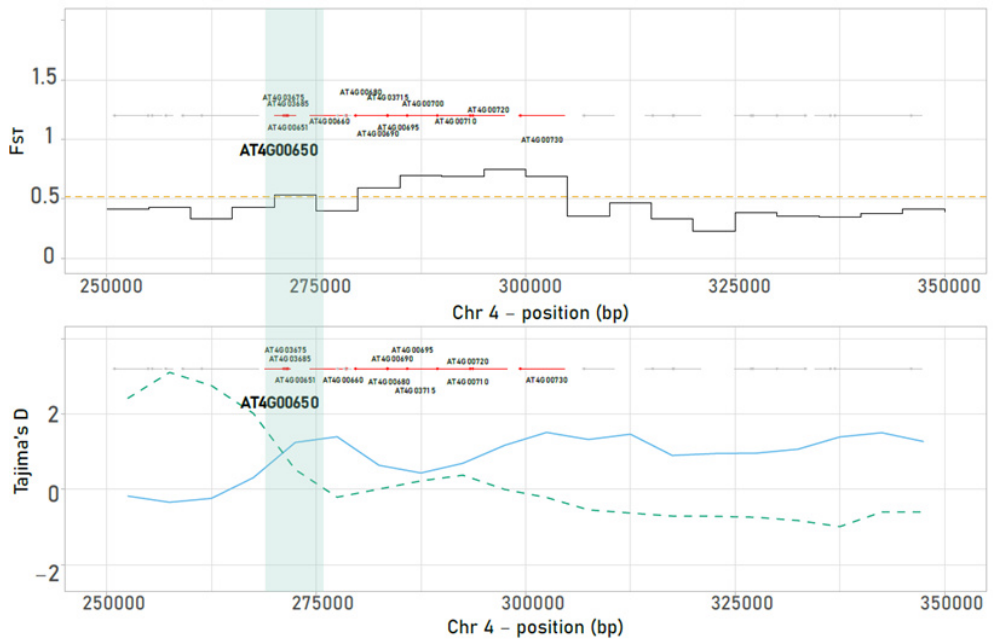
reported to be under positive selection in nature (Zhang & Jiménez-Gómez, 2020). Here, *FRI* was identified as an F_{ST} outlier but not detected as a locus under selection based on site frequency spectrum analysis (i.e., Tajima's D outliers). F_{ST} and Tajima's D index are reported to detect selection acting at different temporal scales (Franks et al., 2016) and genes under recent episodes of balancing selection or recent selective sweeps are difficult to detect by Tajima's D (Carlson et al., 2005). Therefore, the genetic divergence of *FRI* between early flowering and late flowering demes can still imply that an historically recent environmental change has differentiated the habitat of each compared group and favored different allele variants.

Finally, *AGL17* and *AGL19* are MADS-box *SOC1*-like transcription factors which promote flowering in a *CO* and *FLC*-independent manner (Dorca-Fornell et al., 2011; Kim et al., 2013). Besides, Tajima's D values showed opposite trends between groups at the *AGL19* region (early = 1.7; late = -0.75). Alternatively (or complementarily) to *BRR2a*, the presence of hypofunctional *AGL19* or *AGL17* alleles contributing to a delayed flowering transition would explain the T6 phenotype (slower reproductive cycle under the same *FRI-FLC^A* background than the early flowering demes). The polycomb-group (PcG) proteins MSI1, CLF, and EMF2, repress *AGL19* in the absence of cold (Schönrock et al., 2006), and the histone deacetylase HDA9 also prevents *AGL19* transcription (cita; Kim et al., 2013). Likewise, *AGL17* is a CLF target (Shu et al., 2020). *AGL17-19* methylation (a key repressive histone modification) and expression levels should be compared between early and late flowering samples to assess whether hypoacetylation in *AGL17-19* chromatin is causing delayed flowering (Kang et al., 2014) in T6 and T6-like demes.

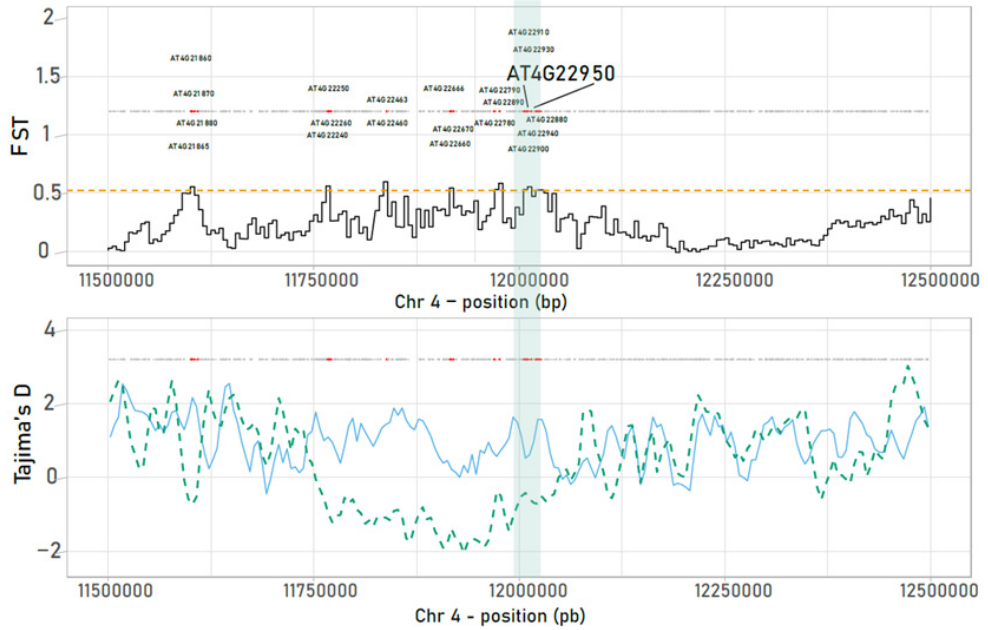
BRR2a



FRI



AGL19



AGL17

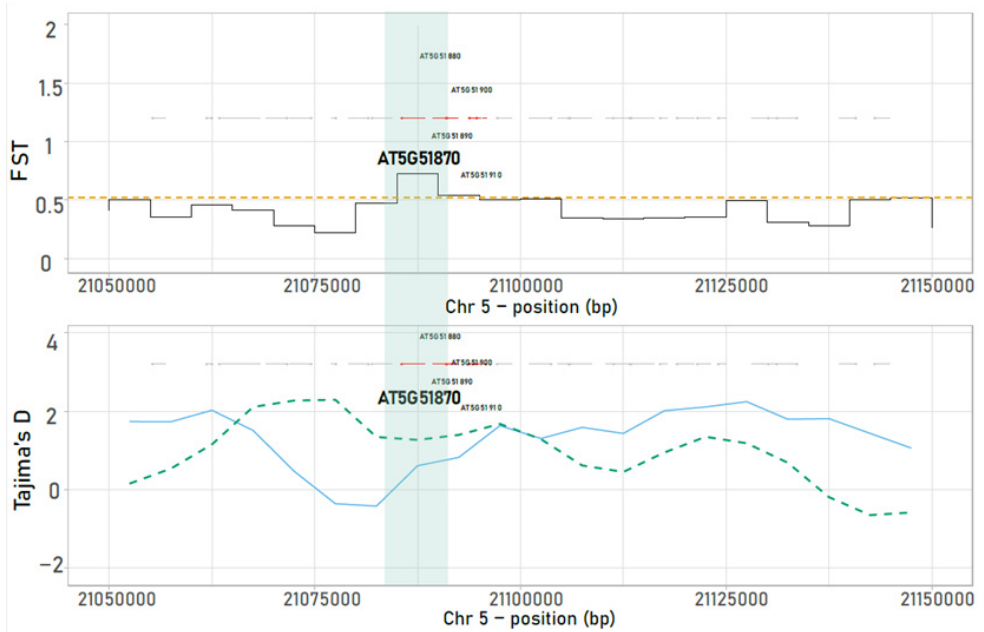


Figure 1.8. Genomic divergence scans. Pairwise F_{ST} estimated in 5 kb windows for the outlier peaks on *BRR2a*, *FRI*, *AGL19* and *AGL17* between early and late flowering groups. Tajima's D, estimated in 5 kb windows, is displayed for each group by the blue (early flowering) and dotted green (late flowering). The locations of gene annotations are shown by bold-typed gene id. The hotspot is shaded. Red bars highlight all genes under the peak. Chromosome and position are shown at the x-axis.

To gain further evidence of the involvement of the proposed candidates in BT variation, the produced WGS data should be used for *BRR2a* and *AGL17-19* genotyping and haplotype analyses in CatDeme. Next, genotyping of *FRI*, *BRR2a*, *AGL17* and *AGL19* should be complemented by pairwise correlations between gene variant expression levels and BT of each deme. Besides, a nonrandom distribution of alleles at these candidate loci across geographic, climatic, and other environmental gradients should be confirmed by association analyses, to get deeper insights into their adaptive role and to identify the driver agent of such adaptation, if present.

Assessing genotype-environment associations (GEA) and genotype-phenotype associations (GPA) in CatDeme under alkaline salinity

Previously, soil salinity on siliceous soils (Busoms, 2015) and soil carbonate content (Terés, 2017) have been reported as selective agents in the CatDeme collection, driving local adaptation processes in coastal and inland demes, respectively. Furthermore, no presence of demes has been detected on calcareous soils at the coastal range (i.e., alkaline salinity) in the study region. Recently, some plant responses from coastal demes (adapted to siliceous soils) have been shown to be deleterious under alkaline salinity, whereas plants from moderately saline-calcareous soils (broadly, areas between inland and coastal areas) outperformed those from coastal or inland demes when grown under alkaline salinity conditions (Pérez-Martín et al., 2022).

The role of the soil nutrient profile as an adaptive driver in the CatDeme collection was addressed by a Genotype-Environmental Association Analysis

(GEA), in which associations between variation in genomic regions and changes in soil composition at a regional scale were assessed. To seek for candidate variants involved in enhanced responses to alkaline salinity, data on leaf nutrition for all demes grown under alkaline salinity was included for a Genotype-Phenotype Association Analysis (GPA). Genomic data of all CatDeme samples and mineral nutrient concentration in leaf and soil of origin were used (Dataset S1.1-S1.3).

First, all studied demes were classified according to Na^+ concentration and $\text{CaCO}_3\%$ content at their native soils: **CN** (Calcareous-Non Saline: CaCO_3 above 4% and Na^+ below 50 mg kg^{-1}), **CS** (Calcareous-Saline: CaCO_3 above 4% and Na^+ above 50 mg kg^{-1}) and **SS** (Siliceous-Saline: CaCO_3 below 4% and Na^+ above 50 mg kg^{-1}) (Figure 1.9A-B). Data on ionomic profiling of the native soil associated with each sequenced individual was obtained from Busoms et al., 2018.

Next, the ionomic profiles of each soil type were compared to characterize elements differentiating alkaline-saline soils (CS) from neutral saline soils (SS). Among the 15 elements investigated, six exhibited consistently different concentration in CS soil, besides $\text{CaCO}_3\%$ and Na^+ (adj. p -value < 0.05, HSD Tukey): K^+ , Ca, Mn and Mo (Figure 1.9C; Table S1.5). Likewise, leaf nutrient profiles of the study demes were compared according to their native soil-type when grown on a natural alkaline-saline soil in greenhouse-controlled conditions (CS-reference soil, see methodology). CS demes exhibited

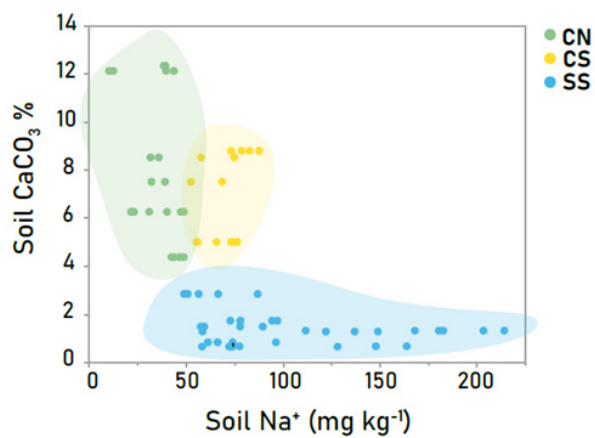
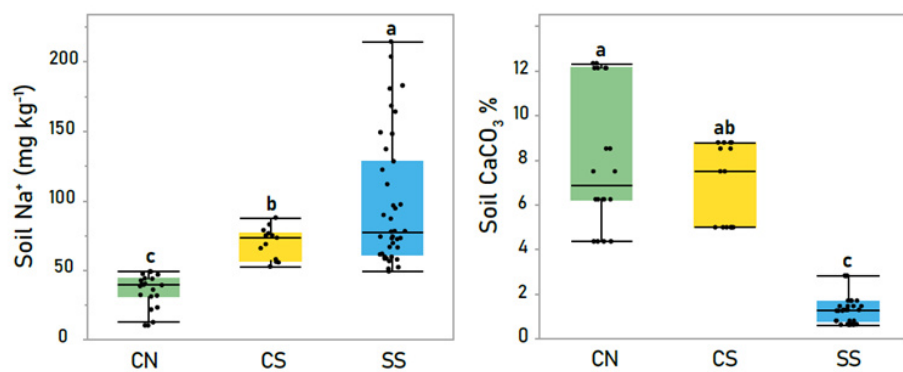
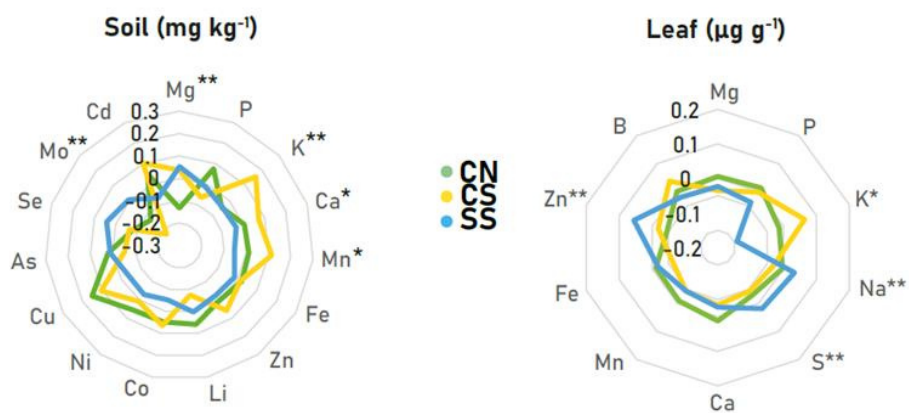
A**Soil-type classification****B****C**

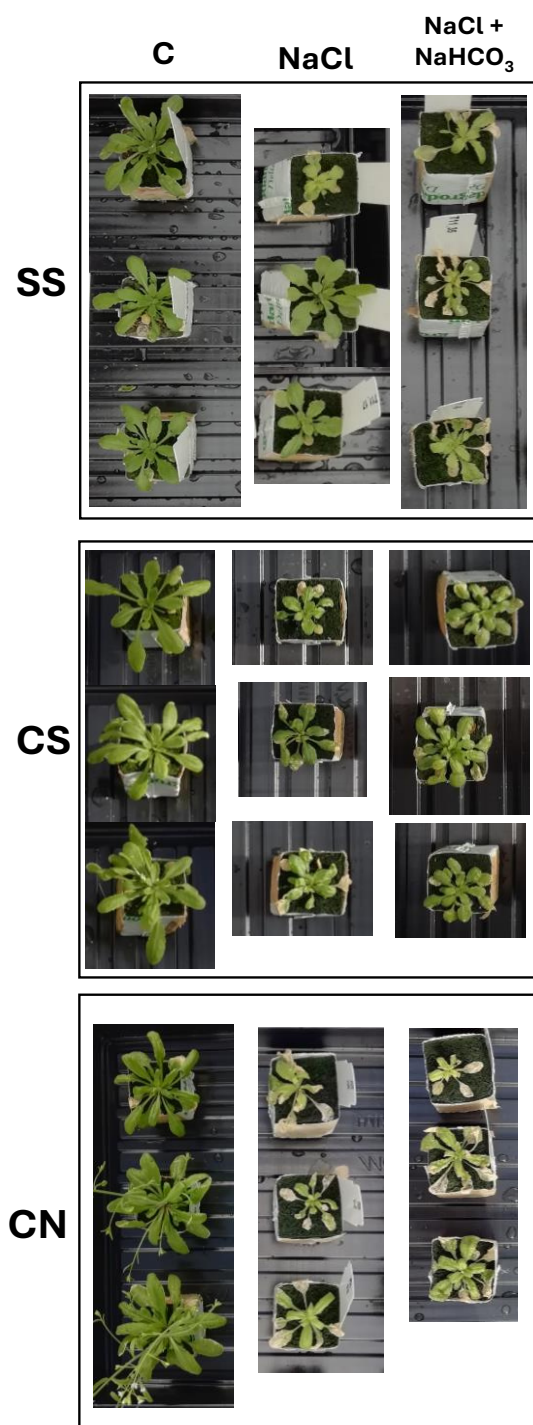
Figure 1.9. Deme classification according to native soil-type. (A) Native soil carbonate (CaCO_3) vs soil Na^+ content. (B) Boxplots of soil Na^+ and CaCO_3 differences and (C) Radial plots with the Z-values of the studied elements in native soils and leaves among the established deme groups. CN, CS and SS demes. Axes display Z-scores calculated per element and asterisks show significant differences among the three groups ($p < 0.05$, HSD Tukey). **CN**: Calcareous-non-saline; **CS**: Calcareous-saline; **SS**: Siliceous-saline.

significantly higher K^+ and lower Na^+ , S and Zn concentrations when compared to the SS deme group (adj. p -value < 0.05 , HSD Tukey) (Figure 1.9C; Table S1.6).

To further assess for differential effects of the reference CS soil in the nutrient profile of the studied demes depending on their origin, multivariate analyses on the differentially accumulated nutrients was performed (Figure 1.10). SS individuals (originating from saline siliceous soils) showed the highest correlation among all selected nutrients when grown on CS soil, being Na^+ and K^+ the most negatively correlated ($r = -0.87$; p -value < 0.0001), pointing to ionic imbalance (Kumari et al., 2021). Contrarily, CN accessions only exhibited moderate positive correlation between Na^+ -S ($r = 0.50$) and S-Zn ($r = 0.46$). Finally, CS accessions displayed increased Na^+ -S correlation ($r = 0.93$) but attenuated correlations between the rest of element combinations. These results point to differential plant ionome dynamics under alkaline salinity in the studied demes depending on their origin, influencing on overall plant performance.

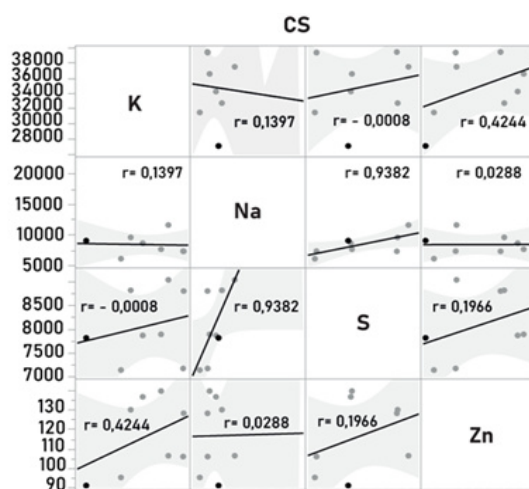
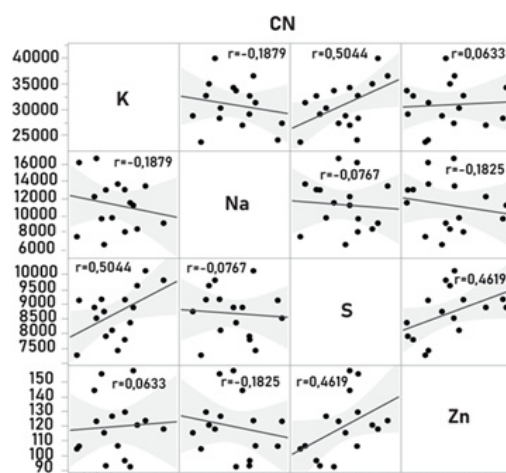
Rockwool irrigation experiments (RI, see methodology) confirmed significantly higher relative K^+ concentration in leaves of CS plants when compared to SS demes under alkaline saline treatment, whereas CS Na^+ and S leaf concentrations were significantly lower than those of CN but not SS plants, and Zn exhibited no significant differences among groups (Table S1.7). These observations prove that irrigation on an inert substrate does not embrace the complexity of soil systems, but provide further evidence that increased leaf K^+ ,

more than decreased leaf Na^+ accumulation, is involved in alkaline salinity tolerance in CatDeme.



Picture 1. RI experiment.
 Example of SS, CS and CN deme performance under control, neutral (NaCl, pH 5.9) and alkaline salinity irrigation treatments (NaCl + NaHCO₃ pH 8.3, see methods).

Based on the established deme classification, we applied latent factor mixed models (LFMM) to infer candidates significantly associated with distinctive CS soil elements (GEA) and with the differential leaf element concentration in the studied demes (GPA).



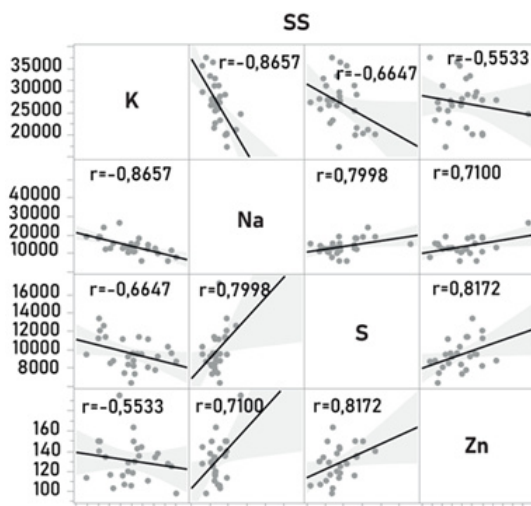


Figure 1.10. Multivariate analysis. Scatterplot matrix of pairwise correlations from leaf nutrition variables differentiating CN, CS and SS demes when grown in an alkaline saline environment. Numbers in each matrix denote linear association via Pearson's correlation coefficient. Y-axis: leaf element concentration ($\mu\text{g g}^{-1}$ DW).

Mutasa between each soil or leaf elemental concentration and the SNPs present across the genome in each individual sample (in total 120 samples). After p -value correction (q -value < 0.01 ; see methods), LFMM identified a total of 439 genes (341 for GEA and 98 for GPA) harboring ≥ 1 SNP significantly associated with at least one variable (Dataset S1.6; Figure S1.2-S1.3). This is a restrictive list compared to LFMM association analyses using larger collections of accessions and less restrictive parameters (Tabas-Madrid et al., 2018; Konečná et al., 2021).

The highest number of significant associations (i.e., variables with most candidate genes associated) were found in soil Ca ($n = 438$ SNPs, mapping to 129 genes) and soil Na^+ phenotypes ($n = 296$ SNPs, mapping to 136 genes). This supports the fact that Na^+ and Ca are primary selective agents in the sampled sites. Moreover, the SNPs with the lowest q -value across all GEA and GPA were associated with soil Na^+ (10 SNPs with q -value $= 3.29\text{E}^{-05}$), followed by leaf K^+ (56 SNPs with q -value $= 3.53\text{E}^{-05}$) (Dataset S1.7). These results are in line with salinity being a major driver of genomic variation in the studied demes, on one

hand, and with differential K^+ nutrition as a key trait under salinity regardless of pH, on the other.

In soil mineral concentration traits (GEA) all candidates (GEA candidates hereafter) were associated with only one variable. Opposite to GEA, candidates from leaf nutrition traits (GPA candidates hereafter) were mostly non-exclusive: 100% of leaf K^+ and Na^+ , 95% of leaf S and 97% of leaf Zn detected candidates were shared among 2 or more variables, and only 4 and 2 genes were exclusive to leaf S and Zn, respectively (Figure 1.11).

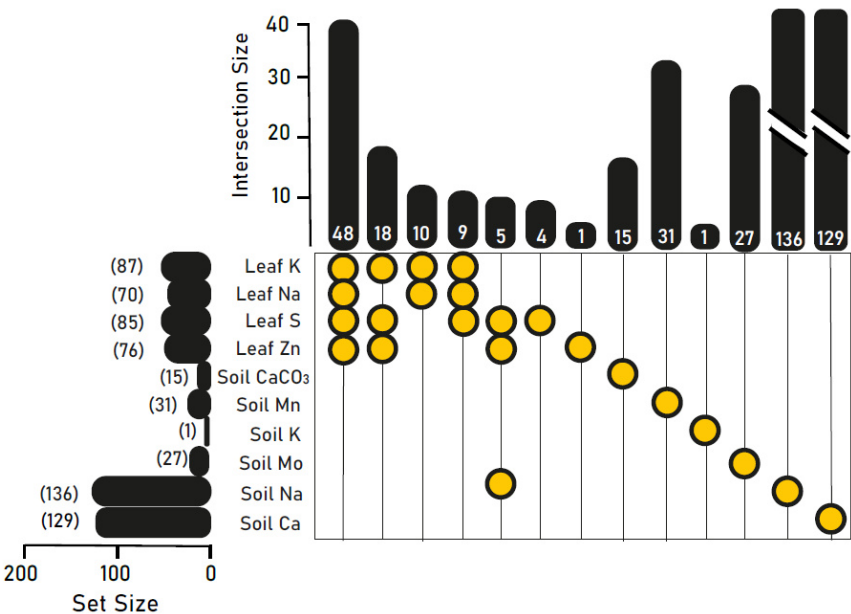


Figure 1.11. UpSet plot of GPA and GEA candidates. Y axis: graph of total number of candidates for each trait. X axis: intersection of sets of genes at multiple traits. Each dot connected by lines represent traits of the intersection set.

The top SNPs associating with soil Na⁺ mapped at AT3G45660. AT3G45660 encodes an extracellular NAXT NPF protein (*NPF6.2*), active in the plasma membrane and involved in transmembrane transport. Among the seven NAXT subfamily- genes described in *Arabidopsis*, proton-dependent transporters of nitrate (AT1G32450, *NPF7.3*) and chloride (AT3G45700, *NPF2.4*) showing downregulation upon salt exposure are found (Lin et al., 2008; Li et al., 2016). Moreover, GA1 and Ile-JA hormones transport activity has been reported in *NPF6.2* by yeast two-hybrid system (Chiba et al., 2015).

The subsequent soil Na⁺ SNPs mapped to AT3G47630 and AT5G62600, two protein kinases involved in RNA regulation and oxidative and phytohormone signaling stress responses (Zhang et al., 2023; Schippers et al., 2008), and to AT3G55880 (*SUE4*), which encodes a plasma membrane regulator of auxin transport and has recently reported to be involved in the sulfur deficiency response (Xiang et al., 2022).

In fact, the whole set of GEA candidates (n=339) classified into catalytic (hydrolase, transferase, protein-modifying, and oxidoreductase) and binding (organic compounds, protein, and ion binding) activities as top molecular functions, and into transmembrane transporter activity as third category (Fig 1.12).

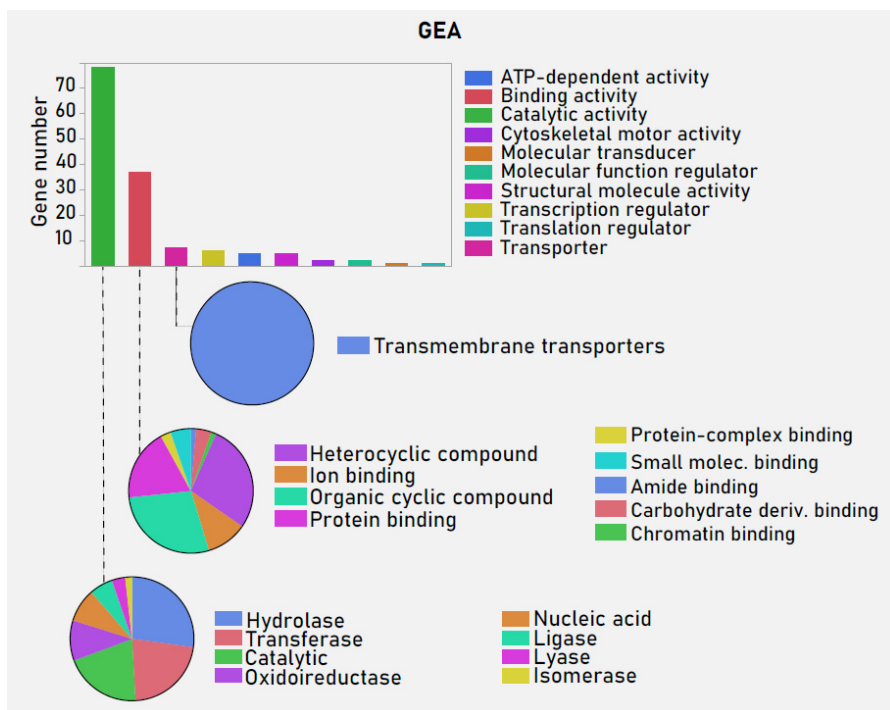


Figure 1.12. Panther gene ontology (GO) term analysis for GEA candidates' dataset. The bar chart of molecular functions (MF) represented by PANTHER GO analysis. Pie charts of PANTHER protein classes below the top three MF categories are shown.

Gene Ontology (GO) Enrichment Analysis of GEA candidates revealed significant enrichment ($FDR < 0.05$) for catalytic activity ($FDR = 0.045$). The enriched set comprised ATP-synthases, such as the proton ATPase-subunit *VHA-c1* (AT4G38920) and a plasma membrane primary transporter: the calcium-transporting ATPase *ACA2* (AT4G37640) (Dataset S1.6). *VHA* genes encode vacuolar H^+ -ATPase, which acidifies intracellular compartments and is essential for tolerance to environmental stress (Sze et al., 2002). The modulation of proton secretion through H^+ -ATPase variation plays an essential role in plant alkalinity responses (Yang et al., 2019; Xie et al., 2022), and its

regulation is reported to be crucial for mediating K^+/Na^+ homeostasis under NaCl stress and promoting salinity tolerance (Zhang et al., 2017; Bose et al., 2015).

Same as *VHA-c1*, sequence variation at the plant Ca^{2+} pump *ACA2* was associated to soil Na^+ . The modification of cytosolic calcium signature promotes adaptive Na^+ adjustments. In fact, *ACA4* and *ACA2* double-mutant *Arabidopsis* plants showed increased sensitivity to NaCl (Anil et al., 2008), and together with *TPC1* (AT4G03560), *ACA4* and *ACA2* are reported to be the important calcium channels for salinity tolerance (Liu et al., 2021). Moreover, *ACA2* is an Endoplasmic Reticulum (ER) Ca^{2+} pump. Intracellular alkalinization increase cytosolic Ca^{2+} , and such increase is not only provided by the increased Ca^{2+} influx but also by ER Ca^{2+} pools.

The presence of membrane ion transporters described for soil Na^+ was not an isolated event, as two other K^+ transporters were associated with soil Ca^{2+} and soil $CaCO_3$ in CatDeme: *KEA5* (AT5G51710, *K⁺ efflux antiporter 5*), *KAT1* (AT5G46240, *K⁺ channel 1*) and *YSL2* (AT5G24380). Whereas *KEA5* mediates pH and K^+ homeostasis in the endomembrane system (Zhu et al., 2018), increased *KAT1* activity is reported to confer tolerance to NaCl stress (Abdelaziz et al., 2017), and *YSL2* is related to the long-distance transport of Fe and Fe deficiency alleviation under NaCl stress (Zhu et al., 2017).

For GPA, variation in K^+ leaf concentration of the contrasted demes contained the most significant associations (Dataset S1.6). This agrees with the detected K^+ transporters, *KEA5* and *KAT1*, influencing the differential tolerance of plants to CS soils. The same as GEA, the 99 GPA candidates classified into catalytic (hydrolase, transferase and protein-modifying) and binding (organic compounds and protein binding) molecular functions, but transcription regulation was the third most represented category, comprising only 3 transcription factors (Figure 1.13).

Although not enriched, proteins involved in the response to oxidative (AT4G21850, *MSRB9*; AT4G21910), osmotic (AT5G16080, *CXE17*; AT1G53165, *MAP4K*) and salt stress (AT1G53080), and proton and transmembrane transport

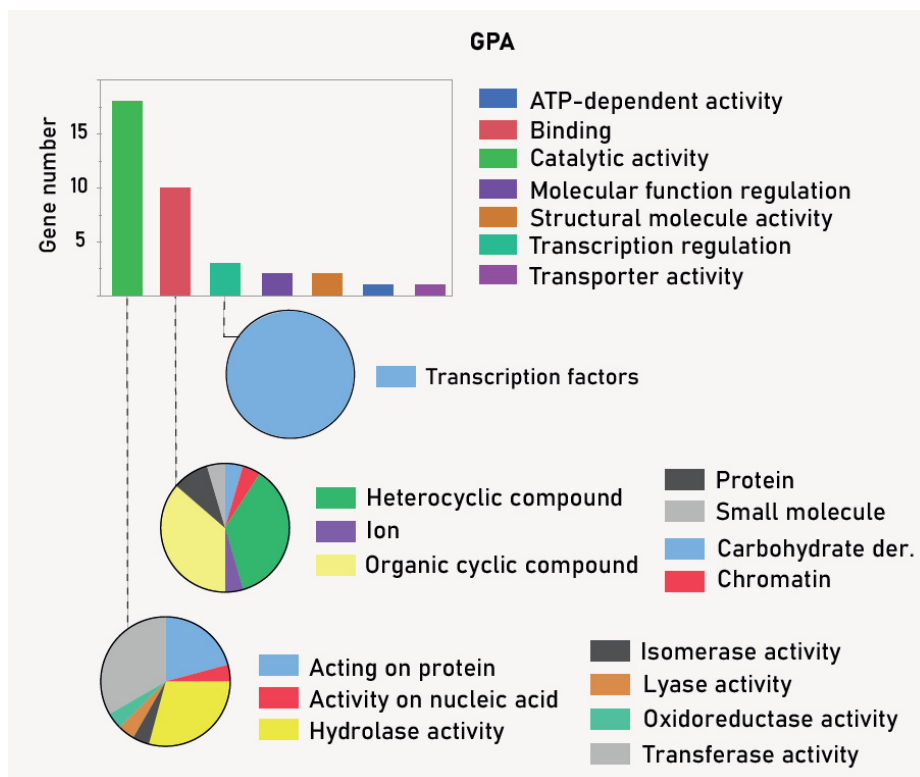


Figure 1.13. Panther gene ontology (GO) term analysis for GPA candidates' dataset. The bar chart of molecular functions (MF) represented by PANTHER GO analysis. Pie charts of PANTHER protein classes below the top three MF categories are shown.

(AT1G53110 and AT5G65687) were found not only for leaf K^+ but also for at least one more leaf element. The clade VI carboxyesterase *CXE17*, speculated to be involved in programmed cell death (Marshall et al., 2003), associated to leaf K^+ and Na^+ ; whereas a series of targeted genes associated to all measured leaf elements: AT4G21910 (MATE efflux family protein active in the membrane), AT4G21850 (*MSRB9*, a methionine sulfoxide reductase involved in protein

repair), AT4G36450 (*MPK14*, a protein kinase involved in the hyperosmotic and salinity response), AT1G53080 (an extracellular lectin family protein acting within the salinity and water deprivation responses) and AT1G53110 (an ER regulator of proton transport) were mapped by significant SNPs at all leaf elements. Finally, AT5G65687 (involved in the monocarboxylic acid metabolism and transmembrane transport processes) was found in K⁺, Na⁺ and Zn leaf concentration traits (Dataset S1.6).

Altogether, the associations from LFMM analysis target promising candidates for being involved in differential tolerance to alkSAL conditions, not only for being plasma membrane-localized anion channels with substrate unspecificity (Corratgé-Faillie et al., 2017), but also for showing RNA and protein regulating roles and for influencing hormone signaling and/or concentrations in plants (Chiba et al., 2015). Studies on causal mutations for the observed allelic variation, as well as the analysis of alkaline salinity effects in gene expression levels of contrasted demes (CS and non-CS-native), would help to further characterize their contribution mechanisms (e.g., the regulation of proton and Ca²⁺ pumps and cell K⁺ status), and their involvement in differential plant fitness under alkaline salinity stress. Moreover, GEA results point to soil factors as important drivers of adaptation; further attention should be paid to candidates involved in mineral ion transmembrane transport, as salinity and alkalinity interfere with plant nutrition by altering the transport of nutrients from the soil to the plant (Safdar et al., 2019).

Unlike GEA candidates, GPA results revealed that differential leaf concentrations of distinct mineral nutrients were frequently associated with the same candidate genes. As suggested by Guerrero and colleagues (Guerrero et al., 2018), probably soil alkaline salinity represents the actual selective pressure, having a direct impact in plant leaf Na⁺ and K⁺ status. Na⁺ - K⁺ would not only affect each other but also the rest of leaf mineral nutrient profiles in a

deme group-dependent way, as reflected by the distinct correlation patterns observed in the multivariate analysis.

Nevertheless, validating experimentally the adaptive role of the identified candidates is a required follow-up step to any genome association inference. Moreover, current associations between allele frequencies of adaptive genes and selective environmental conditions can be used for estimating the required allele frequency change for matching future conditions, which provides a powerful tool for tolerance breeding and biodiversity management (Rellstab et al., 2016; Guerrero et al., 2018).

Addressing soil variables as potential selective pressures at the candidate adaptive loci regulating CatDeme nutrition and flowering responses

As detailed above, F_{ST} outlier lists are based by the assumption that regions with high divergence are under directional selection (Konečná et al., 2021). To test if the adaptive patterns identified in the candidate loci were shaped by environmental heterogeneity in terms of alkaline salinity, the flowering time F_{ST} outlier list and the GPA and GEA candidate lists were combined. By these stringent criteria, only candidate loci for selection which are associated with the selective soil environment (alkaline salinity in this case) were expected to be pulled out. Besides, merging the three datasets allowed to assess if the detected adaptive flowering regulators are potentially under selection for alkSAL tolerance in CatDeme.

VAB2	ATPase, V1 complex, subunit B protein; Non-catalytic subunit of the peripheral V1 complex of vacuolar ATPase. V-ATPase is responsible for acidifying a variety of intracellular compartments in eukaryotic cells; Belongs to the ATPase alpha/beta chains family (494 aa)	Soil Na
AT4G21865	At4g21865; Unknown protein	
EDS5	Susceptible to coronatine-deficient pst dc3000 3; Functions as a multidrug and toxin extrusion transporter in the export of salicylic acid (SA) from the chloroplast to the cytoplasm . Plays an essential function in plant defense via the pathogen-induced salicylic acid (SA) accumulation (543 aa)	Soil Na
VPS34	Encodes a phosphatidylinositol 3-kinase that is expressed in most plant tissues. Defects in VPS34 affect a number of cellular processes. Involved in salt-stress responses; Belongs to the PI3/P14-kinase family (814 aa)	Soil Na
AT4G38500	At4g38500/F20M13_60; Protein of unknown function (DUF616)	
AT5G57610	Protein kinase superfamily protein with octicosapeptide/Phox/Bem1p domain; Its function is described as protein serine/threonine/tyrosine kinase activity, protein kinase activity (1054 aa)	Soil Na

Figure 1.14. Prime candidates under selective pressures associated to salinity.

List of overlapping genes between FST outlier and GEA-GPA candidates.

Only 6 genes overlapped between the two candidate lists and all were associating with soil Na^+ (Figure 1.14). Among them, another vacuolar ATPase (*VAB2*, AT4G38510) was identified, mapping at an extreme F_{ST} outlier region between early and late flowering deme groups. This provides evidence that genomic variation in vacuolar H^+ -ATPases has been subjected to selective pressures and is associated to soil salinity. The Tajima's D values at *VAB2* region showed a significant decrease in the late flowering group, supporting VHA's allele fixation in late flowering but diversity maintenance in early flowering demes.

Another promising candidate, *VPS34*, mapped at an outlier peak in Chr 1 and displayed same signs of balancing selection (high Tajima's D value) in early flowering demes. *VPS34* encodes a phosphatidylinositol 3-kinase reported to regulate salinity-stress responses (Baena-González, 2010).

None of the FT adaptive candidates displayed significantly associated variation with leaf or soil mineral nutrition under alkaline salinity. This lack of environment–allele relationships implies that there is no evidence of prime candidates affecting FT variation for adaptation to soil heterogeneity in CatDeme. However, deme classification according to flowering time exhibited a dominance of CS individuals in the late flowering group (V1, LG5, V3) and of SS individuals in the early flowering group (Ro2, LLO2, PO1) used for the divergence scans. A maintenance of allelic diversity at F_{ST} -LFMM overlapping loci in the early flowering group, like *VPS34*, could indicate that early flowering individuals are in selective advantage under fluctuating seasonal levels of salinity from SS-coastal areas (Bürger et al., 2002). Analogously, allele fixation in CS demes at loci regulating vacuolar H^+ -ATPases, like *VAB2*, is pinpointed as a mechanism involved in the enhanced response of CS demes to alkaline salinity.

As linking soil type classification groups with flowering time was highly speculative, a further attempt to address the role of flowering time in CatDeme performance under neutral and alkaline salinity was carried out. The time of flowering promotion of all LFMM studied individuals was scored under neutral and alkaline salinity treatments in RI (Figure 1.15A) and RS experiments (Figure 1.15B; Table S1.8-S1.13), and genotype*treatment effects were assessed.

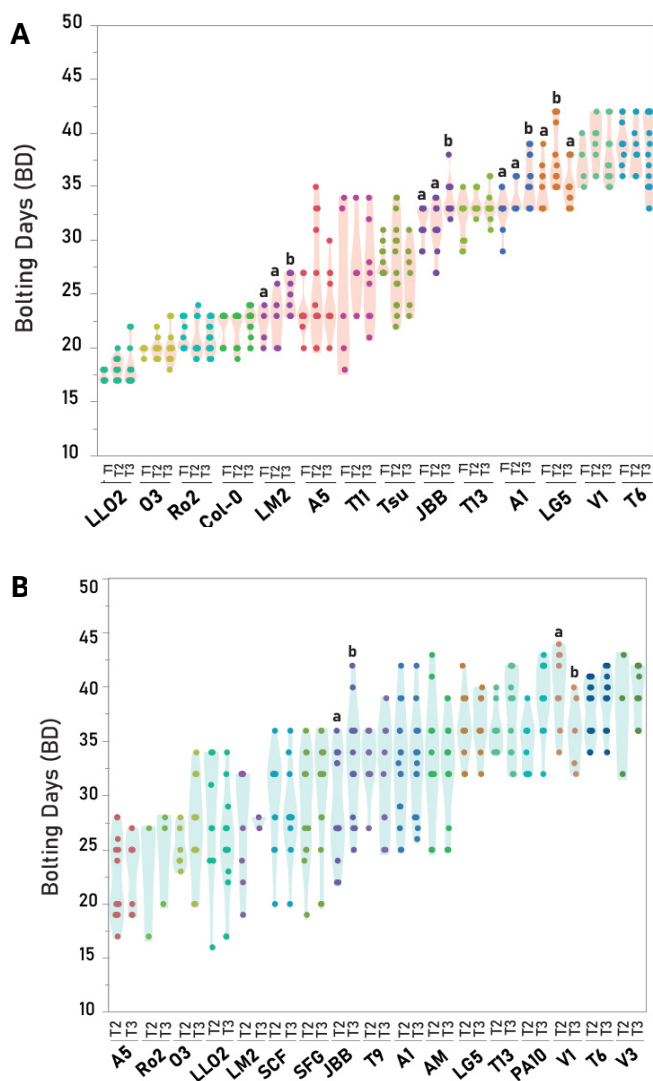


Figure 1.15. Flowering time scored as days to bolting (BD) in all studied demes under RI (A) and RS (B) experiments. **RI:** rockwool irrigation with control (**T1:** 0.5-Hoagland, pH = 5.9), neutral salinity (**T2:** 0.5-Hoagland, 50-75-100 mM NaCl, pH = 5.9) and alkaline salinity (**T3:** 0.5-Hoagland, 20-40-85 mM NaCl + 5 - 10 - 15 mM NaHCO₃, pH = 8.3). **RS:** reciprocal soil experiment with saline siliceous soil (**T2:** BLA, excavated from coastal siliceous region at 41° 40' 37,64"; 2° 48' 3,86") and saline calcareous soil (**T3:** ESC, excavated from coastal calcareous region at 42°13'03"N 3°11'30"E). Plants were maintained under a 10 h photoperiod and 21/16°C temperature.

The range of variation in CatDeme flowering time was genotype-dependent, and significant bolting time differences caused by neutral (T2) or alkaline salinity (T3) at the deme level were rather isolated events (Figure 1.15A-B, Table S1.9-S1.11).



Picture 2. Random block distribution of CatDeme at RI experiment. Nergena greenhouse facilities, Wageningen University, The Netherlands.

Demes were grouped according to native soil groups (CN, CS and SS) and Bolting Days (BT) were compared between groups and between treatments: neutral (T2) and alkaline salinity (T3) in RS (Table S1.8-S1.9); control (T1), neutral (T2) and alkaline salinity (T3) in RI (Table S1.10-S1.13) (see methods). Under neutral salinity (T2), SS individuals tended to flower earlier than under alkaline

salinity (T3) (1.4 and 1.5 days earlier in RS and RI experiments, respectively). The opposite effect was observed in the CS group (1.8 and 1.7 days later under T2 than T3 in RS and RI, respectively). When compared to control, T2 caused 1.2 days earlier but 3 days later bolting in SS and CS, respectively. Moreover, mean BT values between groups did not show significant differences under control (T1) or alkaline salinity (T3), whereas T2 led to SS individuals bolting significantly earlier than the CS group (adj. p -value < 0.05). Therefore, neutral salinity exerted significant differential effects on the BT of the studied demes according to their origin. In fact, two-way ANOVA exhibited significant interaction between deme group and treatment [T2*SS; T2*CS; T3*CS (prob. $|t|$ = 0.039)]. This could suggest certain phenotypic plasticity in the flowering time of SS demes being advantageous under neutral but not under alkaline salinity. In turn, phenotypic plasticity could have promoted balanced polymorphisms in adaptive loci of coastal SS demes (Gulisija et al., 2016) as seen on *FRI* and *AGL19*.

In summary, we gathered evidence supporting the influence of edaphic traits in promoting local adaptation by means of physiological and landscape genomic approaches (LFMM applied to GEA and GPA). A high number of SNPs associated with soil variables were identified, and the major proportion of GEA candidates associated with soil Na⁺ and soil Ca variation, which highlights salinity and alkalinity as the two main selective pressures in CatDeme genomic variation. Candidates associated with soil Na⁺ variation point to regulators of phytohormonal transport (*SUE4*) and the cellular Ca²⁺ pool (*ACA2*) influencing salinity responses in CatDeme. Moreover, allelic variation at major K⁺ (*KEA5* and *KAT1*) and Fe transmembrane transporters (*YSL2*), previously reported to be salinity responsive, significantly associated with variation in soil Ca and CaCO₃ % levels, which supports that enhanced K⁺ and Fe nutrition are key traits for alkaline salinity tolerance.

Despite the limited overlapping among candidates detected through genome divergence scans and GEA, *VAB2* allelic variation exhibited signs of being under

selective pressure in a deme group comprising mostly CS individuals (late flowering group), reinforcing the role of vacuolar H⁺-ATPases in the adaptation to soil alkaline salinity.

Finally, the earliness of BT on SS individuals under neutral salinity, which was observed experimentally, is proposed to be a sign of phenotypic plasticity favored by higher allele diversity in *FRI* and in *FLC*- dependent and independent regulators on the early flowering group as an adaptive trait to coastal areas. Whether soil salinity in terms of Na⁺ or distance to the coast, among others, are drivers of such adaptive patterns remains to be confirmed, as none of the flowering alleles exhibited significant genome-soil element variation. Yet, as all plants in RI and RS experiments were vernalized for 4 weeks, which reduces the effect of *FRI*/*FLC* on flowering time (Sheldon et al., 2000) *FRI* and *FLC* alone may not account for all the variance observed in the BT of CatDeme groups. This supports the presence of a selective environmental factor across the CatDeme distribution favoring an early flowering phenotype in CatDeme.

The adaptive significance of the identified candidates must be necessarily validated experimentally to support the inferences made by this landscape genomics approach. However, the obtained results highlight the importance of integrating plant phenotyping, physiological measurements, population genomics and environmental association studies for the characterization of environmental adaptation at a small geographical scale, in which selection pressures can be heterogeneous and lead to different adaptive signatures within populations.

Methods

Studied Populations

A collection of 20 demes sampled along the north-eastern Spanish Mediterranean coast of Catalonia was analyzed (Figure S1.1). All demes have been in situ georeferenced for latitude, longitude, distance to sea and soil physicochemical characterization (Table S1.9). Screening of physiology and leaf mineral nutrition traits of all demes were performed in multiyear field, common garden, and greenhouse experiments (Busoms, 2015; Terés, 2017; Pérez-Martín, 2021 and current work), and all soils from sample collection have been physico-chemically characterized in previous studies (Busoms et al., 2018).

Native soils

Collection sites belong to coastal – eastern Pyrenees and Serra de Marina coastal range hill system - and adjacent inland locations - Coastal Depression and Pre-Coastal Range geoclimatic regions. Briefly, individuals from eastern Pyrenees (Northeast region) consists of granitic terrains, average annual precipitation of 500-600 mm and average annual temperature variation of 15-17 °C. In contrast, Serra de Marina is characterized by large masses of granitic rocks which eventually get eroded and transformed into sandy texture, average annual precipitation of 550-700 mm and average annual temperature variation of 14-16 °C. Inland locations run 30 to 60 km from the Mediterranean Sea in a parallel trajectory. In the north, it is formed by granitic batholiths and Paleozoic metamorphic rocks, where average annual precipitations are 750 to 1.000 mm and average annual temperature ranges between 14-15 °C. In the south, plutonic rocks emplaced in between metamorphic granodiorites, with 600-800 mm average precipitation and 12-14 °C temperatures reported (Busoms 2015).

Whole-Genome Sequencing

Sequence data on 74 and 70 individuals belonging to the 19 demes sequenced in 2018 (Busoms et al., 2018) and 2021, respectively, were used. DNA was extracted from fresh leaves, libraries for whole-genome sequencing were prepared, and sequencing was done with Illumina HiSeq 2500, paired-end specification. After demultiplexing and removal of adaptor sequences by means of 'Cutadapt', standard quality trimming was performed using Trimmomatic 0.39 (Bolger et al., 2014). Reads were aligned to the reference with Minimap2 2.24 (Li, 2016), and duplicated reads were removed with Picard 2.21.1 (Broad Institute, 2019). Raw sequences were analyzed to genotype 3,665,756 biallelic single nucleotide polymorphisms. Likelihoods for the three possible genotypes in each biallelic site were then calculated from the BAM files with the SAMtools model (Li et al., 2009) in ANGSD 0.939 (Korneliussen et al., 2014). Nucleotides with base qualities lower than 20 and reads with mapping quality lower than 30 were discarded. Sites with coverage at fewer than 72 out of the 90 samples were also excluded. After this quality filtering, an in-house pipeline was used to produce VCFs (Variant Call Format file) from BAM files (https://github.com/mattheatley/ngs_pipe): haplotypes were called with GATK4 4.1.4.0 (Poplin et al., 2018) and genotyped following GATK best practices (De Pisto et al., 2011). Our demographic analysis was based on a genome-wide data set consisting of 102,106 four-fold degenerate SNPs (4dgs). The 4dgs sites are those at which mutations occurring in all nucleotides are synonyms and thus not predicted to change the codified protein codon. For this reason, 4dgs have traditionally been seen as free of selective constraint (Eyre-Walker & Keightley 2002) and have therefore been used as a neutral reference.

Analysis of Genetic Diversity and Population Structure

Demography analysis was performed using adegenet 2.1.7 (Jombart, 2008) by an in-house adegenet script (by Filip Kolar, Sian Bray and Levi Yant). The 4dgs

VCF was used to include Principal Component Analysis (PCA). Isolation by distance analysis (IBD) was performed with StAMPP (“statistical analysis of mixed-ploidy populations”) (Pembleton et al., 2013) in combination with adegenet. Inter-population gene flow was determined by Splitstree (Huson & Bryant, 2006).

To assess spatial genetic patterns of the individuals, a cluster analysis in STRUCTURE v 2.3.4 (Pritchard et al., 2000) was performed. The cluster analysis was based on the admixture model. Admixture proportions were estimated using NGSadmix (Skotte et al., 2013) in the ANGSD package. We ran the analysis for K (the number of expected clusters) values of 2–10, with 10 replicates each and a burn-in period of 20 000 and thereafter 50 000 Markov chain Monte Carlo (MCMC) repeats. The results were summarized in STRUCTURE HARVESTER v.0.6.93 (Earl & Vonholdt, 2012) and the differences between consecutive K values (delta K) were analysed based on the approach of Evanno et al. (2005). The resulting K value ($K=3$) was integrated in the subsequent GEA analyses to correct for demographic processes and to reduce false positive associations of SNPs with environmental factors (Excoffier et al., 2009).

FLC alignment and PCA

PCA of the *FLC* region was performed for the CatDeme SNP dataset using 120 sequenced samples and the worldwide *A. thaliana* accessions collection from the 1,135 *A. thaliana* genomes dataset (1001genomes.org/). *FLC* sequences obtained from the assemblies to National Center for Biotechnological Information database.

Selection scans

We searched for SNPs genomewide showing high levels of genetic differentiation between early- and late-flowering individuals, while controlling for population structure, and used window-based scans to identify potential regions of recent selection associated with flowering time variation. Genetic variation within populations was estimated in ANGSD using the empirical Bayes (EB) method to calculate Tajima's D (Korneliussen et al., 2013).

Allele frequencies for the selection scan were estimated in ANGSD directly from the site allele frequency (saf) likelihoods. The genes in 5kb non-overlapping sliding windows were scanned to detect areas of unexpectedly high differentiation between early and late-flowering populations as a sign of directional selection (Lewontin & Krakauer, 1973). 1% outlier values were identified and considered as candidate regions under selective sweeps. F_{ST} distributions were plotted with *ggplot2* package (Wickham, 2016).

Experimental setup

The phenotyping of flowering time and leaf nutrition traits under alkaline salinity conditions was performed in the studied demes by means of rockwool irrigation (RI) and reciprocal soil experiments (RS). The vernalization sensitivity and *FLC* expression levels of 2 demes with contrasted flowering time were assessed in growth chamber conditions (GC). RI was carried out at WUR (Wageningen University) Nergena greenhouse facilities. RS was performed at the Autonomous University of Barcelona greenhouse facilities by Pérez-Martín (Pérez-Martín et al., 2022). GC was carried out at UAB growth chamber facilities.

Growth conditions. For all experiments performed, seeds were surface sterilized by soaking in 70% (v/v) ethanol for 1 min, suspended in 30% (v/v) commercial Clorox bleach and 1 drop of Tween-20 for 5 min and rinsed 5 times in sterile 18 MΩmilli-Q water. Seeds were placed in filter paper soaked with KNO_3 to promote germination and stratified for 4 days at 4 °C in the dark. For RI

and RS, seedlings were vernalized at 4°C for 6 weeks under 8:16 light/dark photoperiod after 10 days of sowing to assure all lines were able to flower when exposed to inductive photoperiods. Both RI and RS greenhouses were light supplemented to provide a 10h day photoperiod and a constant temperature of 21°C. GC was set at 8:16h light/dark and 22/18°C day/night conditions for 10 days. After that, light was increased by 2h every 3 days until reaching 16:8h light/dark cycle.

Screening Flowering time and reproductive fitness. Bolting Time (BT) – was scored for all demes in RI, RS and GC experiments as the number of days between germination and the date of appearance of the first bud (Clarcke & Dean 1994). Number of siliques was counted at maturity as a proxy of fitness only in RS plants. Data on BT and silique number of RS plants was obtained from Pérez-Martín et al., 2022.

Soil experiment (RS). After local adaptation to neutral salinity (Busoms, 2015) and influence of carbonates in the differential fitness (Terés, 2017; Pérez-Martín, 2021) of *A. thaliana* Catalan demes collection, we performed a reciprocal experiment with natural alkaline-saline and neutral-saline soils to confirm if soil type could be a driver for local adaptation to alkaline salinity (Pérez-Martín et al., 2022). *A. thaliana* native populations from coastal siliceous soils and adjacent inland locations were sown in pots containing soil excavated from two sites with contrasted alkalinity: the saline siliceous soil was excavated from Marimurtra Botanic Garden, Blanes (BLA) (41° 40' 37,64"; 2° 48' 3,86") while saline-alkaline soil was selected from L'Escala (ESC) (42°13'03"N 3°11'30"E) after confirming its suitability as natural alkaline-saline soil (Pérez-Martín, 2020; Almira et al., 2022). After sterilization and stratification, twenty seeds of each deme were sowed individually in 4 x 4 x 8 cm pots in soil excavated from BLA or ESC. Pots were placed in random block distribution and bottom-irrigated twice a week with distilled water.

Rockwool irrigation experiment. To assess specific effects of neutral and alkaline salinity in the variation of flowering time in the study demes, irrigation experiments were carried out on rockwool - pH-neutral rockwool cubes for hydroponic purposes. Forty-five seeds per deme were sown on individual rockwool cubes soaked with Hyponex nutrient solution containing 0 mM of NaCl; pH 5.9 (control), 50 mM of NaCl; pH 5.9 (neutral salinity) and 40 mM NaCl + 10 mM NaHCO₃; pH 8.3 (alkaline salinity) resulting in 15 cubes per deme per treatment. The rockwool cubes were sub irrigated with the appropriate Hyponex nutrient solutions once every 3 days (1-0-0-1) until the end of the experiment.

Elemental analysis of soil and leaf samples

The leaf nutritional status was assessed in plants 14 days after treatment in the RI experiment and 15 days after vernalization period of 6 weeks at RS experiments (70 days-old plants in both cases). Plant material was dried for 4 days at 60°C. Approximately 0.1g was used to perform and open-air digestion in Pyrex tubes using 0,7 mL concentrated HNO₃ at 110 °C for 5 h in a hot-block digestion system (SC154-54-Well Hot Block™, Environmental Express, SC, Charleston, USA). Leaf Na⁺, K⁺, Ca, Mg, S, P, Fe, Mn, Zn and B were determined by inductively coupled plasma optical emission spectroscopy ICP-OES (Thermo Jarrell-Ash, model 61E Polyscan, England) (n = 4). Data on CaCO₃%, Na⁺, K⁺, Ca, Mg, S, P, Fe, Mn, Zn, Mo, Li, Ni, Se, Co, As and Cu in soils from collection sites of the studied demes were extracted from Busoms et al., 2018. Briefly, 5g of soil were dried for 42 h at 60 °C in 50-mL Falcon tubes and diluted to 6.0 mL with 18MΩwater before analysis on an ELAN-DRCe ICP-MS instrument (PerkinElmerSciex) (n = 4). Traceable calibration standards (ULTRA Scientific) from the National Institute of Standards and Technology (NIST) were used.

GPA and GEA analyses

We searched for genomic regions involved in adaptation alkaline salinity and flowering time variation by means of environmental and phenotypic GWA analyses. To detect genes associated with variation in bolting time, silique production or leaf and/or native soil elemental concentration, we carried out an environmental association analysis using a Latent Factor Mixed Model (LFMM) —LFMM 2 (<https://bcmuga.github.io/lfmm/>) (Caye et al., 2019). LFMMs are factor regression models that use a genotypic matrix as a response variable and environmental or physiological traits as explanatory variables, so that genetic polymorphisms associating with ecological gradients or phenotypes can be identified while inferring population structure (Frichot et al., 2013). We tested the association of allele frequencies at each SNP for each individual with leaf nutrients and native soil traits that were significant in Student *t*-Test between alkaline-saline and neutral-saline growth conditions (Pérez-Martín et al., 2021): leaf K⁺, Na⁺, S, Fe and Zn, soil CaCO₃%, soil K, soil Na, soil S, soil Fe and soil Zn. SNPs without missing data and MAF > 0.05 were used as an input for the LFMM analysis. LFMM accounts for a discrete number of ancestral population groups as latent factors. K = 3 latent factors were used reflecting the best K obtained in admixture analyses. To identify SNPs significantly associated to reproductive and leaf and soil nutrition traits, FDR corrected *p*-values (*q*-values) below 0.01 were selected, using the *q*-value R package v.2.20100. Candidate SNPs were annotated to genes (at least one significantly associated SNP per candidate gene) using SnpEff v. 4.3101 following *A. thaliana* version 11 genome annotation (www.arabidopsis.org). We made a final shortlist of soil composition-adaptive candidates involved in FT variation by overlapping the LFMM candidates, reflecting significant association with important soil elements, with the previously identified parallel differentiation candidates, mirroring regions of excessive differentiation found across population BT groups.

GO enrichment analysis

We inferred potential functional consequences of the candidate gene lists using GO enrichment tests within biological processes, molecular functions, and cellular components domains. We applied Fisher's exact test ($p < 0.05$) (www.panther.org).

Chapter 2



Chapter 2

At the core of salinity: convergent and divergent transcriptome response pathways to neutral and alkaline salinity in natural populations of *Arabidopsis thaliana*

Introduction

Differential effects of neutral and alkaline salinity in plant performance

Saline stress is a major agricultural constraint and its co-occurrence with alkalinity is an arising environmental concern, specially under arid and semiarid climates. Based on the most recent soil map of the world by FAO/UNESCO, more than one million hectares of the Earth's land are affected by alkaline salinity stress. This is the case of the Mediterranean region, where excess of soluble Na^+ , Ca^{2+} , Mg^{2+} , K^+ , CO_3^{2-} and HCO_3^- ions get to the superficial soil layers due to high evapotranspiration rates (Singh 2021). Besides the induction of osmotic, ion and ROS stress by neutral salinity, alkaline salinity exacerbates nutrient deficiency (Liu et al., 2021) and is reported to exert greater inhibition on plant germination, growth, photosynthesis, and root system activity (Guo et al., 2010; Marconi et al. 2013; Guo et al., 2017). Although there is increasing evidence that alkaline salinity is more detrimental for overall plant performance than neutral salinity, the mechanisms driving such synergistic effects are not yet clearly established. In this regard, more attention should be paid to the environmental factors that generate local-scale diversity patterns in the model plant *Arabidopsis thaliana*, since understanding natural genetic and phenotypic variation is essential for ecological and evolutionary studies (Bomblies et al., 2010).

Genetic differentiation occurs at all geographic scales in *A. thaliana*, and the study of local populations provides a valuable genetic tool for detecting adaptive traits (Bakker et al., 2006). To this end, differences in tolerance to salinity and moderate levels of carbonate as individual stress factors have been described among CatDeme subsets (Busoms et al. 2015; Terés et al. 2019): although T6 and Ro2 (native from saline siliceous soils) were shown to perform better under neutral salinity on siliceous soils than V1 and LM2 (native from calcareous soils at the pre litoral range), it was proven that tolerance to neutral salinity does not confer tolerance to alkaline salinity in the studied individuals, and that populations from soils with intermediate salinity and carbonate levels like V1 and LM2 performed better under alkaline salinity stress due to enhanced phenotypic plasticity (Pérez-Martín et al., 2022). However, the transcriptomic basis of such differential responses have not been explored.

Plant transcriptomic responses to alkaline salinity

Plants are exposed to the co-occurrence of biotic and abiotic stresses in their natural habitats but the effects of combined stresses at the genetic level are much less extensively reviewed than plant responses to single stress factors. Still, there are several studies targeting the existing interconnection of signaling pathways that regulate the coordination of plant responses to different stresses (Sharma et al., 2018; Hosseini et al., 2021; Georgii et al., 2017; Suzuki et al., 2016; Forieri et al., 2017; Rasmussen et al., 2013), whose results highlight that combinatorial stress triggers responses not evoked by single stressors. Despite the scarcity of studies on the effects of co-occurrence of salinization and alkalization at the transcriptomic level in *Arabidopsis*, transcriptome responses to alkaline salinity have been assessed in several crops. In cotton (*Gossypium hirsutum* L.), shared responses in

transcripts involved in ion homeostasis were observed under NaCl and Na₂CO₃ conditions, while differential expression of genes involved in starch and sucrose metabolism was reported to be exclusive of Na₂CO₃ stress due to high pH (Zhang et al., 2018). Transcriptomics on alkalinity-tolerant and sensitive wheat varieties treated for nine days with 100 mM mixed salts (9:1 NaHCO₃:Na₂CO₃ at pH 8.90) revealed enhanced ability of nutrient uptake, intracellular pH regulation and ROS scavenging activation as the main traits conferring tolerance to alkaline salinity (Sun et al., 2020). Similarly, recent transcriptome analysis in *Brassica napus* revealed higher expression of genes from carbohydrate metabolism, photosynthetic processes, ROS regulating, and response to salt stress attributing tolerance to alkaline salinity (Meng et al., 2017). Enhanced antioxidant capacity was also reported to be a major player in the tolerance response of alfalfa to saline-alkaline stress (An et al., 2016). In rice, alkaline tolerant and sensitive cultivars were compared at the transcriptomic level under 0.5% Na₂CO₃ solution and pH 11, and differentially expressed genes from plant hormone signal transduction pathway were primarily related to the tolerance response (Li et al., 2018).

Linking changes in gene expression profiles to functional consequences is the ultimate goal of transcriptomic analysis on stress tolerance-related traits (Yan et al., 2020). The combination of physiological studies with transcriptomic analyses provides a deeper understanding of biological processes (Yang et al., 2022) and, based on the available studies, some of which are reported above, nutrient homeostasis and changes in endogenous phytohormone levels are considered among the most important mechanisms conferring tolerance in the context of neutral and alkaline salinity. While maintaining nutrient homeostasis starts from ion sensing, uptake, transport, and activation of response mechanisms through regulation of gene networks (Farooq et al., 2018), the alteration in the content of phytohormone implies a specific crosstalk between endogenous plant growth regulators. This leads to the

triggering of signal transduction pathways in response to external conditions and can affect germination (Atici et al., 2005), morphology of root and aerial structures (Mao et al., 2018, Wen et al., 2018, Song et al., 2019), and reproduction, specially flowering (Guo et al., 2019, Shu et al., 2018, Bao et al., 2019). These considerations reinforce the idea that differences in mineral nutrition and phytohormone profile orchestrate adaptive processes in populations grown on specific local environments by modulating their growth and reproductive responses.

Here, we conduct a transcriptomic profiling experiment to analyze plant responses to neutral and alkaline salinity stresses to identify the levels and functions of stress regulatory networks. To this end, 4 *A. thaliana* local populations (demes) from contrasted origin were used: 2 from coastal siliceous soils (**SS**), NaCl-rich and pH between 5.7-6.2; and 2 from pre-litoral calcareous soils (**CS**), considered non-saline and with moderate carbonate content (10-15%). SS and CS categories are defined in Chapter 1 (Figure 1.9; Table S1.5). The 4 demes were subjected to neutral (*neuSAL*) and alkaline salinity (*alkSAL*) under the same light and temperature conditions. The physiological and transcriptomic responses of the 4 demes under each type of salinity are analyzed, and convergent and singular metabolic pathways involved in each type of salinity are described. Finally, co-expression network analysis correlating transcriptomics with physiological data is performed to identify hub pathways in shared and exclusive responses to neutral and alkaline salinity.

Results & Discussion

Four *A. thaliana* demes differing in adaptation to soil salinity type were used. Two demes from coastal siliceous soils (T6^{SS} and Ro2^{SS}) and two demes from pre litoral-calcareous soils (V1^{CS}, LM2^{CS}) were grown on potting mix soil irrigated with neuSAL (100 mM NaCl, pH 5.9) or alkSAL (75 mM NaCl; 15 mM NaHCO₃, pH 8.3) for 2 weeks (Figure 2.1 & 2.2).

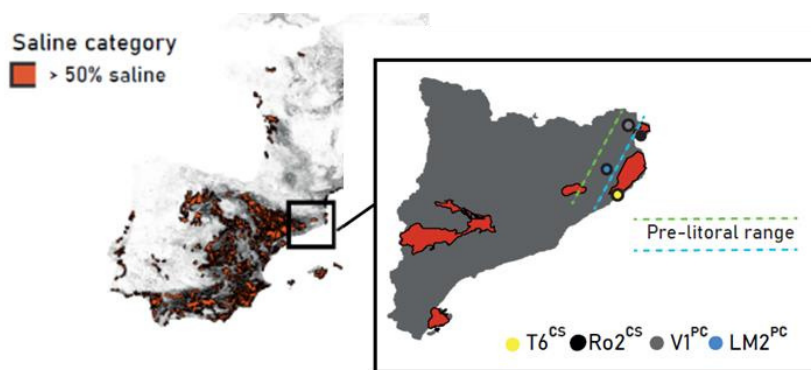


Figure 2.1. Distribution of saline soils in Europe. Red area is categorized as saline (>50% surface). Frame shows studied demes in Catalonia's map.

Physiological responses of A. thaliana demes under neutral and alkaline salinity

To see if the adaptation to saline-siliceous soils in T6^{SS} and Ro2^{SS} (neutral salinity) and to non-saline carbonated soils in V1^{CS}, LM2^{CS} (moderately calcareous) confer tolerance to alkaline salinity, the physiological, nutritional, and phytohormonal responses of the studied demes were assessed.

Multivariate analyses of all measured variables were performed to establish and verify the association between traits and plant stress tolerance.

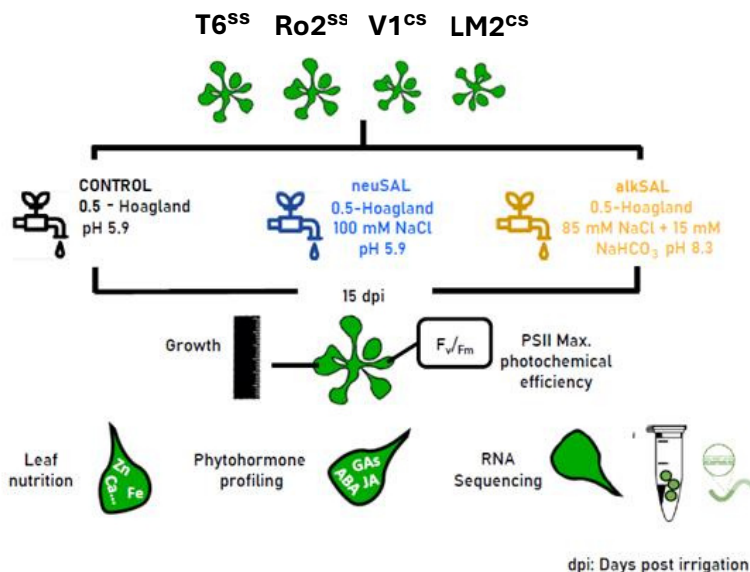


Figure 2.2. Workflow. Schematic overview of the compared sample growth conditions and performed analyses.

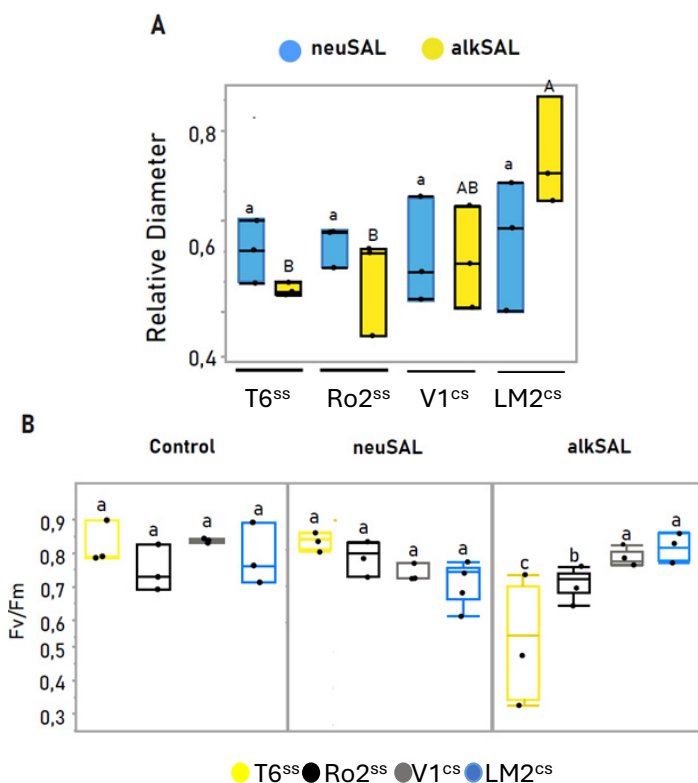
Demes from coastal siliceous soils display reduced growth and photosynthesis under alkaline salinity

Overall, *neuSAL* and *alkSAL* caused 50% decrease in relative rosette diameter (RD) $[(RD_{\text{Treatment}})/(RD_{\text{Control}})]$ regardless of deme and treatment, although LM2^{CS} showed significantly better growth maintenance than the other demes under *alkSAL* conditions ($p\text{-value} \leq 0.05$, Tukey's HSD) (Figure 2.3A; Table S2.1). The chlorophyll (Chl) fluorescence parameter, F_v/F_m , reflects the maximum quantum efficiency of PSII photochemistry in the dark-adapted state and has been widely used for the detection of early stress responses in plants. Under control and *neuSAL* conditions, no significant differences in F_v/F_m among

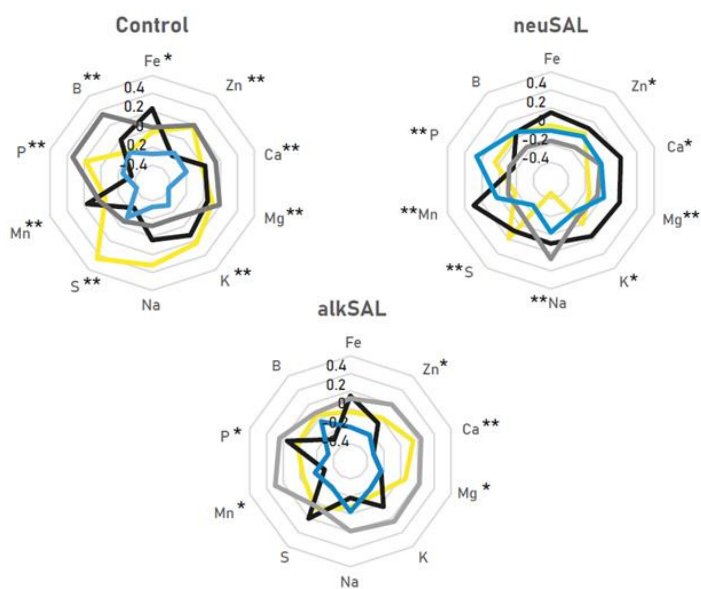
demes were observed and mean F_v/F_m values were comprised in the reading considered as optimal (between 0.79 and 0.84) for stress free plants (Maxwell and Johnson 2004). Under *alkSAL*, T6^{SS} displayed a dramatic decrease in F_v/F_m values (mean F_v/F_m = 0.520) when compared to the rest, while V1^{CS} (mean F_v/F_m = 0.770) and LM2^{CS} (mean F_v/F_m = 0.820) showed better F_v/F_m maintenance (p -value ≤ 0.05 , Tukey's HSD). Contrarily, under *neuSAL*, T6^{SS} and Ro2^{SS} (0.860 and 0.810, respectively) displayed significantly higher F_v/F_m values than V1^{CS} (0.740) and LM2^{CS} (0.730) (Figure 2.3B; Table S2.2). Reduction of total photosynthetic activity is a common feature of plant stress, and the results confirm that the ability to maintain the photosynthetic capacity is a good indicator of tolerance to either *neuSAL* or *alkSAL* in *A. thaliana*. These observations point to a better performance of demes from pre littoral calcareous soils (V1^{CS}, LM2^{CS}) under *alkSAL* in terms of growth maintenance and photosynthesis and agree with the severe reduction in rosette diameter previously reported on coastal demes under *alkSAL* (Pérez-Martín et al., 2022).

K⁺ and Fe uptake efficiency are indicators of plant tolerance to salinity

Mean-standardized values ($-1 < \text{value} < 1$) of leaf and soil elemental contents were used for the analysis. Overall, significantly differentiated leaf nutrient profiles (p -value ≤ 0.05 , Tukey's HSD) were observed for all demes in most elements under control, *neuSAL* and *alkSAL* treatments (Figure 2.3C; Table S2.3). Whereas nutrient profiles were clearly genotype-specific under control conditions, *neuSAL* highlighted a significantly higher K^+ levels in T6^{SS} and Ro2^{SS} when compared to V1^{CS} and LM2^{CS}.



C



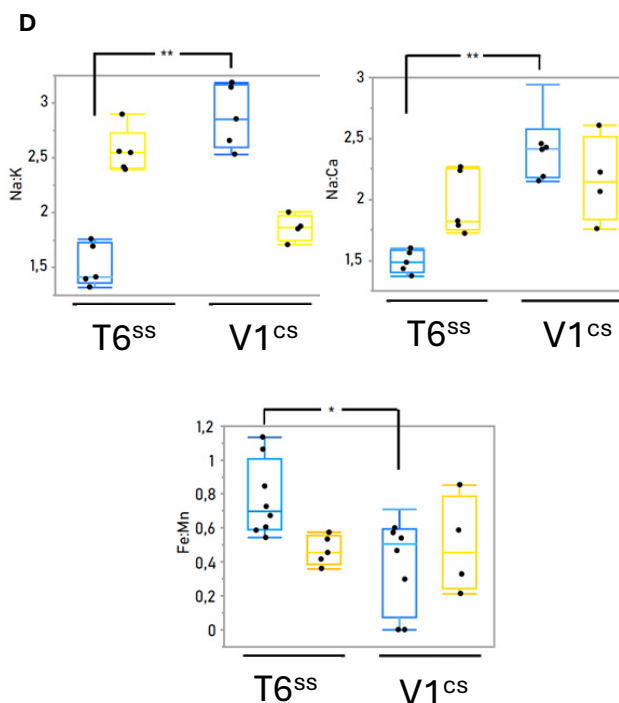


Figure 2.3. Leaf growth, photosynthesis efficiency and mineral nutrition in *A. thaliana* demes under control (C), neutral (neuSAL) and alkaline (alkSAL) salinity. (A) Mean \pm SE of growth (relative rosette diameter) of each deme and treatment. Each dot represents a biological replicate (n=3). Mean values with different letters indicate significant differences (Tukey's HSD, adj. p-value < 0.05). (B) Mean \pm SE of Maximum PSII photochemical efficiency (Fv/Fm) of each deme and treatment. Each dot represents the mean value of 2 technical replicates (2 measurements on each biological replicate) (n=3). Mean values with different letters indicate significant differences (Tukey's HSD, adj. p-value < 0.05). (C) Radial plots showing normalized differences of 10 elements in plant leaf samples from each deme and treatment. Axes display Z-scores calculated per element, and elements exhibiting significant differences in at least 1 deme (Tukey's HSD, adj. p-value < 0.05) are marked with an asterisk on each radial plot. (D) Mean \pm SE of analyzed nutrient ratios in the two contrasted demes T6^{SS} and V1^{CS}. Each dot represents a biological replicate (n=5). Nutrient ratios exhibiting significant differences for each deme between salinity treatments (Student t-Test, adj. p-value < 0.05) are marked with an asterisk (*: adj. p-value < 0.05; **: adj. p-value < 0.01). Plants were grown in potting mix soil and irrigated with C (0.5-Hoagland, pH 5.9), neuSAL (100 mM NaCl, pH 5.9) or alkSAL (85 mM NaCl, 15 mM NaHCO₃, pH 8.3) for 2 weeks.

Moreover, opposite trends in leaf Na⁺ accumulation in coastal demes were observed: T6^{SS} accumulated significantly less leaf Na⁺ when compared to all other demes, but Ro2^{SS} increased leaf Na⁺ due to reported allelic variation at the *HKT1;1* locus, which leads to higher shoot Na⁺ accumulation in individuals bearing the weak *HKT1;1*^{HLS} allele (Rus et al., 2006; Busoms et al., 2018). Still, highest leaf Na⁺ accumulation under *neuSAL* was reported in V1^{CS} (*p*-value = 1,40E-04; Tukey's HSD). Under *alkSAL*, V1^{CS} outrated all other demes in leaf nutritional status, while LM2^{CS} displayed a general significant reduction in leaf nutrient concentration.

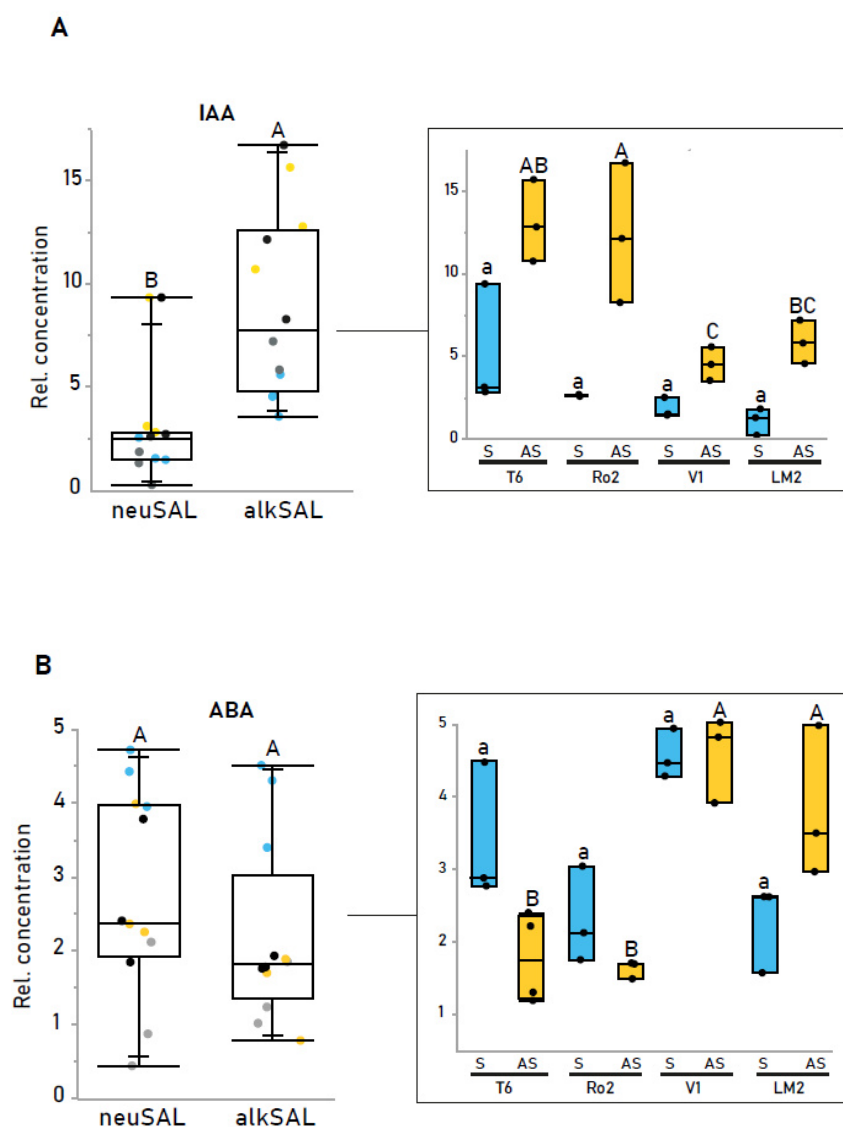
V1^{CS} and LM2^{CS} have been previously classified as good performers under *alkSAL* based on growth, reproductive and physiological traits when compared to coastal T6^{SS} and Ro2^{SS}, and the most tolerance phenotypes under neutral and alkaline salinity were observed for T6^{SS} and V1^{CS}, respectively (Pérez-Martín et al., 2022). Therefore, nutrient ratios with reported biological importance under salinity conditions were compared in T6^{SS} – as tolerant to *neuSAL* but sensitive to *alkSAL* – and V1^{CS} – as sensitive to *neuSAL* but good performer under *alkSAL*, to further explain the implications of the differential nutrient accumulation under each type of salinity (Figure 2.3D; Table S2.4). Na:K ratio in T6^{SS} (1.51) was significantly lower (*p*-value ≤ 0.05, Tukey's HSD) than V1^{CS} (2.88) under *neuSAL*, but higher (2.56 and 1.86 for T6^{SS} and V1^{CS}, respectively) under *alkSAL*. It has been previously concluded that salt tolerance is driven more by a plants ability to retain K⁺ under salt stress, than its ability to simply exclude Na⁺ ions (Wang et al., 2007; Shabala & Cuin, 2008). The Na:Ca ratio followed the same trend as Na:K, being significantly lower in T6^{SS} (1.49) than in V1^{CS} (2.88) under *neuSAL*. Cellular Na⁺ and Ca cell transport pathways are linked via SOS2 (a ser/thr protein kinase activated by SOS3, a calcium sensor protein), as SOS2 regulates SOS1 and NHX1 (plasma membrane and tonoplast Na⁺/H⁺ antiporters) but also CAX1 (a vacuolar Ca/H⁺ antiporter) (Cheng et al., 2004). Decreasing Na:Ca ratio is

shown to enhance K⁺ uptake and reduce Na⁺ uptake, ultimately decreasing Na:K (Garg et al., 2015). This seems to be the case for V1^{CS} under *alkSAL* but not under *neuSAL*, which might be causing its sensitivity to neutral but not to alkaline salinity. Moreover, Fe uptake efficiency is critical in a context of alkalinity, as high pH decreases Fe availability and leads to plant chlorosis (Hsieh et al., 2016). Under *neuSAL*, the Fe:Mn ratio was increased in T6^{SS} (0.77) due to a higher leaf Fe accumulation when compared to V1^{CS} (0.01 vs -0.20). Under *alkSAL*, the maintenance of Fe:Mn despite the high increase in leaf Mn concentration displayed by V1^{CS} (0.30) indicates higher Fe uptake or translocation efficiency (Figure 2.3D). This suggests that T6^{SS} – adapted to moderate levels of neutral salinity - could be hampered by the alkalinity component of *alkSAL*. Overall, the observed response of each deme to *alkSAL* seems driven by other factors than the Na⁺ content in their native soils, as it is the case for *neuSAL* (Busoms et al., 2018), and reinforces the statement that tolerance to salinity in siliceous soils does not confer tolerance to alkaline salinity (Pérez-Martín et al., 2022).

Differential auxin, ABA and CKs alkaline-elicitation is origin-dependent

Considering that regulation of endogenous phytohormone levels is one of the most important described mechanisms that confer tolerance to a wide spectrum of abiotic stresses (Zhang et al., 2019), endogenous phytohormones were quantified in leaf tissue of the studied demes under each treatment. Mean relative concentrations of the analyzed phytohormones can be found in Table S2.5. An increase in all analyzed phytohormones but SA was observed in all demes under *neuSAL* and *alkSAL* when compared to control $[\text{phytohormone}]_T / [\text{phytohormone}]_C$ (Figure 2.4; Figure S2.1). IAA concentration was higher ($p\text{-value} \leq 0.01$, Student's *t*-Test) under *alkSAL* than

under *neuSAL*, and coastal demes had higher leaf IAA under *alkSAL* (Figure 2.4A). It has been shown that the role of auxin under salinity in *Arabidopsis* is specific to ionic stress (Cacket et al., 2022).



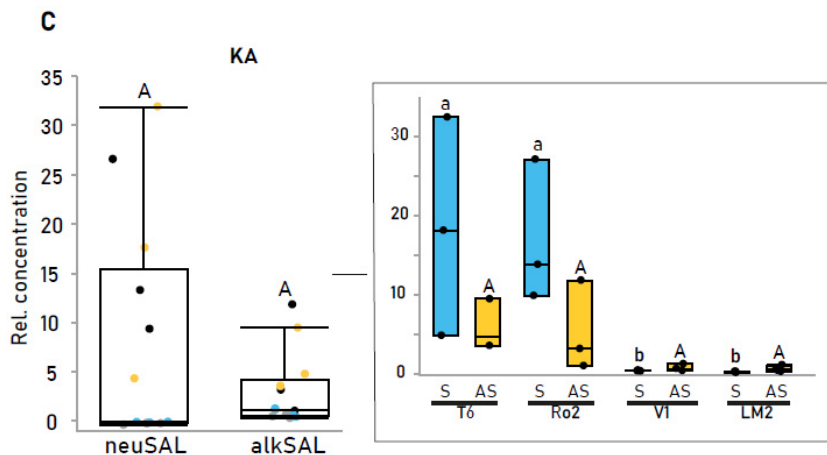


Figure 2. Endogenous phytohormone content in *A.thaliana* demes under neutral (neuSAL) and alkaline (alkSAL) salinity. Mean \pm SE of relative (A) Indole acetic and phenyl acetic acid (IAA), (B) Absciscic acid (ABA), and (C) kinetin (KA) concentration in all demes under control and salinity treatments. Each dot represents a biological replicate ($n=3$), and demes are color-coded (see legend). Zoomed boxplots show relative phytohormone concentration for each deme. Mean values with different letters indicate significant differences (Tukey's HSD, adj. p -value < 0.05). Plants were grown in potting mix soil and irrigated with C (0.5-Hoagland, pH 5.9), neuSAL (100 mM NaCl, pH 5.9) or alkSAL (85 mM NaCl, 15 mM NaHCO₃, pH 8.3) for 2 weeks.

A significantly higher ACC accumulation under alkSAL when compared to neuSAL was observed, but no significant differences in leaf ACC concentration between demes were observed under any of the treatments (Figure S2.1). Thus, the differential tolerance to NaCl and NaHCO₃ among demes may not be attributed to their different abilities to synthesize ACC. For ABA, higher mean relative concentrations were found under neuSAL when compared to alkSAL in coastal demes (mean ABA_{neuSAL} = 2.9 and 1.8; mean ABA_{alkSAL} = 1.2 and 1.1 for T6^{SS} and Ro2^{SS}, respectively), whereas in V1^{CS} and LM2^{CS} higher ABA concentration was observed in alkSAL (mean ABA_{neuSAL} = 4.2 and 2.8; mean ABA_{alkSAL} = 3.9 and 3.3 for V1^{CS} and LM2^{CS}, respectively) (Figure 2.4B). Salinity-induced ABA biosynthesis causing stomatal closure, reducing

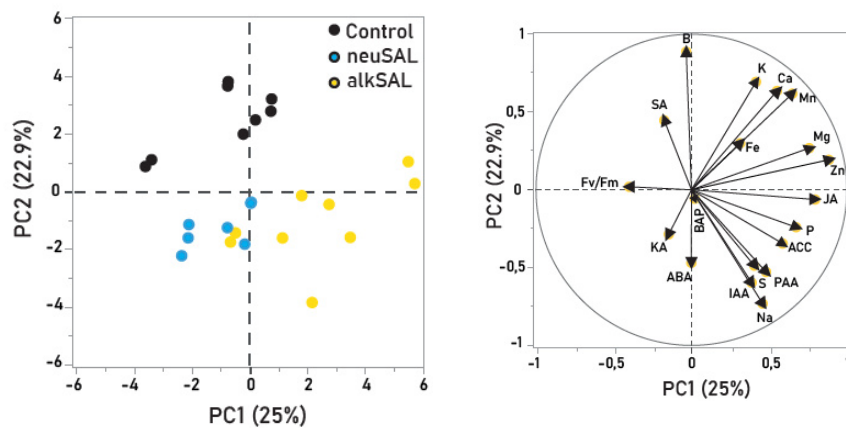
stomatal conductance and water consumption, and promoting overall plant tolerance to salinity is well reported (Lovelli et al., 2012). Quantification of endogenous JA revealed a significantly higher leaf JA concentration in plants submitted to *alkSAL* when compared to *neuSAL*, without differences among demes (Figure S2.1). JA biosynthesis under salinity is well reported in plants and can either trigger the expression of JA-related genes or physiological responses like activation of the antioxidant system, accumulation of amino acids and soluble sugars or regulation of stomatal opening (Wang et al., 2020). SA was the only analyzed phytohormone displaying a significant decrease in relative endogenous concentration under *neuSAL* and *alkSAL* when compared to control (Figure S2.1), which supports previous observations on ABA-SA and JA-SA antagonistic signaling (Kazan & Manners, 2012; Moeder et al., 2010). Finally, CKs quantification showed significant accumulation of KA-like compounds only in coastal demes under *neuSAL* (Figure 2.4C). Kinetin (N6-furfurylaminopurine) has never been found in plants, but naturally occurring kinetin-like substances – mainly *trans*-zeatin – with the same role as KA are usually quantified (Barciszewski et al., 1999).

Here, we report an alkalinity-elicitation of auxin biosynthetic processes in T6^{SS} and Ro2^{SS}, and of ABA in V1^{CS} and LM2^{CS}. While enhanced auxin accumulation is possibly involved in T6^{SS} and Ro2^{SS} smaller rosette size, higher ABA accumulation seems to contribute to the enhanced response of non-saline calcareous demes V1^{CS} and LM2^{CS} to *alkSAL*, as ABA increases water use efficiency and boosts plant antioxidant activity (Cardoso et al., 2020). The biosynthesis of increased KA-like compounds, exclusively triggered in coastal demes by *neuSAL*, might help the plant to alleviate the negative impact of neutral salinity stress by improving ion homeostasis, chlorophyll content or ROS scavenging activity, as observed with exogenous KA application in *Salvia officinalis* (Tounekti et al., 2011).

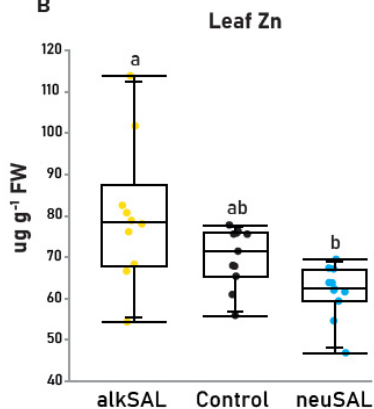
Multivariate analyses reveal new players defining the alkalinity component of salinity

Multivariate analyses on all measured traits were performed for all samples by means of Principal Component (PCA) and Multiple Pearson Correlation (MPC) analyses. The PCA showed that eigenvalues of the two first principal components represented up to 48% (PC1 25%; PC2 23%) of the total variance (p -value = $1.13\text{E-}09$ for PC1 and 0.0002 for PC2 (Table S2.6). A general look at the PC1–PC2 axes plane plot (Fig 2.5A) shows that alkalinity contribute to the construction of component 1 (samples submitted to neutral or alkaline salinity differentiate along the x-axis), whereas salinity contributes to PC2 construction (control samples differentiate from *neuSAL* and *alkSAL* samples along the y-axis). The loading matrix revealed that well correlated mineral nutrient traits (leaf Zn and leaf Mg), as well as endogenous JA, were the variables contributing to PC1 with a loading factor above 0,70 (Dataset S2.7). In fact, *alkSAL* samples contained significantly higher Zn than *neuSAL* samples (p -value ≤ 0.05 , Tukey's HSD) (Figure 2.5B). In turn, MPC results showed that Zn displayed the highest correlation with Mg and JA under *alkSAL* ($R^2 = 0.8$; $R^2 = 0.6$), but correlation with Mg was lost ($R^2 = 0.15$), and correlation with JA was inverted ($R^2 = -0.48$) under *neuSAL* (Figure 2.5C).

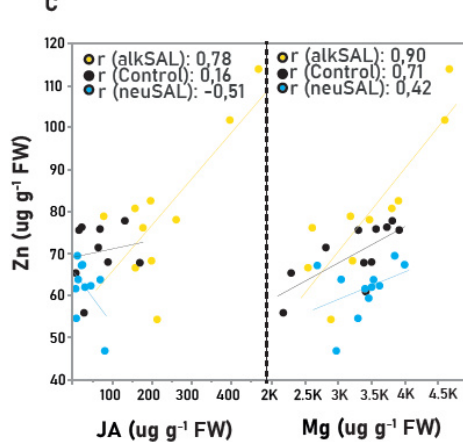
A



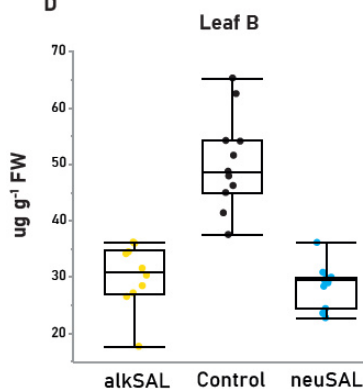
B



C



D



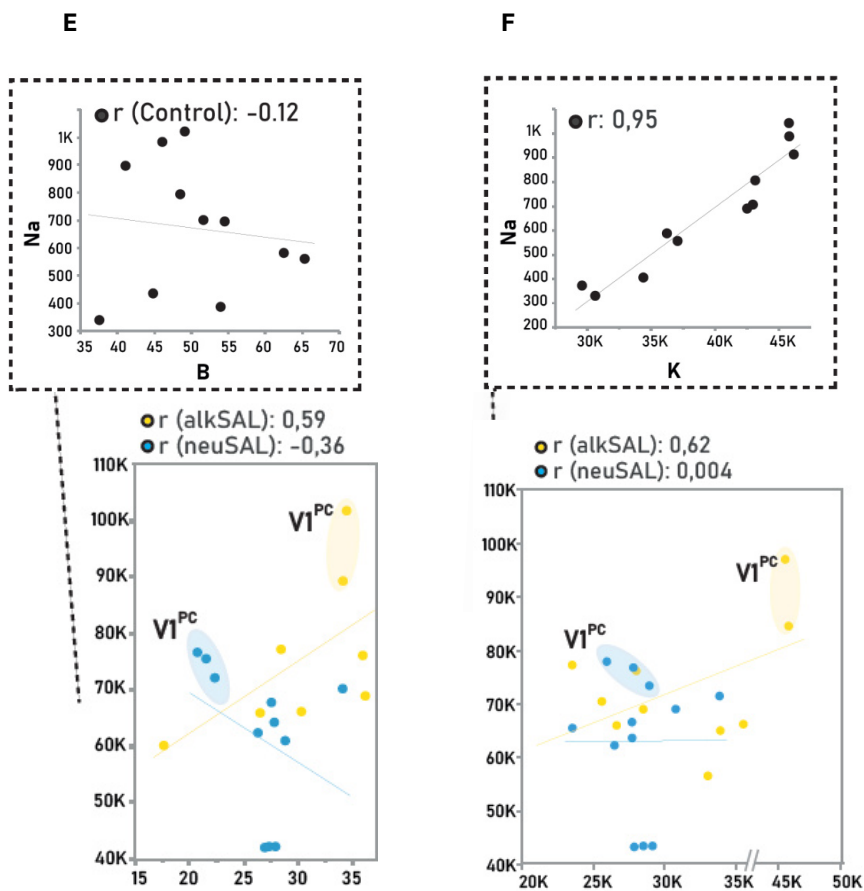


Figure 2.5. Multivariate analysis on physiological traits in *A. thaliana* demes under control (C), neutral (neuSAL) and alkaline (alkSAL) salinity. (A): Principal Component Analysis (PCA). Left: individual factor map with treatment-colored samples distribution on the 2 most informative axes (PC1 and PC2) of the PCA. Right: variable factor map presenting the amount of variance from each trait on the total variance in the PCA. Longer arrows represent larger amount from total variance. **(B)** Mean \pm SE of leaf Zn ($\mu\text{g g}^{-1}$ DW) in all demes under control and salinity treatments. **(C)** Scatter plot matrix section from multivariate correlation analysis of all physiological traits. Scatter plots show correlation between leaf Zn [$\mu\text{g g}^{-1}$ DW], y-axis] and leaf JA and Mg [ng g^{-1} FW], left; ($\mu\text{g g}^{-1}$ DW), right; x-axis] in all samples. **(D)** Mean \pm SE of leaf B ($\mu\text{g g}^{-1}$ DW) in all demes under control and salinity treatments. **(E)** Scatter plot matrix section from multivariate correlation analysis of all physiological traits. Scatter plots show correlation between leaf Na [$\mu\text{g g}^{-1}$ DW], y-axis] and leaf B (left) and K (right) ($\mu\text{g g}^{-1}$ DW); x-axis] in all samples. r = correlation coefficient. Each dot represents a

biological replicate (n=3 per deme) and treatments are color-coded (see legend). Letters indicate significant differences (Tukey's HSD, adj. *p*-value < 0.05). Plants were grown in potting mix soil and irrigated with C (0.5-Hoagland, pH 5.9), *neuSAL* (100 mM NaCl, pH 5.9) or *alkSAL* (85 mM NaCl, 15 mM NaHCO₃, pH 8.3) for 2 weeks.

Leaf Na⁺, leaf K⁺ and leaf B contributed to the construction of component 2, being leaf B dramatically decreased in the presence of salinity regardless of neutral or alkaline (Figure 2.5D). MPC showed how Na-B correlated negatively under *neuSAL* ($R^2 = -0.42$) but positively under *alkSAL* ($R^2 = 0.35$), whereas no correlation was found in control ($R^2 = 0.03$) (Figure 2.5E). While co-toxicity of salinity and B is reported (Pandey et al., 2019), few studies on neutral or alkaline salinity causing B deficiency are found. Boron alleviates salinity and saline-sodicity stress by improving leaf water and soluble carbohydrate contents as well as maintaining osmotic potential (Yousefi et al., 2020; Mehmood et al., 2009). Remarkably, V1^{CS} displayed the highest B and K⁺ maintenance under *alkSAL* and the highest B and K⁺ deficiency under *neuSAL* (Figure 2.5E-F). It is known that efficient plant B acquisition contributes to enhanced HCO₃⁻ tolerance, as high boron requiring transporters (BORs) have been reported to be responsive to saline-alkali stress in *Glycine soja*, and *BOR2* overexpressing conferred enhanced NaHCO₃ tolerance in *Arabidopsis* (Duan et al., 2018).

In summary, the reported results suggest that growth and PSII efficiency maintenance are indicators of differential tolerance to neutral and to alkaline salinity in the studied demes. Whereas neutral salinity tolerance in coastal individuals is driven by a decreased Na⁺ shoot translocation in T6^{SS} and by the ability to retain K⁺ in Ro2^{SS}, the maintenance of leaf K⁺ homeostasis by increasing leaf Ca²⁺ accumulation is a requirement for a better response to alkaline salinity. Moreover, enhanced tolerance to *alkSAL* in V1^{CS} is partially explained by higher Fe, B and K⁺ internal use efficiency. Differential modulation of auxin, ABA and CKs among genotypes is likely involved in

tolerance to either *neuSAL* or *alkSAL* in the studied demes; and differences in leaf Zn concentration under *neuSAL* and *alkSAL* may affect endogenous phytohormone content through the stimulation of tryptophan biosynthesis, which is a precursor of indoleacetic acid and a potential conjugate of IAA and JA.

Transcriptome profiling of A. thaliana under neutral and alkaline salinity

Leaf transcriptome profiling of the 4 demes cultivated under control, *neuSAL* or *alkSAL* conditions was performed to characterize the mechanisms underlying the differential response to neutral and alkaline salinity at the gene expression level. Multi-Dimensional Scaling (MDS) was used to visualize global transcriptional similarity among samples (Figure 2.6A). The transcriptome of each sample was shaped by deme and colored by treatment. Accordingly, individuals showed higher transcriptional similarity between samples corresponding to the same treatment, indicating that the studied transcriptomic response is treatment specific.

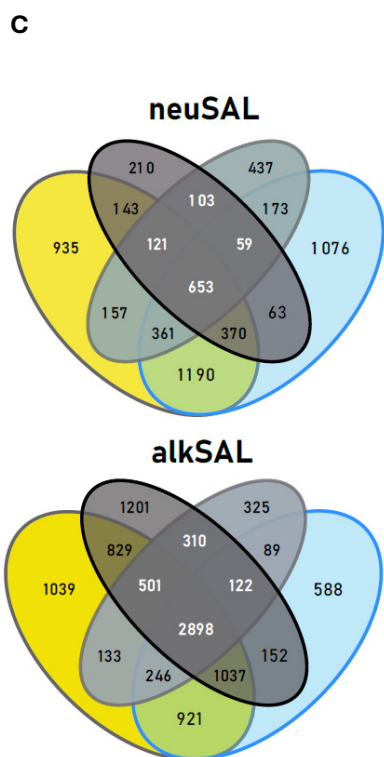
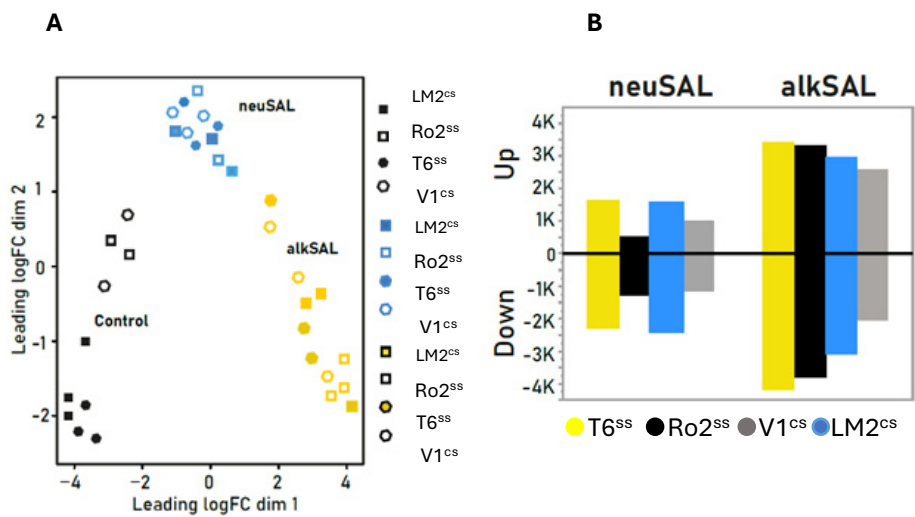
Differentially expressed genes (DEGs) per deme and treatment were declared based on absolute \log_2 fold-change (FC) > 2 under each treatment compared to control conditions (*neuSAL*/Control, *alkSAL*/Control) (q -value < 0.05, Wald test). When considering all demes, a total of 6164 DEGs (2559 up-regulated and 3605 down-regulated) were identified under *neuSAL* and 10487 DEGs (4995 up-regulated and 5492 down-regulated) under *alkSAL*. A 65% of total DEGs from *neuSAL* were found in T6^{SS} and V1^{CS}, while 29% and 34% in Ro2^{SS} and LM2^{CS}. Under *alkSAL*, T6^{SS}, Ro2^{SS}, V1^{CS} and LM2^{CS} displayed 1.9, 4.1, 2.2 and 1.53-times more DEGs than under *neuSAL*. Under *alkSAL*, T6^{SS}, still displayed the most altered transcriptome, followed by Ro2^{SS} (73% and 68% of total *alkSAL* DEGs, respectively), while V1^{CS} and LM2^{CS} transcriptomic response was more attenuated (58% and 44% of total DEGs) (Figure 2.6B-C).

Exclusive and shared molecular components of neutral and alkaline salinity

To gain more insight into commonalities and particularities between treatments, the subset of DEGs shared by at least 3 out of 4 demes in *neuSAL* and *alkSAL* were selected and merged, thus obtaining individual and common DEGs under both treatments (Figure 2.6D). On the one hand, 345 of DEGs were found in response to *neuSAL* but not to *alkSAL* and were referred as *onlyNEUSAL* DEGs set. From these, 141 and 186 (41% and 54% of transcripts, respectively) were commonly upregulated or downregulated among demes, and 18 (5%) showed ambiguous expression trends depending on the deme (Figure 2.7A).

On the other hand, 3585 DEGs changed under *alkSAL* but not under *neuSAL* and were referred to as *onlyALKSAL* DEGs set. From these, 1621 and 1935 (45% and 54% of transcripts, respectively) were upregulated or downregulated, and only a minimal fraction of 29 (0,8%) showed opposite expression trends in at least 1 deme (Figure 2.7B).

Finally, the 1219 of the selected DEGs were shared under both *neuSAL* and *alkSAL* and were referred as *coreSAL* DEGs set.



D

DEGs classification

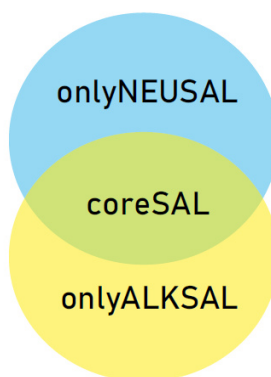


Figure 2.6. Differential Gene Expression (DEG) analysis in *A. thaliana* demes T6^{SS} (yellow), Ro2^{SS} (black), V1^{CS} (blue), and LM2^{CS} (grey). (A) Multidimensional scaling (MDS) plot of RNA expression profiles in the studied samples. Sample relations are plotted using a multidimensional scaling plot (MDS) generated with edgeR showing the variability between replicates and treatments in log2-fold-change distance. The axes represent gene expression levels between the different experimental factors. Each dot represented a sample, color coded by treatment (Black: Control, Blue: *neuSAL*, Yellow: *AlkSAL*) and shape coded by deme (Color-filled square: T6^{SS}, empty square: Ro2^{SS}, color-filled octagon: V1^{CS}, empty octagon: LM2^{CS}). (B) Histogram showing the number of differentially expressed genes for each deme (n=3) and treatment (*neuSAL*/Control; *alkSAL*/Control). (C) Venn diagram showing the mutual overlaps of DEGs among demes under each treatment. DEGs were filtered at log fold change (LFC > 2, LFC < -2), and *q*-value (FDR-adjusted *p*-value) < 0.05.

From these, 406 (65%) were upregulated, 786 (33%) downregulated and 27 (2%) with opposite expression trends in at least one deme (Figure 2.7C). DEGs from *onlyneuSAL*, *alkSAL* and *coreSAL* categories are listed in Datasets S2.1-2.3. It is well known that plants facing complex stress conditions trigger cascade of signals unique to specific stress components as well as shared responses (Zandalinas et al., 2020; Skalak et al., 2021). Studies assessing *Arabidopsis* response to combinatorial stresses described antagonistic expression trends for only 5% to 10% of transcripts, which is in line with the expression trends found for each DEGs subset described above. Moreover, 86% of DEGs from the *coreSAL* were found in the 4 studied demes (Figure S2.2), which reveals that contribution to the *coreSAL* DEGs set is high for all studied demes and, thus, similar strategies in the studied individuals lead to differential responses to *neuSAL* and *alkSAL*.

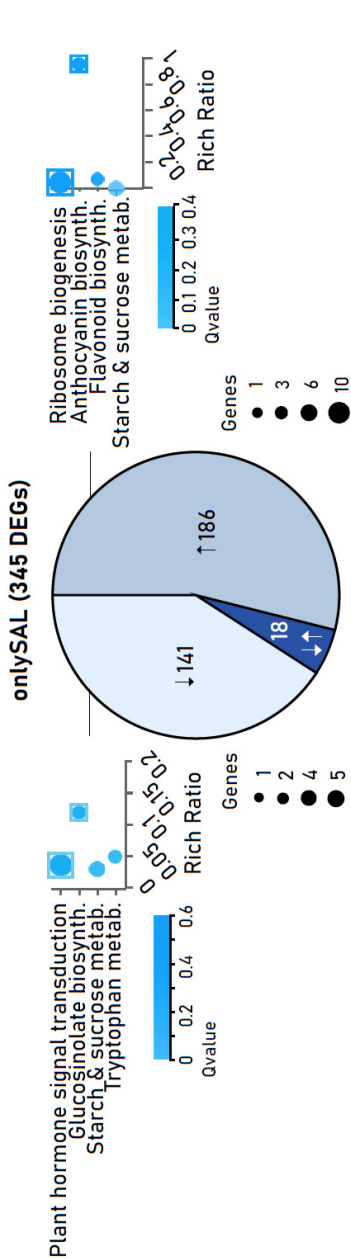
The overall results obtained from DEG analysis and classification provide evidence that the stress imposed on plants by alkaline salinity is distinct from that imposed by salinity in a neutral soil (Guo et al., 2010) and that alkaline

salinity involves more complex processes than neutral salinity at the transcriptomic level (Fang et al., 2021).

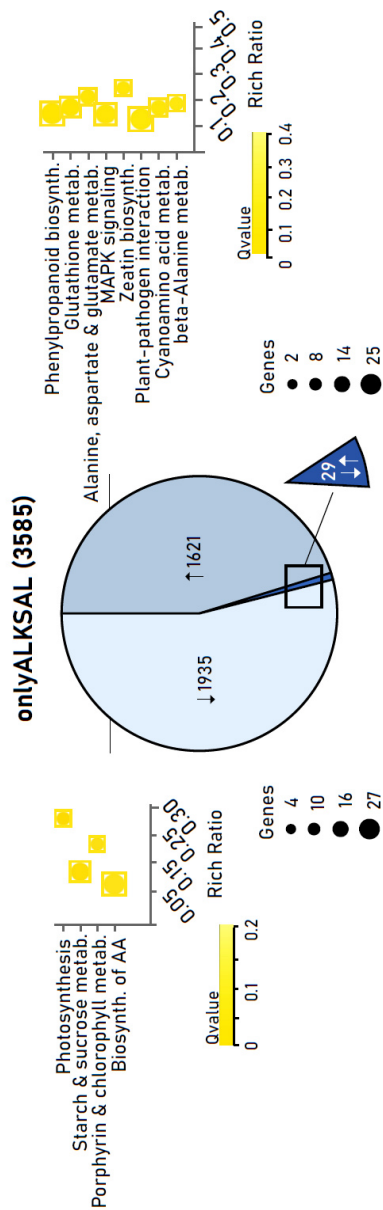
KEGG Enrichment analysis of onlyNEUSAL and onlyALKSAL DEGs

Kyoto Encyclopedia of Genes and Genomes (KEGG) pathway analysis was performed in *onlyNEUSAL* and *onlyALKSAL* DEGs to identify which categories were significantly enriched in metabolic pathways (q -value < 0.05), and thus target the presence of alkalinity-dependent salinity effects in the studied demes. *onlyNEUSAL* and *onlyALKSAL* enriched pathways are listed in Dataset S2.4.1.

A



B



C

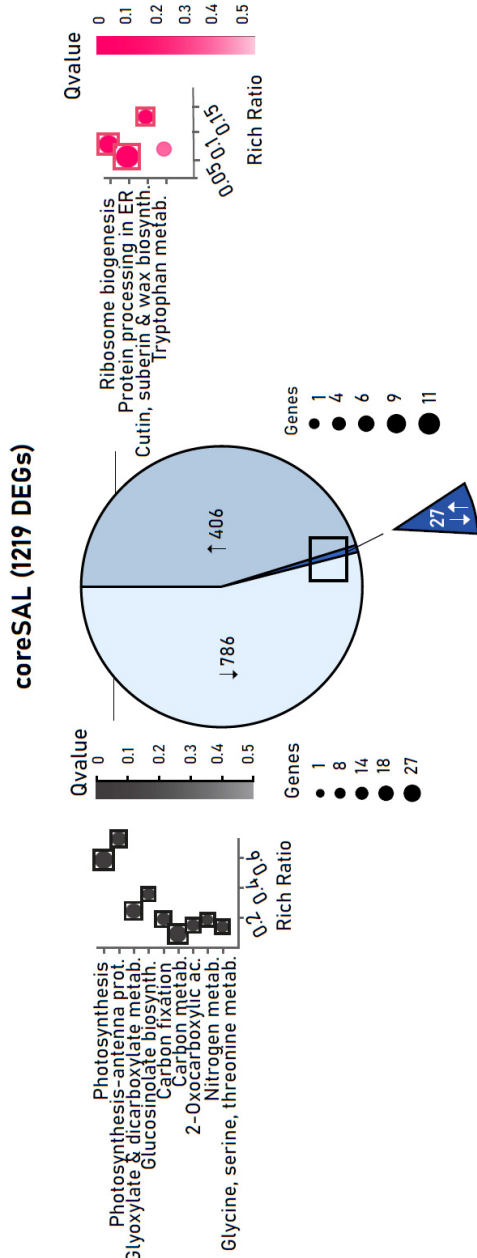


Figure 2.7. Characterization of the onlySAL and onlyALKSAL sets. DEGs were filtered at log fold change ($LFC > 2$, $LFC < -2$), and q -value (FDR-adjusted p -value) < 0.05 . Chart pie showing expression trend of total **(A)** onlySAL, **(B)** onlyALKSAL and **(C)** coreSAL DEGs. KEGG pathway enrichment analyses of downregulated (bubble plot, left) and upregulated DEGs (bubble plot, right) are shown for each corresponding DEG set. In bubble plots, pathways belonging to different classifications are listed on the left. Only the top 4 are presented, which are sorted by the q -value. Rich ratio (x-axis) is the ratio of the DEG number to the total gene number in a certain pathway. Bubble size represents number of DEGs included in each pathway (see legend) and enclosed bubbles indicate significant pathway enrichment. In heatmap: genes were clustered according to their expression pattern (Euclidean distance) and column clustering groups samples based on gene expression similarity. Color scale indicates the expression levels (yellow, low expression; blue, high expression).

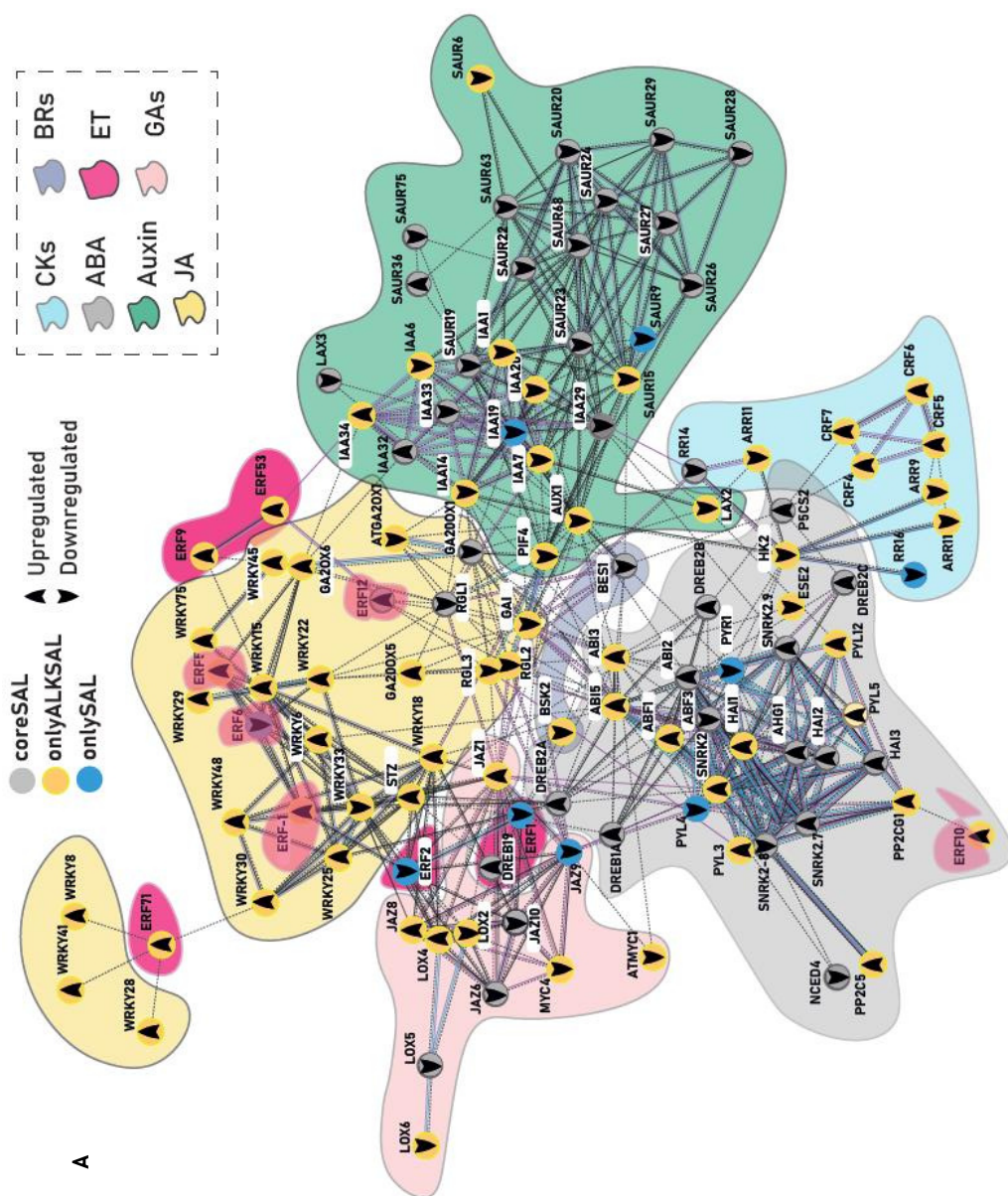
Upregulated transcripts in onlyNEUSAL and onlyALKSAL reveal higher demand for antioxidant protection under alkaline salinity.

In *onlyNEUSAL*, only 2 pathways containing 6 and 2 upregulated transcripts were significantly enriched: “ribosome biogenesis” and “anthocyanin biosynthesis”. This could indicate that expression of such transcripts is triggered by the NaCl component, likely Cl⁻ ion toxicity, which is present in higher extent under *neuSAL* than under *alkSAL* is reported to be the most significant toxic component of the saline solution in some species (Munns & Tester, 2008) and, more specifically, strongly decreases ribosome stability (Brady et al., 1984). The role of anthocyanin accumulation in the positive regulation of tolerance mechanisms to abiotic factors is well reviewed (Perea-Resa et al., 2017; Naing & Kim, 2021; Kubra et al., 2021; Zhang et al., 2019), among others, has been reported. Here, activation of anthocyanin biosynthesis genes (AT4G14090 and AT5G54060) could take place for scavenging ROS excess due to plant oxidative damage (Naing & Kim, 2021). In *onlyALKSAL*, the most enriched pathways with up-regulated transcripts were phenylpropanoid biosynthesis (25 DEGs) and glutathione metabolism (18 DEGs) (Figure S2.3). Phenylpropanoid metabolism is elicited by abiotic stresses such as drought and salinity and, moreover, is reported to contribute to salinity-alkalinity tolerance (Gan et al., 2021). The pH-dependent increase in expression of DEGs from phenylpropanoid and glutathione signaling pathways is in line with that reported in recent studies (Waters et al., 2018, Gan et al., 2021; Han et al., 2018).

The above results point to a pH-dependent response in the studied demes and a higher requirement of the plant antioxidant machinery in the presence of alkaline salinity, which would lead to an enhanced activation of transcripts from the phenylpropanoid and glutathione metabolism.

Convergence and divergence of endogenous phytohormonal pathways under neutral and alkaline salinity.

“Phytohormonal signaling” was the most KEGG enriched pathway containing downregulated transcripts in *onlyNEUSAL*. Plants defense system to abiotic stressors is built, among others, by phytohormone biosynthesis, signaling and metabolism (Yu et al., 2020). Therefore, the contribution of phytohormone signaling to the context dependence (i.e. salinity type) of plant responses was assessed. To identify if different salinity types lead to different strategies to integrate exogenous stress signals with endogenous developmental cues in the studied demes, total DEGs enriched in “plant hormone signal transduction” were further analyzed (Dataset S2.4.2).



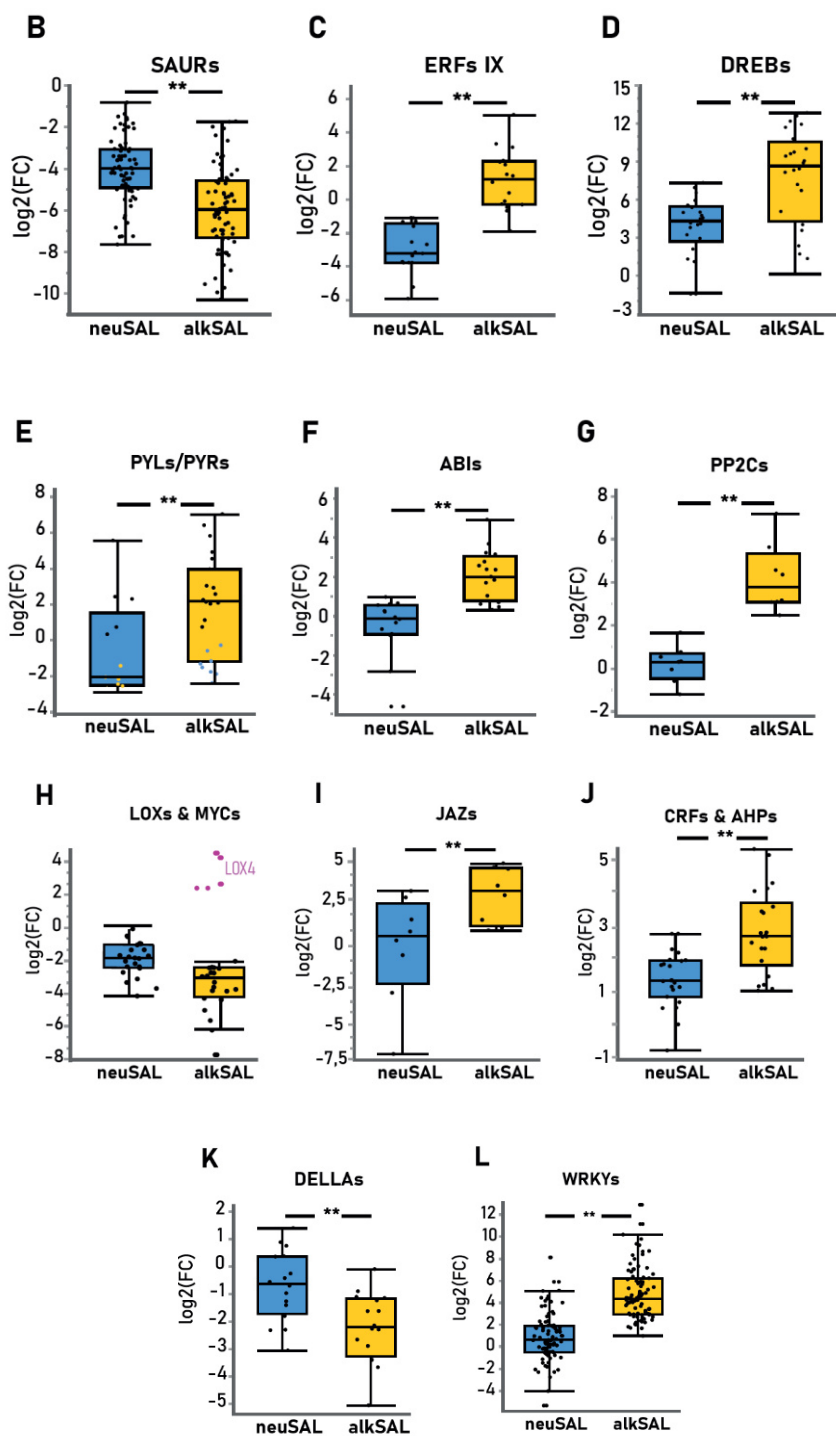


Figure 2.8. Global overview of phytohormone signaling dynamics. (A) Protein-protein interaction (PPI) network of the analyzed DEGs involved in phytohormone signaling based on the STRING online database (<https://string-db.org/>). Nodes are color-coded according to each DEGs subset, arrows inside nodules indicate expression trend and colored surrounding areas distinguish between different hormone classes (see legends). (B) Expression levels [mean \pm SE log₂(FC)] of DEGs from SAURs (n=70), (C) IX clade ERFs (n=12), (D) DREBs (n=24), (E) PYLs/PYRs (n=23), (F) ABIs (n=16), (G) PP2Cs (n=8), (H) LOXs/MYCs (n=20), (I) JAZs (n=8), (J) CRFs/AHPs (n=23), (K) WRKYs (n=88) and (L) DELLAs (n=16) in all demes among treatments. Asterisks indicate significant differences in mean expression values among treatments (Student *t*-test, adj. *p*-value < 0.05; *: adj. *p*-value < 0.05; **: adj. *p*-value < 0.01). Neutral salinity: *neuSAL*; alkaline salinity: *alkSAL*.

First, a global overview of physical interactions according to STRING of DEGs involved in phytohormone signaling under *neuSAL* and *alkSAL* was performed (Figure 2.8A). DEGs lists were dissected according to phytohormone classes (Figure 2.8B-L). Inhibition of Small Auxin Up RNA (SAUR) proteins was present in *coreSAL*, and transcripts displayed an average of x1.5 times enhanced downregulation under *alkSAL* when compared to *neuSAL* (*q*-value < 0.05; Student *t*-Test) (Figure 2.8B). *SAURs* are known for inhibiting PP2C proteins (2C-type Protein Phosphatases), which increases plasma membrane (PM) H⁺-ATPase activity. This process plays an important role in response to alkaline salinity, as PM H⁺-ATPase activity promotes cell wall acidification (Spartz et al., 2014). Moreover, some *SAURs* have been reported to activate proton extrusion involved in the Fe-deficiency response (Sun et al., 2020).

Twelve DEGs from the Ethylene Responsive Factor family (APETALA2/Ethylene Responsive Element Binding Factor – AP2/ERF - superfamily), were found. From these, *ERF2*, 5 and 6, belonging to the *ERF-IXs* clade and reported to suffer a continuous induction upon salinity (Xie et al., 2019) were significantly downregulated under *neuSAL* but activated under *alkSAL* (Figure 2.8C).

The expression pattern of *DREBs* - another major family from the AP2/ERF superfamily –revealed a strong upregulation in 5 *DREBs* in the *coreSAL*

response, with an average of x2 times higher activation under *alkSAL* (Figure 2.8D). Among them, *DREB1A* and *DREB2C*, reported as two of the *DREBs* containing the most types of abiotic stress-related motifs in the promoter region (Xie et al., 2019), were found. The induction of *DREBs* in the *coreSAL* response provides further evidence that *DREBs* form a central response network to control salinity (Sazegari et al., 2015).

The ABA signaling pathway under salinity stress is well described: when facing osmotic pressure, ABA receptors PYR/PLY/RCAR sense the increase in ABA levels and bind to *PP2Cs*. Levels of transcripts encoding ABA receptors – *PYL3*, *5*, *10*, *12* – and ABA responsive genes – *ABI2*, *ABI3*, *ABI5* – were only significantly upregulated by *alkSAL* (Figure 2.8E-F), where *PP2CG1* and *PP2C5* upregulation was also observed (Figure 2.8G). This supports the involvement of ABA-dependent signaling transcripts in the response to *alkSAL* in the studied demes.

The significant upregulation of ABA receptors (PYLs) and ABA responsive genes in *onlyALKSAL* correlated with an enhanced inhibition of JAs responsive transcripts *LOXs* (*LOX2*, *LOX6*) and *MYCs* (*MYC1*, *MYC4*) (Figure 2.8H). Antagonistic interactions between ABA and JA signaling pathways by *MYCs* in the modulation of abiotic stress-responsive gene expression have been described (Anderson et al., 2004; Kazan & Manners, 2013; Sah et al., 2016). Moreover, the expression of JAZs (repressors of JA response) like *JAZ1* and *JAZ8* was inhibited under *neuSAL* but induced in *alkSAL* (Figure 2.8I). The results above suggest that *alkSAL* elicits ABA and JA intercross, whereas hormonal signaling responses are attenuated under *neuSAL*. The increase in JA accumulation together with increase of JAZ-mediated MYC repression seems to be a bicarbonate-specific balance mechanism that cannot be predicted from plant responses to neutral salinity.

In CK signaling, CK receptors (*AHKs*) perceive CKs, phosphotransferase proteins (*AHPs*) transfer phosphate groups from *AHKs* autophosphorylation to type-B *ARRs* and *ARRs* initiate the modulation of expression of downstream genes. A significant downregulation of *ARRs* and *AHKs* but upregulation of *CRFs* (*CRF4-7*) and *AHPs* were observed in the *coreSAL* response (Figure 2.8J). This supports the direct *CRF-AHP* binding independently from *ARRs* (Yu et al., 2021). Finally, in the Gibberellin (GA) signaling pathway, all downregulated DEGs belong to the DELLA protein family. DELLAS *RGL2*, *RGL3* and *GAI* were downregulated only under *alkSAL* (Figure 2.8K). DELLAs are negative regulators of GA signaling and the key repressors of almost all GA responses. The involvement of WRKYs – a big family of transcription factors - in ABA and GA signaling is well known (Rushton et al., 1995), and direct interaction of DELLA and WRKY members has been found (Zhang et al., 2018; Chen et al., 2017). Here, significant activation of 22 WRKYs under *alkSAL* was observed in the 4 demes, while attenuated response under *neuSAL* for all transcripts and demes was shown (Figure 2.8L). Among them, enhancers of the osmotic, ROS and hormone signaling pathways under salinity stress have been recently observed (Price et al., 2022).

Overall, DEGs analysis on all phytohormone signaling under *neuSAL* and *alkSAL* provided further evidence that there is high natural variation in the transcriptional regulation of genes involved in salinity-triggered phytohormone responses, likely driven by alkalinity. In this regard, a complex interplay seems to take place in the core response to salinity, in which central regulatory switches such as PP2Cs might link auxin (through SAURs) to ABA/ET-independent (through DREBs) signaling pathways). Moreover, dynamics in the expression of AP2/ERFs, which show an inhibition under *neuSAL* but activation under *alkSAL* of clade IX ERFs, likely hamper ABA-dependent signaling under *neuSAL* (Hsieh et al., 2013). This supports a signature of salinity-type responses mediated by ET/ABA signaling and highlights the

flexibility of the ET pathway in the response to salinity stress type (Llanes et al., 2016). The activation of the ABA-dependent signaling cascade (through ABIs, PYLs and PYRs) under *alkSAL* but not under *neuSAL* potentially contributes to further differentiation between salinity types by negative regulation of JA signaling. This could constitute a mechanism of minimizing JA inhibitory effect on plant growth and avoid further biomass loss under *alkSAL* in an attempt of acclimation process (Riemann et al., 2015). More importantly, maintaining ABA accumulation could be a requirement under *alkSAL* for PP2Cs inhibition and thus PM H⁺-ATPases activation, which would allow stress-responsive adjustment of plasma membrane proton fluxes (Spartz et al., 2014). If so, the abrupt decay in ABA levels observed in coastal demes in *alkSAL* would lead to reduced cell pH homeostasis. Moreover, increased leaf PM H⁺-ATPase activity is reported to favor cell expansion and carbon sink strength (Sibole et al., 2005), enhancing CO₂ assimilation. This would agree with the lower photosynthate deficiency (Munns, 1993) observed in V1^{CS} and LM2^{CS} under *alkSAL*, together with a better maintenance of cytosolic pH and enhanced *alkSAL* tolerance. The significantly higher accumulation of KA-like substances in coastal demes under *neuSAL* supports the role of CK signaling in the differential plant response to *neuSAL* and *alkSAL* by ARR_s-independent modulation. Finally, the neutral and alkaline salinity response in the studied demes converge in the activation of GA signaling through WRKYs regulation, which suggests a salinity response modulated by WRKYs activation of phytohormone and ROS signaling processes rather than an ABA-dependent stabilization of DELLAs, as generally reported (Achard et al., 2006; Julkowska & Testerink, 2015).

KEGG Enrichment analysis of coreSAL DEGs

KEGG pathway analysis was performed in *coreSAL* DEGs to identify significantly enriched metabolic pathways (q -value < 0.05) in the general salinity stress response and the presence of genotype-dependent salinity effects in the studied demes. *coreSAL* enriched pathways are listed in Dataset S2.4.3.

coreSAL transcript activation reflects shared salinity stress responses.

The significantly enriched pathways in the *coreSAL* set were “Ribosome biogenesis in eukaryotes”, “Protein processing in endoplasmic reticulum” and “Cutin, suberin and wax biosynthesis” (Figure 2.7C). Ribosome biogenesis and protein synthesis in the ER are the two pathways comprising cellular processes with highest metabolic cost (Piazzi et al., 2019). Here, we report a consistent upregulation of genes involved in pre rRNA and RNA processing and maturation (FIB2, PWP2, AT4G04940, AT1G67120, AT3G06530), nucleolytic cleavage (AT5G22100), and cell differentiation (AT2G18900) in all 4 demes under neutral and alkaline salinity, followed by the activation of 11 Heat Shock Proteins – which encode for molecular chaperones that interact with ribosomes ensuring their stability (Piazzi et al., 2019) (Figure 2.4A-B). This indicates nucleolar stress (Yang et al., 2018) triggered by both *neuSAL* and *alkSAL* that leads to the activation of the protein synthetic machinery in the studied demes. Moreover, enhanced activation of 2 genes involved in suberin deposition (FAR1, FAR5) – previously reported to be transcriptionally induced by salinity (Domergue et al., 2010) - were observed in all demes under *neuSAL* and *alkSAL* (Figure S2.4C), which suggests that increase of suberin deposition may enhance tolerance to neutral and alkaline salinity (Zhang et al., 2021).

coreSAL transcript inhibition reveals differential sensitivities to alkSAL in the studied demes.

The significantly enriched pathways containing down-regulated transcripts detected in the *coreSAL* set were ‘Photosynthesis’ and ‘Photosynthesis antenna proteins’, ‘Glucosinolate biosynthesis’ ‘Glyoxylate and dicarboxylate metabolism’, ‘Carbon fixation’, ‘Carbon metabolism’, ‘2-Oxocarboxylic acid metabolism’, ‘Nitrogen metabolism’, and ‘Glycine, serine and threonine metabolism’ (Figure 2.9). T6^{SS} suffered the highest inhibition of all DEGs from “Photosynthesis” and “photosynthesis antenna proteins” (an average of 1.5 and x1.8 times more downregulation than V1^{CS} and LM2^{CS}, respectively), followed by Ro2^{SS} in 2 transcripts: PSAH1-2 (an average of x1.5 times more downregulation in T6^{SS}, Ro2^{SS} when compared to V1^{CS} and LM2^{CS} under *alkSAL*) (Figure 2.9A). PSAH1 and PSAH2 encode subunits H of photosystem I reaction center and their up-regulation under neutral salinity has been reported in halophytes (Hao et al., 2020). The downregulation of photosynthesis-related transcripts in the *coreSAL* response agrees with previous transcriptome studies under neutral salinity reporting a correlation between down regulation of antenna proteins and higher salt sensitivity (Guo et al., 2017; Jing et al., 2019). Similarly, DEGs from “glucosinolate biosynthesis” and a DEG subset from “carbon metabolism” displayed an average of x1.7 times more downregulation in T6^{SS} and Ro2^{SS} when compared to V1^{CS} and LM2^{CS} under *alkSAL* (Figure 2.9B). Glucosinolates are secondary metabolites mainly found in Brassicaceae. Downregulation of genes involved in glucosinolates biosynthesis has been reported under several types of salts (Aghajanzadeh et al., 2017). A previous study (Pérez-Martín et al., 2021) characterized the response to bicarbonate exposure of T6^{SS} and A1_i – as a carbonate sensitive and carbonate tolerant deme, respectively – and reported the downregulation of several GSTU genes involved in glucosinolate metabolism only in T6^{SS}. Two

Ribulose Biphosphate Carboxylase Subunits (RBCS1-2B), an Hydroxypyruvate Reductase (HPR) and a Fumarase (FUM2) comprised the DEG subset from “carbon metabolism” sharing expression pattern with the glucosinolate pathway in coastal demes (Figure 2.9C).

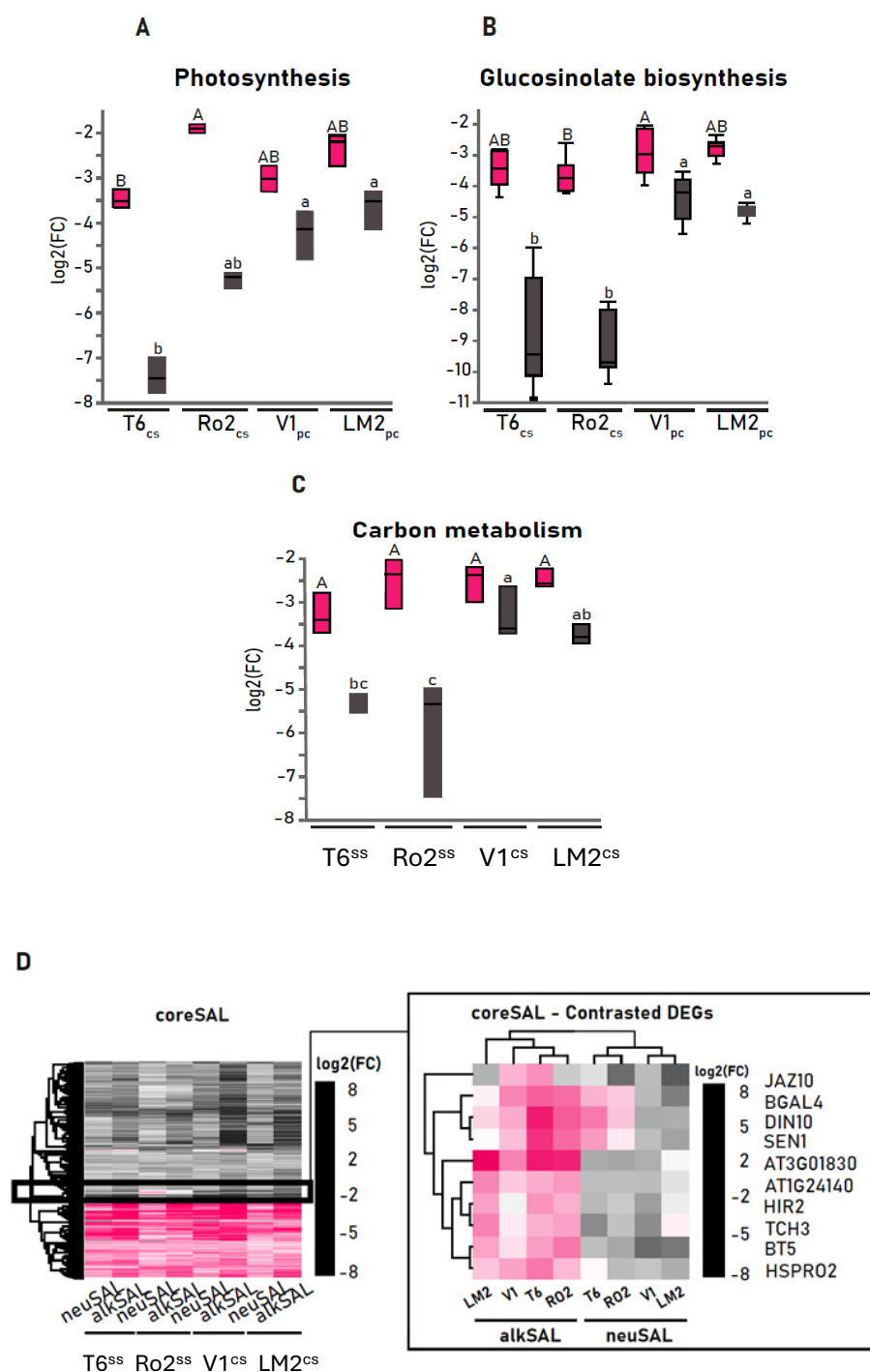


Figure 2.9. Characterization of the coreSAL DEGs set. DEGs were filtered at log fold change ($LFC > 2$, $LFC < -2$), and q -value (FDR-adjusted p -value) < 0.05 . Expression levels [mean \pm SE $\log_2(FC)$] of (A) “photosynthesis”, (B) “glucosinolate metabolism” and (C) “carbon metabolism” DEGs in each deme ($n=3$) and treatment. Letters indicate significant differences in mean expression values among demes (Tukey’s HSD, adj. p -value < 0.05). (D) Heat map showing the expression profile of coreSAL DEGs (1219 genes) for each deme between neutral and alkaline salinity when compared to control (neuSAL/C; alkSAL/C). Genes were clustered according to their expression pattern (Euclidean distance). In frame, heatmap showing the expression profiles of coreSAL DEGs with contrasted expression trends among salinity types and/or demes. The color scale indicates the expression levels (grey, low expression; pink, high expression). Genes were clustered according to their expression pattern (Euclidean distance), while column clustering groups samples based on gene expression similarity.

The last three KEGG pathways significantly enriched in the downregulated transcript set from *coreSAL* were “glyoxylate and decarboxylate metabolism” (19 DEGs), “glycine, serine and threonine metabolism” (10 DEGs) and “nitrogen metabolism” (8 DEGs) (Figure S2.5). *PGLP1* (AT5G36700, from the glyoxylate decarboxylate metabolism) suffered x1.4 times more downregulation in coastal demes under *alkSAL*. *PGLP1* is one of the core metabolite repair enzymes of plant photosynthetic carbon assimilation, as it degrades 2-phosphoglycolate (2PG) for its reconversion to Calvin cycle metabolites (Flügel et al., 2017). After 2PG degradation to glycolate, glyoxylate is generated, ultimately being catalyzed to glycine (Dellero et al., 2016). Thus, *coreSAL* inhibition of glyoxylate and decarboxylate transcripts in the studied demes is likely affecting glycine, serine, and threonine metabolism. In this regard, 10 DEGs enriched in the “glycine, serine and threonine metabolism” pathway were downregulated in the 4 demes under neutral and alkaline salinity, and *AK3* (AT3G02020) was x1.6 times more downregulated in T6^{SS} and Ro2^{SS} when compared to V1^{CS} and LM2^{CS} under *alkSAL*. *AK3* codes for an aspartate kinase that catalyzes the first step in aspartate-derived amino acids (Clark et al., 2015). *AK3* upregulation was also reported in A1 – carbonate

tolerant deme – under bicarbonate exposure when compared to control, but not in T6^{SS} – carbonate sensitive deme (Pérez-Martín et al., 2021).

Finally, inhibition of transcripts from the α -CA and β -CA (Carbonic Anhydrases) (α -CA1, α -CA2, β -CA1, β -CA2 and β -CA4), and the glutamine synthetases 1;4 (GLN1;4) and 2 (GS) family proteins comprised the “Nitrogen metabolism” down-regulated set. From these, *β CA-1* (At3G01500) and *α -CA1* (At3G52720) displayed x1.7 times more inhibition in T6^{SS} when compared to V1^{CS} and LM2^{CS} under *alkSAL* (Figure S2.5). β CA-1 is reported to regulate CO₂ controlled stomatal movements in guard cells together with *β CA4* (AT1G70410). Previous electrophysiological assays reported *β CA4* reduction in T6^{SS} under bicarbonate conditions (Pérez-Martín, 2021), and *β ca1ca4* mutant under NaHCO₃ conditions show reduced photosynthetic efficiency (F_v/F_m) and increased total ion leakage (as reporter for cell death) under NaHCO₃ treatment (Dąbrowska-Bronk et al., 2016). α -CA1 belongs to the α -CA family and is involved in the transformation of HCO₃³⁻ to CO₂ in chloroplast stroma to supply it at the active site of Rubisco (Burén 2010).

Considering the high demand of Fe cofactors by photosynthetic enzymes (Kroh & Pilon, 2020), the above results raise the hypothesis that the defective Fe use efficiency in coastal demes under *alkSAL* (especially T6^{SS}) leads to a stronger photosynthetic inhibition. This would result in the observed unbalance in carbon fixation and metabolism in T6^{SS} and Ro2^{SS}, which ultimately would compromise their total energetic investment into secondary metabolism. In such a scenario, the stronger downregulation of ***PGLP1*** (entry enzyme into one of the major pathways of primary plant metabolism) and the chloroplast carbonic anhydrases ***β -CA1*** and ***α -CA1*** in coastal demes under *alkSAL* is consistent with their reduced photosynthesis efficiency (F_v/F_m

values) and stronger downregulation of transcripts from photosynthesis (**PSAH1-2**), carbon fixation and metabolism (**RBCS1-2B**, **HPR** and **FUM2**). **FUM2** (Fumarate hydratase 2 - AT5G50950, encoding a cytosolic chloroplast fumarase) would link primary metabolism to secondary metabolism (Figure S2.6), leading to the downregulation of all transcripts involved in glucosinolate metabolism and some transcripts from the glycine, serine and threonine metabolism reported to enhance alkalinity tolerance, like **AK3**. Likewise, the results confirm that a significant inhibition of glucosinolate signaling in coastal demes is caused in an alkalinity-specific manner, likely by decreased availability of ferrous ions (Fahey et al., 2001; Wittstock et al., 2002).

A reduced coreSAL DEG subset orchestrate contrasted plant response to neuSAL and alkSAL.

All shared DEGs displaying opposite expression trends between neutral and alkaline salinity in more than 2 demes were analyzed to seek for contrasted transcriptomic responses among the studied demes potentially driving their differential performance under each salinity type (Figure 2.9D). **BGAL4** (AT5G56870), **DIN10** (AT5G20250) and **SEN1** (AT4G35770) exhibited contrasted expression trends among V1^{CS} and LM2^{CS} (down-regulated) and T6^{SS} and Ro2^{SS} (up-regulated) under *neuSAL* (Figure 2.10A). This suggests that activation of **BGAL4**, **DIN10** and/or **SEN1** is advantageous under *neuSAL* but not under *alkSAL*. Therefore, the genomic sequences of **BGAL4**, **DIN10** and **SEN1** in the 4 study demes were extracted from the Catalan demes germplasm Whole Genome Sequencing (WGS) data (Busoms et al., 2018) to identify sequence variation likely causal of the contrasted expression trends in the studied demes under *neuSAL* and *alkSAL* (Figure S2.7; Table S2.15). A SNP located only 4 bp upstream the 5'UTR at **BGAL4** promoter was consistent for all replicates of each deme and, moreover, differentiated coastal from non-

coastal demes (Figure 2.10B). BGAL4 encodes a glycosyl hydrolase regulated by SNF1-related Kinase 1 (SnRK1), a kinase involved in key plant stress responses (Peixoto et al., 2021). Degradation of structural polysaccharides in plant cell wall by cell wall-remodeling enzymes - like BGAL4 – forms part of the stress-regulated cell wall rearrangement (Moneo-Sánchez et al., 2016). A study comparing *A. thaliana* Wild Type vs salt-tolerant mutant roots exposed to NaCl stress reported higher expression of glycosyl hydrolases in the salt-tolerant mutant root, which was hypothesized to increase its potential of salt resistance (Guo et al., 2014). In contrast, β -galactosidases are reported to dramatically decrease enzymatic activity at high pH and to have pH optima ranging from 3.5 to 5.0 (Ross et al., 1994; Smith & Gross, 2000; Kotake et al., 2005, Hussien et al., 2021).

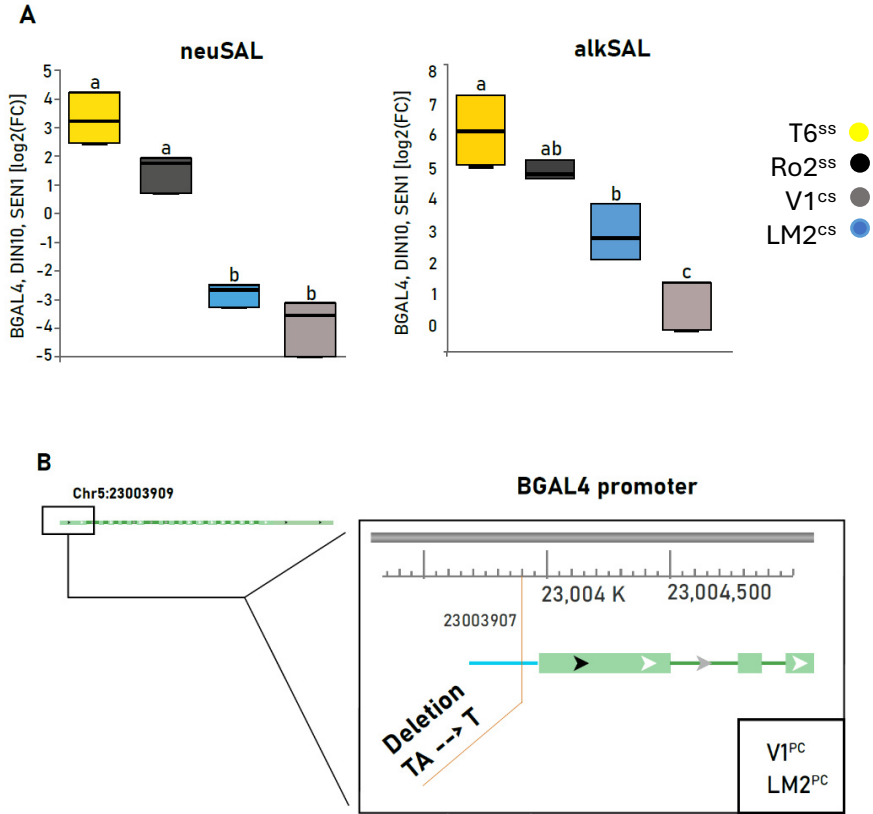


Figure 2.10. Characterization of *BGAL4* expression and sequence variation in *A. thaliana* demes. (A) Expression levels [mean \pm SE log₂(FC)] of *BGAL4*, *DIN10* and *SEN1* in each deme (n=3) and treatment. Letters indicate significant differences in mean expression values among demes (Tukey's HSD, adj. *p*-value < 0.05). T6^{ss} (yellow), Ro2^{ss} (black), V1^{cs} (blue), and LM2^{cs} (grey). **(B)** SNP polymorphisms surrounding the *BGAL4* locus. Triangles: candidate SNPs position. Amino acid change is indicated below each SNP. Gene orientation is indicated with an arrow on the right. Exons are indicated with boxes and introns with lines connecting them. Chromosome positions are indicated at the top left (picture from <https://www.arabidopsis.org/index.jsp>). Reference and alternative allele nucleotide changes, variant type and deme bearing the SNP can be found in Figure S9.

Thus, enhanced upregulation of *BGAL4* in T6^{SS} and Ro2^{SS} could point to an enhanced activation of plant energy management functions under *neuSAL*, whereas a lack of ability to modulate *BGAL4* activity for the prioritization of compounds more suitable under alkaline conditions could compromise their energy budget (Tsai & Schmidt, 2020). Moreover, the decline in photosynthesis and carbon fixation efficiency observed in coastal demes under *alkSAL* may cause further stimulation of the hydrolase enzymes, as these are triggered by sugar starvation (Lee et al., 2007). Transcription factor binding is the strongest contributor to variation in mRNA levels (Pai et al., 2015). This might be the case for *BGAL4*, where the SNP change in the promoter region of V1^{CS} and LM2^{CS} could contain cis-regulatory elements responsible for its consistently lower expression.

WGCNA Network

To combine transcriptomic and physiological datasets and detect possible correlations between genes determining traits of interest, all DEGs detected in each deme under *neuSAL* and *alkSAL* were retained for WGCNA unsigned co-expression network analysis. This involved a total of 11432 DEGs (11K WGCNA hereafter). The soft threshold power of 7 ($\beta = 7$) was selected according to the preconditions of approximate scale-free topology (Figure S2.8). WGCNA 11K analysis identified sixteen distinct co-expression modules which were assigned to different colors shown in the dendrogram (Figure S2.9). The obtained module-trait correlation matrix displayed two major contrasted patterns defined by correlation trends in 3 main traits: leaf Na⁺, leaf B and relative rosette biomass (Figure 2.11). This confirmed that correlation patterns observed in the performed multivariate analyses of physiological traits (PCA and MPC) were maintained when integrating co-expressed

transcriptome data into trait correlations (WGCNA). Besides, most co-expression modules that negatively correlated with leaf Na^+ but positively correlated with leaf B and sample biomass were also displaying positive correlation with leaf K^+ and F_v/F_m values, confirming their biological relevance in the context of salinity stress. Considering all the above, modules showing significant negative correlation with Na^+ and positive correlation with B, K^+ or FW were picked for further analysis of their implication in tolerance mechanisms to salinity stress and GO and KEGG enrichment analysis of each selected co-expression module was performed for each significant selected module. After that, DEGs comprised in the significantly enriched pathways of each module were merged with the representative set of DEGs from *coreSAL*, *onlyNEUSAL* and *onlyALKSAL*, and results confirmed that DEGs selection criteria carried for transcriptome analysis – picking only DEGs detected in at least 3 out of the 4 demes comprised in the shared and the exclusive response to neutral and alkaline salinity - accurately reflected the behavior of the entire dataset (Table S2.16). Moreover, all the genes highlighted from previous analysis have also been identified in the 3 modules explored (Figure 2.12).

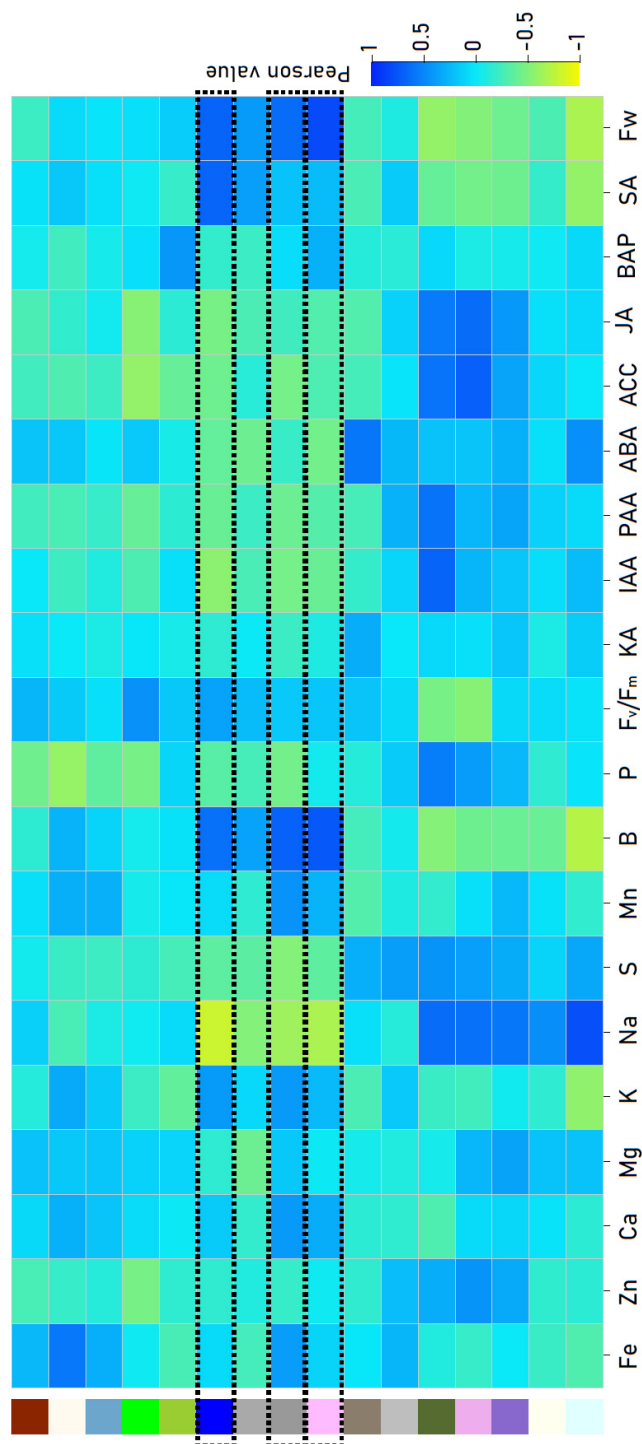
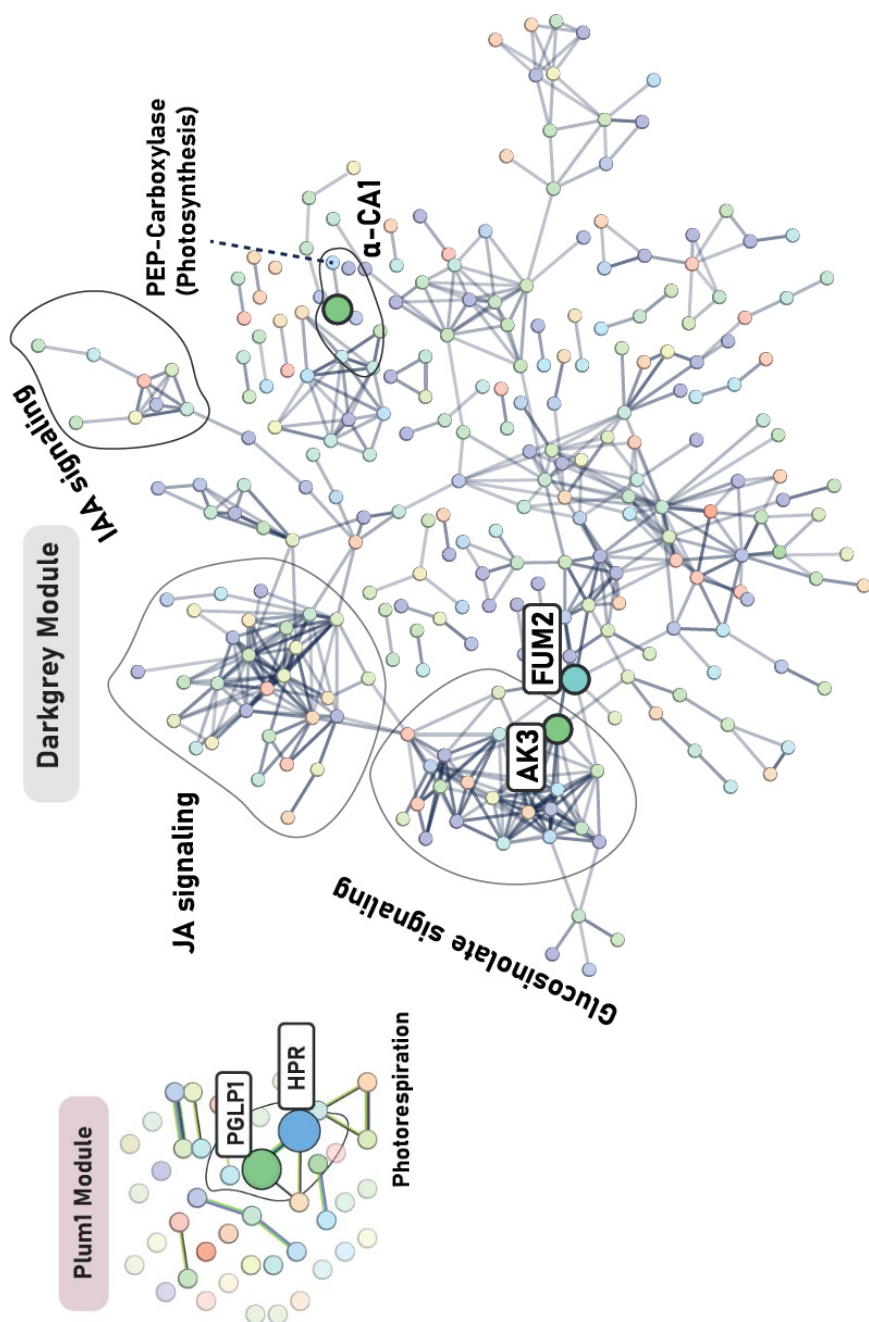


Figure 2.11. WGCNA analysis. Relationships of co-expression modules and analyzed physiological traits. Each row in the table corresponds to a co-expression module, and each column to a trait. Numbers in the matrix report the correlations of the corresponding module genes and each trait, with the p values below the correlations in parentheses. The table is color coded by correlation according to the color legend.



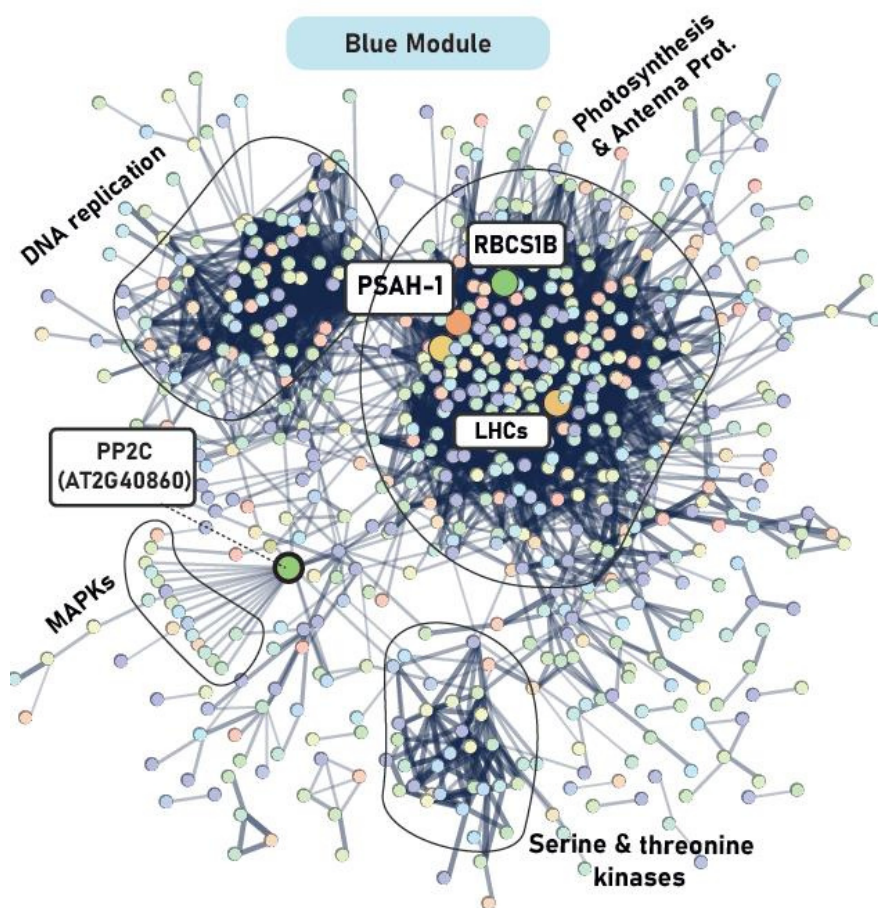


Figure 2.12. Overview of WGCNA co-expression modules significantly correlating to alkaline salinity tolerance traits. Protein-protein interaction (PPI) network of all DEGs comprised in darkgrey, plum1 and blue WGCNA co-expression modules, based on the STRING online database (<https://stringdb.org/>). Proposed candidates identified in each module and appearing on each PPI Network are indicated, and main signaling pathways enriched per module encircled.

Overall, the combination of multivariate analysis on physiological traits, transcriptome analysis and WGCNA results prove that the selection criteria

performed to assess effects of salinity in the studied demes are an accurate reflection of the whole dataset behavior. This combination provides knowledge on the hub biological processes and metabolic pathways that reflect the differential responses of neutral-salinity-adapted demes when compared to demes with tolerance to moderate alkaline-salinity. Moreover, it gives evidence supporting the involvement of key nutritional (K^+ homeostasis, B sufficiency, Na^+ uptake reduction and Zn limitation) and phytohormonal cues (ethylene, ABA-dependent and independent, JA and CKs contrasted signaling) driving tolerance to salinity.

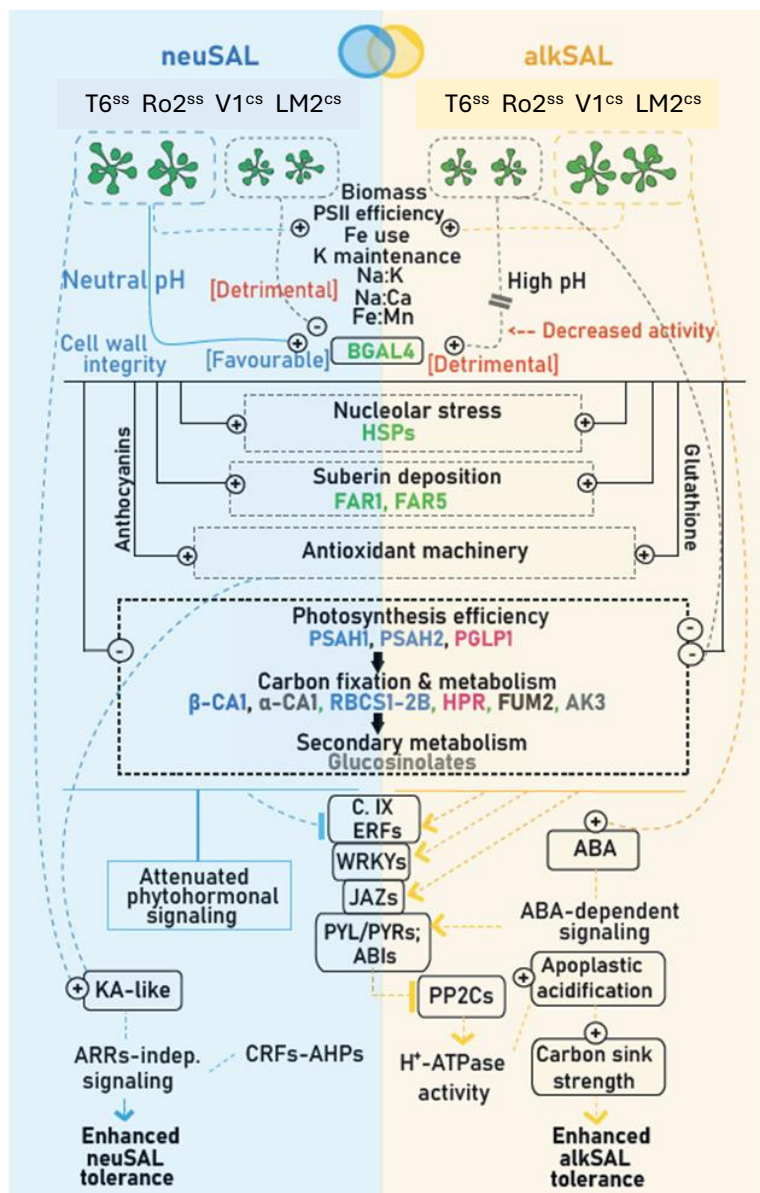


Figure 2.13. Graphical abstract. Blue and yellow blocks represent neutral (neuSAL) and alkaline (alkSAL) treatments. Size of rosette drawings show plant higher (big) or decreased (small) performance under each treatment. Results in-between blocks represent shared responses to neuSAL and alkSAL (coreSAL responses), results on the left (blue block) shows exclusive neuSAL responses and results on the right (yellow block) represents exclusive alkSAL responses. Symbol “+” indicates enhancement of physiology and nutrition traits in the connected demes, transcript up-regulation or pathway activation. Symbol “-” indicates transcript down-regulation or pathway inhibition. “+ +” and “- -” indicate stronger effects in the specified treatment. Gene symbols colored in blue, grey or plum indicate coexpression module to which they are assigned according to WGCNA. All gene symbols point to candidate genes and pathways for *neuSAL* and *alkSAL* tolerance breeding.

Through screening of DEGs with contrasted expression profiles among demes, we propose that a smart regulation of BGAL4, a cell wall and tonoplast hydrolase, is key to tolerate different salt stresses, and identify a SNP at the 5'UTR of V1^{CS} and LM2^{CS} as a pinpointed candidate for the differential regulation of gene expression levels. In contrast, dissection on the down-regulated transcripts at the *coreSAL* set confirms that tolerance to neutral salinity does not confer advantageous features under alkaline salinity. Key genes involved in the photorespiratory cycle – PGLP1, β CA1, RBCS1-2 -, organic acid accumulation – FUM2 - and other secondary metabolism processes for abiotic stress resistance – AK3, glucosinolate biosynthesis genes – could be targets for alkaline salinity resistance breeding. WGCNA analysis confirms that the presented candidates are comprised in co-expression modules significantly correlating with favorable responses to *alkSAL*. In this concern, increasing internal Fe use efficiency for maintenance of photosynthesis rate and Ca, B and K accumulation for decreasing Na-K, Na-Ca, Na-B ratios must be essential targets when facing alkaline salinity stress. The enhanced activation of ABA-dependent signaling is highlighted as a key trait for enhanced performance under *alkSAL* in V1^{CS} and LM2^{CS}, likely by

PYL/PYRs binding to PP2Cs and consequent activation of H⁺ATP-ase activity, allowing enhanced apoplastic acidification.

Methods

Plant material

Seeds of 2 coastal-siliceous (T6^{SS} and Ro2^{SS}) and 2 intermediate-calcareous (V1^{CS}, LM2^{CS}) *A. thaliana* demes were collected from the natural habitat (Figure 2.1) and propagated in the laboratory. The flowchart in Figure 2.2 summarizes the experimental procedures of the study.

Irrigation experiment

Seeds were surface sterilized by soaking them in 30% (v/v) commercial Clorox bleach and 1 drop of Tween-20 for 15 min and rinsed 5 times in 18 MΩmilli-Q sterile water. Seeds were stratified at 4°C for 1 week in the dark and sowed on wet soil. Pots were covered with PVC film until the seedlings germinated. Pots with germinated seedlings were placed in a growth chamber (Conviron CMP5090) with 8 h light / 16 h dark photoperiod, an irradiance of 80 mmol·m⁻²·s⁻¹ and a constant temperature of 22 °C. Plants were watered with 0,5-strength Hoagland solution every 3 days. After 2 weeks, all plants were irrigated every 3 days with 0,5-strength Hoagland solution containing 0,5-strength Hoagland solution alone (control), with 100 mM NaCl (neutral salinity: **neuSAL**) or with 75 mM NaCl and 15 mM NaHCO₃ at pH 8.3 (alkaline salinity, **alkSAL**) for two weeks. The Rosette Diameter (RD) of each sample and the PSII efficiency for 2 different leaves were measured in 3 samples of each deme and condition after two weeks of treatment. After harvest, samples for ionomic analysis were dried and samples for RNA extraction and hormone determination were immediately frozen in liquid nitrogen and stored at -80 °C (n=6 per deme and treatment).

Leaf nutrition

Plant tissues were sampled by removing 2–3 leaves or cutting roots (1–5 mg dry weight). They were then washed with 18 M Ω water before placing them in Pyrex digestion tubes. The sampled plant material was dried for 2 days at 60 °C and weighed before open-air digestion in Pyrex tubes using 0.7 mL concentrated HNO₃ at 110 °C for 5 h in a hot-block digestion system (SC154-54-Well Hot Block, Environmental Express, Charleston, SC, United States). Concentrations of the selected elements (Ca, K, Mg, Na, P, S, Mo, Cu, Fe, Mn, Zn) were determined by ICP-MS (Perkin ElmerInc., ELAN 6000, MA, United States) or ICP-OES (Thermo Jarrell-Ash, model 61E Polyscan, England) (n=4 per deme and treatment).

PSII efficiency

The maximal photochemical efficiency of PSII was calculated from the ratio of variable (F_v) to maximum (F_m) fluorescence [$F_v/F_m = (F_m - F_o)/F_m$] using a MINI-PAM-II/B portable chlorophyll fluorometer (Walz) connected to an Arabidopsis Leaf Clip holder (model 2060-B). The minimum fluorescence yield (F_o) was measured under measuring light (650 nm) with very low intensity (0.8 mmol m⁻² s⁻¹). To estimate the maximum fluorescence yield (F_m), a saturating pulse of white light (3000 mmol m⁻² s⁻¹ for 1 s) was applied. Leaves were dark-adapted for 30 min before measurements and the analysis was performed in a dark room with stable ambient conditions (n=4 per deme and treatment).

Endogenous phytohormones

Phytohormones extraction was done according to the protocol of Pan et al. (2008) with modifications from Delatorre et al. (2017). The phytohormones analyzed were abscisic acid (ABA), indoleacetic acid (IAA), 2-phenylacetic acid (PAA), kinetin (KA), 6-benzylaminopurine (BAP), 1-aminocyclopropane-1-carboxylic acid (ACC), jasmonic acid (JA), and salicylic acid (SA). The following

deuterated standards were employed: ABA-²H₆, IAA-d₅, PAA-d₅, ACC-d₄, JA-d₅, MeJA-d₂ and SA-d₆. All of them were supplied by Olchemim Ltd. (Czech Republic) except SA-d₆ obtained from Sigma Aldrich (St. Louis, MO, USA). Briefly, 0.05 g fresh weight of leaf samples were homogenized in liquid N₂ and extracted with 250 µL of extraction buffer (2- propanol/Mili Q water/Hydrochloric acid; 2:1:0.002; v/v/v) in 1.5 mL Eppendorf tubes (Eppendorf Safe Lock England) and agitated by repeated inversion (60 rpm) for 20 min, at 4 °C, in the dark. The resulting homogenate was transferred to a Teflon tube (Thermo Scientific, England) with 450 µL dichloromethane and reextracted by repeated and inverted agitation for 30 min, at 4 °C in the dark. Three phases were obtained, an aqueous, a material debris and an organic phase. The organic phase (bottom) was recovered, and the intermediate debris phase was also re-extracted. The combined extracts were evaporated under N₂ flow to remove propanol and resuspended 150 µL of 100% methanol. Resuspended extracts were filtered through a 0.22 µm cellulose acetate Spin-X centrifuge tube filter (Costar, Corning Inc., Salt Lake City, USA). Samples were injected into a QTrap4000 LC–ESI(–)–MS/MS system following the method described by Segarra et al. (2006) and modified by Llugany et al. (2013) using HPLC Agilent 1100 (Waldrom, Germany) on a Discovery C18 2.1 × 150 mm ID, 5 µm column (Supelco, Bellefonte, USA) at 50 °C, a constant flow rate of 0.6 mL min⁻¹ and 10 µL injected volume. MS/MS experiments were performed on an API 3000 triple quadrupole mass spectrometer (PE Sciex, Concord, Ontario, Canada). All the analyses were performed using the Turbo Ionspray source in negative ion mode for SA, JA, ABA, IAA, and PAA and in positive mode for ACC, KA and BAP. Quantification was performed by injection of extracted and spiked samples in multiple reaction monitoring (MRM) mode (n=4 per deme and treatment).

Transcriptome profiling

Total RNA Exaction and RNA-Seq Library Preparation. Total RNA was extracted using Maxwell plant RNA kit (Promega Corporation, Madison, WI, USA) following the manufacturer's instruction. The RNA concentration was measured using Qubit® 2.0 Fluorometer (Invitrogen). 4 µg total RNA was used to prepare RNA-seq libraries using the TruSeq Stranded mRNA Library Prep Kit (Illumina, San Diego, US). Strand specific paired-end mRNA sequencing was performed on DNBSEQ platform at the Next-Generation Sequencing Core of the BGI Genomics Service (Hong Kong, China) (n=3 per deme and treatment).

RNA-Seq analysis. We used Bowtie2 (Langmead & Salzberg, 2012) was used to map the clean reads to the reference gene sequence (transcriptome), and then used RSEM (Li & Dewey, 2011) to calculate the transcript abundance of each sample. Quality check of raw sequence data was performed using Fastqc. Reads containing adapters and poly-N and low-quality reads from raw data were removed with Qualimap. Simultaneously, Q20 (percentage of bases with the quality score greater than 20; sequencing error rate less than 1%), Q30 (percentage of bases with the quality score greater than 30; sequencing error rate less than 0.1%), and GC (or guanine-cytosine) content of the clean data were calculated. Paired-end reads were mapped to the TAIR10 reference genome using the STAR aligner and the .sam output of STAR was then converted to its compressed format .bam and sorted by gene identifier with samtools. The overlap of reads with annotation features found in the reference.gtf was calculated using HT-seq (Putri et al., 2022). The output computed for each sample (raw read counts) were imported into BGI data visualization system (<https://www.bgi.com/global/service/dr-tom>) and parsed using DESeq2 (v 1.8.1). Raw counts were normalized using DESeq2's function "rlog," which normalizes sequences according to library size to make them comparable among replicates and transforms the original count data to the log scale. The DEseq2 method is based on the principle of negative binomial distribution (Love et al., 2014). This method was used to perform

differential gene expression analysis (DEG) with an absolute $|FC| > 2$. The p -values were corrected for multiple error testing according to Benjamini-Hochberg (q -value) and q -value threshold of 0.05 was set. According to the results of differential gene detection, the R package pheatmap was used to perform hierarchical clustering analysis and extract expression trends on the union set differential genes.

Gene functional annotation. Gene Ontology (GO) functional significant enrichment analysis - used to analyze molecular functions, cellular components and biological processes - was performed by mapping all candidate genes to each entry in the Gene Ontology database (<http://www.geneontology.org/>). A hypergeometric test was applied to find the GO function significantly enriched in candidate genes compared to all background genes of the species. p -value was calculated using the basis function `phyper` (<https://stat.ethz.ch/R-manual/R-devel/library/stats/html/Hypergeometric.html>) of R and then corrected for multiple error testing according to Benjamini-Hochberg (<https://bioconductor.org/packages/release/bioc/html/qvalue.html>). Finally, a q -value threshold of 0.05 was set, and the GO term that satisfied this condition was defined as the GO term that was significantly enriched in candidate genes. Kyoto Encyclopedia of Genes and Genomes (KEGG) pathway-based enrichment analysis – which links gene sets with a network of interacting molecules in the cell, such a pathway or complex - was performed following the same methodology and significance threshold than for GO functional enrichment analysis. Pathways significantly enriched in differentially expressed genes were identified and visualized through BGI data visualization system (<https://www.bgi.com/global/service/dr-tom>)

Protein-Protein Interaction (PPI) Network Analysis. Protein–protein Interaction (PPI) networks of differential expressed genes were performed on STRING version 11.0. Active interaction sources, including text mining, experiments, databases, and co-expression as well as species limited to “*Arabidopsis thaliana*” and an interaction score > 0.4 were applied to construct the PPI networks.

WGCNA network analysis

Weighted gene co-expression network analysis (WGCNA) was conducted with the “WGCNA” package (Langfelder and Horvath, 2008) on BGI’s Dr.Tom system (<http://biosys.bgi.com>). Gene expression file and trait file were combined, and the soft thresholding power (β value) was filtered based on the calculation of scale-free topological fit index and mean connectivity. The topological overlap matrix (TOM) was constructed based on the topological overlap between pairwise genes, and hierarchical clustering analysis was performed. Cluster dendrogram plot and clustering tree of co-expression modules of DEGs were created. The co-expression relationships among different modules were analyzed and modules with high similarity were merged at a similarity threshold of 0.25 and a minimum module size of 20 genes.

Statistical Analysis

All statistical analyses were performed using JMP SAS software (SAS Institute, Cary, NC, United States). Significant differences for multiple comparisons were determined by one-way or two-way ANOVA as indicated in figure legends, treatment or treatment relative to control (neuSAL/Control; alkSAL/Control) and deme (T6^{SS}, Ro2^{SS}, V1^{CS}, LM2^{CS}) or deme origin [coastal-siliceous_(T6+Ro2); intermediate-calcareous_(V1+LM2)] as independent factors. Comparisons among demes were followed by post hoc Tukey HSD test (adj.

p -value < 0.05). Multivariate Correlation Analysis was performed to determine the level of association among the measured physiological traits for each deme and treatment. Pearson's correlation coefficients were calculated for all pairs of measured parameters under *neuSAL* and *alkSAL* at a level of 5% significance. Principal Component Analysis, eigenvalues and relative proportion of the variance explained by each trait included in MCA were calculated.

Chapter 3



Chapter 3

A genome-wide association study identifies novel players in Na and Fe homeostasis in *Arabidopsis thaliana* under alkaline-salinity stress

Introduction

Plant responses to abiotic stress are presumably shaped by a combination of adaptation to the local environment, accumulation of mutations, gene flow between the populations and random effects. Local adaptation is particularly relevant in the face of the global changes our planet is exposed to, because locally adapted populations can become maladapted if environmental conditions change rapidly (Olivas et al., 2017). When studying the genetic mechanisms and the extent of local adaptation, understanding the genetic basis of fitness variation across different ecological conditions is of major importance. This includes identifying the loci associated with individual fitness in different natural environments, the distribution pattern and environment specificity of adaptive variants and the type of genes involved.

The diversity of stress responses present within one species can be harnessed by screening natural diversity panels and performing subsequent Genome-Wide Association Studies (GWAS) to identify genetic components of various stress responses, as has been done in the past for e.g., salinity (Rus et al., 2006, Baxter et al., 2010, Katori et al., 2010), carbonates (Pérez-Martín, 2021; Terés, 2017) or combinations of stress factors (Kawa et al., 2016, Olivas et al., 2017). GWA studies enumerate underlying SNPs (single nucleotide polymorphisms) responsible for certain phenotypic traits by exploiting the natural variation in a population or collection of populations of the studied species (Weigel, 2012, Ogura & Busch, 2015). More specifically, GWAS evaluate the statistical significance of associations between differences in a quantitative phenotype and genetic polymorphisms tested across many

genetically different individuals by using linkage disequilibrium (LD), based on non-random association between alleles and phenotypes (Uffelmann, 2021). GWAS identifies associations between marker SNPs and phenotypes without the need of constructing special mapping populations, and it uses high recombination in natural populations instead (Korte & Farlow, 2013, He et al., 2017, Bazakos et al., 2017). The candidate genes identified by GWAS can eventually serve to guide marker-assisted breeding and the genetic modification of crops (Li, 2020). In this regard, recent reviews (Liu et al., 2020) point to GWA studies as an increasingly successful analysis in the identification of key genes that are useful for agronomic traits of interest.

In the model plant *Arabidopsis thaliana*, GWAS are a powerful approach to identify loci associated with fitness and abiotic stress responses. Multiple growth and reproductive life history traits showing natural variation along geographical gradients such as flowering time, seed dormancy, growth rate, resistance to abiotic stresses, defense related traits, ionome profile or root growth have proven to be good input data sets for GWA analyses. Atwell (2010) demonstrated for the first time the power of GWAS for describing the genetics of natural variation in such traits in *A. thaliana*, many of them of great agricultural importance.

Stress resistance is one of the most ecologically relevant traits in a plant species. Due to its agronomic importance, salinity is among the most studied abiotic stress factors (Knight et al., 1997; Shabala, 2005; Julkowska, 2014). Since the start of GWAS in *A. thaliana*, important achievements have been obtained in revealing new genes and mapping new Quantitative Trait Loci (QTLs) for salinity tolerance. For example, by means of association mapping of ionome profile data of 394 *Arabidopsis* accessions, Baxter (2010) identified *HKT1* as one of the major contributing factors to natural variation in Na⁺ accumulation in shoots. *HKT1* was previously known to be involved in sodium-driven potassium uptake (Rubio et al., 1995), sodium uniport in roots (Laurie

et al., 2002; Haro et al., 2005), differential Na⁺ accumulation in aerial parts (Rus et al., 2006), and shoot Na⁺ exclusion and salt tolerance (Møller et al., 2009). *HKT1*, together with *CYTOCHROME P450 FAMILY 79 SUBFAMILY B2* and *B3* (*CYP79B2/B3*) were later confirmed as new components contributing to lateral root hair development under salt stress by performing GWAS on root traits from the *Arabidopsis* HapMap collection (Julkowska et al., 2017). GWA mapping of salinity tolerance in cultivars of interest like rice (Kumar et al., 2015; Warraich et al., 2020; Nayyeripasand et al., 2021), barley (Fan et al., 2016, Hazzouri et al., 2018, Mwando et al., 2020), soybean (Zeng et al., 2017, Do et al., 2019, Zhang et al., 2019, Jin et al., 2021), cotton (Yasir et al., 2019), or wheat (Chaurasia et al., 2021) have been cutting-edge studies performed in recent years.

Alkaline-sodic environments are defined by a high OH⁻ concentration in the waters and soils accompanied by the dominance of sodium base cations in both dissolved and exchangeable forms. In this context, excess of dissolved carbonate species is required for the development of alkalinity and the increase of the dispersive power of sodium (Jobágyi et al., 2017). Soil carbonates have been much less explored through GWAS as a potential driving agent of natural variation. Most studies focus on the deficiency of iron (Mamidi et al., 2014, Satbhai et al., 2017, Assefa et al., 2020 and Xu et al., 2022, in *Arabidopsis*, chickpea, soybean and maize, respectively) or phosphorus (Liu et al., 2015 and Reddy et al., 2020, in mungbean) when studying the effects of alkalinity stress. The cited studies lead to the identification of new candidate iron responsive genes such as AT1G01580/*FRO2* (Mamidi et al., 2014; Satbhai et al., 2017) and At5g53970/*NAAT1*, Os03g0237100/*DMAS1*, GRMZM5G812538/*YSL11*, AT4G19690/*IRT1*, AT1G10970/*ZIP4* and AT2G25490/*EBF1* (Xu et al., 2022).

In nature, multiple stress factors occur simultaneously. Thus, assessing how plants respond to a combination of stresses is ecologically more

representative of how their performance will be under field conditions. In areas with arid and semi-arid climates, like the Mediterranean region, soil salinity often co-occurs with alkalinity due to the movement of soluble ions like Na^+ , Ca^{2+} , Mg^{2+} , K^+ , CO_3^{2-} and HCO_3^- to the superficial soil layers produced by the increase in evapotranspiration rates (Singh, 2021). Alkaline-salinity stress has gained importance, in the last decade, as a major limiting factor for world crop production (Huang et al., 2015, Bai et al., 2018, Zhao et al., 2021). Around 831 million hectares of the Earth are covered by alkaline-saline soils (FAO 1973). Alkaline-saline stress exerts complex harmful effects on plants in the form of osmotic pressure, ion toxicity, nutrient deficiency, and high pH (Liu et al., 2021). Alkaline salts inhibit germination, growth, photosynthesis, and root system activity, and are reported to increase shoot Na^+ and ion imbalance with higher intensity than neutral salts in *Lathyrus quinquenervius* (Zhang et al., 2009). When compared to NaCl stress, alkaline-saline stress can increase the activities of H^+ -ATPase and H^+ -VPPases, which are proton-driven forces for Na transport at the cell and vacuolar membranes (Deinlein et al., 2014; Ye et al., 2019). Sodium sequestration into vacuoles takes place through SOS2/SOS3 kinase-regulated *SOS1* and *NHX1*, a process sensitive to Ca^{2+} ions (Bahmani et al., 2015; Fang et al., 2021). Thus, adequate Ca levels are essential under alkaline salinity. To a limited extent, alkaline salt tolerance has been explored by means of association mapping in the last decade. A major QTL allele from wild soybean was identified for increasing alkaline salt tolerance (Tuyen et al., 2010). Epistatic association mapping in 257 soybean cultivars with 135 SSR markers was performed to assess salt tolerance under control, NaCl or Na_2CO_3 conditions and small-effect QTLs were identified for further confirmation (Zhang et al., 2014). More recent association studies have provided novel candidate locus to crop breeders for improving saline-alkaline adaptation (Cao et al., 2020).

Here, we use a natural alkaline saline soil to assess the variation in growth and nutritional status in a set of 270 natural accessions of the widely distributed model species *A. thaliana* and we explore the molecular genetic mechanisms underlying possible stress responses to alkaline salinity. In this study, soil complexity was embraced by performing GWAS on natural saline calcareous soil from a coastal Mediterranean region. There is high variation in the mineral nutrient accumulation among different populations within a species depending on the chemical composition, nutrient, and trace element bioavailability from their native soils (Baxter et al., 2012). Therefore, the natural variation in the ionic profiles of the studied *A. thaliana* accessions was used as the main phenotype for this GWAS.

Results

Arabidopsis thaliana HapMap performance on saline calcareous soil

A total of 270 accessions constituting the HapMap collection (Horton et al., 2012) were grown for 8 weeks on a saline carbonated soil (SCS) excavated from a coastal region of the northeast of Spain. The geographical location of the accessions used in this study and the physicochemical properties of the SCS are described in Dataset S3.1 and Figure 3.2A-B. Figure 3.1 details the workflow and the *A. thaliana* accessions and mutants used in each experiment.

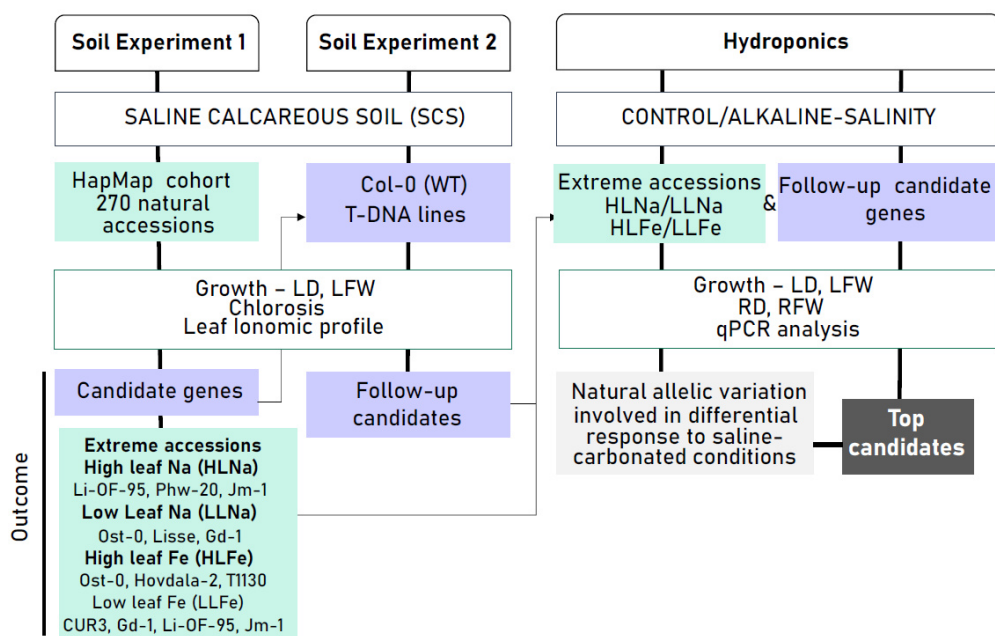
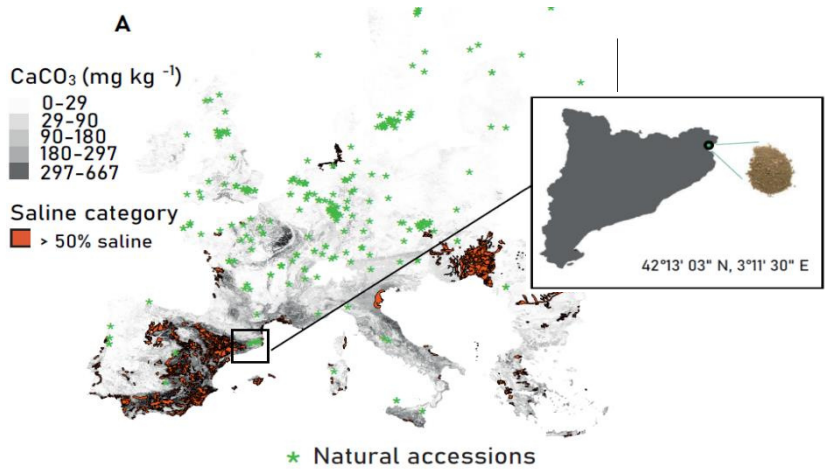


Figure 3.1. Flowchart of the experimental procedure. Different color boxes define plant material used at each experimental stage: Turquoise: HapMap cohort accessions; Purple: Col-0 (Wild-Type) and T-DNA insertion mutant lines.

Selecting an adequate soil to mimic the conditions of representative saline carbonated soils in Mediterranean areas was prioritized. As soil-forming factors and dynamics are interdependent processes that create a unique and high complex system, no commercial soil was considered reliable as a control and plant performance was only assessed on SCS.

High natural variability was observed for rosette diameter (RD) of 8-weeks-old plants among all the accessions (Dataset S3.2). We classified the studied accessions according to their RD into low diameter (LD) and high diameter (HD) groups, based on the 10% tails of the RD normal distribution. Differences in RD were statistically significant among the two groups (Table S3.1; Figure 3.3A).

Elemental profiling of leaf tissue was performed for three plants of each of the 270 studied accessions (Dataset S3.2). To understand the relationship between the elemental concentrations, we performed multivariate correlation analysis on the 10 quantified leaf mineral nutrients and the rosette diameter traits and clustered the elements based on their degree of correlation. The



B

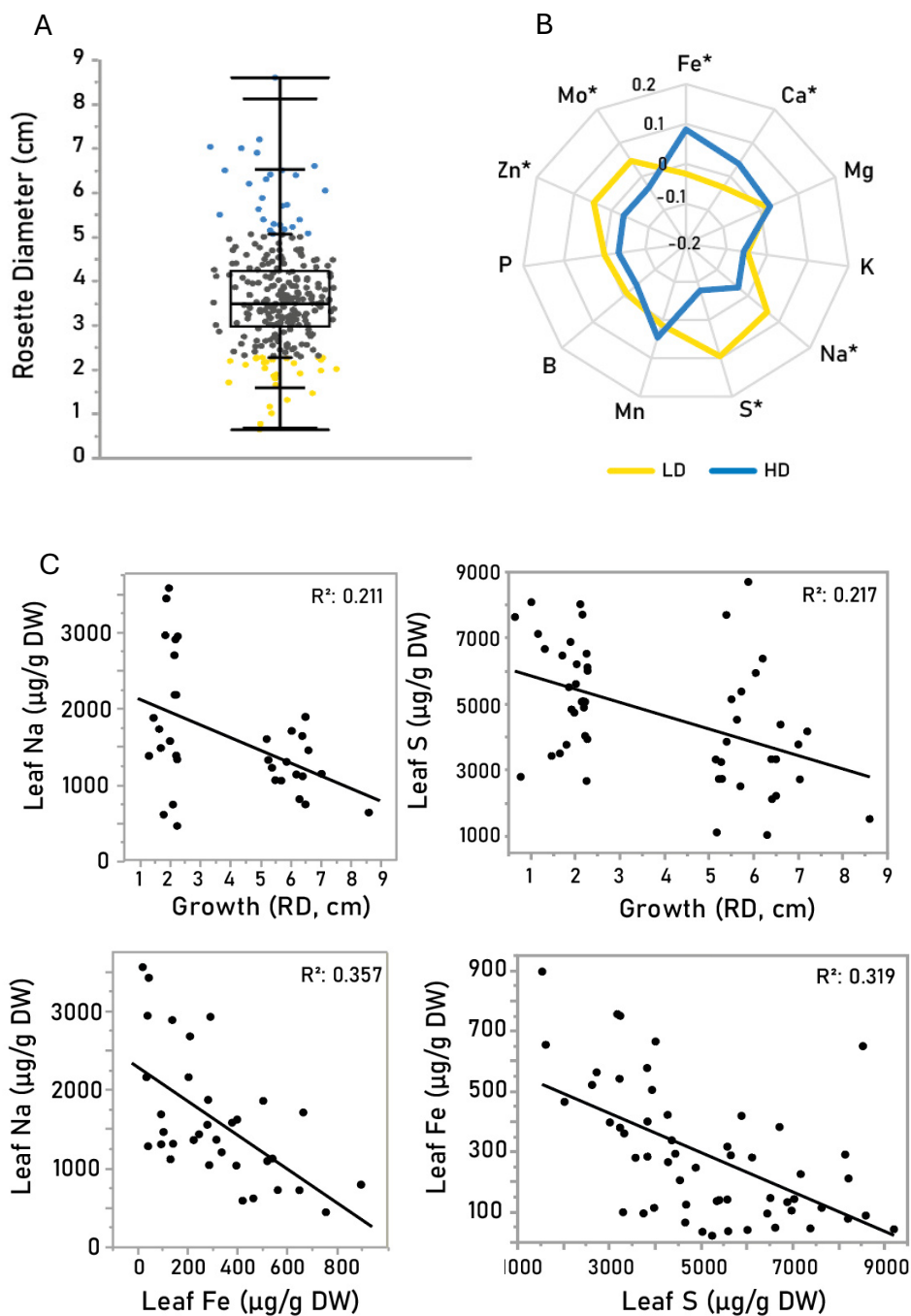
SCS Study Soil

pH (1:2.5)	8.44 ± 0.05
CE uS/cm	486.63 ± 20.4
%CaCO ₃	18.86 ± 5.02
Na (µg/g)	92.28 ± 31.6
K (µg/g)	63.23 ± 2.5
Ca (µg/g)	395.91 ± 13.4
Mg (µg/g)	27.02 ± 4.4
P (µg/g)	6.01 ± 0.4
S (µg/g)	15.98 ± 5.0
Fe (µg/g)	12.12 ± 0.8
Mn (µg/g)	9.65 ± 0.4
Mo (µg/g)	0.02 ± 0.01
Zn (µg/g)	0.92 ± 0.06

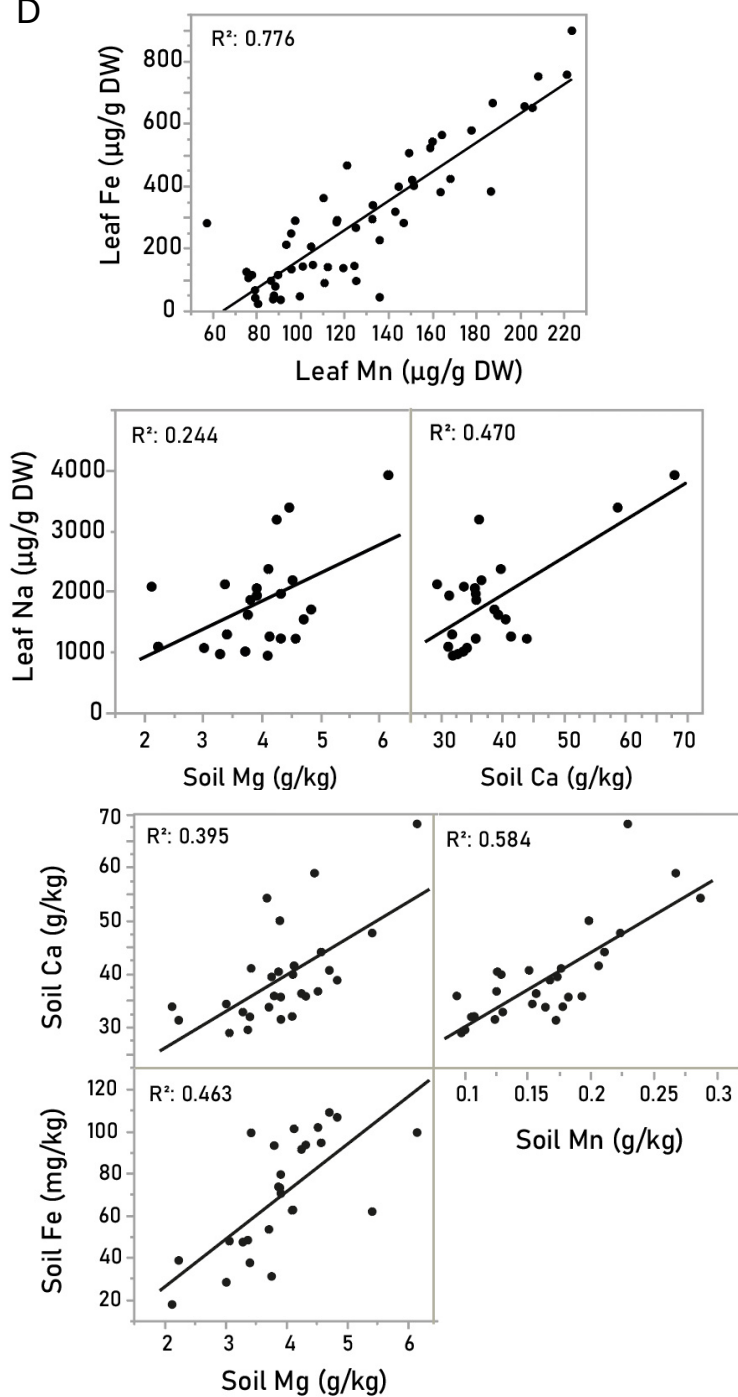
Figure 3.2. Plant material and soil of study. (A) Distribution of saline and calcareous soils in Europe. Green dots indicate the location of origin of the 360 accessions of the HapMap collection. Red area is categorized as saline (>50% surface), and CaCO₃ content (mg kg⁻¹) is shown (grey-scale legend). Frame shows the map of Catalunya, indicating the location of the saline calcareous soil (SCS) used in the experiment; (B) physico-chemical characterization of SCS.

highest positive and negative correlations were found between leaf Fe - Mn ($R^2=0.78$) and Fe - K ($R^2=0.64$), respectively. Leaf Fe concentrations were strongly correlated to several elements under SCS alkaline salinity conditions besides Mn and K and showed a positive correlation to Ca ($R^2=0.29$) and negative correlation to S and P ($R^2=0.27$). Although to a less degree, leaf Na displayed significant positive and negative correlations only with Fe ($R^2= 0.10$) and S ($R^2= 0.10$). Na and S were the only measured elements showing a significant negative correlation with rosette diameter (RD) ($R^2 = 0.05$; $R^2 = 0.06$). Results are represented in the correlogram, clustered heatmap and scatter plot matrix (Figure S3.1A-C).

Next, leaf element concentrations were compared among the established growth performance groups to further characterize element interactions under SCS and their effects on plant performance. Overall, accessions from both LD and HD (worst and best performance, respectively) showed remarkably different ionic profiles when compared to each other. Individuals from LD had significantly lower Fe concentration and higher leaf Na concentration than individuals from HD. In turn, HD accessions contained significantly less Zn, S and Mo and more Ca than those from LD (Figure 3.3B). Nutrient ratios with known biological significance in plant growth and nutrition were also assessed in the two groups of accessions. LD plants showed significantly higher Na:K, Mg:Ca, Zn:Fe, S:Fe ratios and significantly lower Fe:Mn ratios than those from the HD group (Figure S3.2). We confirmed that RD was negatively correlated to leaf Na and S content. In turn, the negative correlations between leaf Fe - leaf Na and leaf Fe - leaf S were endorsed, whereas strong positive correlation between leaf Fe – leaf Mn was found (Figure 3.3C).



D



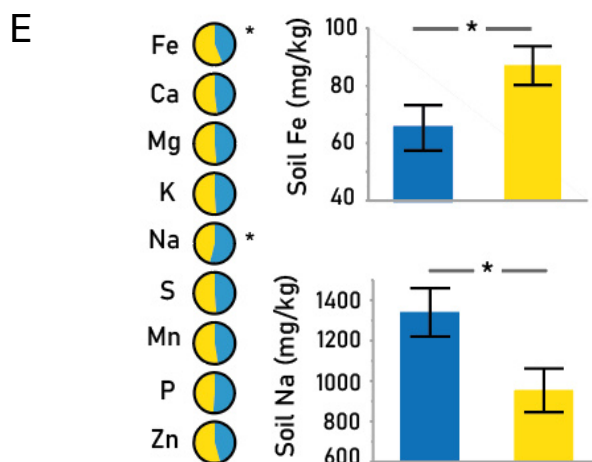


Figure 3.3. Phenotypic analysis of the studied accessions grown on saline calcareous soil (SCS). (A) Scatter plot of the rosette diameter (cm) of all accessions grown on SCS. Each dot represents an accession. Growth categories were established by selecting accessions on the 10% top (blue) and 10% lowest (yellow) rosette diameter. HD: High Diameter group; LD: Low Diameter group; (B) Radial plot with the Z-values of the studied elements in leaves of HD and LD accessions. Axes display Z-scores calculated per element and asterisks show significant differences among the two extreme groups (Student *t*-Test, $p < 0.05$); (C) Pairwise correlation between leaf mineral nutrients and growth performance (Leaf Na and RD, leaf S and RD, expressed as $\mu\text{g g}^{-1}$ DW and cm, respectively), and between different leaf mineral nutrients (Na and Fe, Fe and S, Fe and Mn, expressed as $\mu\text{g g}^{-1}$ DW); (D) Pairwise correlation between leaf mineral nutrients and SCS soil element concentrations (Leaf Na and soil Mg and Ca, expressed as $\mu\text{g g}^{-1}$ DW and g Kg^{-1} respectively), and between different SCS soil element concentrations (Ca and Mg, Fe and Mg, Ca and Mn, expressed as g Kg^{-1}). The lines represent the result of linear regression. R^2 : Squared Pearson correlation's coefficient; (E) Chart pie of nutrient content in the native soil of HD (blue) and LD (yellow) accessions. Asterisks and histograms show the two elements displaying significant differences among the two groups (Student *t*-Test, $p < 0.05$). Plants were grown on SCS for 8 weeks ($n = 4$).

The leaf ionome is largely dependent on the soil nutrient availability. It is well known that geographically widespread *A. thaliana* accessions have evolved mechanisms to balance their nutritional needs based on availability of

nutrients in the site of origin (Campos et al., 2021). Thus, we further considered the correlations between the leaf and soil nutrients in the study accessions, and the relations among different soil nutrients at their natural habitats. Leaf Na concentrations correlated positively with concentrations of Mg and Ca in the soil of origin. Likewise, high soil Mg and Ca strongly correlated with high soil Fe and Mn, respectively (Figure 3.3D).

Finally, we analyzed the correlation between RD and leaf elemental profile on SCS and the properties of their soil of origin to further explore the possible relationship between geographic regions and the leaf ionome under alkaline salinity (Figure 3.3E). Estimated soil Na content and other elemental profile data of the native soils of the tested accessions were extracted from public maps of the European Soil Data Centre (ESDAC) and previous studies (Busoms et al., 2021) (Dataset S3.2). As shown, accessions from HD belong to soils with more elevated Na and more limited Fe concentrations than accessions from LD.

Detection of SNPs associated with differential leaf elemental profile on saline calcareous soil

To identify genomic regions underlying the differential growth and ionic responses to alkaline salinity, we conducted GWA analysis on leaf elemental profiles of the accessions grown for 8 weeks on SCS. We identified several significantly associated SNPs using a 25% FDR threshold calculated by the Benjamini-Hochberg procedure. From the 10 phenotypes analyzed, two traits gave significant associations: LNa and LFe (Figure 3.4). Manhattan plots for rest of leaf ion concentration phenotypes are provided in Figure S3.3. A single strong peak of SNPs associated with leaf Na⁺ at Chr 4, with the peak centered

on *AtHKT1*. Previous QTL mapping and GWAS identified QTLs for leaf Na^+ centered on *AtHKT1* (Rus et al., 2006; Baxter et al., 2010). Such genetic evidence supports that the peaks of SNPs associated with leaf Na^+ and Fe^+ observed in our GWA analysis represent true positive associations and not a false positive caused by high degree of population structure present in *A. thaliana* (Atwell et al., 2010). To account for a possible effect of the *HKT1* locus on the identification of the other loci identified in this GWAs, *HKT1* allelic variations in HD and LD accessions were assessed. The strong *HKT1* variant was confirmed for all accessions used in further analyses. Other significantly associated SNPs [$-\log_{10}(p) > 6.42$; see Methodology] were identified on chromosomes (Chr) 1 (SNP 1) and 4 (SNP 2) for LNa, and on Chr 1 for LFe (SNP 3). A SNP for LNa at Chr 4 with LOD score 5.56 mapping 40 Kb upstream SNP 3 was included in the analyses (SNP 4) for being in moderate LD with SNP 3 ($R^2 = 0.4$), in order not to rule out any potential candidate, as sub-threshold signals with proximity to putative candidate genes have been previously selected to identify novel loci involved in the studied response (Wang et al., 2016). The scores, positions, genes associated with the detected SNPs and genes included in the linkage disequilibrium (LD) regions are detailed in Table S3.3. The function and localization of all candidate genes included in the quantitative trait locus (QTL) regions was examined for all described peaks. This led to a total of 22 candidate genes for analysis from which AT4G28900 was a transposable element and discarded. The other 21 genes were selected to identify the causal gene(s) underlying each QTL association to the observed phenotypes.

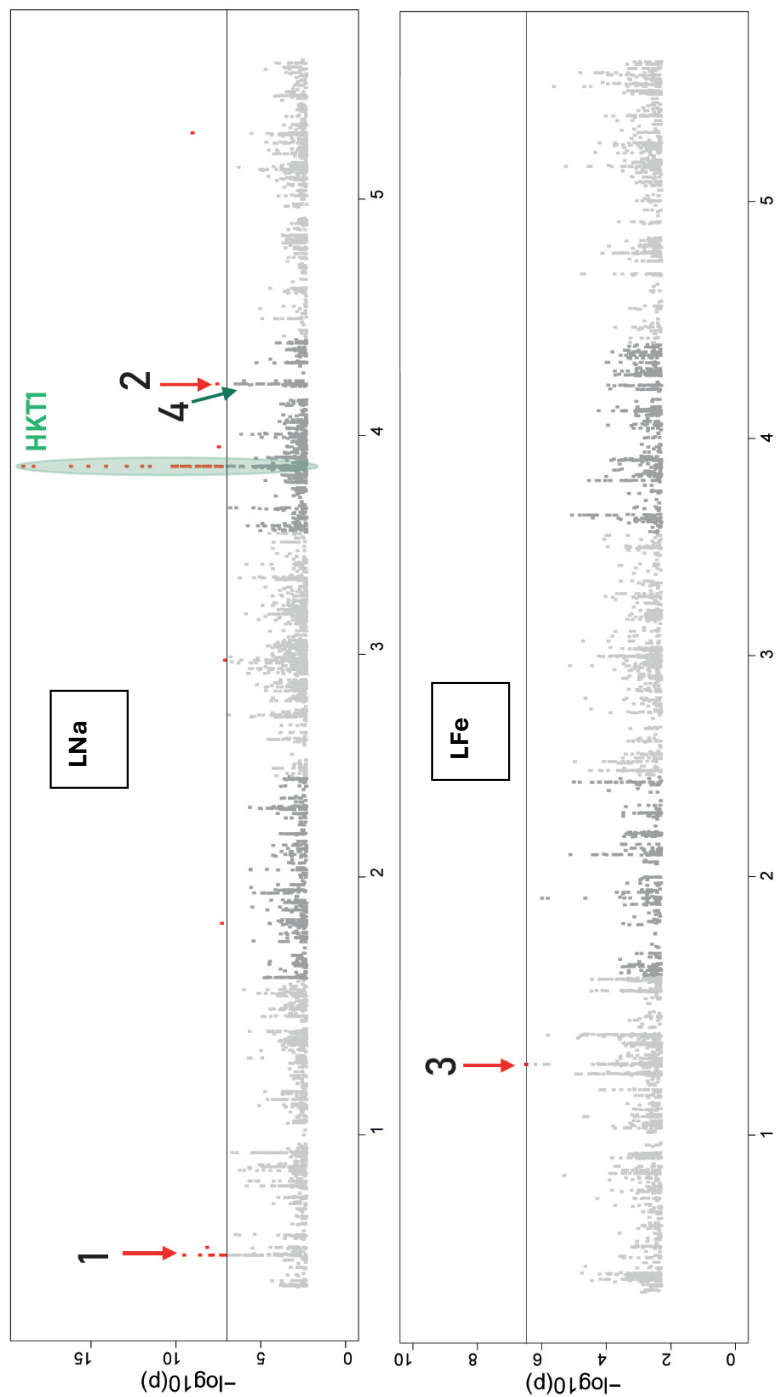


Figure 3.4 Genome wide association studies (GWAS) for leaf ionome traits of HapMap accessions grown on SCS. Manhattan plots displaying the GWAS results for (a) leaf Na concentration and (b) leaf Fe concentration in the studied accessions. The horizontal grey dash-line corresponds to a nominal 0.05 significance threshold after Benjamini Hochberg (False Discovery Rate) correction. Numbers, red dots and arrows indicate the regions containing the significantly associated locus. Peak of SNPs centered on *HKT1* is circled and labeled. Blue arrow indicates SNP included independently from SNP 3 in the analysis. X-axis: chromosomal position of SNP; Y-axis: $-\log_{10}(\text{p-value})$. Plants were grown on SCS for 8 weeks (n = 4).

Among the selected candidates three transporters were found: one mitochondrial transporter, AT1G10680 (*P-glycoprotein 10*, *PGP10*), one cytoplasmic vesicle transporter AT1G10730 (*Adaptor protein-1 mu-adaptin 1*, *AP1M1*) and one Golgi to plasma membrane transporter, AT1G59820 (*Aminophospholipid ATPase 3*, *ALA3*). *PGP10* encodes a P-glycoprotein from the ABC Transporter Family. It associates with differential leaf Na accumulation together with *AP1M1*, which encodes a protein belonging to the clathrin adaptor complex medium subunit family (Qiao et al., 2010). *ALA3* encodes a transporter involved in Golgi to plasma membrane phospholipid transport (Poulsen et al., 2008) and associated with differential leaf Fe accumulation.

Another four genes are regulating or involved in kinase activity: one encoding a nuclear kinase inhibitor, AT1G10690 (*Siamese-Related 8*, *SMR8*), one encoding a phosphoribosyl pyrophosphate synthase, AT1G10700 (*Phosphoribosyl pyrophosphate synthase 3*, *PRS3*) and two Casein-Kinase-I-like protein coding genes, AT4G28880 (*CKL3*) and AT4G28860 (*CKL4*). All four genes associated with differential leaf Na accumulation. *SMR8* and *PRS3* mapped to Chr1. *CKL3* and *CKL4* mapped to chromosome 4 and both CKL proteins act as signal transducers mainly in the blue light signaling pathway (Tan et al., 2013).

Two genes associated with the two SNPs mapping on Chr 4 for leaf Na accumulation are involved in phytohormone biosynthesis and signaling pathways: AT4G28720 (*YUC8*) and AT4G28910 (*NOVEL INTERACTOR OF JAZ, NINJA*). *YUC8* encodes a member of the flavin-binding monooxygenase family protein, which is involved in auxin biosynthesis and active in the nucleus. The gene is expressed mainly in flowers and shown to be ethylene responsive (Qin et al., 2017). *NINJA* encodes a transcriptional repressor that functions in the jasmonic acid (JA) signaling pathway, has a role in root development, and a key role in leaf development (Pauwels et al., 2010). It is also involved in the adaptive responses to salt stress (Ismail et al., 2014). Two other genes included in the same LD region as *YUC8* and *NINJA*, are AT4G28730 (*GrXC5*) and AT4G28850 (*ATXTH26*), respectively. *GrXC5* encodes a Glutaredoxin Family Protein with glutathione disulfide oxidoreductase activity. It belongs to the Class I or “Classic” *GRX*’s, which are involved in stress response (Couturier et al., 2011). Specifically, *GrxC5* is present only in Brassicaceae and its dimeric holoprotein incorporates a [2Fe-2S] cluster. *ATXTH26* encodes a xyloglucan endotransglucosylase/hydrolase involved in root growth and cell wall extension (Maris et al., 2009). Another gene with a known biological function in this LD region is AT4G28750 (*PSAE-1*), encoding a protein from the Photosystem I reaction center subunit IV, involved in the response to light stimulus and mRNA binding.

Another gene with promising roles in nutrient homeostasis present in the LD region of SNP 4 associated with differential leaf Fe concentration: AT1G59830 (*Protein phosphatase 2a-1, PP2A-1*). *PP2A-1* encodes a serine/threonine phosphatase, which reverses the actions of protein kinases. It is a regulator of stomatal development (Bian et al., 2020) and involved in the response to several abiotic stress factors such as heat (Wang et al., 2010), salt (Hu et al., 2017), oxidative stress (Máthé et al., 2017) or drought (Rahikainen et al., 2016).

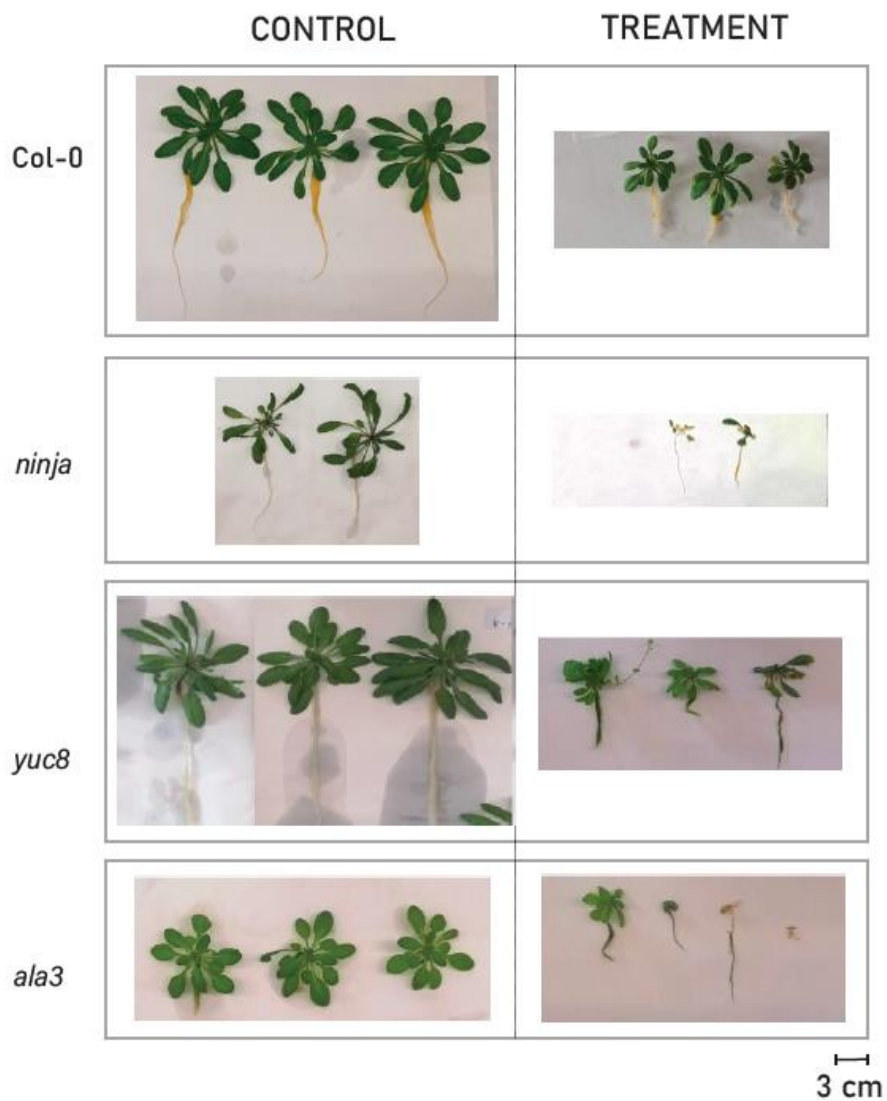
The other genes included in the analyses have roles in secondary metabolic processes (AT1G10690), cellular lipid metabolism (AT1G10720), homologous chromosome pairing at meiosis (AT1G10710), ubiquitin protein ligase binding (AT1G59800) or are described to encode nuclear proteins (AT4G28890 and AT1G59810), with so far unknown functions.

To verify which of the candidate genes included in the analyses were more likely to be responsible for the observed differential LNa and LFe observed under alkaline salinity conditions, we examined available homozygous T-DNA insertion mutant lines for each gene (Table S3.4). No seed viability or homozygous lines were obtained for T-DNA insertion lines for AT1G10690 (*SMR8*), AT1G59810 (*AGL50*), AT4G28750 (*PSAE-1*), AT4G28880 (*CKL-3*), AT1G10730 (*AP1M1*) and AT4G28890 (*ATL42*). A total of 12 KO lines were analyzed.

Mutant phenotyping

The 12 KO lines were grown together with Col-0 (wild type control) on SCS to perform the same phenotyping as conducted with the HapMap studied accessions for the GWAS. In parallel, a plate experiment was performed to observe severity of alkaline salinity effects on seed germination and

distinguish this from seed non viability (lines with no germination neither in control nor in treatment conditions). The effects of alkaline salinity



Picture 1. Phenotyping of mutant T-DNA insertion lines.

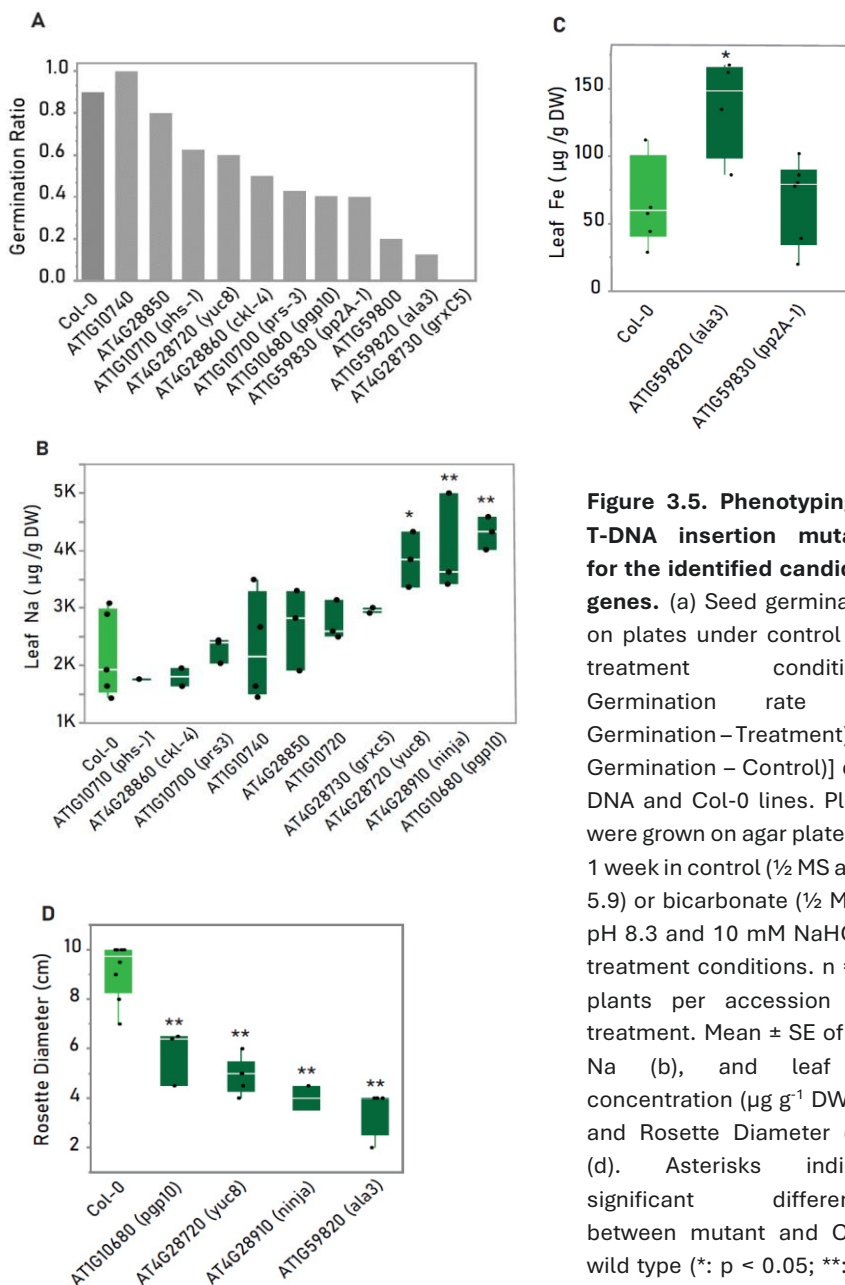


Figure 3.5. Phenotyping of T-DNA insertion mutants for the identified candidate genes. (a) Seed germination on plates under control and treatment conditions. Germination rate $[(\% \text{ Germination} - \text{Treatment}) / (\% \text{ Germination} - \text{Control})]$ of T-DNA and Col-0 lines. Plants were grown on agar plates for 1 week in control ($\frac{1}{2}$ MS at pH 5.9) or bicarbonate ($\frac{1}{2}$ MS at pH 8.3 and 10 mM NaHCO_3) treatment conditions. $n = 10$ plants per accession and treatment. Mean \pm SE of leaf Na (b), and leaf Fe concentration ($\mu\text{g g}^{-1}$ DW) (c) and Rosette Diameter (cm) (d). Asterisks indicate significant differences between mutant and Col-0 wild type (*: $p < 0.05$; **: $p < 0.01$, Dunnett's test). Plants were grown on SCS for 8 weeks ($n =$ up to 6 plants per accession and treatment).

conditions on seed germination for all mutant lines and Col-0 and the performance of each line on SCS are shown in Figure 3.5 A-C. All lines suffered a dramatic inhibition in germination under alkaline salinity conditions (alkSAL) (Figure 3.5A). For both SNPs with the highest associations with LNa on Chr 1 and 4 (SNPs 1 and 3, respectively, at positions 3562288 and 14258447), the Col-0 reference allele was associated with low LNa. From the candidate genes located in the respective LD regions, *pgp10* (Chr 1), *yuc8* (Chr 4) and *ninja* (Chr 4) accumulated significantly higher leaf Na concentrations on SCS (Figure 3.5B). For LFe, the Col-0 reference allele for SNP4 on chromosome 1 (located at position 22010370) associated with low leaf Fe concentration. Significantly higher leaf Fe was observed in *ala3* when compared to Col-0 (Figure 3.5C). Growth constraints were observed in all selected lines when compared to WT (Figure 3.5D). The selected mutant lines for the candidate genes mapping to differential LNa did not show significant alterations in LFe when compared to Col-0 except for *ninja*, which also displayed reduced LFe (p 0.034, Dunnett's Test). Similarly, none of the selected mutants for LFe exhibited an altered LNa phenotype in comparison to WT. This indicates the trait specificity of each locus association except for AT4G28910 (*NINJA*) (Figure S3.4).

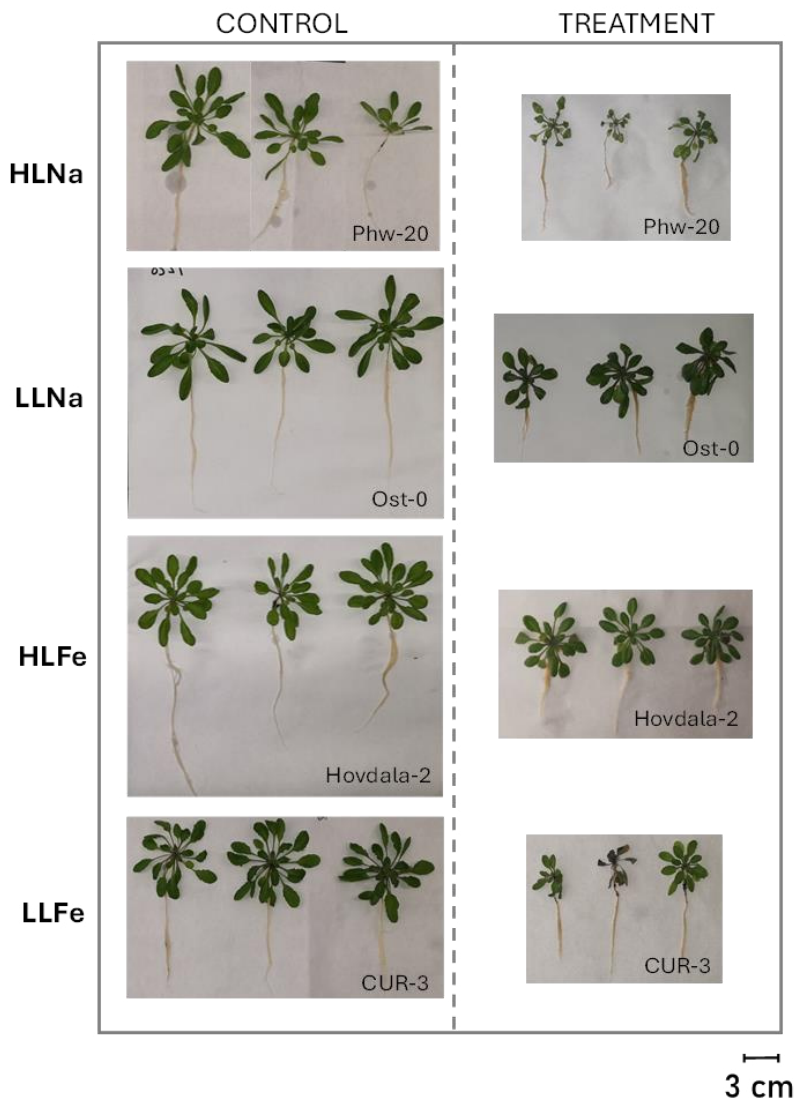
Effects of natural allelic variation of the locus of interest in gene expression and plant growth performance under alkaline salinity

To further identify the causal genes underlying SNP associations, HapMap accessions showing extreme phenotypes (ExtP) for the studied traits were selected as "High Leaf Na" (HLNa), "Low Leaf Na" (LLNa), "High Leaf Fe" (HLFe) or "Low Leaf Fe" (LLFe) accessions according to their leaf Na and Fe contents, respectively (Table S3.5). Plants were re-examined for alkaline-salinity-induced changes in rosette size and ionic profile under hydroponic conditions. The selected ExtP accessions were grown in control and treatment

solutions (0.5-strength Hoagland solution at pH 5.7 for control; 40+10 mM NaCl + NaHCO₃ at pH 8.3 for the alkSAL treatment). Rosette diameter, root length, rosette and root biomass and leaf ionome profiles were assessed after 35 days. Allelic variation at the locus of interest was associated with differential growth (LD, HD) and ionomic responses (HLNa/LLNa; HLF_e/LLF_e) of the studied ExtP accessions. For the locus associated to differential LNa, the alternative variant correlated to the phenotype LD and HLNa (sensitive accession with high leaf Na accumulation) while the common variant correlated to HD, LLNa (tolerant accession with low leaf Na accumulation) (Figure 3.6A). For the locus associated to differential leaf Fe, LD and LLF_e phenotype (sensitive accession with low leaf Fe accumulation) correlated to the common allele variant, while accessions bearing the alternative allele related to HD and HLF_e groups (tolerant accession with high leaf Fe accumulation) (Figure 3.6B).

We measured the expression of the candidate genes in ExtP accessions under control and alkSAL hydroponic conditions. Accessions bearing the alternative and common allele variants for each SNP were pooled separately. On the genes surrounding the LNa peak, *PGP10* expression was not significantly different based on this comparison ($p = 0.89$, Student *t*-test), while *YUC8* and *NINJA* showed significant differential expression in leaves between accessions from group 1 (bearing the alternative allele) and group 2 (bearing the common allele) ($p = 0.003$, $p = 0.015$, $p = 0.046$; Student *t*-Test). Transcript

levels of *PGP10* did not correlate with plant growth ($R^2 < 0.001$) but the relative expressions of *YUC8* and *NINJA* were highly correlated with rosette diameter of each accession under alkSAL conditions ($R^2 = 0.55$; $R^2 = 0.50$ and $R^2 = 0.42$,



Picture 2. Phenotyping of ExtP contrasted accessions.

coefficient of determination of the pairwise correlation) (Figure 3.7A). For LFe

peak, differences in *ALA3* expression were not found in shoots (Figure 3.7B) but roots (Figure 3.9B) ($p = 0.0002$), where gene expression levels correlated positively with plant performance under alkSAL conditions ($R^2=0.45$; $R^2=0.30$, respectively).

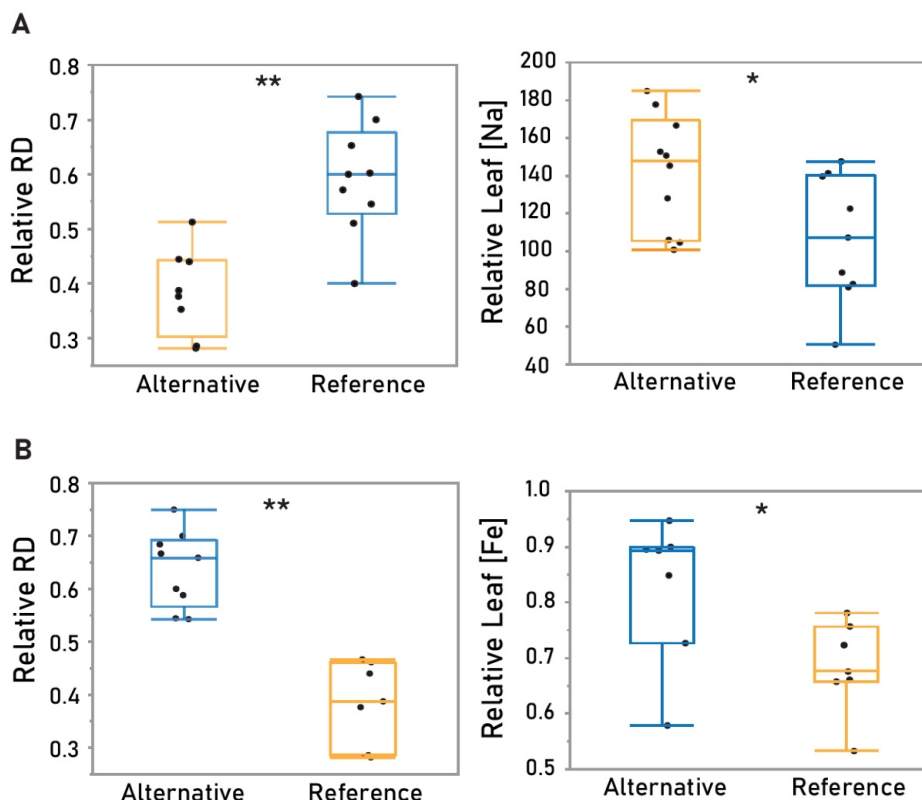


Figure 3.6. Phenotyping of selected accessions displaying extreme phenotypes and contrasted alleles for each SNP of interest under hydroponic conditions. From left to right, mean \pm SE of relative rosette diameter (Relative RD) per allele variant and relative leaf element concentration per allele variant for all LNa (A) and LFe (B) SNPs. Each dot represents 1 individual. Color boxes indicate advantageous (blue) and detrimental (yellow) alleles for each SNP. Plants treated with 0 or 40 mM NaCl + 10 mM NaHCO₃ (pH 8.3) for 2 weeks. Three populations with up to 3 plants per population were pooled per each group. Asterisks indicate significant differences (*: $p < 0.05$; **: $p < 0.01$, Student *t*-Test).

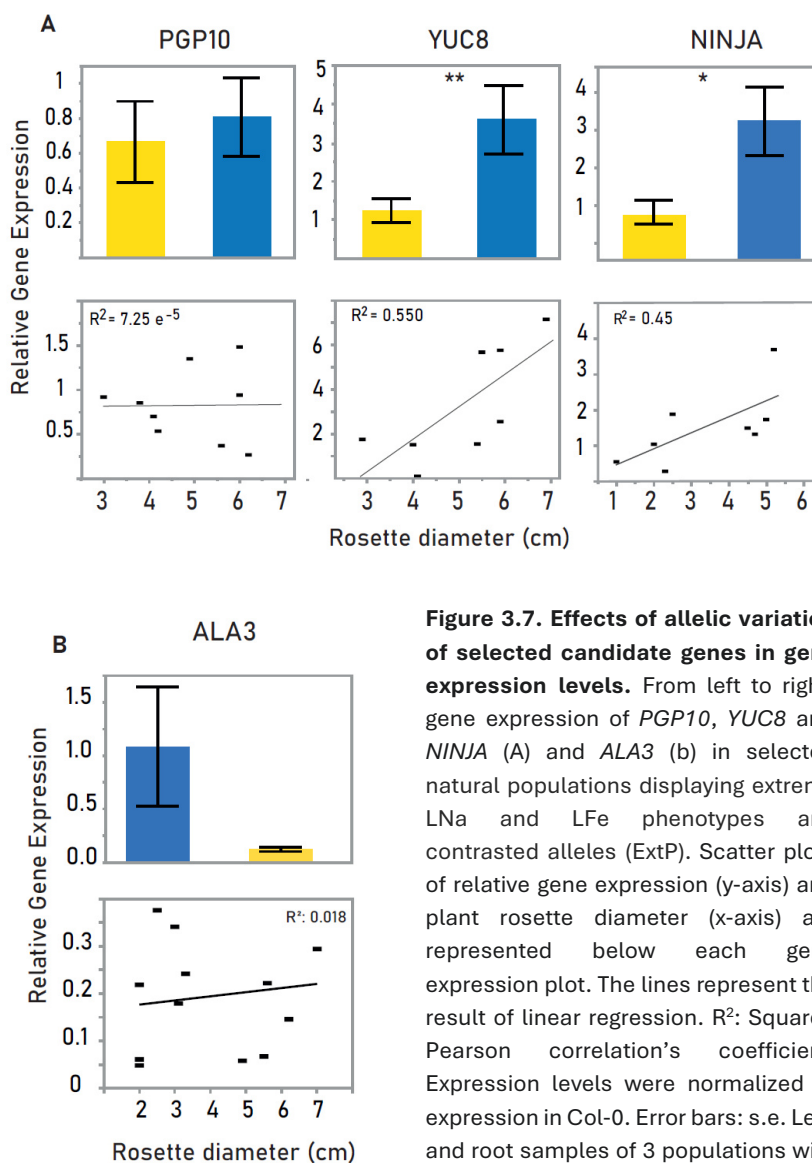


Figure 3.7. Effects of allelic variation of selected candidate genes in gene expression levels. From left to right, gene expression of *PGP10*, *YUC8* and *NINJA* (A) and *ALA3* (b) in selected natural populations displaying extreme LNa and LFe phenotypes and contrasted alleles (ExtP). Scatter plots of relative gene expression (y-axis) and plant rosette diameter (x-axis) are represented below each gene expression plot. The lines represent the result of linear regression. R^2 : Squared Pearson correlation's coefficient. Expression levels were normalized to expression in Col-0. Error bars: s.e. Leaf and root samples of 3 populations with 3 plants per population were pooled per each group. Populations used are listed in Table S5. Data from three independent biological replicates each with two technical replicates are analyzed. Asterisks indicate significant differences (*: $p < 0.05$; **: $p < 0.01$, Student *t*-Test).

Causal polymorphisms at the NINJA, YUC8 and ALA3 locus

After observing that allelic variation at the pinpointed candidates is causal for the differential gene expression level and ultimately for the differential response to alkaline salinity in the study accessions, the identification of most causal sequence polymorphisms was addressed by conducting haplotype analysis on a 50-kb region centered on each candidate gene. The pattern of polymorphisms of different haplotypes that associated with contrasted phenotypes was compared by the analysis of SNPs in intermediate ($R^2 > 0.6$) and high LD ($R^2 > 0.8$) with the GWAS marker SNP.

Three splice variants are associated to the *NINJA* locus. AT4G28910.1 and AT4G28910.2 are 2753 bp, while AT4G28910.3 is 207 bp shorter (2546 bp). The haplotypes of the accessions with highest leaf Na – bearing the alternative allele of the marker SNP – and accessions with lowest leaf Na – possessing the non-reference allele at the marker SNP - exhibit 5 SNPs: one in the 3' UTR, 2 in the first intron for all 3 variants, 1 in the first intron of variant 1 but within the splice region of variants 2 and 3, and one in the first intron of variants 1 and 2 but within the splice region of variant 3. *YUC8* is 1734 bp long with one exon.

Three SNPs in LD with the marker SNP surrounding the *YUC8* coding region were found at the upstream, exon and downstream *YUC8* region. The exonic SNP is a synonymous variant. *ALA3* is a 9083-bp gene. Haplotypes of the marker SNP – and accessions with lowest leaf Fe – possessing the accessions with highest leaf Fe – bearing the reference allele of the alternative allele at the marker SNP - exhibit 4 SNPs: 970 bp upstream the gene coding region, 2 at the promoter region (639 and 529 bp upstream the coding region) and 1 at the third intron. SNP polymorphisms around the *NINJA*, *YUC8* and *ALA3* locus and SNPs differing from the Col-0 reference genome sequence are shown in Table S3.11 and Figure 3.8A-C.

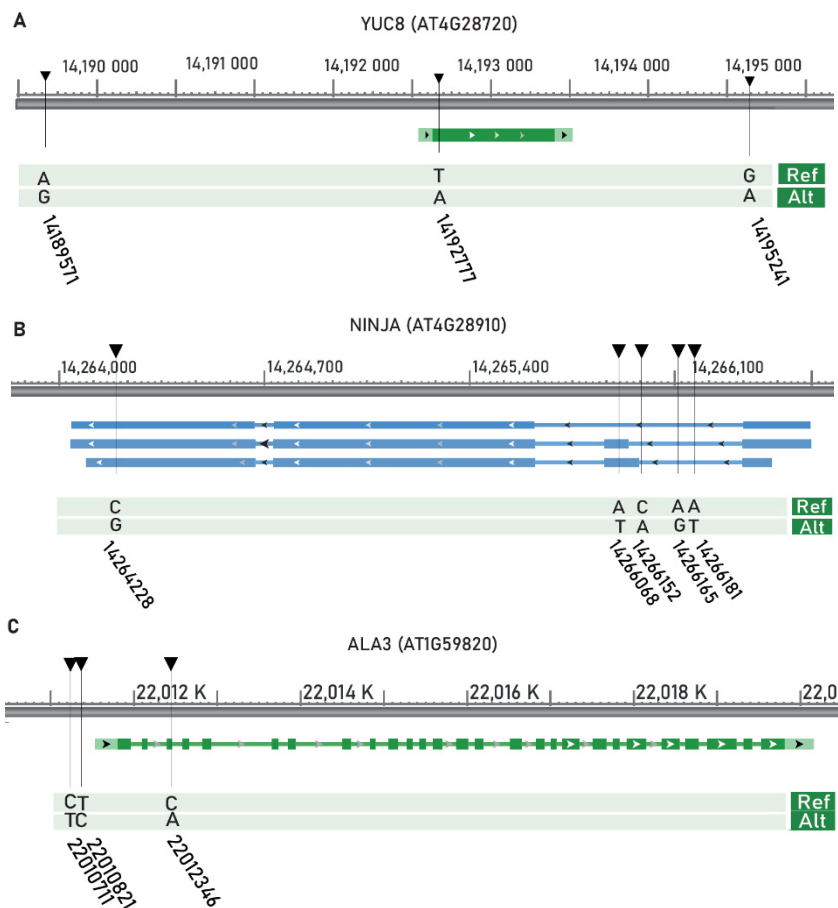


Figure 3.8. SNP polymorphisms surrounding the *NINJA*, *YUC8* and *ALA3* locus. Black triangles and orange lines: most likely candidate SNPs underlying the allelic effects. Gene orientation is indicated with an arrow on the right (A, C) and left (B). Exons are indicated with yellow boxes and introns with lines connecting them. Splice variants are shown when present. Reference and alternative allele nucleotydic changes and SNP position are marked below; chromosome positions are indicated at the top (picture from <https://www.arabidopsis.org/index.jsp>).

Identified novel loci are not masked by effects of known major players in Na and Fe homeostasis

To assess if expression patterns in the pinpointed candidate genes are determined by expression patterns of known major players in salinity and

alkalinity tolerance, the expression levels of *HKT1* and *SOS1* (for the leaf Na SNP) and *FRO2* and *IRT1* (for the leaf Fe SNP) were analyzed in ExtP root samples. *YUC8*, *NINJA* (leaf Na SNP) and *ALA3* (leaf Fe SNP) were included. *SOS1* and *YUC8* did not show differences in root expression levels when comparing the two ExtP pools, while *NINJA* displayed significantly enhanced expression in the ExtP pool bearing the alternative allele ($p < 0.0001$) (Table S3.10.1; Figure 3.9A). *HKT1* followed the same trend and its expression level increased significantly, but these differences were not caused by effects of *HKT1* allelic variation in the ExtP pools, as all used accessions were confirmed to carry the *HKT1* reference (*HLS*, Col-0 -type) allele (Table S3.7). Root *IRT1* and *FRO2* did not show expression differences according to the study group classification, while *ALA3* expression levels were dramatically increased in ExtP accessions bearing the alternative allele ($p=0.0003$) (Table S3.10.2; Figure 3.9B).

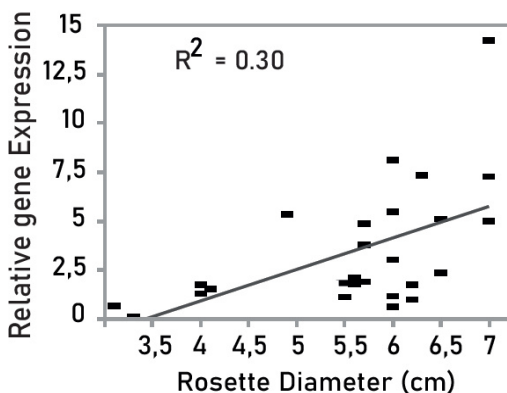
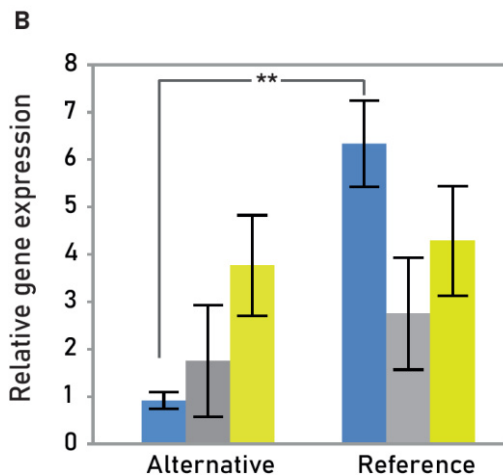
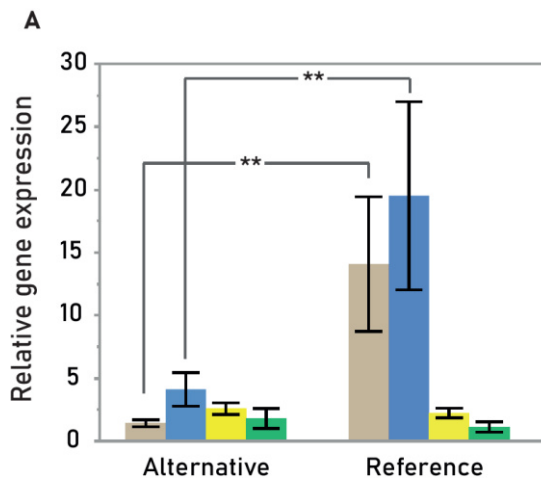


Figure 3.9. Expression pattern of major players in salinity and iron deficiency in roots of ExtP accessions. Gene expression of *NINJA*, *YUC8*, *HKT1* and *SOS1* (A) and *ALA3*, *IRT1* and *FRO2* (B) in roots of ExtP accessions. Scatter plots of relative gene expression (y-axis) and plant rosette diameter (x-axis) are represented below *ALA3* gene expression plot. The lines represent the result of linear regression. R²: Squared Pearson correlation's coefficient. Expression levels were normalized to expression in Col-0. Error bars: s.e. Root samples of three accessions with three plants per accession were pooled per each group. Populations used are listed in Table S5. Data from three independent biological replicates each with two technical replicates are analyzed. Letters a and b indicate significant differences between mRNA expression levels ($p < 0.05$, HSD Tukey).

Discussion

Natural variation in the response of Arabidopsis thaliana HapMap accessions to alkaline salinity

In this study, growth and nutritional status in a set of 270 natural accessions of *A. thaliana* were screened under a natural saline-carbonate soil and the molecular genetic mechanisms underlying stress responses to alkaline salinity were explored by conducting GWAS. Among all accessions surviving to the end of the experiment, two groups were established: LD accessions (Low Diameter – plants below the 10% quartile), with poor adaptation to SCS and HD accessions (High Diameter – plants above the 90% quartile), with good adaptation to SCS. Differences in leaf nutrition, allelic variants of final candidate genes and differential gene expression levels between HD and LD groups under alkaline salinity are discussed.

Footprint of eco-geographical adaptation in the ionomic profiles of A. thaliana natural populations

High natural variation in the ionomic profiles of the 270 *A. thaliana* accessions was observed, in accordance with the high biodiversity in the mineral nutrient accumulation known to exist among different populations within a species reflecting the chemical composition, and the nutrient and trace element bioavailability from their native soils (Baxter et al., 2012). The *A. thaliana* HapMap set of natural accessions comes from habitats with a broad range of soil physicochemical parameters, including Na, Fe and CaCO_3 concentrations. Using a geographically widely distributed collection of accessions offers the opportunity of identifying causal genetic variants important for local adaptation, including those constituting adaptation to a combined stress like alkaline salinity (Miller & Busch 2021). We noticed that

HD accessions originate from sites with higher Na and lower Fe soil concentrations. As expected for poorly adapted accessions, when grown on SCS LD plants display higher leaf Na and lower leaf Fe concentrations than HD plants. SCS study soil has an average EC of $487 \mu\text{S cm}^{-1}$, pH above 8 and an average CaCO_3 concentration of 19%. Thus, it is classified as moderately saline (Fan et al., 2011) and calcareous (Santiago-Martin et al., 2013; Terés, 2017). In arid and semiarid climates, high evapotranspiration rates move soluble Na^+ , Ca^{2+} , Mg^{2+} , K^+ , CO_3^{2-} and HCO_3^- ions to the superficial soil layers leading to the co-occurrence of alkaline-saline soils, which are estimated to cover 831 million hectares of Earth (FAO, 1973). In this context, Fe uptake efficiency is critical to prevent chlorosis under conditions of high soil pH (Hsieh et al., 2016) and salinity aggravates this problem by negatively affecting the acquisition and internal use of Fe by plants (Rabhi et al., 2007, Ben Abdallah et al., 2017; Zhou et al., 2017). The observed results point to the presence of a footprint of eco-geographical adaptation to alkaline saline soils in the study accessions, where not only a reduction in Na uptake or an enhancement in Na compartmentalization (Volkmar et al., 1998), but also an efficient acquisition of iron is advantageous (Li et al., 2016; Yousfi et al., 2007). Altogether it suggests that the enhanced response of HD plants to SCS is shaped by alkaline salinity fitness promoting trade-offs.

HD accessions displayed lower Na:K under SCS when compared to LD individuals. It has been proven that alkaline salinity has a larger effect on the rice root Na:K ratio than salinity alone (Shi & Sheng, 2005). This indicates that maintaining a low Na:K ratio in response to alkaline salinity is a main mechanism of ion homeostasis regulation, as it is for salinity alone (Hu et al., 2022).

The HD group also showed significantly better Fe-S adjustment, as the decreased leaf Fe accumulation in LD accessions was accompanied by a strong increase in leaf S concentration. There is dynamic crosstalk between plant Fe and S networks, which is reported to be critical under low Fe availability (Hantzis et al., 2018) but also under S deficiency (Ostaszewska et al., 2014; Vigani et al., 2016). Here, maintenance of Fe:S is favoring HD individuals under SCS likely by optimizing Iron-sulfur (Fe-S) clusters, which are at the center of photosynthesis, respiration, amino acid, and DNA metabolism (Mendoza-Cózatl et al., 2019). Iron-sulfur clusters are also required for most molybdo-enzymes to function (Bittner, 2014). HD accessions showed significantly lower leaf Mo accumulation. Molybdenum is a primary mineral nutrient highly available in alkaline soils which can interfere with Fe acquisition when present in high concentrations (Alloway, 2013). Mo levels of the study accessions on SCS (2 to 380 $\mu\text{g g}^{-1}$) are much larger than what was found for shoot Mo concentration ranges (0.7 to 50 $\mu\text{g g}^{-1}$) in *A. thaliana* accessions grown in potting mix or hydroponics (Baxter et al., 2008). Thus, an adjustment in Mo accumulation may favor, among others, Fe nutrition in HD accessions, which in turn maintains Fe:S ratios and ultimately Mo co-factor (Moco) biosynthetic activity (Teschner et al., 2010).

We observe significantly higher leaf Ca accumulation in HD accessions (Figure 2B). Interaction between salinity and Ca seems to play a pivotal role in the overall performance of the studied accessions: higher Ca concentrations under salinity inhibit Na^+ -induced K^+ efflux by counteracting the plasma membrane (PM) depolarization induced by salt stress and thereby increase K^+ absorption (Shabala et al., 2006; Bacha et al., 2015). In turn, high Ca levels in calcareous soils can alter Mg uptake and induce Mg deficiency in plants (Mengel & Kirkby 2001, Shaul, 2002), as Mg and Ca are strongly antagonistic (Voogt, 1998). Our results suggest that enhancing Ca nutrition - resulting in a

decrease in the Na:Ca ratio and an increase of K content –, rather than maintaining low Ca:Mg ratios to avoid Mg deficiency, favors plant performance under alkaline salinity.

HD accessions accumulated significantly less Zn than LD accessions on SCS. Both high soil carbonate/bicarbonate and high Na affect Zn availability (Akhtar et al., 2019) and our data show a significant negative correlation between RD and leaf Zn concentration (Figure S3 B). However, plants generally exhibit Zn deficiency symptoms at shoot concentrations below 15 – 20 $\mu\text{g g}^{-1}$ (Babu et al., 2014) and HD accessions display higher average Zn concentration in leaf on SCS (73 $\mu\text{g g}^{-1}$). Moreover, Fe:Zn ratios are significantly higher in HD accessions. Crosstalk in Zn and Fe nutrition has been extensively reviewed (Pineau et al., 2012; Rai et al., 2021). Several Zn membrane transporters (mainly IRT-like proteins) are regulated by Fe status and can transport both Fe and Zn (Vert et al., 2001, Yuan et al., 2008; Shanmugam et al., 2013). Here, the enhanced Fe accumulation lead by alkalinity in HD plants could be related to the observed decrease in leaf Zn concentration in these accessions and thus be a tolerance mechanism on SCS. These results are in line with previous studies in which Zn deficiency led to increased Fe accumulation in bean (Cakmak, 2000) and, in the opposite trend, iron deficiency led to Zn excess in maize (Akhtar et al., 2019).

HD accessions displayed significantly higher Fe:Mn ratio than LD accessions under SCS. Plants grown in SCS showed Fe:Mn ratios ranging from 0.8 to 4. From the 12 study accessions displaying Fe:Mn ratio below 1.5, 8 belonged to LD group. On the opposite trend, 15 out of 20 accessions showing Fe:Mn ratio above 2 were from HD group. Classically, the optimum Fe:Mn ratio in plants has been given as 1.5 to 2.5 (Shive, 1941). It is well established that Fe, Mn

and other divalent ions share transporters (e.g. IRT1) and that Fe-dependent chlorosis in *A. thaliana* can be alleviated by means of sequestration of Mn in root vacuoles (Eroglu et al., 2016). Thus, HD accessions might be more able to adjust Fe:Mn homeostasis by reducing Mn root-to-shoot translocation (Milner et al., 2013) or increasing Mn import into root vacuoles (Li et al., 2019) leading to increased Fe:Mn ratios under SCS

Detection of SNPs Associated With Differential Leaf Elemental Profile on Saline Calcareous Soil

In this study, we report significant natural variation of leaf Na (LNa) and Fe (LFe) content in a panel of 270 *Arabidopsis* natural populations exposed to saline carbonated soil. We identified allelic variation in *NINJA* and *YUC8* genes to be likely causal for the variation in leaf sodium concentration (LNa) and in *ALA3* for the variation in leaf iron concentration (LFe). Allelic variation in these genes leads to changes in their mRNA expression and is not associated to allelic variation in the main genes responsible for differential plant responses to either salinity (*HKT1*, *SOS1*) or alkalinity (*IRT1*, *FRO2*).

Two out of the five SNPs detected in the *NINJA* gene are splice-site mutations - as they are found within splice sites (the boundary of an exon and an intron) in one or more *NINJA* splice variants. Both SNPs emerge as the top candidates contributing to genotype-specific splicing events under alkaline salinity at the *NINJA* locus, as alternative splicing (AS) regulates transcript levels (Grodecká et al., 2017) and contributes to plant adaptation to their environment (Syed et al., 2012). One SNP in *YUC8* causes an exonic synonymous variant. Far from having no effects on the synthesized protein, coding synonymous variants can have a significant impact on mRNA structure, translation rate and expression (Edwards et al., 2012). *ALA3* contains 2 of the 4 assessed SNPs in the

promoter region, which have a high potential to alter gene expression for being close to transcription start sites (Greenbaum & Deng, 2017). The rest of potentially causal SNPs are in non-coding intragenic regions (Fig. 8) and therefore they do not have an obvious impact on gene expression or protein conformation (Robert & Pelletier, 2018). Still, they might be good indicators for the leaf Na and Fe accumulation phenotypes and for the expression level changes detected in the proximal genes. This suggests that *YUC8*, *NINJA*, and *ALA3* could be genes under selection and might be affected by structural variation that should be further explored.

NINJA (AT4G28910, Novel interactor of JAZ) acts as a transcriptional repressor and is a negative regulator of jasmonate responses. *NINJA* interaction with JAZ proteins (jasmonate ZIM-domain repressor proteins) has been experimentally determined. In turn, *MYC2* interacts physically with JAZ proteins, thus regulating JA-Ile-responsive gene expression. JA-Ile is a plant hormone that regulates a broad array of plant defense and developmental processes (Pauwels et al., 2010). Transcriptomic analysis has revealed the importance of JA-Ile in the response of *A. thaliana* plants to overcome moderate saline stress (Erice et al., 2017).

YUC8 (AT4G28720) is an auxin biosynthetic gene and *yuc8* null mutants have previously been shown to suffer reduction in hypocotyl and petiole length under both high and low red to far-red (R:FR) conditions. We showed that the *yuc8* line developed significantly smaller rosette, shorter roots, and higher leaf Na⁺ accumulation under alkaline salinity conditions when compared to WT plants. It has been hypothesized that down-regulation of auxin signaling might be part of *A. thaliana* acclimation to neutral salinity (Iglesias et al., 2014). More recent studies have shown that exogenous auxin application alters sodium ion

accumulation and plays a protective role in salinity challenged strawberry (Zhang et al., 2021). Furthermore, a link between enhanced auxin accumulation mediated by *YUCCA* genes and a better developed root system architecture for the acquisition of salinity stress tolerance has been hypothesized in rice (Saini et al., 2021). Several auxin biosynthetic genes have been reported as direct targets of *YUC8*: *AUF1*, *TAA1*, *TAR1*, *TAR2*, shown to regulate local auxin biosynthesis in primary root tips (Ursache et al., 2014). The jasmonic acid signaling pathway has shown to be linked to auxin homeostasis through the modulation of *YUC8*, and roots of *yuc8* and *yuc9* knockout mutants displayed a reduced response to methyl jasmonate (MeJA) (Hentrich et al., 2013). Phytohormones modulate a wide range of responses during the whole plant life cycle and the alteration of endogenous phytohormonal levels is a key factor for the regulation of plant growth and reproductive responses to environmental stimuli. Here we suggest a role of *YUC8* and *NINJA* expression levels in the regulation of auxin and jasmonic signaling pathways thus affecting plant tolerance to alkaline salinity. Quantification of endogenous phytohormone concentrations and expression levels of direct targets of *YUC8* and *NINJA* knockout and overexpressing lines grown on alkaline salinity stress will help to confirm its involvement in tolerance acquisition to saline calcareousness in the soil and to elucidate their mechanism of action and possible mutual interaction.

ALA3 encodes a phospholipid translocase active in plasma membrane and the trans Golgi network. It has been reported to be important for vegetative growth and reproductive success in *A. thaliana*. Screening of *ala3* knockout mutants showed that *ala3* was growth-defective dependent upon both temperature and soil when compared to Col-0 (McDowell et al., 2013). *ALA3* contributes to secretory vesicle formation by assisting in the formation of slime vesicles in root tip cells (Poulsen et al., 2008a) and helps regulate polar

growth by controlling phosphatidylserine exposure at the plasma membrane cytoplasmic face (López-Marqués et al., 2021). Physical interaction between AtALA3 and two ARFGEFs (ADPribosylation factor GTPases) - BIG3 (Brefeldin A-Inhibited Guanine Nucleotide-Exchange Protein3) and GNOM, which is essential for proper trafficking of PIN auxin transporters – has been observed in endomembrane, thus regulating trafficking events in the late secretory pathway and *ala3* mutants are defective in auxin mediated developmental processes (Zhang et al., 2020). There is increasing evidence for a role of auxin in plant response to both the Fe deficiency (Celletti et al., 2020) and salinity (Cacket et al., 2022). Plant P4 ATPases are expected to have a major role in any physiological process involving lipid signaling, vesicle formation and/or lipid-dependent protein recruitment to membranes. Plants sense environmental stimuli and transduce the signal into downstream biological responses often through the plasma membrane, which is the interface between the cell and the environment and the source for signaling lipids. Salinity is well known to change membrane lipid composition in plants, and to alter membrane permeability for water, ions, and metabolites (Tsydendambaev et al., 2013). Moreover, membrane lipids are directly affected by pH, due to their acid-basic properties. The assessment of the effects of an *ALA3* hyper-functional allele in membrane fluidity and permeability, regulation of lipid-dependent signaling cascades and control of other gene clusters that might activate plant adaptation under alkaline salinity should be addressed using loss of function, homozygous knockout, and overexpressing mutant lines for *ALA3*.

Altogether, we demonstrate Na-Fe homeostasis are key features in the adaptation of *A. thaliana* to saline alkaline conditions. Our GWAS approach using a saline calcareous natural soil allowed the identification of new players in this crucial ion homeostasis regulation: *YUC8* and *NINJA* associated with

Na leaf exclusion (providing a low leaf Na phenotype) and *ALA3* with high Fe leaf accumulation. The importance of these genes for tolerance to saline alkaline conditions is further highlighted by the fact that, excepting *HKT-1*, for which absence of allelic variation in the study accessions has been confirmed, the study populations bearing alternative and common allelic variants for each identified locus do not differ in the expression of well-established genes involved in Na and Fe homeostasis such as *SOS1*, *FRO1* and *IRT1*. Recent studies have shown that accessions with tolerance to moderate salinity regulate Na:K ratios under salinity by enhancing *HKT1* expression in roots but are unable to increase *HKT1* root expression under alkaline salinity (Pérez-Martín et al., 2022). This suggests that mechanisms for a better maintenance of Na:K balance under salinity conditions are likely to differ from those under alkaline salinity and that the latter need to be better understood.

Methods

HapMap phenotyping and GIS Data Extrapolation

Seeds of the *Arabidopsis thaliana* HapMap cohort (354 natural accessions) were obtained from Nottingham *A. thaliana* Stock Centre (NASC, Nottingham, United Kingdom). The list and information of the accessions is detailed in Dataset S1. Seeds were surface sterilized using 5% sodium hypochlorite (NaOCl) solution under constant agitation for 10 min and rinsed with sterile water six times. Seeds were stratified for 4 days at 4°C after sowing to synchronize germination, then four seeds per accession were sown in saline-carbonated soil (SCS) into Aratrays of 51 individual pots especially suited for *A. thaliana* (www.arasystem.com).

The SCS used for treatment was a mix of soil originating from a parcel of natural saline-carbonated soil in L'Escala, NE Catalunya, Spain (42°13'03"N 3°11'30"E) and perlite (3:1). The SCS had previously been characterized as suitable for saline-carbonate stress analysis (Supplementary Table 1) (Pérez-Martín, 2020). Aratrays were placed in a growth chamber with 150 $\mu\text{mol m}^{-2}\text{s}^{-1}$ of PAR, 10 h light/14 h dark photoperiod, and 25°C/20°C day/night temperature. Trays were bottom-watered twice weekly with deionized water with no further nutrients added, and aratrays were rotated horizontally to help reduce gradient effects for light, temperature, and humidity.

Germination and seedling survival were monitored. Fifty-five-days old plants were harvested to measure their nutrient mineral contents and Rosette Diameter (RD), Rosette Leaf Area (RLA) and Fresh Weight (FW) of three individuals per accession were measured at the end of the experiment.

To estimate the edaphic parameters of the native soil of each *A. thaliana* accession, location coordinates and public maps from the European Soil Data Centre (ESDAC) database (Panagos et al., 2012) were combined using Q-GIS1. Natural accession coordinates were extracted from GWAPP2 in WGS84 system (latitude and longitude). Maps of soil properties at European scale, based on Lucas, 2009/2012 topsoil data from the European Soil Data Centre (ESDAC) were used to extract the following variables: pH (measured in H₂O), pH (in CaCl₂ 0.01 M solution), Cation Exchange Capacity (CEC), Calcium carbonates (CaCO₃), C:N ratio, and N, P, and K concentrations (mg.kg⁻¹).

Elemental Composition of Soils and Plants

To analyze the composition of the SCS, six independent samples from the trays used for the pot experiment (three at the beginning and three at the end

of the experiment) were collected. The soil characterization was performed on the 2-mm fraction samples following the extraction method described by Busoms et al. (2018). Plant tissues were sampled by removing 2–3 leaves (1–5 mg dry weight) and washing them with 18 milli-Q water before being placed in Pyrex digestion tubes. Sampled plant material was dried for 2 days at 60°C and weighed before open-air digestion in Pyrex tubes using 0.7 mL concentrated HNO₃ at 110°C for 5 h in a hot-block digestion system (SC154-54-Well Hot Block, Environmental Express, Charleston, SC, United States). Concentrations of the selected elements (Fe, Ca, K, Mg, S, Na, P, Mn, Mo, Cu, B, Zn and Ni) were determined by ICP-MS (Perkin ElmerInc., ELAN 6000, MA, United States) or ICP-OES (Thermo Jarrell-Ash, model 61E Polyscan, England).

GWA Studies and Candidate Genes Selection

Genome Wide Association Studies (GWAS) was performed on the phenotypes obtained from the 270 *A. thaliana* natural accessions that survived and grew on the SCS. Phenotypes included leaf mineral concentrations of 11 elements (Fe, Mg, Ca, K, Na, S, Mn, B, P, Zn and Mo) of three 55-days old plants. Cu and Ni were below the level of detection and could not be quantified. All the phenotypes are detailed in Table S1.

GWA mapping was performed in GEMMA (version 0.98) (Zhou 2012) with a univariate linear mixed model and the minor allele frequency cut-off set at 0.1. GWAS was run with the imputed 1348843 SNP set (Arabidopsis_2029_Maf001_Filter80) (Arouisse et al., 2020). A kinship matrix was constructed in GEMMA to correct for population structure and individual relatedness. The Benjamini & Hochberg threshold (BH) was implemented using the formula $(i/m) Q$, where: i = the individual p-value's rank, m = total

number of tests, Q = the false discovery rate set at 25%. This corresponded to a BH threshold of 6.42. SNPs with score above BH correction and $m.a.f > 0.1$ were selected and the linkage disequilibrium (LD) region associated with the highest score SNP was explored to identify candidate genes for the causal allelic variant. All genes associated with the significant SNPs and their SNPs in strong LD ($r^2 > 0.8$) were explored (Table S3). Genes were annotated according to TAIR 10 (Araport11).

Candidate genes validation

Seeds from 12 selected *A. thaliana* accessions, Col-0 and 17 T-DNA insertion lines were obtained from the *A. thaliana* Stock Centre (NASC, Nottingham, United Kingdom). Figure S1 details the workflow and the *A. thaliana* accessions and mutants used in each experiment. *A. thaliana* natural accessions were classified as “High Leaf Na” (HLNa), “Low Leaf Na Lead” (LLNa), “High Leaf Fe Lead” (HLFe) or “Low Leaf Fe” (LLFe) based on their leaf Na and Fe concentrations on SCS. In all soil, hydroponic and plate experiments, seeds were surface sterilized and stratified as described above to synchronize germination.

Potted Soil culture

Seeds were sown into the same soil type used for the HapMap screening. Each tray contained 24 individuals in a random block design with a total of six individuals per accession and soil type. Plants were allowed to germinate and grow at 10 h light/14 h dark at 25°C to 20°C day/night temperature, 150 $\mu\text{mol m}^{-2} \cdot \text{s}^{-1}$ and 40% humidity. Trays were bottom watered twice weekly with deionized water. Rosette diameter (RD) from the third week to the end of the

experiment from aerial pictures. Two leaves from 55-day-old plants were collected from up to six plants per accession and soil type.

Hydroponic culture

Seeds were germinated in a mix of sand and perlite (3:1) and 10-day old seedlings were transferred to individual round hydroponic containers (100 mL) filled with 0.5-strength Hoagland solution (pH 5.7) and no NaCl or NaHCO₃ added (control) or containing 40 mM NaCl + 10 mM NaHCO₃, set at pH 8.3 (treatment). Plants germinated and grew at 10 h light/14 h dark, 25°C to 20°C day/night temperature, 150 $\mu\text{mol. cm}^{-2}\cdot\text{s}^{-1}$ PAR and 40% humidity. The hydroponic solution was changed every 3 days to maintain a relatively constant concentration of nutrients in the solution and treatment concentrations were increased two times - 20 mM NaCl + 5 mM NaHCO₃ at pH 8.3, and 30 mM NaCl + 15 mM NaHCO₃ at pH 8.3 - until reaching the final concentration of 40 mM NaCl + 10 mM NaHCO₃, at pH 8.3, when plants were 21 days old. Plants remained at these conditions for two more weeks. 35-days old plants were harvested and root length, rosette diameter and total fresh weight (biomass) of the six individuals per accession and per treatment were measured. Roots and leaves from the six plants per accession were stored for ionome and gene expression analysis.

Plate culture

For germination assays, 10 seeds from each accession were sown in plates in a laminar air flow cabinet with sterile material. Plates were made for two treatments: control ($\frac{1}{2}$ MS at pH 5.9) and bicarbonate ($\frac{1}{2}$ MS at pH 8.3 and 10 mM NaHCO₃). All plates contained Phyto-agar 0.6% (Duchefa, Haarlem, The Netherlands), and solutions were buffered with MES (2-(N-

morpholino)ethanesulfonic acid) and BTP (Bis-Tris Propane) depending on final pH. Plates with seeds were kept at 4 °C for synchronizing germination. After 7 days under stratification treatment, plates were moved to a growth chamber (12 h light/12 h dark, 150 $\mu\text{mol m}^{-2} \text{s}^{-1}$, 40% humidity and 25 °C). Germination was checked every day for 2 weeks and treatment effects were recorded as (% alkSal germination / % C-germination). Seeds of *ninja* and SALK_069095.55.25 mutant were not available at the time of plate experimental setup and were not assessed for germination.

Gene Expression Analysis

Total RNA of about 100 mg of plant leaf material was extracted using the MaxwellR RSC plant RNA kit (Promega Corporation, WI, United States) following the manufacturer's instructions. Two micrograms of total RNA were used as a template to synthesize first-strand cDNA with the iScriptTM cDNA Synthesis Kit (Bio-Rad, United States). The cDNA was used as a template for Reverse-Transcriptase quantitative real-time PCR (RT-qPCR) using iTaqTM Universal SYBR Green Supermix (Bio-Rad, CA, United States). Real-time detection of fluorescence emission was performed on a CFX384 Real-Time System (Bio-Rad, CA, United States), and plates were edited using the CFX manager version 3.1 software. Primers used for pinpointed candidate genes transcript quantification - *PGP10*, *NINJA*, *YUC8*, *ALA3* – in selected natural accessions showing contrasted phenotypes are detailed in Table S2. Relative quantifications were performed for all genes with the *Actin2* gene (AT3G18780) used as an internal reference. For each sample, the average value from triplicate RT-qPCRs was used to estimate transcript abundance. Four samples per line were used. The mean Ct values were normalized against *Actin2* and dCt values were calculated as (dCtGene- dCtActin2). The data are expressed as means \pm SE relative to the Col-0 value (defined as 1).

Statistical Analyses

All the statistical analyses were conducted using JMP SAS software (SAS Institute, Cary, NC, United States). No data normalization was applied. To compensate for variation between and within trays, outlier samples that were 4.5 times higher than the interquartile range across all trays per each element were excluded from the descriptive analysis. This threshold was chosen over the more standard 1.5 times threshold according to Campos et al. (2021), to include accessions with an extreme phenotype. In all soil and hydroponic cultures, mean-standardized values ($-1 < \text{value} < 1$) of elemental contents of soil and leaf material were used to represent the radar plots and compare between soil types, treatments or accessions, and One-way ANOVA was used to test for significant differences ($P < 0.05$) between means of phenotypic responses, gene expression, and between means of elemental contents of soil and leaf material. To perform multiple comparisons of group means we used Tukey's HSD and to compare elemental profiles of each mutant with Col-0 (WT) we used Dunnett's test.

To investigate changes in root length (RL), rosette diameter (RD) and fresh weight (Biomass) in the hydroponic experiment, where a control treatment was available, the phenotypic responses to saline-carbonated conditions were quantified and compared to the respective control conditions [relative measurements: $\text{mean}(X_{\text{Treatment}}) = \text{mean}(X_{\text{Control}})$].

Conclusions



Concluding remarks

The specific conclusions that address the objectives of this thesis (1-11) and further considerations based on the general trends observed throughout the different experimental procedures carried out (12, 13) are listed below.

1. The variations in the responses to environmental factors among and within populations of *A. thaliana* can be exploited for studying local adaptation processes through the combination of phenotyping techniques and *omic* approaches at a wide range of geographical scales. This is supported by the existing phenotypic, genomic, and transcriptomic variations in the studied CatDeme collection, which have shown to be large enough to detect differential plant responses to environmental heterogeneity in terms of soil composition.

2. The *A. thaliana* CatDeme collection exhibits continuous isolation by distance along the studied distribution range without natural breaks, that would correspond to the classical notion of population. Population structure is only supported for the northeastern group of demes, where a geographic pattern of genomic divergence is observed, whereas considerable genetic interbreed appears to be present for the rest of the studied demes. An exception which deserves further attention is the T6/T11/CALA coastal group of demes, proven to be a differentiated genetic cluster by both PCA, NJ Tree and admixture clustering algorithms.

3. Genotyping of the *FRI* and *FLC* regions has led to the classification of the the CatDeme collection into the functional *FRI-FLC^A* haplogroup. However, genomic divergence is present at the *FRI* locus and at other loci regulating flowering time in an *FLC* dependent and independent manner between CatDeme

early and late flowering groups. Such divergence is shown to be driven by both balancing and positive selective pressures and potentially accounts for the existing variation in the flowering time of CatDeme stands.

4. Soil composition heterogeneity along the studied distribution range is an environmental driver of selection in CatDeme. Soil Na^+ and $\text{CaCO}_3\%$ are the two major agents differentiating CatDeme native soils, and leaf Na^+ , K^+ , Zn and S profiles differ between demes with contrasted tolerance to neutral (SS) and alkaline salinity (CS). This provides evidence that the leaf elemental composition is affected by genotypic variation and soil nutrient environment in *Arabidopsis* even at small geographical scales.

5. The landscape genomics approach, based on the spatial distribution of alleles and their association with variation in traits characteristic from alkaline saline soils, confirmed that allelic variation at loci regulating transmembrane K^+ and Ca transport and intracellular pH contributes to local adaptation processes in CatDeme, and highlighted soil Na^+ and Ca as major selective pressures for local adaptation to alkaline salinity.

6. Alkaline salinity stress exerts more deleterious effect than neutral salinity in the performance of the studied demes in terms of plant leaf growth, photosynthesis efficiency, nutrient balance maintenance, endogenous phytohormone regulation and transcriptome response pathways.

7. Plant growth, leaf nutrition, photosynthesis, and secondary metabolites regulation mechanisms under alkaline salinity cannot be predicted from neutral salinity responses in the studied demes. Therefore, the assessment of the effects

of saline calcareous soil on plant responses must be approached by applying alkaline salinity as a combinatorial stress.

8. Local adaptation of the studied demes to their native soil, which contains either the salinity or the alkalinity component of saline calcareous soils, but not the combination of both, leads to differential plant core responses to salinity at the gene expression level (i.e., genes altered under both neutral and alkaline salinity are differentially regulated in an origin-dependent manner). The contrasted expression profiles in the convergent salinity response pathways contributed more to the differential plant tolerance to alkaline salinity than the individual responses to either neutral or alkaline salinity. Moreover, the detrimental effect of local adaptation to saline siliceous soils for tolerance to saline calcareousness is corroborated at the transcriptome level.

9. The GWAS performed on the *A. thaliana* HapMap diversity panel grown on the saline calcareous soil allowed the identification and description of the molecular bases of natural variations in leaf Na⁺ and Fe concentrations under alkaline salinity. There is a geographic adaptation imprint on leaf nutrient profiles by which plants from soils with limited Fe and elevated Na⁺ perform better under alkaline salinity in terms of rosette diameter, leaf sodium limitation and leaf iron maintenance.

10. The combination of ionomics and genomic data allows for both the simultaneous association mapping of all foliar elemental traits and the identification of the common alleles potentially affecting each trait. In the HapMap collection, changes in leaf Na⁺ concentration under alkaline salinity significantly associate to allelic variations at the *NINJA* and *YUC8* loci, whereas

an alternative allelic variant of *ALA3* associates with enhanced leaf Fe concentration.

11. A correlation between *NINJA*, *YUC8* and *ALA3* allele version and gene expression levels has been demonstrated to contribute to the differential plant performance observed under alkaline salinity in terms of growth of the studied HapMap accessions. This suggests that knockout mutant phenotyping must be complemented with other phenotyping approaches to understand allelic variation effects on a trait of interest.

Further considerations

12. Integrating studies performed with more than one panel of populations is a powerful approach to target prime candidates for alkaline salinity tolerance at different geographical scales. Here, maintaining K^+ homeostasis is targeted as a desirable trait for alkaline salinity tolerance based on genome divergence, transcriptome, and GWAS studies using both local and regional collections; however, $Na^+ : K^+$ maintenance is achieved by enhanced K^+ accumulation in CatDeme, while reduced leaf Na^+ results in higher alkaline salinity tolerance in HapMap individuals. Similarly, ecogeographical footprints of adaptation to alkaline salinity are revealed by differential Fe at soils of origin across Europe (HapMap collection), but neither soil nor leaf Fe concentrations seem distinctive traits when phenotyping native soils and plant responses to alkaline salinity in CatDeme; in this case, the CatDeme transcriptomic profiling points to an enhanced internal Fe use efficiency rather than differential Fe concentration as a key trait for alkaline salinity tolerance at a local scale.

13. In line with the previous statement, plant leaf mineral nutrients have been shown not to correlate always with the same sets of other nutrients (or with the same trend) across different tested environments, genotype groups, and sample sizes. Thus, addressing the plant and soil ionome as a whole is recommended for crop breeding research, to account for the complex regulatory networks determining plant growth and performance under each studied scenario. For instance, results from the GPA, transcriptome, and GWA studies with local and European *A. thaliana* accessions agree in that reduced $\text{Na}^+:\text{K}^+$ and $\text{Na}^+:\text{Ca}$ ratios correlate with enhanced physiological status under neutral and alkaline salinity, and plasma membrane (PM) and vacuolar (V) H^+ -ATPases are present in GEA, GPA and RNA-Seq candidate lists. In fact, the maintenance of leaf K^+ and Ca and the enhanced intracellular acidification as key mechanisms for improving plant response to alkaline salinity deserve further attention: in individuals with better performance under alkaline salinity, the increase of cytosolic Ca^{2+} seems to enhance H^+ -ATPase activity, which contributes to conserve high leaf K^+ concentrations. Likewise, limiting Zn leaf concentration is a favorable trait for tolerance to saline calcareousness in *A. thaliana*, as the physiological measurements in both CatDeme and HapMap collections converge in the negative correlation between leaf Zn concentrations and plant physiological performance under alkaline salinity. The observations compiled through the presented research allow to state that a tight regulation of Zn availability, uptake and translocation is crucial when dealing with alkaline salinity conditions, to avoid Zn competition with Fe and P without reaching a Zn deficiency status caused by the presence of bicarbonates. This suggest that Zn optimal ranges in saline calcareous soils should be revisited, accounting for pH dependent salinity-Zn interactions.

References

- Abdelaziz, M. E., Kim, D., Ali, S., Fedoroff, N. V., & Al-Babili, S.** (2017). The endophytic fungus *Piriformospora indica* enhances *Arabidopsis thaliana* growth and modulates Na⁺/K⁺ homeostasis under salt stress conditions. *Plant Science*, 263, 107-115.
<https://doi.org/10.1016/j.plantsci.2017.07.006>
- Achard, P., Cheng, H., De Grauwe, L., Decat, J., Schoutteten, H., Moritz, T., ... & Harberd, N. P.** (2006). Integration of plant responses to environmentally activated phytohormonal signals. *Science*, 311(5757), 91-94. <https://doi.org/10.1126/science.1118642>
- Aghajanzadeh, T. A., Reich, M., Kopriva, S., & De Kok, L. J.** (2018). Impact of chloride (NaCl, KCl) and sulphate (Na₂SO₄, K₂SO₄) salinity on glucosinolate metabolism in *Brassica rapa*. *Journal of Agronomy and Crop Science*, 204(2), 137-146.
<https://doi.org/10.1111/jac.12243>
- Ahmad, P., Ozturk, M., Sharma, S., & Gucel, S.** (2014). Effect of sodium carbonate-induced salinity–alkalinity on some key osmoprotectants, protein profile, antioxidant enzymes, and lipid peroxidation in two mulberry (*Morus alba* L.) cultivars. *Journal of plant interactions*, 9(1), 460-467. <https://doi.org/10.1080/17429145.2013.855271>
- Ahuja, I., de Vos, R. C., Bones, A. M., & Hall, R. D.** (2010). Plant molecular stress responses face climate change. *Trends in plant science*, 15(12), 664-674.
<https://doi.org/10.1016/j.tplants.2010.08.002>
- Akhtar, M., Yousaf, S., Sarwar, N., & Hussain, S.** (2019). Zinc biofortification of cereals—role of phosphorus and other impediments in alkaline calcareous soils. *Environmental geochemistry and health*, 41(5), 2365-2379.
<https://doi.org/10.1007/s10653-019-00279-6>
- Alloway, B. J.** (2013). Molybdenum. In *Heavy Metals in Soils*. Springer, Dordrecht (pp. 527-534).
- Alonso-Blanco, C., Aarts, M. G., Bentsink, L., Keurentjes, J. J., Reymond, M., Vreugdenhil, D., & Koornneef, M.** (2009). What has natural variation taught us about plant development, physiology, and adaptation?. *The Plant Cell*, 21(7), 1877-1896.
- Amasino, R. M., & Michaels, S. D.** (2010). The timing of flowering. *Plant Physiology*, 154(2), 516-520. <https://doi.org/10.1104/pp.110.161653>
- An, Y. M., Song, L. L., Liu, Y. R., Shu, Y. J., & Guo, C. H.** (2016). De novo transcriptional analysis of alfalfa in response to saline-alkaline stress. *Frontiers in Plant Science*, 7(931).
<https://doi.org/10.3389/fpls.2016.00931>

- Anderson, J. P., Badruzsaufari, E., Schenk, P. M., Manners, J. M., Desmond, O. J., Ehlert, C., ... & Kazan, K.** (2004). Antagonistic interaction between abscisic acid and jasmonate-ethylene signaling pathways modulates defense gene expression and disease resistance in *Arabidopsis*. *The Plant Cell*, 16(12), 3460-3479.
<https://doi.org/10.1105/tpc.104.025833>
- Andrés, F., & Coupland, G.** (2012). The genetic basis of flowering responses to seasonal cues. *Nature Reviews Genetics*, 13(9), 627-639. <https://doi.org/10.1038/nrg3291>
- Anil, V. S., Rajkumar, P., Kumar, P., & Mathew, M. K.** (2008). A plant Ca^{2+} pump, ACA2, relieves salt hypersensitivity in yeast: modulation of cytosolic calcium signature and activation of adaptive Na^+ homeostasis. *Journal of Biological Chemistry*, 283(6), 3497-3506.
<https://doi.org/10.1074/jbc.M700766200>
- Araki, T.** (2001). Transition from vegetative to reproductive phase. *Current opinion in plant biology*, 4(1), 63-68. [https://doi.org/10.1016/S1369-5266\(00\)00137-0](https://doi.org/10.1016/S1369-5266(00)00137-0)
- Arouisse, B., Korte, A., van Eeuwijk, F., & Kruijer, W.** (2020). Imputation of 3 million SNPs in the *Arabidopsis* regional mapping population. *The Plant Journal*, 102(4), 872-882.
<https://doi.org/10.1111/tpj.14659>
- Assefa, T., Zhang, J., Chowda-Reddy, R. V., Moran Lauter, A. N., Singh, A., O'Rourke, J. A., ... & Singh, A. K.** (2020). Deconstructing the genetic architecture of iron deficiency chlorosis in soybean using genome-wide approaches. *BMC plant biology*, 20(1), 1-13.
<https://doi.org/10.1186/s12870-020-2237-5>
- Atici, Ö., Açar, G., & Battal, P. E. Y. A. M. İ.** (2005). Changes in phytohormone contents in chickpea seeds germinating under lead or zinc stress. *Biologia plantarum*, 49(2), 215-222. <https://doi.org/10.1007/s10535-005-5222-9>
- Atwell, S., Huang, Y. S., Vilhjálmsson, B. J., Willems, G., Horton, M., Li, Y., ... & Nordborg, M.** (2010). Genome-wide association study of 107 phenotypes in *Arabidopsis thaliana* inbred lines. *Nature*, 465(7298), 627-631. <https://doi.org/10.1038/nature08800>
- Babuin, M. F., Campestre, M. P., Rocco, R., Bordenave, C. D., Escaray, F. J., Antonelli, C., ... & Menendez, A. B.** (2014). Response to long-term NaHCO_3 -derived alkalinity in model *Lotus japonicus* ecotypes Gifu B-129 and Miyakojima MG-20: transcriptomic profiling and physiological characterization. *PLoS One*, 9(5), e97106.
<https://doi.org/10.1371/journal.pone.0097106>
- Bacha, H., Ródenas, R., López-Gómez, E., García-Legaz, M. F., Nieves-Cordones, M., Rivero, R. M., ... & Rubio, F.** (2015). High Ca^{2+} reverts the repression of high-affinity K^+ uptake produced by Na^+ in *Solanum lycopersicum* L.(var. microtom) plants. *Journal of plant physiology*, 180, 72-79. <https://doi.org/10.1016/j.jplph.2015.03.014>
- Baena-González, E.** (2010). Energy signaling in the regulation of gene expression during stress. *Molecular plant*, 3(2), 300-313. <https://doi.org/10.1093/mp/ssp113>

- Bai, J., Yan, W., Wang, Y., Yin, Q., Liu, J., Wight, C., & Ma, B.** (2018). Screening oat genotypes for tolerance to salinity and alkalinity. *Frontiers in plant science*, 9, 1302. <https://doi.org/10.3389/fpls.2018.01302>
- Bakker, E. G., Stahl, E. A., Toomajian, C., Nordborg, M., Kreitman, M., & Bergelson, J.** (2006). Distribution of genetic variation within and among local populations of *Arabidopsis thaliana* over its species range. *Molecular ecology*, 15(5), 1405-1418. <https://doi.org/10.1111/j.1365-294X.2006.02884.x>
- Balasubramanian, S., Sureshkumar, S., Agrawal, M., Michael, T. P., Wessinger, C., Maloof, J. N., ... & Weigel, D.** (2006). The PHYTOCHROME C photoreceptor gene mediates natural variation in flowering and growth responses of *Arabidopsis thaliana*. *Nature genetics*, 38(6), 711-715. <https://doi.org/10.1038/ng1818>
- Bao, S., Hua, C., Huang, G., Cheng, P., Gong, X., Shen, L., & Yu, H.** (2019). Molecular basis of natural variation in photoperiodic flowering responses. *Developmental cell*, 50(1), 90-101. <https://doi.org/10.1016/j.devcel.2019.05.018>
- Barciszewski, J., Rattan, S. I., Siboska, G., & Clark, B. F.** (1999). Kinetin—45 years on. *Plant science*, 148(1), 37-45. [https://doi.org/10.1016/S0168-9452\(99\)00116-8](https://doi.org/10.1016/S0168-9452(99)00116-8)
- Baxter, I. & Dilkes, B.P.** (2012) Elemental profiles reflect plant adaptations to the environment. *Science*, 336(6089), 1661– 1663. <https://doi.org/10.1126/science.1219992>.
- Baxter, I., Brazelton, J. N., Yu, D., Huang, Y. S., Lahner, B., Yakubova, E., Li, Y., Bergelson, J., Borevitz, J., Nordborg, M., Vitek, O., Salt, D. E.** (2010). A coastal cline in sodium accumulation in *Arabidopsis thaliana* is driven by natural variation of the sodium transporter AtHKT1; 1. *PLoS genetics*, 6(11), e1001193. <https://doi.org/10.1371/journal.pgen.1001193>
- Baxter, I., Muthukumar, B., Park, H. C., Buchner, P., Lahner, B., Danku, J., ... & Salt, D. E.** (2008). Variation in molybdenum content across broadly distributed populations of *Arabidopsis thaliana* is controlled by a mitochondrial molybdenum transporter (MOT1). *PLoS Genetics*, 4(2), e1000004. <https://doi.org/10.1371/journal.pgen.1000004>
- Bazakos, C., Hanemian, M., Trontin, C., Jimenez-Gomez, J. M., & Loudet, O.** (2017). New strategies and tools in quantitative genetics: how to go from the phenotype to the genotype. *Annual review of plant biology*, 68(435-455). <https://doi.org/10.1146/annurev-arplant-042916-040820>
- Ben Abdallah, H., Mai, H. J., Álvarez-Fernández, A., Abadía, J., & Bauer, P.** (2017). Natural variation reveals contrasting abilities to cope with alkaline and saline soil among different *Medicago truncatula* genotypes. *Plant and Soil*, 418(1), 45-60. <https://doi.org/10.1007/s11104-017-3379-6>

- Bian, C., Guo, X., Zhang, Y., Wang, L., Xu, T., DeLong, A., & Dong, J.** (2020). Protein phosphatase 2A promotes stomatal development by stabilizing SPEECHLESS in *Arabidopsis*. *Proceedings of the National Academy of Sciences*, 117(23), 13127-13137. <https://doi.org/10.1073/pnas.1912075117>
- Bittner, F.** (2014). Molybdenum metabolism in plants and crosstalk to iron. *Frontiers in plant science*, 5(28). <https://doi.org/10.3389/fpls.2014.00028>
- Blanvillain, R., Wei, S., Wei, P., Kim, J. H., & Ow, D. W.** (2011). Stress tolerance to stress escape in plants: role of the OXS2 zinc-finger transcription factor family. *The EMBO journal*, 30(18), 3812-3822. <https://doi.org/10.1038/emboj.2011.270>
- Bloomer, R. H., & Dean, C.** (2017). Fine-tuning timing: natural variation informs the mechanistic basis of the switch to flowering in *Arabidopsis thaliana*. *Journal of Experimental Botany*, 68(20), 5439-5452. <https://doi.org/10.1093/jxb/erx270>
- Bolger, A. M., Lohse, M., & Usadel, B.** (2014). Trimmomatic: a flexible trimmer for Illumina sequence data. *Bioinformatics*, 30(15), 2114-2120. <https://doi.org/10.1093/bioinformatics/btu170>
- Bomblies, K., Yant, L., Laitinen, R. A., Kim, S. T., Hollister, J. D., Warthmann, N., ... & Weigel, D.** (2010). Local-scale patterns of genetic variability, outcrossing, and spatial structure in natural stands of *Arabidopsis thaliana*. *PLoS Genetics*, 6(3), e1000890. <https://doi.org/10.1371/journal.pgen.1000890>
- Bose, J., Rodrigo-Moreno, A., Lai, D., Xie, Y., Shen, W., & Shabala, S.** (2015). Rapid regulation of the plasma membrane H⁺-ATPase activity is essential to salinity tolerance in two halophyte species, *Atriplex lentiformis* and *Chenopodium quinoa*. *Annals of botany*, 115(3), 481-494. <https://doi.org/10.1093/aob/mcu219>
- Brachi, B., Faure, N., Bergelson, J., Cuguen, J., & Roux, F.** (2013). Genome-wide association mapping of flowering time in *Arabidopsis thaliana* in nature: genetics for underlying components and reaction norms across two successive years. *Acta Botanica Gallica*, 160(3-4), 205-219. <https://doi.org/10.1080/12538078.2013.807302>
- Brennan, A. C., Méndez-Vigo, B., Haddioui, A., Martínez-Zapater, J. M., Picó, F. X., & Alonso-Blanco, C.** (2014). The genetic structure of *Arabidopsis thaliana* in the south-western Mediterranean range reveals a shared history between North Africa and southern Europe. *BMC plant biology*, 14(1), 1-14. <https://doi.org/10.1186/1471-2229-14-17>
- Burén, S.** (2010). *Targeting and function of CAH1: Characterization of a novel protein pathway to the plant cell chloroplast* (Doctoral dissertation, Institutionen för fysiologisk botanik, Umeå universitet). DiVA, id: [diva2:284338](https://diva2.org/284338)
- Bürger, R., & Gimelfarb, A.** (2002). Fluctuating environments and the role of mutation in maintaining quantitative genetic variation. *Genetics Research*, 80(1), 31-46. DOI: <https://doi.org/10.1017/S0016672302005682>

- Burghardt, L. T., Edwards, B. R., & Donohue, K.** (2016). Multiple paths to similar germination behavior in *Arabidopsis thaliana*. *New Phytologist*, 209(3), 1301-1312.
<https://doi.org/10.1111/nph.13685>
- Busoms, S.** (2015). Local adaptation of wild populations of *Arabidopsis thaliana* to coastal and inland habitats in Catalonia. <http://hdl.handle.net/10803/401010>
- Busoms, S., Paajanen, P., Marburger, S., Bray, S., Huang, X. Y., Poschenrieder, C., ... & Salt, D. E.** (2018). Fluctuating selection on migrant adaptive sodium transporter alleles in coastal *Arabidopsis thaliana*. *Proceedings of the National Academy of Sciences*, 115(52), E12443-E12452. <https://doi.org/10.1073/pnas.1816964115>
- Busoms, S., Teres, J., Huang, X. Y., Bomblies, K., Danku, J., Douglas, A., ... & Salt, D. E.** (2015). Salinity is an agent of divergent selection driving local adaptation of *Arabidopsis* to coastal habitats. *Plant Physiology*, 168(3), 915-929.
<https://doi.org/10.1104/pp.15.00427>
- Busoms, S., Terés, J., Yant, L., Poschenrieder, C., & Salt, D. E.** (2021). Adaptation to coastal soils through pleiotropic boosting of ion and stress hormone concentrations in wild *Arabidopsis thaliana*. *New Phytologist*, 232(1), 208-220.
<https://doi.org/10.1111/nph.17569>
- Cackett, L., Cannistraci, C. V., Meier, S., Ferrandi, P., Pěnčík, A., Gehring, C., ... & Donaldson, L.** (2022). Salt-specific gene expression reveals elevated auxin levels in *Arabidopsis thaliana* plants grown under saline conditions. *Frontiers in plant science*, 15. <https://doi.org/10.3389/fpls.2022.804716>
- Caicedo, A. L., Stinchcombe, J. R., Olsen, K. M., Schmitt, J., & Purugganan, M. D.** (2004). Epistatic interaction between *Arabidopsis* FRI and FLC flowering time genes generates a latitudinal cline in a life history trait. *Proceedings of the National Academy of Sciences*, 101(44), 15670-15675. <https://doi.org/10.1073/pnas.0406232101>
- Cakmak, I.** (2000). Tansley Review No. 111 Possible roles of zinc in protecting plant cells from damage by reactive oxygen species. *The New Phytologist*, 146(2), 185-205.
<https://doi.org/10.1046/j.1469-8137.2000.00630.x>
- Cao, Y., Zhang, M., Liang, X., Li, F., Shi, Y., Yang, X., & Jiang, C.** (2020). Natural variation of an EF-hand Ca²⁺-binding-protein coding gene confers saline-alkaline tolerance in maize. *Nature communications*, 11(1), 1-14. <https://doi.org/10.1038/s41467-019-14027-y>
- Cardoso, A. A., Gori, A., Da-Silva, C. J., & Brunetti, C.** (2020). Absciscic acid biosynthesis and signaling in plants: Key targets to improve water use efficiency and drought tolerance. *Applied Sciences*, 10(18), 6322. <https://doi.org/10.3390/app10186322>
- Carlson, C. S., Thomas, D. J., Eberle, M. A., Swanson, J. E., Livingston, R. J., Rieder, M. J., & Nickerson, D. A.** (2005). Genomic regions exhibiting positive selection identified from dense genotype data. *Genome research*, 15(11), 1553-1565.
<https://doi.org/10.1101/gr.4326505>

- Castilla, A. R., Méndez-Vigo, B., Marcer, A., Martínez-Minaya, J., Conesa, D., Picó, F. X., & Alonso-Blanco, C.** (2020). Ecological, genetic and evolutionary drivers of regional genetic differentiation in *Arabidopsis thaliana*. *BMC Evolutionary Biology*, 20(1), 1-13. <https://doi.org/10.1186/s12862-020-01635-2>
- Celletti, S., Pii, Y., Valentinuzzi, F., Tiziani, R., Fontanella, M. C., Beone, G. M., ... & Astolfi, S.** (2020). Physiological responses to Fe deficiency in split-root tomato plants: Possible roles of auxin and ethylene?. *Agronomy*, 10(7), 1000. <https://doi.org/10.3390/agronomy10071000>
- Chaurasia, S., Singh, A. K., Kumar, A., Songachan, L. S., Yadav, M. C., Kumar, S., ... & Singh, K.** (2021). Genome-wide association mapping reveals key genomic regions for physiological and yield-related traits under salinity stress in wheat (*Triticum aestivum* L.). *Genomics*, 113(5), 3198-3215. <https://doi.org/10.1016/j.ygeno.2021.07.014>
- Chen, L., Xiang, S., Chen, Y., Li, D., & Yu, D.** (2017). *Arabidopsis* WRKY45 interacts with the DELLA protein RGL1 to positively regulate age-triggered leaf senescence. *Molecular Plant*, 10(9), 1174-1189. <https://doi.org/10.1016/j.molp.2017.07.008>
- Chen, Q., Bai, L., Wang, W., Shi, H., Ramón Botella, J., Zhan, Q., ... & Song, C. P.** (2021). COP1 promotes ABA-induced stomatal closure by modulating the abundance of ABI/HAB and AHG3 phosphatases. *New Phytologist*, 229(4), 2035-2049. <https://doi.org/10.1111/nph.17001>
- Cheng, N. H., Liu, J. Z., Nelson, R. S., & Hirschi, K. D.** (2004). Characterization of CXIP4, a novel *Arabidopsis* protein that activates the H⁺/Ca²⁺ antiporter, CAX1. *FEBS letters*, 559(1-3), 99-106. [https://doi.org/10.1016/S0014-5793\(04\)00036-5](https://doi.org/10.1016/S0014-5793(04)00036-5)
- Che-Othman, M. H., Millar, A. H., & Taylor, N. L.** (2017). Connecting salt stress signaling pathways with salinity-induced changes in mitochondrial metabolic processes in C3 plants. *Plant, cell & environment*, 40(12), 2875-2905. <https://doi.org/10.1104/pp.106.085555>
- Chew, Y. H., & Halliday, K. J.** (2011). A stress-free walk from *Arabidopsis* to crops. *Current Opinion in Biotechnology*, 22(2), 281-286. <https://doi.org/10.1016/j.copbio.2010.11.011>
- Chiba, Y., Shimizu, T., Miyakawa, S., Kanno, Y., Koshiba, T., Kamiya, Y., & Seo, M.** (2015). Identification of *Arabidopsis thaliana* NRT1/PTR FAMILY (NPF) proteins capable of transporting plant hormones. *Journal of plant research*, 128, 679-686. <https://doi.org/10.1007/s10265-015-0710-2>
- Clark, T. J., & Lu, Y.** (2015). Analysis of loss-of-function mutants in aspartate kinase and homoserine dehydrogenase genes points to complexity in the regulation of aspartate-derived amino acid contents. *Plant Physiology*, 168(4), 1512-1526. <https://doi.org/10.1104/pp.15.00364>

- Clarke, J. H., & Dean, C.** (1994). Mapping FRI, a locus controlling flowering time and vernalization response in *Arabidopsis thaliana*. *Molecular and General Genetics MGG*, 242, 81-89.
<https://doi.org/10.1007/BF00277351>
- Colebrook, E. H., Thomas, S. G., Phillips, A. L., & Hedden, P.** (2014). The role of gibberellin signalling in plant responses to abiotic stress. *Journal of experimental biology*, 217(1), 67-75. <https://doi.org/10.1242/jeb.089938>
- Conti, L.** (2017). Hormonal control of the floral transition: can one catch them all?. *Developmental Biology*, 430(2), 288-301. <https://doi.org/10.1016/j.ydbio.2017.03.024>
- Coolen, S., Proietti, S., Hickman, R., Davila Olivas, N. H., Huang, P. P., Van Verk, M. C., ... & Van Wees, S. C.** (2016). Transcriptome dynamics of *Arabidopsis* during sequential biotic and abiotic stresses. *The Plant Journal*, 86(3), 249-267.
<https://doi.org/10.1111/tpj.13167>
- Corratgé-Faillie, C., & Lacombe, B.** (2017). Substrate (un) specificity of *Arabidopsis* NRT1/PTR FAMILY (NPF) proteins. *Journal of Experimental Botany*, 68(12), 3107-3113.
<https://doi.org/10.1093/jxb/erw499>
- Couturier, J., Ströher, E., Albetel, A. N., Roret, T., Muthuramalingam, M., Tarrago, L., ... & Rouhier, N.** (2011). *Arabidopsis* chloroplastic glutaredoxin C5 as a model to explore molecular determinants for iron-sulfur cluster binding into glutaredoxins. *Journal of Biological Chemistry*, 286(31), 27515-27527. <https://doi.org/10.1074/jbc.M111.228726>
- Crimmins, T. M., Crimmins, M. A., & David Bertelsen, C.** (2010). Complex responses to climate drivers in onset of spring flowering across a semi-arid elevation gradient. *Journal of Ecology*, 98(5), 1042-1051. <https://doi.org/10.1111/j.1365-2745.2010.01696.x>
- Dąbrowska-Bronk, J., Komar, D. N., Rusaczonek, A., Kozłowska-Makulska, A., Szechyńska-Hebda, M., & Karpiński, S.** (2016). β -carbonic anhydrases and carbonic ions uptake positively influence *Arabidopsis* photosynthesis, oxidative stress tolerance and growth in light dependent manner. *Journal of plant physiology*, 203, 44-54.
<https://doi.org/10.1016/j.jplph.2016.05.013>
- Davila Olivas, N. H., Coolen, S., Huang, P., Severing, E., van Verk, M. C., Hickman, R., ... & Dicke, M.** (2016). Effect of prior drought and pathogen stress on *Arabidopsis* transcriptome changes to caterpillar herbivory. *New Phytologist*, 210(4), 1344-1356.
<https://doi.org/10.1111/nph.13847>
- Davila Olivas, N. H., Frago, E., Thoen, M., Kloth, K. J., Becker, F., van Loon, J., Gort, G., Keurentjes, J., van Heerwaarden, J., & Dicke, M.** (2017). Natural variation in life history strategy of *Arabidopsis thaliana* determines stress responses to drought and insects of different feeding guilds. *Molecular ecology*, 26(11), 2959-2977.
<https://doi.org/10.1111/mec.14100>

- de Kraker, J. W., Luck, K., Textor, S., Tokuhisa, J. G., & Gershenzon, J.** (2007). Two *Arabidopsis* genes (IPMS1 and IPMS2) encode isopropylmalate synthase, the branchpoint step in the biosynthesis of leucine. *Plant physiology*, 143(2), 970–986.
<https://doi.org/10.1104/pp.106.085555>
- De Pristo, M. A., Banks, E., Poplin, R., Garimella, K. V., Maguire, J. R., Hartl, C., & Philippakis, A. A.** (2011). A framework for variation discovery and genotyping using next-generation DNA sequencing data. *Nature genetics*, 43(5), 491. <https://doi.org/10.1038/ng.806>
- de Vitry, C.** (2011). Cytochrome c maturation system on the negative side of bioenergetic membranes: CCB or System IV. *The FEBS journal*, 278(22), 4189–4197.
<https://doi.org/10.1111/j.1742-4658.2011.08373.x>
- Dellero, Y., Jossier, M., Schmitz, J., Maurino, V. G., & Hodges, M.** (2016). Photorespiratory glycolate–glyoxylate metabolism. *Journal of Experimental Botany*, 67(10), 3041–3052.
<https://doi.org/10.1093/jxb/erw090>
- Do, T. D., Vuong, T. D., Dunn, D., Clubb, M., Valliyodan, B., Patil, G., ... & Shannon, J. G.** (2019). Identification of new loci for salt tolerance in soybean by high-resolution genome-wide association mapping. *BMC genomics*, 20(1), 1–16.
<https://doi.org/10.1186/s12864-019-5662-9>
- Domergue, F., Vishwanath, S. J., Joubès, J., Ono, J., Lee, J. A., Bourdon, M., ... & Rowland, O.** (2010). Three *Arabidopsis* fatty acyl-coenzyme A reductases, FAR1, FAR4, and FAR5, generate primary fatty alcohols associated with suberin deposition. *Plant physiology*, 153(4), 1539–1554. <https://doi.org/10.1104/pp.110.158238>
- Dorca-Fornell, C., Gregis, V., Grandi, V., Coupland, G., Colombo, L., & Kater, M. M.** (2011). The *Arabidopsis* SOC1-like genes AGL42, AGL71 and AGL72 promote flowering in the shoot apical and axillary meristems. *The Plant Journal*, 67(6), 1006–1017.
<https://doi.org/10.1111/j.1365-313X.2011.04653.x>
- Dubois, M., Skirycz, A., Claeys, H., Maleux, K., Dhondt, S., De Bodt, S., ... & Inzé, D.** (2013). ETHYLENE RESPONSE FACTOR6 acts as a central regulator of leaf growth under water-limiting conditions in *Arabidopsis*. *Plant physiology*, 162(1), 319–332.
<https://doi.org/10.1104/pp.113.216341>
- Dubois, M., Van den Broeck, L., Claeys, H., Van Vlierberghe, K., Matsui, M., & Inzé, D.** (2015). The ETHYLENE RESPONSE FACTORS ERF6 and ERF11 antagonistically regulate mannitol-induced growth inhibition in *Arabidopsis*. *Plant physiology*, 169(1), 166–179.
<https://doi.org/10.1104/pp.15.00335>
- Earl, D. A., & VonHoldt, B. M.** (2012). STRUCTURE HARVESTER: a website and program for visualizing STRUCTURE output and implementing the Evanno method. *Conservation genetics resources*, 4, 359–361. <https://doi.org/10.1007/s12686-011-9548-7>
- Epstein, E.** (1998). How calcium enhances plant salt tolerance. *Science*, 280(5371), 1906–1907.
<https://doi.org/10.1126/science.280.5371.1906>

- Erice, G., Ruíz-Lozano, J. M., Zamarreño, Á. M., García-Mina, J. M., & Aroca, R.** (2017). Transcriptomic analysis reveals the importance of JA-Ile turnover in the response of *Arabidopsis* plants to plant growth promoting rhizobacteria and salinity. *Environmental and Experimental Botany*, 143 (10-19).
<https://doi.org/10.1016/j.envexpbot.2017.08.006>
- Eroglu, S., Meier, B., von Wirén, N., & Peiter, E.** (2016). The vacuolar manganese transporter MTP8 determines tolerance to iron deficiency-induced chlorosis in *Arabidopsis*. *Plant physiology*, 170(2), 1030-1045. <https://doi.org/10.1104/pp.15.01194>
- Evanno, G., Regnaut, S., & Goudet, J.** (2005). Detecting the number of clusters of individuals using the software STRUCTURE: a simulation study. *Molecular ecology*, 14(8), 2611-2620. <https://doi.org/10.1111/j.1365-294X.2005.02553.x>
- Excoffier, L., Foll, M., & Petit, R. J.** (2009). Genetic consequences of range expansions. *Annual Review of Ecology, Evolution, and Systematics*, 40, 481-501.
<https://doi.org/10.1146/annurev.ecolsys.39.110707.173414>
- Eyre-Walker, A., Keightley, P. D., Smith, N. G., & Gaffney, D.** (2002). Quantifying the slightly deleterious mutation model of molecular evolution. *Molecular Biology and Evolution*, 19(12), 2142-2149. <https://doi.org/10.1093/oxfordjournals.molbev.a004039>
- Fahey, J. W., Zalcman, A. T., & Talalay, P.** (2001). The chemical diversity and distribution of glucosinolates and isothiocyanates among plants. *Phytochemistry*, 56(1), 5-51.
[https://doi.org/10.1016/S0031-9422\(00\)00316-2](https://doi.org/10.1016/S0031-9422(00)00316-2)
- Fan, Y., Zhou, G., Shabala, S., Chen, Z. H., Cai, S., Li, C., & Zhou, M.** (2016). Genome-wide association study reveals a new QTL for salinity tolerance in barley (*Hordeum vulgare* L.). *Frontiers in plant science*, 7, 946. <https://doi.org/10.3389/fpls.2016.00946>
- Fang, S., Hou, X., & Liang, X.** (2021). Response mechanisms of plants under saline-alkali stress. *Frontiers in Plant Science*, 12, 667458. <https://doi.org/10.3389/fpls.2021.667458>
- FAO** (1973) Report of the FAO/UNDP regional seminar on reclamations and management of calcareous soils FAO Soils Bulletin 21, Calcareous soils. FAO-UN Rome. ISBN 92-5-100276-2. <https://www.fao.org/3/x5868e/x5868e00.htm>
- Farooq, S., Ahmad, S., Hussain, S., & Hussain, M.** (2018). Nutrient homeostasis and salt stress tolerance. In *Plant Nutrients and Abiotic Stress Tolerance*, 391-413. Springer, Singapore.
https://doi.org/10.1007/978-981-10-9044-8_17
- Feng, L., Liang, X., Zhou, Y., Zhang, Y., Liu, J., Cai, M., ... & Pan, H.** (2020). Functional Analysis of Aux/IAA s and SAURs on Shoot Growth of *Lagerstroemia indica* through Virus-Induced Gene Silencing (VIGS). *Forests*, 11(12), 1288. <https://doi.org/10.3390/f11121288>
- Flügel, F., Timm, S., Arrivault, S., Florian, A., Stitt, M., Fernie, A. R., & Bauwe, H.** (2017). The photorespiratory metabolite 2-phosphoglycolate regulates photosynthesis and starch accumulation in *Arabidopsis*. *The Plant Cell*, 29(10), 2537-2551.
<https://doi.org/10.1105/tpc.17.00256>

- Forieri, I., Sticht, C., Reichelt, M., Gretz, N., Hawkesford, M. J., Malagoli, M., ... & Hell, R.** (2017). System analysis of metabolism and the transcriptome in *Arabidopsis thaliana* roots reveals differential co-regulation upon iron, sulfur and potassium deficiency. *Plant, cell & environment*, 40(1), 95-107. <https://doi.org/10.1111/pce.12842>
- Franks, S. J., Kane, N. C., O'Hara, N. B., Tittes, S., & Rest, J. S.** (2016). Rapid genome-wide evolution in *Brassica rapa* populations following drought revealed by sequencing of ancestral and descendant gene pools. *Molecular ecology*, 25(15), 3622-3631. <https://doi.org/10.1111/mec.13615>
- Gan, T., Lin, Z., Bao, L., Hui, T., Cui, X., Huang, Y., ... & Qian, Y.** (2021). Comparative proteomic analysis of tolerant and sensitive varieties reveals that phenylpropanoid biosynthesis contributes to salt tolerance in mulberry. *International journal of molecular sciences*, 22(17), 9402. <https://doi.org/10.3390/ijms22179402>
- Gan, X., Stegle, O., Behr, J., Steffen, J. G., Drewe, P., Hildebrand, K. L., ... & Mott, R.** (2011). Multiple reference genomes and transcriptomes for *Arabidopsis thaliana*. *Nature*, 477(7365), 419-423. <https://doi.org/10.1038/nature10414>
- Garg, N., & Pandey, R.** (2015). Effectiveness of native and exotic arbuscular mycorrhizal fungi on nutrient uptake and ion homeostasis in salt-stressed *Cajanus cajan* L. (Millsp.) genotypes. *Mycorrhiza*, 25(3), 165-180. <https://doi.org/10.1007/s00572-014-0600-9>
- Gazzani, S., Gendall, A. R., Lister, C., & Dean, C.** (2003). Analysis of the molecular basis of flowering time variation in *Arabidopsis* accessions. *Plant physiology*, 132(2), 1107-1114. <https://doi.org/10.1104/pp.103.021212>
- Georgii, E., Jin, M., Zhao, J., Kanawati, B., Schmitt-Kopplin, P., Albert, A., ... & Schäffner, A. R.** (2017). Relationships between drought, heat and air humidity responses revealed by transcriptome-metabolome co-analysis. *BMC plant biology*, 17(1), 1-23. <https://doi.org/10.1186/s12870-017-1062-y>
- Greenbaum, J., & Deng, H. W.** (2017). A statistical approach to fine mapping for the identification of potential causal variants related to bone mineral density. *Journal of Bone and Mineral Research*, 32(8), 1651-1658. <https://doi.org/10.1002/jbmr.3154>
- Grodecká, L., Buratti, E., & Freiburger, T.** (2017). Mutations of pre-mRNA splicing regulatory elements: are predictions moving forward to clinical diagnostics? *International journal of molecular sciences*, 18(8), 1668. <https://doi.org/10.3390/ijms18081668>
- Guerrero, J., Andreollo, M., Burgarella, C., & Manel, S.** (2018). Soil environment is a key driver of adaptation in *Medicago truncatula*: new insights from landscape genomics. *New Phytologist*, 219(1), 378-390. <https://doi.org/10.1111/nph.15171>
- Gulisija, D., Kim, Y., & Plotkin, J. B.** (2016). Phenotypic plasticity promotes balanced polymorphism in periodic environments by a genomic storage effect. *Genetics*, 202(4), 1437-1448. <https://doi.org/10.1534/genetics.115.185702>

- Guo, L., Wang, J., Li, M., Liu, L., Xu, J., Cheng, J., ... & Luedeling, E.** (2019). Distribution margins as natural laboratories to infer species' flowering responses to climate warming and implications for frost risk. *Agricultural and Forest Meteorology*, 268, 299-307. <https://doi.org/10.1016/j.agrformet.2019.01.038>
- Guo, M., Li, H., Li, L., Cheng, X., Gao, W., Xu, Y., ... & Liu, X.** (2014). Comparative proteomic analysis of *Arabidopsis thaliana* roots between wild type and its salt-tolerant mutant. *Journal of Plant Interactions*, 9(1), 330-337. <https://doi.org/10.1080/17429145.2013.833653>
- Guo, R., Shi, L., Ding, X., Hu, Y., Tian, S., Yan, D., ... & Yang, Y.** (2010). Effects of saline and alkaline stress on germination, seedling growth, and ion balance in wheat. *Agronomy journal*, 102(4), 1252-1260. <https://doi.org/10.2134/agronj2010.0022>
- Guo, R., Shi, L., Yan, C., Zhong, X., Gu, F., Liu, Q., ... & Li, H.** (2017). Ionic and metabolic responses to neutral salt or alkaline salt stresses in maize (*Zea mays* L.) seedlings. *BMC Plant Biology*, 17(1), 1-13. <https://doi.org/10.1186/s12870-017-0994-6>
- Gupta, A., Hisano, H., Hojo, Y., Matsuura, T., Ikeda, Y., Mori, I. C., & Senthil-Kumar, M.** (2017). Global profiling of phytohormone dynamics during combined drought and pathogen stress in *Arabidopsis thaliana* reveals ABA and JA as major regulators. *Scientific reports*, 7(1), 1-13. <https://doi.org/10.1038/s41598-017-03907-2>
- Gupta, A., Sarkar, A. K., & Senthil-Kumar, M.** (2016). Global transcriptional analysis reveals unique and shared responses in *Arabidopsis thaliana* exposed to combined drought and pathogen stress. *Frontiers in plant science*, 7 (686). <https://doi.org/10.3389/fpls.2016.00686>
- Han, H., Wang, Q., Wei, L., Liang, Y., Dai, J., Xia, G., & Liu, S.** (2018). Small RNA and degradome sequencing used to elucidate the basis of tolerance to salinity and alkalinity in wheat. *BMC plant biology*, 18(1), 1-17. <https://doi.org/10.1186/s12870-018-1415-1>
- Hantzis, L. J., Kroh, G. E., Jahn, C. E., Cantrell, M., Peers, G., Pilon, M., & Ravet, K.** (2018). A program for iron economy during deficiency targets specific Fe proteins. *Plant Physiology*, 176(1), 596-610. <https://doi.org/10.1104/pp.17.01497>
- Hao, X., Li, J., Gao, S., Tuerxun, Z., Chang, X., Hu, W., ... & Huang, Q.** (2020). SsPsaH, a H subunit of the photosystem I reaction center of *Suaeda salsa*, confers the capacity of osmotic adjustment in tobacco. *Genes & Genomics*, 42(12), 1455-1465. <https://doi.org/10.1007/s13258-020-00970-4>
- Haro, R., Bañuelos, M. A., Senn, M. E., Barrero-Gil, J., & Rodríguez-Navarro, A.** (2005). HKT1 mediates sodium uniport in roots. Pitfalls in the expression of HKT1 in yeast. *Plant Physiology*, 139(3), 1495-1506. <https://doi.org/10.1104/pp.105.067553>

- Hartmann, L., Pedrotti, L., Weiste, C., Fekete, A., Schierstaedt, J., Göttler, J., ... & Dröge-Laser, W.** (2015). Crosstalk between two bZIP signaling pathways orchestrates salt-induced metabolic reprogramming in *Arabidopsis* roots. *The Plant Cell*, 27(8), 2244-2260. <https://doi.org/10.1105/tpc.15.00163>
- Hazzouri, K. M., Khraiweh, B., Amiri, K. M., Pauli, D., Blake, T., Shahid, M., ... & Masmoudi, K.** (2018). Mapping of HKT1; 5 gene in barley using GWAS approach and its implication in salt tolerance mechanism. *Frontiers in Plant Science*, 9, 156. <https://doi.org/10.3389/fpls.2018.00156>
- He, Y., Wu, D., Wei, D., Fu, Y., Cui, Y., Dong, H., ... & Qian, W.** (2017). GWAS, QTL mapping and gene expression analyses in *Brassica napus* reveal genetic control of branching morphogenesis. *Scientific reports*, 7(1), 1-9. <https://doi.org/10.1038/s41598-017-15976-4>
- Heidari, P., Entazari, M., Ebrahimi, A., Ahmadzadeh, M., Vannozzi, A., Palumbo, F., & Barcaccia, G.** (2021). Exogenous EBR ameliorates endogenous hormone contents in tomato species under low-temperature stress. *Horticulturae*, 7(4), 84. <https://doi.org/10.3390/horticulturae7040084>
- Hentrich, M., Böttcher, C., Dückting, P., Cheng, Y., Zhao, Y., Berkowitz, O., ... & Pollmann, S.** (2013). The jasmonic acid signaling pathway is linked to auxin homeostasis through the modulation of YUCCA 8 and YUCCA 9 gene expression. *The Plant Journal*, 74(4), 626-637. <https://doi.org/10.1111/tpj.12152>
- Hirayama, T., & Shinozaki, K.** (2010). Research on plant abiotic stress responses in the post-genome era: past, present and future. *The Plant Journal*, 61(6), 1041-1052. <https://doi.org/10.1111/j.1365-3113X.2010.04124.x>
- Horton, M. W., Hancock, A. M., Huang, Y. S., Toomajian, C., Atwell, S., Auton, A., ... & Bergelson, J.** (2012). Genome-wide patterns of genetic variation in worldwide *Arabidopsis thaliana* accessions from the RegMap panel. *Nature genetics*, 44(2), 212-216. <https://doi.org/10.1038/ng.1042>
- Hosseini, S. Z., Ismaili, A., Nazarian-Firouzabadi, F., Fallahi, H., Nejad, A. R., & Sohrabi, S.** (2021). Dissecting the molecular responses of lentil to individual and combined drought and heat stresses by comparative transcriptomic analysis. *Genomics*, 113(2), 693-705. <https://doi.org/10.1016/j.ygeno.2020.12.038>
- Hsieh, E. J., & Waters, B. M.** (2016). Alkaline stress and iron deficiency regulate iron uptake and riboflavin synthesis gene expression differently in root and leaf tissue: implications for iron deficiency chlorosis. *Journal of Experimental Botany*, 67(19), 5671-5685. <https://doi.org/10.1093/jxb/erw328>
- Hsieh, E. J., Cheng, M. C., & Lin, T. P.** (2013). Functional characterization of an abiotic stress-inducible transcription factor AtERF53 in *Arabidopsis thaliana*. *Plant molecular biology*, 82(3), 223-237. <https://doi.org/10.1007/s11103-013-0054-z>

- Hu, R., Zhu, Y., Shen, G., & Zhang, H.** (2017). Overexpression of the PP2A-C5 gene confers increased salt tolerance in *Arabidopsis thaliana*. *Plant signaling & behavior*, 12(2), e1276687. <https://doi.org/10.1080/15592324.2016.1276687>
- Hu, X., Wang, D., Ren, S., Feng, S., Zhang, H., Zhang, J., ... & Zhou, A.** (2022). Inhibition of root growth by alkaline salts due to disturbed ion transport and accumulation in *Leymus chinensis*. *Environmental and Experimental Botany*, 104907. <https://doi.org/10.1016/j.envexpbot.2022.104907>
- Huang, R. D.** (2018). Research progress on plant tolerance to soil salinity and alkalinity in sorghum. *Journal of Integrative Agriculture*, 17(4), 739-746. [https://doi.org/10.1016/S2095-3119\(17\)61728-3](https://doi.org/10.1016/S2095-3119(17)61728-3)
- Huijser, P., & Schmid, M.** (2011). The control of developmental phase transitions in plants. *Development*, 138(19), 4117-4129. <https://doi.org/10.1242/dev.063511>
- Huson, D. H., & Bryant, D.** (2006). Application of phylogenetic networks in evolutionary studies. *Molecular biology and evolution*, 23(2), 254-267. <https://doi.org/10.1093/molbev/msj030>
- Hussain, A., Shah, M., Hamayun, M., Iqbal, A., Murad, W., Irshad, M., ... & Kim, H. Y.** (2021). *Pseudocitrobacter anthropi* reduces heavy metal uptake and improves phytohormones and antioxidant system in *Glycine max* L. *World Journal of Microbiology and Biotechnology*, 37(11), 1-19. <https://doi.org/10.1007/s11274-021-03156-6>
- Hussien, S. A., & Doosh, K.** (2021). Extraction, Purification and Characterization of β -Galactosidase from Tomato (*Lycopersicon esculentum*). In *IOP Conference Series: Earth and Environmental Science* (Vol. 761, No. 1, p. 012123). IOP Publishing. <https://doi.org/10.1088/1755-1315/761/1/012123>
- Iglesias, M. J., Sellaro, R., Zurbriggen, M. D., & Casal, J. J.** (2018). Multiple links between shade avoidance and auxin networks. *Journal of Experimental Botany*, 69(2), 213-228. <https://doi.org/10.1093/jxb/erx295>
- Ismail, A., Seo, M., Takebayashi, Y., Kamiya, Y., Eiche, E., & Nick, P.** (2014). Salt adaptation requires efficient fine-tuning of jasmonate signalling. *Protoplasma*, 251(4), 881-898. <https://doi.org/10.1007/s00709-013-0591-y>
- Jin, H., Plaha, P., Park, J. Y., Hong, C. P., Lee, I. S., Yang, Z. H., ... & Lim, Y. P.** (2006). Comparative EST profiles of leaf and root of *Leymus chinensis*, a xerophilous grass adapted to high pH sodic soil. *Plant Science*, 170(6), 1081-1086. <https://doi.org/10.1016/j.plantsci.2006.01.002>
- Jin, T., Sun, Y., Shan, Z., He, J., Wang, N., Gai, J., & Li, Y.** (2021). Natural variation in the promoter of GsERD15B affects salt tolerance in soybean. *Plant biotechnology journal*, 19(6), 1155-1169. <https://doi.org/10.1111/pbi.13536>

- Jing, Y., Shi, L., Li, X., Zheng, H., Gao, J., Wang, M., ... & Zhang, W. (2019). OXS2 is required for salt tolerance mainly through associating with salt Inducible genes, CA1 and Araport11, in *Arabidopsis*. *Scientific reports*, 9(1), 1-11.
<https://doi.org/10.1038/s41598-019-56456-1>
- Jobbágy, E. G., Tóth, T., Nasetto, M. D., & Earman, S. (2017). On the fundamental causes of high environmental alkalinity (pH \geq 9): an assessment of its drivers and global distribution. *Land Degradation & Development*, 28(7), 1973-1981.
<https://doi.org/10.1002/ldr.2718>
- Johanson, U., West, J., Lister, C., Michaels, S., Amasino, R., & Dean, C. (2000). Molecular analysis of FRIGIDA, a major determinant of natural variation in *Arabidopsis* flowering time. *Science*, 290(5490), 344-347. <https://doi.org/10.1126/science.290.5490.344>
- Jombart, T. (2008). adegenet: a R package for the multivariate analysis of genetic markers. *Bioinformatics* 24(11), 1403-1405. <https://doi.org/10.1093/bioinformatics/btn129>
- Julkowska, M. M., & Testerink, C. (2015). Tuning plant signaling and growth to survive salt. *Trends in plant science*, 20(9), 586-594. <https://doi.org/10.1016/j.tplants.2015.06.008>
- Julkowska, M. M., Hoefsloot, H. C., Mol, S., Feron, R., de Boer, G. J., Haring, M. A., & Testerink, C. (2014). Capturing *Arabidopsis* root architecture dynamics with ROOT-FIT reveals diversity in responses to salinity. *Plant Physiology*, 166(3), 1387-1402.
<https://doi.org/10.1104/pp.114.248963>
- Julkowska, M. M., Koevoets, I. T., Mol, S., Hoefsloot, H., Feron, R., Tester, M. A., ... & Testerink, C. (2017). Genetic components of root architecture remodeling in response to salt stress. *The plant cell*, 29(12), 3198-3213. <https://doi.org/10.1105/tpc.16.00680>
- Jung, C., Pillen, K., Staiger, D., Coupland, G., & Von Korff, M. (2017). Recent advances in flowering time control. *Frontiers in plant science*, 7, 2011.
<https://doi.org/10.3389/fpls.2016.02011>
- Kang, M. J., Jin, H. S., Noh, Y. S., & Noh, B. (2015). Repression of flowering under a noninductive photoperiod by the HDA 9-AGL 19-FT module in *Arabidopsis*. *New Phytologist*, 206(1), 281-294. <https://doi.org/10.1111/nph.13161>
- Katori T, Ikeda A, Iuchi S, Kobayashi M, Shinozaki K, Maehashi K, Sakata Y, Tanaka S, Taji T. (2010). Dissecting the genetic control of natural variation in salt tolerance of *Arabidopsis thaliana* accessions. *Journal of Experimental Botany* 61, 1125–1138.
<https://doi.org/10.1093/jxb/erp376>
- Kawa, D., Julkowska, M. M., Sommerfeld, H. M., Ter Horst, A., Haring, M. A., & Testerink, C. (2016). Phosphate-dependent root system architecture responses to salt stress. *Plant physiology*, 172(2), 690-706. <https://doi.org/10.1104/pp.16.00712>
- Kazan, K., & Lyons, R. (2016). The link between flowering time and stress tolerance. *Journal of experimental botany*, 67(1), 47-60. <https://doi.org/10.1093/jxb/erv441>

- Kazan, K., & Manners, J. M.** (2012). JAZ repressors and the orchestration of phytohormone crosstalk. *Trends in plant science*, 17(1), 22-31.
<https://doi.org/10.1016/j.tplants.2011.10.006>
- Kazan, K., & Manners, J. M.** (2013). MYC2: the master in action. *Molecular plant*, 6(3), 686-703.
<https://doi.org/10.1093/mp/sss128>
- Khare, R., Dhar, Y. V., Sandhu, G., Singh, S., Kumar, S., Khan, A., ... & Trivedi, P. K.** (2022). Genome-wide expression and variation in nucleotide sequences lead to differential response of *Arabidopsis thaliana* ecotypes towards arsenic stress under sulfur limiting condition. *Environmental and Experimental Botany*, 195, 104764.
<https://doi.org/10.1016/j.envexpbot.2021.104764>
- Kim, W., Latrasse, D., Servet, C., & Zhou, D. X.** (2013). *Arabidopsis* histone deacetylase HDA9 regulates flowering time through repression of AGL19. *Biochemical and biophysical research communications*, 432(2), 394-398.
<https://doi.org/10.1016/j.bbrc.2012.11.102>
- Knight, H., Trewavas, A. J., & Knight, M. R.** (1997). Calcium signalling in *Arabidopsis thaliana* responding to drought and salinity. *The Plant Journal*, 12(5), 1067-1078.
<https://doi.org/10.1046/j.1365-313X.1997.12051067.x>
- Konečná, V., Bray, S., Vlček, J., Bohutínská, M., Požárová, D., Choudhury, R. R., ... & Kolář, F.** (2021). Parallel adaptation in autopolyploid *Arabidopsis arenosa* is dominated by repeated recruitment of shared alleles. *Nature communications*, 12(1), 4979.
<https://doi.org/10.1038/s41467-021-25256-5>
- Koornneef, M., Hanhart, C. J., & Van der Veen, J. H.** (1991). A genetic and physiological analysis of late flowering mutants in *Arabidopsis thaliana*. *Molecular and General Genetics*, 229, 57-66. <https://doi.org/10.1007/BF00264213>
- Kooyers, N. J.** (2015). The evolution of drought escape and avoidance in natural herbaceous populations. *Plant science*, 234, 155-162.
<https://doi.org/10.1016/j.plantsci.2015.02.012>
- Korneliussen, T. S., Moltke, I., Albrechtsen, A., & Nielsen, R.** (2013). Calculation of Tajima's D and other neutrality test statistics from low depth next-generation sequencing data. *BMC bioinformatics*, 14(1), 1-14. <https://doi.org/10.1186/1471-2105-14-289>
- Korte, A., & Farlow, A.** (2013). The advantages and limitations of trait analysis with GWAS: a review. *Plant methods*, 9(1), 1-9. <https://doi.org/10.1186/1746-4811-9-29>
- Korves, T. M., Schmid, K. J., Caicedo, A. L., Mays, C., Stinchcombe, J. R., Purugganan, M. D., & Schmitt, J.** (2007). Fitness effects associated with the major flowering time gene FRIGIDA in *Arabidopsis thaliana* in the field. *The American Naturalist*, 169(5), E141-E157. <https://doi.org/10.1086/513111>

- Kotake, T., Dina, S., Konishi, T., Kaneko, S., Igarashi, K., Samejima, M., ... & Tsumuraya, Y.** (2005). Molecular cloning of a β -galactosidase from radish that specifically hydrolyzes β -(1 \rightarrow 3)-and β -(1 \rightarrow 6)-galactosyl residues of arabinogalactan protein. *Plant Physiology*, 138(3), 1563-1576. <https://doi.org/10.1104/pp.105.062562>
- Kroh, G. E., & Pilon, M.** (2020). Regulation of iron homeostasis and use in chloroplasts. *International Journal of Molecular Sciences*, 21(9), 3395. <https://doi.org/10.3390/ijms21093395>
- Kubra, G., Khan, M., Munir, F., Gul, A., Shah, T., Hussain, A., ... & Amir, R.** (2021). Expression characterization of flavonoid biosynthetic pathway genes and transcription factors in peanut under water deficit conditions. *Frontiers in Plant Science*, 12, 680368. <https://doi.org/10.3389/fpls.2021.680368>
- Kumar, D., Datta, R., Hazra, S., Sultana, A., Mukhopadhyay, R., & Chattopadhyay, S.** (2015). Transcriptomic profiling of *Arabidopsis thaliana* mutant pad 2.1 in response to combined cold and osmotic stress. *PLoS One*, 10(3), e0122690. <https://doi.org/10.1371/journal.pone.0122690>
- Kumar, D., Hazra, S., Datta, R., & Chattopadhyay, S.** (2016). Transcriptome analysis of *Arabidopsis* mutants suggests a crosstalk between ABA, ethylene and GSH against combined cold and osmotic stress. *Scientific reports*, 6(1), 1-13. <https://doi.org/10.1038/srep36867>
- Kumar, V., Singh, A., Mithra, S. A., Krishnamurthy, S. L., Parida, S. K., Jain, S., ... & Mohapatra, T.** (2015). Genome-wide association mapping of salinity tolerance in rice (*Oryza sativa*). *DNA research*, 22(2), 133-145. <https://doi.org/10.1093/dnares/dsu046>
- Kumari, S., Chhillar, H., Chopra, P., Khanna, R. R., & Khan, M. I. R.** (2021). Potassium: A track to develop salinity tolerant plants. *Plant Physiology and Biochemistry*, 167, 1011-1023. <https://doi.org/10.1016/j.plaphy.2021.09.031>
- Langmead, B., & Salzberg, S. L.** (2012). Fast gapped-read alignment with Bowtie 2. *Nature methods*, 9(4), 357-359. <https://doi.org/10.1038/nmeth.1923>
- Laurie, S., Feeney, K. A., Maathuis, F. J., Heard, P. J., Brown, S. J., & Leigh, R. A.** (2002). A role for HKT1 in sodium uptake by wheat roots. *The Plant Journal*, 32(2), 139-149. <https://doi.org/10.1046/j.1365-313X.2002.01410.x>
- Le Corre, V., Roux, F., & Reboud, X.** (2002). DNA polymorphism at the FRIGIDA gene in *Arabidopsis thaliana*: extensive nonsynonymous variation is consistent with local selection for flowering time. *Molecular biology and evolution*, 19(8), 1261-1271. <https://doi.org/10.1093/oxfordjournals.molbev.a004187>
- Lee, E. J., Matsumura, Y., Soga, K., Hoson, T., & Koizumi, N.** (2007). Glycosyl hydrolases of cell wall are induced by sugar starvation in *Arabidopsis*. *Plant and cell physiology*, 48(3), 405-413. <https://doi.org/10.1093/pcp/pcm009>

- Li, B., & Dewey, C. N.** (2011). RSEM: accurate transcript quantification from RNA-Seq data with or without a reference genome. *BMC bioinformatics*, 12(1), 1-16. <https://doi.org/10.1093/bioinformatics/btq009>
- Lee, H. Y., Chen, Y. C., Kieber, J. J., & Yoon, G. M.** (2017). Regulation of the turnover of ACC synthases by phytohormones and heterodimerization in *Arabidopsis*. *The Plant Journal*, 91(3), 491-504. <https://doi.org/10.1111/tpj.13585>
- Lempe, J., Balasubramanian, S., Sureshkumar, S., Singh, A., Schmid, M., & Weigel, D.** (2005). Diversity of flowering responses in wild *Arabidopsis thaliana* strains. *PLoS genetics*, 1(1), e6. <https://doi.org/10.1371/journal.pgen.0010006>
- Lewontin, R. C., & Krakauer, J.** (1973). Distribution of gene frequency as a test of the theory of the selective neutrality of polymorphisms. *Genetics*, 74(1), 175-195. <https://doi.org/10.1093/genetics/74.1.175>
- Lezhneva, L., Kuras, R., Ephritikhine, G., & De Vitry, C.** (2008). A novel pathway of cytochrome c biogenesis is involved in the assembly of the cytochrome b6f complex in *Arabidopsis* chloroplasts. *Journal of Biological Chemistry*, 283(36), 24608-24616. <https://doi.org/10.1074/jbc.M803869200>
- Li, B.** (2020). Identification of genes conferring plant salt tolerance using GWAS: current success and perspectives. *Plant and Cell Physiology*, 61(8), 1419-1426. <https://doi.org/10.1093/bioinformatics/btq073>
- Li, B., Byrt, C., Qiu, J., Baumann, U., Hrmova, M., Evrard, A., ... & Roy, S. J.** (2016). Identification of a stelar-localized transport protein that facilitates root-to-shoot transfer of chloride in *Arabidopsis*. *Plant Physiology*, 170(2), 1014-1029. <https://doi.org/10.1104/pp.15.01163>
- Li, H.** (2016). Minimap and miniasm: fast mapping and de novo assembly for noisy long sequences. *Bioinformatics*, 32(14), 2103-2110. <https://doi.org/10.1093/bioinformatics/btw152>
- Li, J., Jia, Y., Dong, R., Huang, R., Liu, P., Li, X., ... & Chen, Z.** (2019). Advances in the mechanisms of plant tolerance to manganese toxicity. *International Journal of Molecular Sciences*, 20(20), 5096. <https://doi.org/10.3390/ijms20205096>
- Li, N., Liu, H., Sun, J., Zheng, H., Wang, J., Yang, L., ... & Zou, D.** (2018). Transcriptome analysis of two contrasting rice cultivars during alkaline stress. *Scientific reports*, 8(1), 1-16. <https://doi.org/10.1038/s41598-018-27940-x>
- Li, P., Filiault, D., Box, M. S., Kerdaffrec, E., van Oosterhout, C., Wilczek, A. M., ... & Dean, C.** (2014). Multiple FLC haplotypes defined by independent cis-regulatory variation underpin life history diversity in *Arabidopsis thaliana*. *Genes & Development*, 28(15), 1635-1640. <http://www.genesdev.org/cgi/doi/10.1101/gad.245993.114>

- Li, Z., Zhang, Z., He, Z., Tang, W., Li, T., Zeng, Z., ... & Shi, Y.** (2009). A partition-ligation-combination-subdivision EM algorithm for haplotype inference with multiallelic markers: update of the SHESis (<http://analysis.bio-x.cn>). *Cell research*, 19(4), 519-523. <https://doi.org/10.1038/cr.2009.33>
- Lin, S. H., Kuo, H. F., Canivenc, G., Lin, C. S., Lepetit, M., Hsu, P. K., ... & Tsay, Y. F.** (2008). Mutation of the *Arabidopsis* NRT1. 5 nitrate transporter causes defective root-to-shoot nitrate transport. *The Plant Cell*, 20(9), 2514-2528. <https://doi.org/10.1105/tpc.108.060244>
- Liu, J., Hu, J., Li, Y., Li, G., & Wu, H.** (2021). Calcium channels and transporters in plants under salinity stress. *Calcium transport elements in plants*, 157-169. <https://doi.org/10.1016/B978-0-12-821792-4.00002-3>
- Liu, L., & Wang, B.** (2021). Protection of halophytes and their uses for cultivation of saline-alkali soil in China. *Biology*, 10(5), 353. <https://doi.org/10.3390/biology10050353>
- Liu, P., Huang, R., Hu, X., Jia, Y., Li, J., Luo, J., ... & Chen, Z.** (2019). Physiological responses and proteomic changes reveal insights into *Stylosanthes* response to manganese toxicity. *BMC plant biology*, 19(1), 1-21. <https://doi.org/10.1186/s12870-019-1822-y>
- Liu, Q., Zhang, Y. C., Wang, C. Y., Luo, Y. C., Huang, Q. J., Chen, S. Y., ... & Chen, Y. Q.** (2009). Expression analysis of phytohormone-regulated microRNAs in rice, implying their regulation roles in plant hormone signaling. *FEBS letters*, 583(4), 723-728. <https://doi.org/10.1016/j.febslet.2009.01.020>
- Liu, S., Zhong, H., Meng, X., Sun, T., Li, Y., Pinson, S. R., ... & Peng, Z.** (2020). Genome-wide association studies of ionomic and agronomic traits in USDA mini core collection of rice and comparative analyses of different mapping methods. *BMC plant biology*, 20(1), 1-18. <https://doi.org/10.1186/s12870-020-02603-0>
- Liu, Y., Chen, X., Xue, S., Quan, T., Cui, D., Han, L., ... & Xu, Z. Y.** (2021). SET DOMAIN GROUP 721 protein functions in saline-alkaline stress tolerance in the model rice variety Kitaake. *Plant biotechnology journal*, 19(12), 2576. <https://doi.org/10.1111/pbi.13683>
- Llanes, A., Andrade, A., Masciarelli, O., Alemano, S., & Luna, V.** (2016). Drought and salinity alter endogenous hormonal profiles at the seed germination phase. *Seed Science Research*, 26(1), 1-13. <https://doi.org/10.1017/S0960258515000331>
- Llugany, M., Martin, S. R., Barceló, J., & Poschenrieder, C.** (2013). Endogenous jasmonic and salicylic acids levels in the Cd-hyperaccumulator *Noccaea (Thlaspi) praecox* exposed to fungal infection and/or mechanical stress. *Plant cell reports*, 32(8), 1243-1249. <https://doi.org/10.1007/s00299-013-1427-0>
- Lopez-Berenguer, C., Martínez-Ballesta, M. D. C., Moreno, D. A., Carvajal, M., & Garcia-Viguera, C.** (2009). Growing hardier crops for better health: salinity tolerance and the nutritional value of broccoli. *Journal of Agricultural and Food Chemistry*, 57(2), 572-578. <https://doi.org/10.1021/jf802994p>

- López-Marqués, R. L., Davis, J. A., Harper, J. F., & Palmgren, M.** (2021). Dynamic membranes: the multiple roles of P4 and P5 ATPases. *Plant Physiology*, 185(3), 619-631. <https://doi.org/10.1093/plphys/kiaa065>
- Love, M.I., Huber, W. & Anders, S.** (2014). Moderated estimation of fold change and dispersion for RNA-seq data with DESeq2. *Genome Biol* 15(550). <https://doi.org/10.1186/s13059-014-0550-8>
- Lovelli, S., Scopa, A., Perniola, M., Di Tommaso, T., & Sofo, A.** (2012). Absciscic acid root and leaf concentration in relation to biomass partitioning in salinized tomato plants. *Journal of plant physiology*, 169(3), 226-233. <https://doi.org/10.1016/j.jplph.2011.09.009>
- Ma, H. & Wang, P.** (2021). Regulation of plant responses to salt stress. *International Journal of Molecular Sciences*, 22(9), 4609. <https://doi.org/10.3389/fpls.2019.00498>
- Mahrez, W., Shin, J., Munoz-Viana, R., Figueiredo, D. D., Trejo-Arellano, M. S., Exner, V., ... & Hennig, L.** (2016). BRR2a affects flowering time via FLC splicing. *PLoS genetics*, 12(4), e1005924. <https://doi.org/10.1371/journal.pgen.1005924>
- Malone, L. A., Proctor, M. S., Hitchcock, A., Hunter, C. N., & Johnson, M. P.** (2021). Cytochrome b6f-Orchestrator of photosynthetic electron transfer. *Biochimica et Biophysica Acta (BBA)-Bioenergetics*, 1862(5), 148380. <https://doi.org/10.1016/j.bbabi.2021.148380>
- Mamidi, S., Lee, R. K., Goos, J. R., & McClean, P. E.** (2014). Genome-wide association studies identifies seven major regions responsible for iron deficiency chlorosis in soybean (*Glycine max*). *PloS one*, 9(9), e107469. <https://doi.org/10.1371/journal.pone.0107469>
- Manzano-Piedras, E., Marcer, A., Alonso-Blanco, C., & Pico, F. X.** (2014). Deciphering the adjustment between environment and life history in annuals: lessons from a geographically explicit approach in *Arabidopsis thaliana*. *PloS one*, 9(2), e87836. <https://doi.org/10.1371/journal.pone.0087836>
- Mao, B., Yin, H., Wang, Y., Zhao, T. H., Tian, R. R., Wang, W., & Ye, J. S.** (2017). Combined effects of O₃ and UV radiation on secondary metabolites and endogenous hormones of soybean leaves. *PloS one*, 12(8), e0183147. <https://doi.org/10.1371/journal.pone.0183147>
- Mao, F., Nan, G., Cao, M., Gao, Y., Guo, L., Meng, X., & Yang, G.** (2018). The metal distribution and the change of physiological and biochemical process in soybean and mung bean plants under heavy metal stress. *International journal of phytoremediation*, 20(11), 1113-1120. <https://doi.org/10.1080/15226514.2017.1365346>
- Marconi, G., Pace, R., Traini, A., Raggi, L., Lutts, S., Chiusano, M., ... & Albertini, E.** (2013). Use of MSAP markers to analyse the effects of salt stress on DNA methylation in rapeseed (*Brassica napus* var. *oleifera*). *PloS one*, 8(9), e75597. <https://doi.org/10.1371/journal.pone.0075597>

- Maris, A., Suslov, D., Fry, S. C., Verbelen, J. P., & Vissenberg, K.** (2009). Enzymic characterization of two recombinant xyloglucan endotransglucosylase/hydrolase (XTH) proteins of *Arabidopsis* and their effect on root growth and cell wall extension. *Journal of Experimental Botany*, 60(13), 3959-3972. <https://doi.org/10.1093/jxb/erp229>
- Martinez-Zapater, J. M., Coupland, G., Dean, C., & Koornneef, M.** (1994). The transition to flowering in *Arabidopsis*. In E. M. Meyerowitz, & C. R. Somerville (Eds.), *Arabidopsis* (pp. 403-433). Cold Spring Harbor Laboratory Press.
- Martos, S., Gallego, B., Cabot, C., Llugany, M., Barceló, J., & Poschenrieder, C.** (2016). Zinc triggers signaling mechanisms and defense responses promoting resistance to *Alternaria brassicicola* in *Arabidopsis thaliana*. *Plant Science*, 249, 13-24. <https://doi.org/10.1016/j.plantsci.2016.05.001>
- Máthé, C., Garda, T., Freytag, C., & M-Hamvas, M.** (2019). The role of serine-threonine protein phosphatase PP2A in plant oxidative stress signaling—facts and hypotheses. *International journal of molecular sciences*, 20(12), 3028. <https://doi.org/10.3390/ijms20123028>
- McDowell, S. C., Lopez-Marques, R. L., Poulsen, L. R., Palmgren, M. G., & Harper, J. F.** (2013). Loss of the *Arabidopsis thaliana* P4-ATPase ALA3 reduces adaptability to temperature stresses and impairs vegetative, pollen, and ovule development. *PloS one*, 8(5), e62577. <https://doi.org/10.1371/journal.pone.0062577>
- Mehmood, E., R. Kausar, M. Akram and S.M. Shahzad.** (2009). Is boron required to improve rice growth and yield in saline environment. *Pak. J. Bot.*, 41(3):1339-1350.
- Méndez-Vigo, B., Picó, F. X., Ramiro, M., Martínez-Zapater, J. M., & Alonso-Blanco, C.** (2011). Altitudinal and climatic adaptation is mediated by flowering traits and FRI, FLC, and PHYC genes in *Arabidopsis*. *Plant physiology*, 157(4), 1942-1955. <https://doi.org/10.1104/pp.111.183426>
- Mendoza-Cózatl, D. G., Gokul, A., Carelse, M. F., Jobe, T. O., Long, T. A., & Keyster, M.** (2019). Keep talking: crosstalk between iron and sulfur networks fine-tunes growth and development to promote survival under iron limitation. *Journal of Experimental Botany*, 70(16), 4197-4210. <https://doi.org/10.1093/jxb/erz290>
- Meng, C., Quan, TY., Li, ZY. et al.** (2017). Transcriptome profiling reveals the genetic basis of alkalinity tolerance in wheat. *BMC Genomics* 18-24. <https://doi.org/10.1186/s12864-016-3421-8>
- Mengel, K., & Kirkby, E. A.** (2012). *Principles of plant nutrition*. Springer Science & Business Media. <https://doi.org/10.1093/aob/mch063>
- Michaels, S. D., & Amasino, R. M.** (1999). FLOWERING LOCUS C encodes a novel MADS domain protein that acts as a repressor of flowering. *The Plant Cell*, 11(5), 949-956. <https://doi.org/10.1105/tpc.11.5.949>

- Michaels, S. D., & Amasino, R. M.** (2001). Loss of FLOWERING LOCUS C activity eliminates the late-flowering phenotype of FRIGIDA and autonomous pathway mutations but not responsiveness to vernalization. *The Plant Cell*, 13(4), 935-941.
<https://doi.org/10.1105/tpc.13.4.935>
- Miller, C. N., & Busch, W.** (2021). Using natural variation to understand plant responses to iron availability. *Journal of Experimental Botany*, 72(6), 2154-2164.
<https://doi.org/10.1093/jxb/erab012>
- Milner, M. J., Seamon, J., Craft, E., & Kochian, L. V.** (2013). Transport properties of members of the ZIP family in plants and their role in Zn and Mn homeostasis. *Journal of experimental botany*, 64(1), 369-381. <https://doi.org/10.1093/jxb/ers315>
- Moeder, W., Ung, H., Mosher, S., & Yoshioka, K.** (2010). SA-ABA antagonism in defense responses. *Plant signaling & behavior*, 5(10), 1231-1233.
<https://doi.org/10.4161/psb.5.10.12836>
- Møller, I. S., Gilliam, M., Jha, D., Mayo, G. M., Roy, S. J., Coates, J. C., ... & Tester, M.** (2009). Shoot Na⁺ exclusion and increased salinity tolerance engineered by cell type-specific alteration of Na⁺ transport in *Arabidopsis*. *The Plant Cell*, 21(7), 2163-2178.
<https://doi.org/10.1105/tpc.108.064568>
- Moneo-Sánchez, M., Izquierdo, L., Martín, I., Labrador, E., & Dopico, B.** (2016). Subcellular location of *Arabidopsis thaliana* subfamily a1 β -galactosidases and developmental regulation of transcript levels of their coding genes. *Plant Physiology and Biochemistry*, 109, 137-145. <https://doi.org/10.1016/j.plaphy.2016.09.016>
- Munns, R.** (1993). Physiological processes limiting plant growth in saline soils: some dogmas and hypotheses. *Plant, Cell & Environment*, 16(1), 15-24.
<https://doi.org/10.1111/j.1365-3040.1993.tb00840.x>
- Mutasa-Göttgens, E., & Hedden, P.** (2009). Gibberellin as a factor in floral regulatory networks. *Journal of experimental botany*, 60(7), 1979-1989. <https://doi.org/10.1093/jxb/erp040>
- Mwando, E., Han, Y., Angessa, T. T., Zhou, G., Hill, C. B., Zhang, X. Q., & Li, C.** (2020). Genome-wide association study of salinity tolerance during germination in barley (*Hordeum vulgare* L.). *Frontiers in plant science*, 11, 118.
<https://doi.org/10.3389/fpls.2020.00118>
- Naing, A. H., & Kim, C. K.** (2021). Abiotic stress-induced anthocyanins in plants: Their role in tolerance to abiotic stresses. *Physiologia Plantarum*, 172(3), 1711-1723.
<https://doi.org/10.1111/ppl.13373>
- Nam, Y. J., Herman, D., Blomme, J., Chae, E., Kojima, M., Coppens, F., ... & Gonzalez, N.** (2017). Natural variation of molecular and morphological gibberellin responses. *Plant Physiology*, 173(1), 703-714. <https://doi.org/10.1104/pp.16.01626>
- Napp-Zinn, K.** (1969). *Arabidopsis thaliana* (L.) Heynh. In LT Evans, (Eds.), *The Induction of Flowering: Some Case Histories*. MacMillan, Melbourne, Australia, pp 291-304

- Nayeripasand, L., Garoosi, G. A., & Ahmadikhah, A.** (2021). Genome-wide association study (GWAS) to identify salt-tolerance QTLs carrying novel candidate genes in rice during early vegetative stage. *Rice*, 14(1), 1-21. <https://doi.org/10.1186/s12284-020-00433-0>
- Nei, Masatoshi.** (1972). Genetic distance between populations. *The American Naturalist* 106(949), 283-292. <https://doi.org/10.2307/2459777>
- Nielsen, R., Korneliussen, T., Albrechtsen, A., Li, Y., & Wang, J.** (2012). SNP calling, genotype calling, and sample allele frequency estimation from new-generation sequencing data. <https://doi.org/10.1371/journal.pone.0037558>
- Ogura, T., & Busch, W.** (2015). From phenotypes to causal sequences: using genome wide association studies to dissect the sequence basis for variation of plant development. *Current opinion in plant biology*, 23, 98–108. <https://doi.org/10.1016/j.pbi.2014.11.008>
- Osnato, M., Cota, I., Nebhnani, P., Cereijo, U., & Pelaz, S.** (2022). Photoperiod control of plant growth: Flowering time genes beyond flowering. *Frontiers in plant science*, 12, 3359. <https://doi.org/10.3389/fpls.2021.805635>
- Ostaszewska, M., Juszczuk, I. M., Kołodziejek, I., & Rychter, A. M.** (2014). Long-term sulphur starvation of *Arabidopsis thaliana* modifies mitochondrial ultrastructure and activity and changes tissue energy and redox status. *Journal of plant physiology*, 171(7), 549-558. <https://doi.org/10.1016/j.jplph.2013.12.013>
- Pai, A. A., Pritchard, J. K., & Gilad, Y.** (2015). The genetic and mechanistic basis for variation in gene regulation. *PLoS genetics*, 11(1), e1004857. <https://doi.org/10.1016/j.plophy.2016.09.016>
- Panagos, P., Meusburger, K., Alewell, C., & Montanarella, L.** (2012). Soil erodibility estimation using LUCAS point survey data of Europe. *Environmental Modelling & Software*, 30, 143-145. <https://doi.org/10.1016/j.envsoft.2011.11.002>
- Pandey, A., Khan, M. K., Hakki, E. E., Gezgin, S., & Hamurcu, M.** (2019). Combined boron toxicity and salinity stress - An insight into its interaction in plants. *Plants*, 8(10), 364. <https://doi.org/10.3390/plants8100364>
- Pauwels, L., Barbero, G. F., Geerinck, J., Tilleman, S., Grunewald, W., Pérez, A. C., ... & Goossens, A.** (2010). NINJA connects the co-repressor TOPLESS to jasmonate signalling. *Nature*, 464(7289), 788-791. <https://doi.org/10.1038/nature08854>
- Peixoto, B., Moraes, T. A., Mengin, V., Margalha, L., Vicente, R., Feil, R., ... & Baena-González, E.** (2021). Impact of the SnRK1 protein kinase on sucrose homeostasis and the transcriptome during the diel cycle. *Plant physiology*, 187(3), 1357-1373. <https://doi.org/10.1093/plphys/kiab350>
- Pembleton, L. W., Cogan, N. O., & Forster, J. W.** (2013). St AMPP: An R package for calculation of genetic differentiation and structure of mixed-ploidy level populations. *Molecular ecology resources*, 13(5), 946-952. <https://doi.org/10.1111/1755-0998.12129>

- Perea-Resa, C., Rodríguez-Milla, M. A., Iniesto, E., Rubio, V., & Salinas, J.** (2017). Prefoldins negatively regulate cold acclimation in *Arabidopsis thaliana* by promoting nuclear proteasome-mediated HY5 degradation. *Molecular plant*, 10(6), 791-804.
<https://doi.org/10.1016/j.molp.2017.03.012>
- Pérez-Martín, L.** (2020). Physiological, molecular and genetic mechanisms of adaptation to alkaline and saline soils in *Arabidopsis thaliana* populations. *Universitat Autònoma de Barcelona*. <https://ddd.uab.cat/record/256996>
- Pérez-Martín, L., Busoms, S., Almira, M. J., Azagury, N., Terés, J., Tolrà, R., ... & Barcelo, J.** (2022). Evolution of salt tolerance in *Arabidopsis thaliana* on siliceous soils does not confer tolerance to saline calcareous soils. *Plant and Soil*, 1-21.
<https://doi.org/10.1007/s11104-022-05439-9>
- Pérez-Martín, L., Busoms, S., Tolrà, R., & Poschenrieder, C.** (2021). Transcriptomics reveals fast changes in salicylate and jasmonate signaling pathways in shoots of carbonate-tolerant *Arabidopsis thaliana* under bicarbonate exposure. *International journal of molecular sciences*, 22(3), 1226. <https://doi.org/10.3390/ijms22031226>
- Piazzzi, M., Bavelloni, A., Gallo, A., Faenza, I., & Blalock, W. L.** (2019). Signal transduction in ribosome biogenesis: a recipe to avoid disaster. *International journal of molecular sciences*, 20(11), 2718. <https://doi.org/10.3390/ijms20112718>
- Pigliucci, M.** (2003). Selection in a model system: ecological genetics of flowering time in *Arabidopsis thaliana*. *Ecology*, 84(7), 1700-1712.
[https://doi.org/10.1890/0012-9658\(2003\)084](https://doi.org/10.1890/0012-9658(2003)084)
- Pineau, C., Loubet, S., Lefoulon, C., Challes, C., Fizames, C., Lacombe, B., ... & Richard, O.** (2012). Natural variation at the FRD3 MATE transporter locus reveals cross-talk between Fe homeostasis and Zn tolerance in *Arabidopsis thaliana*. *PLoS genetics*, 8(12), e1003120. <https://doi.org/10.1371/journal.pgen.1003120>
- Poplin, R., Chang, P. C., Alexander, D., Schwartz, S., Colthurst, T., Ku, A., ... & DePristo, M. A.** (2018). A universal SNP and small-indel variant caller using deep neural networks. *Nature biotechnology*, 36(10), 983-987. <https://doi.org/10.1038/nbt.4235>
- Poulsen, L.R., López-Marqués, R.L., McDowell, S.C., Okkeri, J., Licht, D., Schulz, A., Pomorski, T., Harper, J.F., Palmgren, M.G.** (2008a). The *Arabidopsis* P4-ATPase ALA3 localizes to the golgi and requires a β -subunit to function in lipid translocation and secretory vesicle formation. *Plant Cell* 20:658–676.
<https://doi.org/10.1105/tpc.107.054767>
- Prerostova, S., Dobrev, P. I., Gaudinova, A., Hosek, P., Soudek, P., Knirsch, V., & Vankova, R.** (2017). Hormonal dynamics during salt stress responses of salt-sensitive *Arabidopsis thaliana* and salt-tolerant *Thellungiella salsuginea*. *Plant Science*, 264, 188-198.
<https://doi.org/10.1016/j.plantsci.2017.07.020>

- Price, L., Han, Y., Angessa, T., & Li, C.** (2022). Molecular Pathways of WRKY Genes in Regulating Plant Salinity Tolerance. *International Journal of Molecular Sciences*, 23(18), 10947. <https://doi.org/10.3390/ijms231810947>
- Pritchard, J. K., Stephens, M., & Donnelly, P.** (2000). Inference of population structure using multilocus genotype data. *Genetics*, 155(2), 945-959. <https://doi.org/10.1093/genetics/155.2.945>
- Putri, G. H., Anders, S., Pyl, P. T., Pimanda, J. E., & Zanini, F.** (2022). Analysing high-throughput sequencing data in Python with HTSeq 2.0. *Bioinformatics*, 38(10), 2943-2945. <https://doi.org/10.1093/bioinformatics/btac166>
- Qasim, M., Ashraf, M., Ashraf, M. Y., Rehman, S. U., & Rha, E. S.** (2003). Salt-induced changes in two canola cultivars differing in salt tolerance. *Biologia plantarum*, 46(4), 629-632. <https://doi.org/10.1023/A:1024844402000>
- Qiao, Y., Jiang, W., Lee, J., Park, B., Choi, M. S., Piao, R., ... & Koh, H. J.** (2010). SPL28 encodes a clathrin-associated adaptor protein complex 1, medium subunit $\mu 1$ (AP1M1) and is responsible for spotted leaf and early senescence in rice (*Oryza sativa*). *New Phytologist*, 185(1), 258-274. <https://doi.org/10.1111/j.1469-8137.2009.03047.x>
- Qin, H., Zhang, Z., Wang, J., Chen, X., Wei, P., & Huang, R.** (2017). The activation of OsEIL1 on YUC8 transcription and auxin biosynthesis is required for ethylene-inhibited root elongation in rice early seedling development. *PLoS Genetics*, 13(8), e1006955. 185(1), 258-274. <https://doi.org/10.1371/journal.pgen.1006955>
- Rabhi, M., Barhoumi, Z., Ksouri, R., Abdelly, C., & Gharsalli, M.** (2007). Interactive effects of salinity and iron deficiency in *Medicago ciliaris*. *Comptes Rendus Biologies*, 330(11), 779-788. <https://doi.org/10.1016/j.crv.2007.08.007>
- Radovich, T. J., Kleinhenz, M. D., & Streeter, J. G.** (2005). Irrigation timing relative to head development influences yield components, sugar levels, and glucosinolate concentrations in cabbage. *Journal of the American Society for Horticultural Science*, 130(6), 943-949. <https://doi.org/10.21273/JASHS.130.6.943>
- Rahikainen, M., Pascual, J., Alegre, S., Durian, G., & Kangasjärvi, S.** (2016). PP2A phosphatase as a regulator of ROS signaling in plants. *Antioxidants*, 5(1), 8. <https://doi.org/10.3390/antiox5010008>
- Rai, S., Singh, P. K., Mankotia, S., Swain, J., & Satbhai, S. B.** (2021). Iron homeostasis in plants and its crosstalk with copper, zinc, and manganese. *Plant Stress*, 1, 100008. <https://doi.org/10.1016/j.stress.2021.100008>
- Rasmussen, S., Barah, P., Suarez-Rodriguez, M. C., Bressendorff, S., Friis, P., Costantino, P., ... & Mundy, J.** (2013). Transcriptome responses to combinations of stresses in *Arabidopsis*. *Plant physiology*, 161(4), 1783-1794. <https://doi.org/10.1104/pp.112.210773>

- Reddy, V. R. P., Das, S., Dikshit, H. K., Mishra, G. P., Aski, M., Meena, S. K., ... & Sharma, T. R.** (2020). Genome-wide association analysis for phosphorus use efficiency traits in mungbean (*Vigna radiata* L. Wilczek) using genotyping by sequencing approach. *Frontiers in plant science*, 11, 537766. <https://doi.org/10.3389/fpls.2020.537766>
- Rédei, G. P.** (1970). *Arabidopsis thaliana* (L.) Heynh. A review of the genetics and biology. *Bibliographia Genetica.*, 20(2).
- Rellstab, C., Zoller, S., Walthert, L., Lesur, I., Pluess, A. R., Graf, R., ... & Gugerli, F.** (2016). Signatures of local adaptation in candidate genes of oaks (*Quercus* spp.) with respect to present and future climatic conditions. *Molecular Ecology*, 25(23), 5907-5924. <https://doi.org/10.1111/mec.13889>
- Riboni, M., Robustelli Test, A., Galbiati, M., Tonelli, C., & Conti, L.** (2014). Environmental stress and flowering time: the photoperiodic connection. *Plant Signaling & Behavior*, 9(7), e29036. <https://doi.org/10.4161/psb.29036>
- Riemann, M., Dhakarey, R., Hazman, M., Miro, B., Kohli, A., & Nick, P.** (2015). Exploring jasmonates in the hormonal network of drought and salinity responses. *Frontiers in plant science*, 6, 1077. <https://doi.org/10.3389/fpls.2015.01077>
- Rosloski, S. M., Jali, S. S., Balasubramanian, S., Weigel, D., & Grbic, V.** (2010). Natural diversity in flowering responses of *Arabidopsis thaliana* caused by variation in a tandem gene array. *Genetics*, 186(1), 263-276. <https://doi.org/10.1534/genetics.110.116392>
- Ross, G. S., Wegrzyn, T., MacRae, E. A., & Redgwell, R. J.** (1994). Apple [beta]-Galactosidase (Activity against Cell Wall Polysaccharides and Characterization of a Related cDNA Clone). *Plant Physiology*, 106(2), 521-528. <https://doi.org/10.1104/pp.106.2.521>
- Rubio, F., Gassmann, W., & Schroeder, J. I.** (1995). Sodium-driven potassium uptake by the plant potassium transporter HKT1 and mutations conferring salt tolerance. *Science*, 270(5242), 1660-1663. <https://doi.org/10.1126/science.270.5242.1660>
- Rus, A., Baxter, I., Muthukumar, B., Gustin, J., Lahner, B., Yakubova, E., & Salt, D. E.** (2006). Natural variants of At HKT1 enhance Na⁺ accumulation in two wild populations of *Arabidopsis*. *PLoS genetics*, 2(12), e210. <https://doi.org/10.1371/journal.pgen.0020210>
- Safdar, H., Amin, A., Shafiq, Y., Ali, A., Yasin, R., Shoukat, A., ... & Sarwar, M. I.** (2019). A review: Impact of salinity on plant growth. *Nat. Sci*, 17(1), 34-40. <https://doi.org/10.7537/marsnsj170119.06>
- Sah, S. K., Reddy, K. R., & Li, J.** (2016). Absciscic acid and abiotic stress tolerance in crop plants. *Frontiers in plant science*, 7, 571. <https://doi.org/10.3389/fpls.2016.00571>
- Saini, S., Kaur, N., & Pati, P. K.** (2021). Phytohormones: Key players in the modulation of heavy metal stress tolerance in plants. *Ecotoxicology and Environmental Safety*, 223, 112578. <https://doi.org/10.1016/j.ecoenv.2021.112578>

- Saini, S., Kaur, N., Marothia, D., Singh, B., Singh, V., Gantet, P., & Pati, P. K.** (2021). Morphological analysis, protein profiling and expression analysis of auxin homeostasis genes of roots of two contrasting cultivars of rice provide inputs on mechanisms involved in rice adaptation towards salinity stress. *Plants*, 10(8), 1544. <https://doi.org/10.3390/plants10081544>
- Samach, A., & Wigge, P. A.** (2005). Ambient temperature perception in plants. Current opinion in plant biology, 8(5), 483-486. <https://doi.org/10.1016/j.pbi.2005.07.011>
- Samis, K. E., Heath, K. D., & Stinchcombe, J. R.** (2008). Discordant longitudinal clines in flowering time and phytochrome C in *Arabidopsis thaliana*. *Evolution: International Journal of Organic Evolution*, 62(12), 2971-2983. <https://doi.org/10.1111/j.1558-5646.2008.00484.x>
- Sánchez-bermejo, E., Méndez-Vigo, B., Picó, F., Martínez-Zapater, J. M., & Alonso-Blanco, C.** (2012). Novel natural alleles at FLC and LVR loci account for enhanced vernalization responses in *Arabidopsis thaliana*. *Plant, Cell & Environment*, 35(9), 1672-1684. <https://doi.org/10.1111/j.1365-3040.2012.02518.x>
- Santner, A., Calderon-Villalobos, L. I. A., & Estelle, M.** (2009). Plant hormones are versatile chemical regulators of plant growth. *Nature chemical biology*, 5(5), 301-307. <https://doi.org/10.1038/nchembio.165>
- Sasaki, E., Zhang, P., Atwell, S., Meng, D., & Nordborg, M.** (2015). "Missing" G x E variation controls flowering time in *Arabidopsis thaliana*. *PLoS Genetics*, 11(10), e1005597. <https://doi:10.1371/journal.pgen.1005597>
- Satbhai, S. B., Setzer, C., Freynschlag, F., Slovak, R., Kerdaffrec, E., & Busch, W.** (2017). Natural allelic variation of FRO2 modulates *Arabidopsis* root growth under iron deficiency. *Nature communications*, 8(1), 1-10. <https://doi.org/10.1038/ncomms15603>
- Sazegari, S., Niazi, A., & Ahmadi, F. S.** (2015). A study on the regulatory network with promoter analysis for *Arabidopsis* DREB-genes. *Bioinformation*, 11(2), 101. <https://doi.org/10.6026/97320630011101>
- Schansker, G., Tóth, S. Z., Holzwarth, A. R., & Garab, G.** (2014). Chlorophyll a fluorescence: beyond the limits of the QA model. *Photosynthesis research*, 120(1), 43-58. <https://doi.org/10.1007/s11120-013-9806-5>
- Schippers, J. H., Ellens, R., Hille, J., & Dijkwel, P. P.** (2008). Early leaf senescence of old13 is partially dependent on salicylic acid and associated with increased oxidative stress and altered water balance. *Molecular aspects of ageing and the onset of leaf senescence*, 67. [Thesis fully internal (DIV), University of Groningen]. s.n.
- Schönrock, N., Bouveret, R., Leroy, O., Borghi, L., Köhler, C., Gruissem, W., & Hennig, L.** (2006). Polycomb-group proteins repress the floral activator AGL19 in the FLC-independent vernalization pathway. *Genes & development*, 20(12), 1667-1678. <https://doi:10.1101/gad.377206>

- Schöttler, M. A., Tóth, S. Z., Boulouis, A., & Kahlau, S.** (2015). Photosynthetic complex stoichiometry dynamics in higher plants: biogenesis, function, and turnover of ATP synthase and the cytochrome b 6 f complex. *Journal of experimental botany*, 66(9), 2373-2400. <https://doi.org/10.1093/jxb/eru495>
- Segarra, G., Jáuregui, O., Casanova, E., & Trillas, I.** (2006). Simultaneous quantitative LC–ESI–MS/MS analyses of salicylic acid and jasmonic acid in crude extracts of *Cucumis sativus* under biotic stress. *Phytochemistry*, 67(4), 395-401. <https://doi.org/10.1016/j.phytochem.2005.11.017>
- Seifikalhor, M., Aliniaiefard, S., Shomali, A., Azad, N., Hassani, B., Lastochkina, O., & Li, T.** (2019). Calcium signaling and salt tolerance are diversely entwined in plants. *Plant signaling & behavior*, 14(11), 1665455. <https://doi.org/10.1080/15592324.2019.1665455>
- Shabala, L., Cuin, T. A., Newman, I. A., & Shabala, S.** (2005). Salinity-induced ion flux patterns from the excised roots of *Arabidopsis* sos mutants. *Planta*, 222(6), 1041-1050. <https://doi.org/10.1007/s00425-005-0074-2>
- Shabala, S., & Cuin, T. A.** (2008). Potassium transport and plant salt tolerance. *Physiologia plantarum*, 133(4), 651-669. <https://doi.org/10.1111/j.1399-3054.2007.01008.x>
- Shabala, S., Demidchik, V., Shabala, L., Cuin, T. A., Smith, S. J., Miller, A. J., ... & Newman, I. A.** (2006). Extracellular Ca²⁺ ameliorates NaCl-induced K⁺ loss from *Arabidopsis* root and leaf cells by controlling plasma membrane K⁺-permeable channels. *Plant physiology*, 141(4), 1653-1665. <https://doi.org/10.1104/pp.106.082388>
- Shanmugam, V., Lo, J. C., & Yeh, K. C.** (2013). Control of Zn uptake in *Arabidopsis halleri*: a balance between Zn and Fe. *Frontiers in Plant science*, 4, 281. <https://doi.org/10.3389/fpls.2013.00281>
- Sharma, R., Singh, G., Bhattacharya, S., & Singh, A.** (2018). Comparative transcriptome meta-analysis of *Arabidopsis thaliana* under drought and cold stress. *PloS one*, 13(9), e0203266. <https://doi.org/10.1371/journal.pone.0203266>
- Shaul, O.** (2002). Magnesium transport and function in plants: the tip of the iceberg. *Biometals*, 15(3), 307-321. <https://doi.org/10.1023/A:1016091118585>
- Sheldon CC, Conn AB, Dennis ES, Peacock WJ.** (2002). Different regulatory regions are required for the vernalization-induced repression of FLOWERING LOCUS C and for the epigenetic maintenance of repression. *Plant Cell* 14, 2527-2537. <https://doi.org/10.1105/tpc.004564>
- Shi, D., & Sheng, Y.** (2005). Effect of various salt–alkaline mixed stress conditions on sunflower seedlings and analysis of their stress factors. *Environmental and experimental Botany*, 54(1), 8-21. <https://doi.org/10.1016/j.envexpbot.2004.05.003>

- Shimizu-Mitao, Y., & Kakimoto, T.** (2014). Auxin sensitivities of all *Arabidopsis* Aux/IAAs for degradation in the presence of every TIR1/AFB. *Plant and Cell Physiology*, 55(8), 1450-1459. <https://doi.org/10.1093/pcp/pcu077>
- Shindo, C., Aranzana, M. J., Lister, C., Baxter, C., Nicholls, C., Nordborg, M., & Dean, C.** (2005). Role of FRIGIDA and FLOWERING LOCUS C in determining variation in flowering time of *Arabidopsis*. *Plant physiology*, 138(2), 1163-1173. <https://doi.org/10.1104/pp.105.061309>
- Shive, J. W.** (1941). Significant roles of trace elements in the nutrition of plants. *Plant physiology*, 16(3), 435. <https://doi.org/10.1104%2Fpp.16.3.435>
- Shu, J., Chen, C., Kohalmi, S. E., & Cui, Y.** (2020). Evidence that AGL17 is a significant downstream target of CLF in floral transition control. *Plant Signaling & Behavior*, 15(7), 1766851. <https://doi.org/10.1080/15592324.2020.1766851>
- Shu, J., Liu, Y., Zhang, L., Li, Z., Fang, Z., Yang, L., ... & Lv, H.** (2018). QTL-seq for rapid identification of candidate genes for flowering time in broccoli^x cabbage. *Theoretical and applied genetics*, 131(4), 917-928. <https://doi.org/10.1007/s00122-017-3047-5>
- Sibole, J., Cabot, C., Michalke, W., Poschenrieder, C., & Barceló, J.** (2005). Relationship between expression of the PM H⁺-ATPase, growth and ion partitioning in the leaves of salt-treated *Medicago* species. *Planta*, 221(4), 557-566. <https://doi.org/10.1007/s00425-004-1456-6>
- Singh, A.** (2021). Soil salinization management for sustainable development: a review. *J Environ Manag* 277:111383. <https://doi.org/10.1016/j.jenvman.2020.111383>
- Skalak, J., Nicolas, K. L., Vankova, R., & Hejatk, J.** (2021). Signal integration in plant abiotic stress responses via multistep phosphorelay signaling. *Frontiers in Plant Science*, 12, 644823. <https://doi.org/10.3389/fpls.2021.644>
- Skotte, L., Korneliussen, T. S., & Albrechtsen, A.** (2013). Estimating individual admixture proportions from next generation sequencing data. *Genetics*, 195(3), 693-702. <https://doi.org/10.1534/genetics.113.154138>
- Smith, D. L., & Gross, K. C.** (2000). A family of at least seven β -galactosidase genes is expressed during tomato fruit development. *Plant Physiology*, 123(3), 1173-1184. <https://doi.org/10.1104/pp.123.3.1173>
- Song, Y., Lv, J., Ma, Z., & Dong, W.** (2019). The mechanism of alfalfa (*Medicago sativa* L.) response to abiotic stress. *Plant Growth Regulation*, 89(3), 239-249. <https://doi.org/10.1007/s10725-019-00530-1>
- Spartz, A. K., Ren, H., Park, M. Y., Grandt, K. N., Lee, S. H., Murphy, A. S., ... & Gray, W. M.** (2014). SAUR inhibition of PP2C-D phosphatases activates plasma membrane H⁺-ATPases to promote cell expansion in *Arabidopsis*. *The Plant Cell*, 26(5), 2129-2142. <https://doi.org/10.1105/tpc.114.126037>

- Sun, S., Song, H., Li, J., Chen, D., Tu, M., Jiang, G., ... & Zhou, Z.** (2020). Comparative transcriptome analysis reveals gene expression differences between two peach cultivars under saline-alkaline stress. *Hereditas*, 157(1), 1-10.
<https://doi.org/10.1186/s41065-020-00122-4>
- Sun, Y., Hao, P., Lv, X., Tian, J., Wang, Y., Zhang, X., ... & Wu, T.** (2020). A long non-coding apple RNA, MSTRG. 85814.11, acts as a transcriptional enhancer of SAUR32 and contributes to the Fe-deficiency response. *The Plant Journal*, 103(1), 53-67.
<https://doi.org/10.1111/tpj.14706>
- Suzuki, N., Bassil, E., Hamilton, J. S., Inupakutika, M. A., Zandalinas, S. I., Tripathy, D., ... & Mittler, R.** (2016). ABA is required for plant acclimation to a combination of salt and heat stress. *PloS one*, 11(1), e0147625. <https://doi.org/10.1371/journal.pone.0147625>
- Swarbreck D, Wilks C, Lamesch P, Berardini TZ, Garcia-Hernandez M, Foerster H, ... & Huala, E.** (2008). The *Arabidopsis* Information Resource (TAIR): gene structure and function annotation. *Nucleic Acids Res. Jan;36(Database issue) D1009-14*.
<https://doi:10.1093/nar/gkm965>
- Syed, N. H., Kalyna, M., Marquez, Y., Barta, A., & Brown, J. W.** (2012). Alternative splicing in plants—coming of age. *Trends in plant science*, 17(10), 616-623.
<https://doi.org/10.1016/j.tplants.2012.06.001>
- Sze, H., Schumacher, K., Müller, M. L., Padmanaban, S., & Taiz, L.** (2002). A simple nomenclature for a complex proton pump: VHA genes encode the vacuolar H⁺-ATPase. *Trends in plant science*, 7(4), 157-161.
[https://doi.org/10.1016/S1360-1385\(02\)02240-9](https://doi.org/10.1016/S1360-1385(02)02240-9)
- Tabas-Madrid, D., Méndez-Vigo, B., Arteaga, N., Marcer, A., Pascual-Montano, A., Weigel, D., ... & Alonso-Blanco, C.** (2018). Genome-wide signatures of flowering adaptation to climate temperature: Regional analyses in a highly diverse native range of *Arabidopsis thaliana*. *Plant, cell & environment*, 41(8), 1806-1820.
<https://doi.org/10.1111/pce.13189>
- Takeno, K.** (2016). Stress-induced flowering: the third category of flowering response. *Journal of Experimental Botany*, 67(17), 4925-4934. <https://doi.org/10.1093/jxb/erw272>
- Tan, S. T., Dai, C., Liu, H. T., & Xue, H. W.** (2013). *Arabidopsis* casein kinase1 proteins CK1. 3 and CK1. 4 phosphorylate cryptochrome2 to regulate blue light signaling. *The Plant Cell*, 25(7), 2618-2632. <https://doi.org/10.1105/tpc.113.114322>
- Tang, X., Chang, L., Wu, S., Li, P., Liu, G., & Wang, N. N.** (2008). Auto-regulation of the promoter activities of *Arabidopsis* 1-aminocyclopropane-1-carboxylate synthase genes AtACS4, AtACS5, and AtACS7 in response to different plant hormones. *Plant Science*, 175(1-2), 161-167.
<https://doi.org/10.1016/j.plantsci.2008.01.002>

- Terés, J.** (2017). Characterization of natural populations of *A. thaliana* differing in tolerance to carbonate soil. Doctoral dissertation, Ph. D. Thesis Universitat Autònoma de Barcelona. <https://ddd.uab.cat/record/187700>
- Terés, J., Busoms, S., Perez Martín, L., Luís-Villarroya, A., Flis, P., Álvarez-Fernández, A., ... & Poschenrieder, C.** (2019). Soil carbonate drives local adaptation in *Arabidopsis thaliana*. *Plant, cell & environment*, 42(8), 2384-2398. <https://doi.org/10.1111/pce.13567>
- Teschner, J., Lachmann, N., Schulze, J., Geisler, M., Selbach, K., Santamaria-Araujo, J., ... & Bittner, F.** (2010). A novel role for *Arabidopsis* mitochondrial ABC transporter ATM3 in molybdenum cofactor biosynthesis. *The Plant Cell*, 22(2), 468-480. <https://doi.org/10.1105/tpc.109.068478>
- Torun, H., Novák, O., Mikulík, J., Strnad, M., & Ayaz, F. A.** (2022). The Effects of exogenous salicylic acid on endogenous phytohormone status in *Hordeum vulgare* L. under salt stress. *Plants*, 11(5), 618. <https://doi.org/10.3390/plants11050618>
- Tounekti, T., Hernández, I., Müller, M., Khemira, H., & Munné-Bosch, S.** (2011). Kinetin applications alleviate salt stress and improve the antioxidant composition of leaf extracts in *Salvia officinalis*. *Plant Physiology and Biochemistry*, 49(10), 1165-1176. <https://doi.org/10.1016/j.plaphy.2011.07.011>
- Tsai, H. H., & Schmidt, W.** (2020). pH-dependent transcriptional profile changes in iron-deficient *Arabidopsis* roots. *BMC genomics*, 21(1), 1-11. <https://doi.org/10.1186/s12864-020-07116-6>
- Tsydendambaev, V. D., Ivanova, T. V., Khalilova, L. A., Kurkova, E. B., Myasoedov, N. A., & Balnokin, Y. V.** (2013). Fatty acid composition of lipids in vegetative organs of the halophyte *Suaeda altissima* under different levels of salinity. *Russian journal of plant physiology*, 60(5), 661-671. <https://doi.org/10.1134/S1021443713050142>
- Tuyen, D. D., Lal, S. K., & Xu, D. H.** (2010). Identification of a major QTL allele from wild soybean (*Glycine soja* Sieb. & Zucc.) for increasing alkaline salt tolerance in soybean. *Theoretical and Applied Genetics*, 121(2), 229-236. <https://doi.org/10.1007/s00122-010-1304-y>
- Uffelmann, E., Huang, Q. Q., Munung, N. S., De Vries, J., Okada, Y., Martin, A. R., ... & Posthuma, D.** (2021). Genome-wide association studies. *Nature Reviews Methods Primers*, 1(1), 1-21. <https://doi.org/10.1038/s43586-021-00056-9>
- Ursache, R., Miyashima, S., Chen, Q., Vatén, A., Nakajima, K., Carlsbecker, A., ... & Dettmer, J.** (2014). Tryptophan-dependent auxin biosynthesis is required for HD-ZIP III-mediated xylem patterning. *Development*, 141(6), 1250-1259. <https://doi.org/10.1242/dev.103473>
- Van Veen, H., Vashisht, D., Akman, M., Girke, T., Mustroph, A., Reinen, E., ... & Sasidharan, R.** (2016). Transcriptomes of eight *Arabidopsis thaliana* accessions reveal core

- conserved, genotype-and organ-specific responses to flooding stress. *Plant Physiology*, 172(2), 668-689. <https://doi.org/10.1104/pp.16.00472>
- Vert, G., Briat, J. F., & Curie, C.** (2001). *Arabidopsis* IRT2 gene encodes a root-periphery iron transporter. *The Plant Journal*, 26(2), 181-189. <https://doi.org/10.1046/j.1365-313x.2001.01018.x>
- Vigani, G., & Briat, J. F.** (2016). Impairment of respiratory chain under nutrient deficiency in plants: does it play a role in the regulation of iron and sulfur responsive genes?. *Frontiers in Plant Science*, 6, 1185. <https://doi.org/10.3389/fpls.2015.01185>
- Voogt, W.** (1987, April). The growth of beefsteak tomato as affected by K/Ca ratios in the nutrient solution. In *Symposium on the Fertilization of Vegetables under Protected Cultivation* 222 (pp. 155-166). <https://doi.org/10.17660/ActaHortic.1988.222.18>
- Wadgyamar, S. M., Ogilvie, J. E., Inouye, D. W., Weis, A. E., & Anderson, J. T.** (2018). Phenological responses to multiple environmental drivers under climate change: insights from a long-term observational study and a manipulative field experiment. *New Phytologist*, 218(2), 517-529. <https://doi.org/10.1111/nph.15029>
- Wang, J., Shi, X., Zhou, Z., Qin, M., Wang, Y., Li, W., ... & Lei, Z.** (2022). Genetic dissection of grain iron concentration in hexaploid wheat (*Triticum aestivum* L.) using a genome-wide association analysis method. *PeerJ*, 10, e13625. <https://doi.org/10.7717/peerj.13625>
- Wang, J., Song, L., Gong, X., Xu, J., & Li, M.** (2020). Functions of jasmonic acid in plant regulation and response to abiotic stress. *International Journal of Molecular Sciences*, 21(4), 1446. <https://doi.org/10.3390/ijms21041446>
- Wang, T., Yu, Q., Chen, J., Deng, B., Qian, L., & Le, Y.** (2010). PP2A mediated AMPK inhibition promotes HSP70 expression in heat shock response. *PloS one*, 5(10), e13096. <https://doi.org/10.1371/journal.pone.0013096>
- Wang, X. S., & Han, J. G.** (2007). Effects of NaCl and silicon on ion distribution in the roots, shoots and leaves of two alfalfa cultivars with different salt tolerance. *Soil Science & Plant Nutrition*, 53(3), 278-285. <https://doi.org/10.1111/j.1747-0765.2007.00135.x>
- Warraich, A. S., Krishnamurthy, S. L., Sooch, B. S., Vinaykumar, N. M., Dushyanthkumar, B. M., Bose, J., & Sharma, P. C.** (2020). Rice GWAS reveals key genomic regions essential for salinity tolerance at reproductive stage. *Acta Physiologiae Plantarum*, 42(8), 1-15. <https://doi.org/10.1007/s11738-020-03123-y>
- Waters, B. M., Amundsen, K., & Graef, G.** (2018). Gene expression profiling of iron deficiency chlorosis sensitive and tolerant soybean indicates key roles for phenylpropanoids under alkalinity stress. *Frontiers in plant science*, 9(10). <https://doi.org/10.3389/fpls.2018.00010>
- Weigel, D.** (2012). Natural variation in *Arabidopsis*: from molecular genetics to ecological genomics. *Plant physiology*, 158(1), 2-22. <https://doi.org/10.1104/pp.111.189845>

- Weigel, D., & Nordborg, M.** (2015). Population genomics for understanding adaptation in wild plant species. *Annual review of genetics*, 49(1), 315-338.
<https://doi.org/10.1146/annurev-genet-120213-092110>
- Wen, R., Lv, H. N., Jiang, Y., & Tu, P. F.** (2018). Anti-inflammatory flavone and chalcone derivatives from the roots of *Pongamia pinnata* (L.) Pierre. *Phytochemistry*, 149, 56-63.
<https://doi.org/10.1016/j.phytochem.2018.02.005>
- Werner, J. D., Borevitz, J. O., Uhlenhaut, N. H., Ecker, J. R., Chory, J., & Weigel, D.** (2005). FRIGIDA-independent variation in flowering time of natural *Arabidopsis thaliana* accessions. *Genetics*, 170(3), 1197-1207.
<https://doi.org/10.1534/genetics.104.036533>
- Wickham, H., & Wickham, H.** (2016). Programming with ggplot2. *Ggplot2: elegant graphics for data analysis*, 241-253. https://doi.org/10.1007/978-3-319-24277-4_12
- Wittstock, U., & Halkier, B. A.** (2002). Glucosinolate research in the *Arabidopsis* era. *Trends in plant science*, 7(6), 263-270. [https://doi.org/10.1016/S1360-1385\(02\)02273-2](https://doi.org/10.1016/S1360-1385(02)02273-2)
- Wright, S.** (1943). Isolation by distance. *Genetics*, 28(2): 114.
<https://doi.org/10.1093/genetics/28.2.114>
- Wu, Q., Han, T. S., Chen, X., Chen, J. F., Zou, Y. P., Li, Z. W., ... & Guo, Y. L.** (2017). Long-term balancing selection contributes to adaptation in *Arabidopsis* and its relatives. *Genome biology*, 18(1), 1-15. <https://doi.org/10.1186/s13059-017-1342-8>
- Xiang, C. B., & Xu, P.** (2022). SUE4, a novel PIN1-interacting membrane protein, regulates acropetal auxin transport in response to sulfur deficiency. *New Phytologist*, 1. <https://doi.org/10.1111/nph.18536>
- Xie, Q., Yang, Y., Wang, Y., Pan, C., Hong, S., Wu, Z., ... & Jiang, X.** (2022). The calcium sensor CBL10 negatively regulates plasma membrane H⁺-ATPase activity and alkaline stress response in *Arabidopsis*. *Environmental and Experimental Botany*, 194, 104752.
<https://doi.org/10.1016/j.envexpbot.2021.104752>
- Xie, Z., Nolan, T. M., Jiang, H., & Yin, Y.** (2019). AP2/ERF transcription factor regulatory networks in hormone and abiotic stress responses in *Arabidopsis*. *Frontiers in plant science*, 10, 228. <https://doi.org/10.3389/fpls.2019.00228>
- Yan, F., Zhu, Y., Zhao, Y., Wang, Y., Li, J., Wang, Q., & Liu, Y.** (2020). De novo transcriptome sequencing and analysis of salt-, alkali-, and drought-responsive genes in *Sophora alopecuroides*. *BMC genomics*, 21(1), 1-15.
<https://doi.org/10.1186/s12864-020-06823-4>
- Yan, W., Wang, B., Chan, E., & Mitchell-Olds, T.** (2021). Genetic architecture and adaptation of flowering time among environments. *New Phytologist*, 230(3), 1214-1227.
<https://doi.org/10.1111/nph.17229>

- Yang, H., Wu, Y., Duan, Y., Zhang, C., Huang, Z., Wu, W., ... & Li, W.** (2022). Metabolomics combined with physiological and transcriptomic analyses reveal regulatory features associated with blueberry growth in different soilless substrates. *Scientia Horticulturae*, 302, 111145. <https://doi.org/10.1016/j.scienta.2022.111145>
- Yang, K., Yang, J., & Yi, J.** (2018). Nucleolar Stress: hallmarks, sensing mechanism and diseases. *Cell Stress*, 2(6), 125. <https://doi.org/10.15698/cst2018.06.139>
- Yang, Y., Wang, L., Zhang, D., Cheng, H., Wang, Q., Yang, H., & Yu, D.** (2020). GWAS identifies two novel loci for photosynthetic traits related to phosphorus efficiency in soybean. *Molecular Breeding*, 40(3), 1-14. <https://doi.org/10.1007/s11032-020-01112-0>
- Yang, Y., Wu, Y., Ma, L., Yang, Z., Dong, Q., Li, Q., ... & Guo, Y.** (2019). The Ca²⁺ sensor SCaBP3/CBL7 modulates plasma membrane H⁺-ATPase activity and promotes alkali tolerance in Arabidopsis. *The Plant Cell*, 31(6), 1367-1384. <https://doi.org/10.1105/tpc.18.00568>
- Yasir, M., He, S., Sun, G., Geng, X., Pan, Z., Gong, W., ... & Du, X.** (2019). A genome-wide association study revealed key SNPs/genes associated with salinity stress tolerance in upland cotton. *Genes*, 10(10), 829. <https://doi.org/10.3390/genes10100829>
- Yousefi, H., Dalir, N., Rahnemaie, R., & Babaei, A.** (2020). The alleviation of salinity-induced stress by using boron in soilless grown rose. *Journal of plant nutrition*, 43(4), 526-537. <https://doi.org/10.1080/01904167.2019.1685103>
- Yu, H., Du, Q., Campbell, M., Yu, B., Walia, H., & Zhang, C.** (2021). Genome-wide discovery of natural variation in pre-mRNA splicing and prioritizing causal alternative splicing to salt stress response in rice. *New Phytologist*, 230 (3), 1273-1287. <https://doi.org/10.1111/nph.17189>
- Yu, Y., Li, Y., Yan, Z., & Duan, X.** (2021). The role of cytokinins in plant under salt stress. *Journal of Plant Growth Regulation*, 1-13. <https://doi.org/10.1007/s00344-021-10441-z>
- Yuan, Y., Wu, H., Wang, N., Li, J., Zhao, W., Du, J., ... & Ling, H. Q.** (2008). FIT interacts with AtbHLH38 and AtbHLH39 in regulating iron uptake gene expression for iron homeostasis in Arabidopsis. *Cell research*, 18(3), 385-397. <https://doi.org/10.1038/cr.2008.26>
- Zandalinas, S. I., Sengupta, S., Fritschi, F. B., Azad, R. K., Nechushtai, R., & Mittler, R.** (2021). The impact of multifactorial stress combination on plant growth and survival. *New Phytologist*, 230(3), 1034-1048. <https://doi.org/10.1111/nph.17232>
- Zeng, A., Chen, P., Korth, K., Hancock, F., Pereira, A., Brye, K., ... & Shi, A.** (2017). Genome-wide association study (GWAS) of salt tolerance in worldwide soybean germplasm lines. *Molecular Breeding*, 37(3), 1-14. <https://doi.org/10.1007/s11032-017-0634-8>
- Zhang, J., Wang, F., Zhang, C., Zhang, J., Chen, Y., Liu, G., ... & Zhang, J.** (2018). A novel VIGS method by agroinoculation of cotton seeds and application for elucidating functions of GhBI-1 in salt-stress response. *Plant cell reports*, 37(8), 1091-1100. <https://doi.org/10.1007/s00299-018-2294-5>

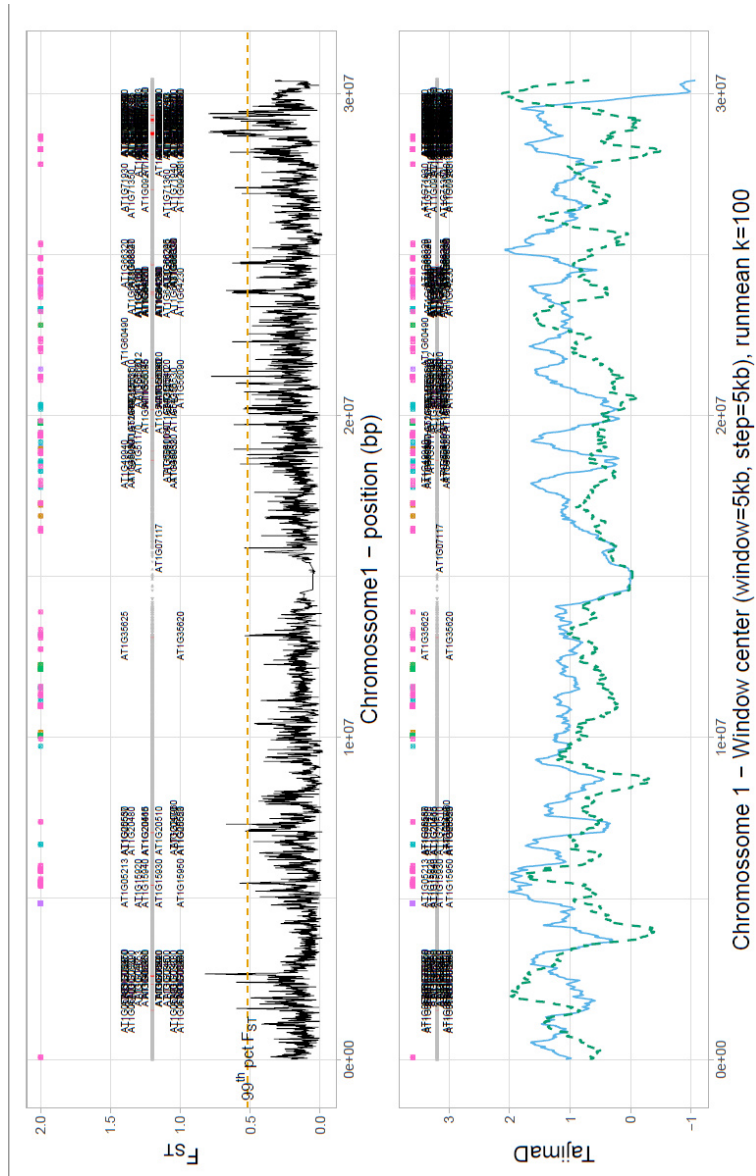
- Zhang, L., & Jiménez-Gómez, J. M.** (2020). Functional analysis of FRIGIDA using naturally occurring variation in *Arabidopsis thaliana*. *The Plant Journal*, 103(1), 154-165.
<https://doi.org/10.1111/tpj.14716>
- Zhang, L., Chen, L., & Yu, D.** (2018). Transcription factor WRKY75 interacts with DELLA proteins to affect flowering. *Plant Physiology*, 176(1), 790-803.
<https://doi.org/10.1104/pp.17.00657>
- Zhang, Q., Boundjou, N. B., Jia, L., Wang, X., Zhou, L., Peisker, H., ... & Zhou, Y.** (2023). A Cytidinediphosphate Diacylglycerol Synthase is essential for mitochondrial structure and energy production in *Arabidopsis thaliana*. *The Plant Journal*. In press.
<https://doi.org/10.1111/tpj.16139>.
- Zhang, Q., Zhai, J., Shao, L., Lin, W., & Peng, C.** (2019). Accumulation of anthocyanins: an adaptation strategy of *Mikania micrantha* to low temperature in winter. *Frontiers in Plant Science*, 10, 1049. <https://doi.org/10.3389/fpls.2019.01049>
- Zhang, R., Xu, C., Bao, Z., Xiao, R., Chen, X., Xiao, W., ... & Li, L.** (2021). Auxin alters sodium ion accumulation and nutrient accumulation by playing protective role in salinity challenged strawberry. *Plant Physiology and Biochemistry*, 164, 1-9.
<https://doi.org/10.1016/j.plaphy.2021.04.008>
- Zhang, S. X., Wu, S. H., Chao, J. Q., Yang, S. G., Bao, J., & Tian, W. M.** (2022). Genome-Wide Identification and Expression Analysis of MYC Transcription Factor Family Genes in Rubber Tree (*Hevea brasiliensis* Muell. Arg.). *Forests*, 13(4), 531.
<https://doi.org/10.3390/f13040531>
- Zhang, S., Quartararo, A., Betz, O. K., Madahosseini, S., Heringer, A. S., Le, T., ... & Drakakaki, G.** (2021). Root vacuolar sequestration and suberization are prominent responses of *Pistacia* spp. rootstocks during salinity stress. *Plant Direct*, 5(5), e00315.
<https://doi.org/10.1002/pld3.315>
- Zhang, W. J., Niu, Y., Bu, S. H., Li, M., Feng, J. Y., Zhang, J., ... & Zhang, Y. M.** (2014). Epistatic association mapping for alkaline and salinity tolerance traits in the soybean germination stage. *PloS one*, 9(1), e84750. <https://doi.org/10.1371/journal.pone.0084750>
- Zhang, W., Liao, X., Cui, Y., Ma, W., Zhang, X., Du, H., ... & Yu, D.** (2019). A cation diffusion facilitator, GmCDF1, negatively regulates salt tolerance in soybean. *PLoS Genetics*, 15(1), e1007798. <https://doi.org/10.1371/journal.pgen.1007798>
- Zhang, W., Wang, J., Huang, Z., Mi, L., Xu, K., Wu, J., ... & Jiang, D.** (2019). Effects of low temperature at booting stage on sucrose metabolism and endogenous hormone contents in winter wheat spikelet. *Frontiers in Plant Science*, 10, 498.
<https://doi.org/10.3389/fpls.2019.00498>
- Zhang, X., Adamowski, M., Marhava, P., Tan, S., Zhang, Y., Rodriguez, L., ... & Friml, J.** (2020). *Arabidopsis* flippases cooperate with ARF GTPase exchange factors to regulate the

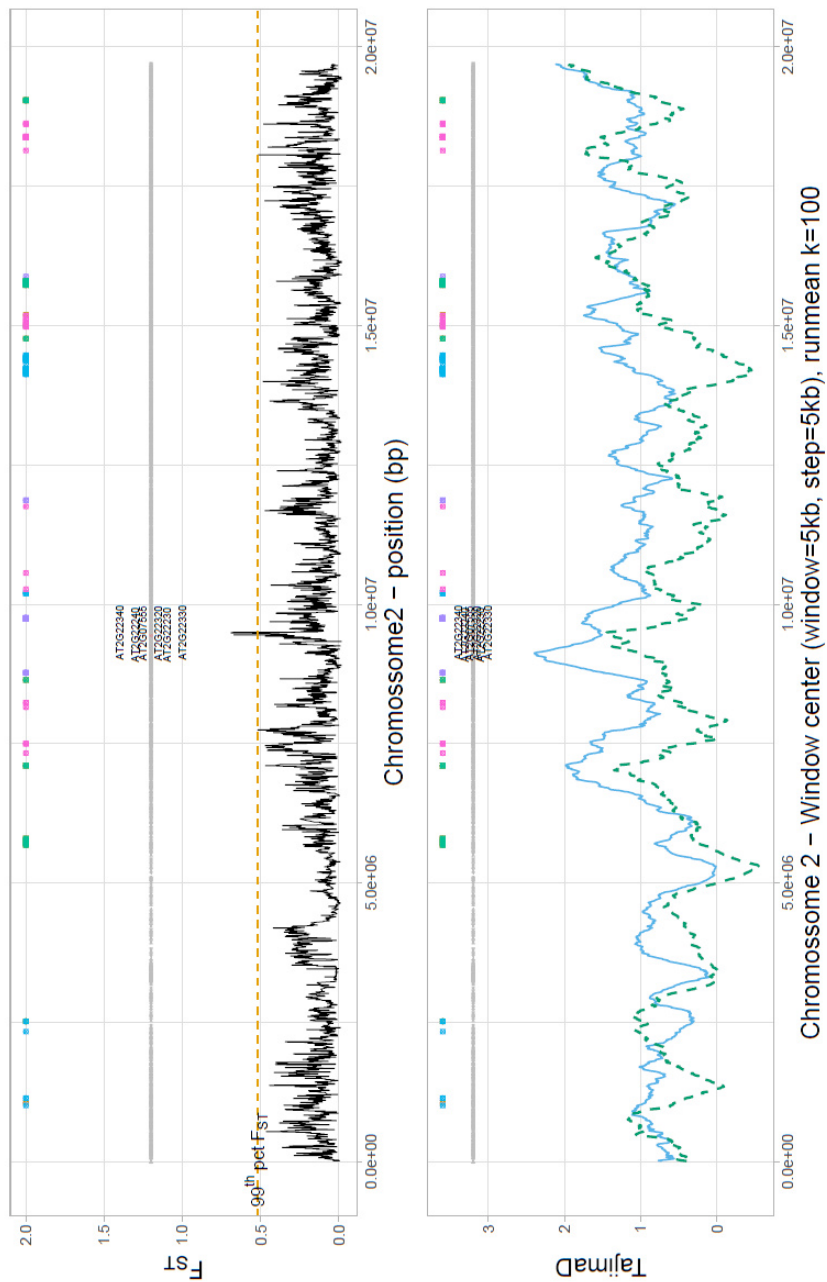
- trafficking and polarity of PIN auxin transporters. *The Plant Cell*, 32(5), 1644-1664. <https://doi.org/10.1105/tpc.19.00869>
- Zhang, Y., Wang, Y., Sa, G., Zhang, Y., Deng, J., Deng, S., ... & Chen, S.** (2017). *Populus euphratica* J3 mediates root K⁺/Na⁺ homeostasis by activating plasma membrane H⁺-ATPase in transgenic *Arabidopsis* under NaCl salinity. *Plant Cell, Tissue and Organ Culture (PCTOC)*, 131, 75-88. <https://doi.org/10.1007/s11240-017-1263-y>
- Zhao, S., Zhang, Q., Liu, M., Zhou, H., Ma, C., & Wang, P.** (2021). Regulation of plant responses to salt stress. *International Journal of Molecular Sciences*, 22(9), 4609. <https://doi.org/10.3390/ijms22094609>
- Zhao, Y., Wang, G., Zhao, M., Wang, M., Xue, Z., Liu, B., & Jiang, M.** (2021). Seed limitation and saline-alkaline stress restrict wetland restoration potential in the Songnen Plain, northeastern China. *Ecological Indicators*, 129, 107998. <https://doi.org/10.1016/j.ecolind.2021.107998>
- Zheng, L., Ma, H., Jiao, Q., Ma, C., & Wang, P.** (2020). Phytohormones: important participators in plant salt tolerance. *International Journal of Agriculture and Biology*, 24(2), 319-332. <https://doi.org/10.17957/ijab.15.1441>
- Zhou, C., Zhu, L., Xie, Y., Li, F., Xiao, X., Ma, Z., & Wang, J.** (2017). *Bacillus licheniformis* SA03 confers increased saline–alkaline tolerance in Chrysanthemum plants by induction of abscisic acid accumulation. *Frontiers in plant science*, 8, 1143. <https://doi.org/10.3389/fpls.2017.01143>
- Zhou, X., & Stephens, M.** (2012). Genome-wide efficient mixed-model analysis for association studies. *Nature genetics*, 44(7), 821-824. <https://doi.org/10.1038/ng.2310>
- Zhu, X. F., Wu, Q., Zheng, L., & Shen, R. F.** (2017). NaCl alleviates iron deficiency through facilitating root cell wall iron reutilization and its translocation to the shoot in *Arabidopsis thaliana*. *Plant and Soil*, 417, 155-167. <https://doi.org/10.1007/s11104-017-3248-3>
- Zhu, X., Pan, T., Zhang, X., Fan, L., Quintero, F. J., Zhao, H., ... & Qiu, Q. S.** (2018). K⁺ efflux antiporters 4, 5, and 6 mediate pH and K⁺ homeostasis in endomembrane compartments. *Plant Physiology*, 178(4), 1657-1678. <https://doi.org/10.1104/pp.18.01053>
- Zhu, Y. J., Fan, Y. Y., Wang, K., Huang, D. R., Liu, W. Z., Ying, J. Z., & Zhuang, J. Y.** (2017). Rice Flowering Locus T 1 plays an important role in heading date influencing yield traits in rice. *Scientific reports*, 7(1), 1-10. <https://doi.org/10.1038/s41598-017-05302-3>
- Zou, Y. N., Wang, P., Liu, C. Y., Ni, Q. D., Zhang, D. J., & Wu, Q. S.** (2017). Mycorrhizal trifoliate orange has greater root adaptation of morphology and phytohormones in response to drought stress. *Scientific reports*, 7(1), 1-10. <https://doi.org/10.1038/srep41134>

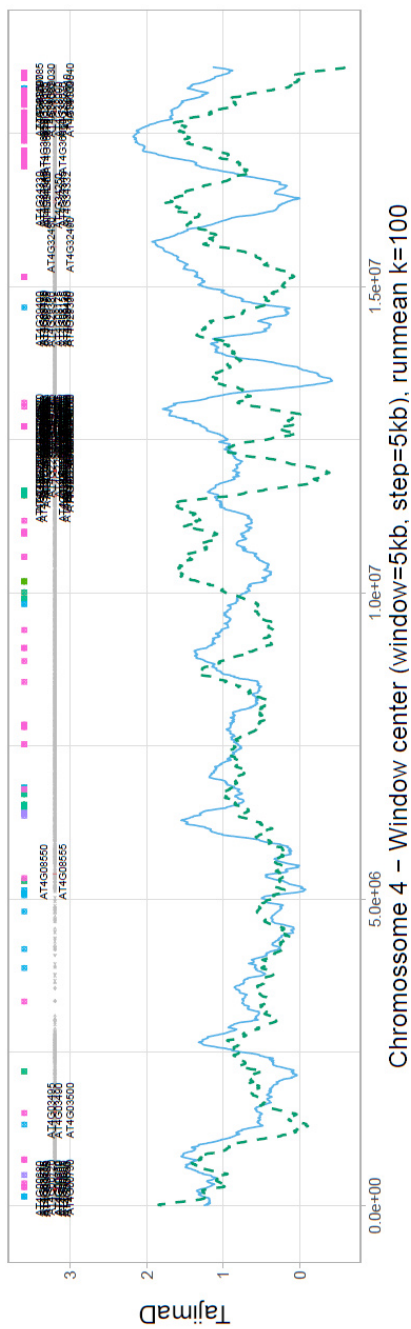
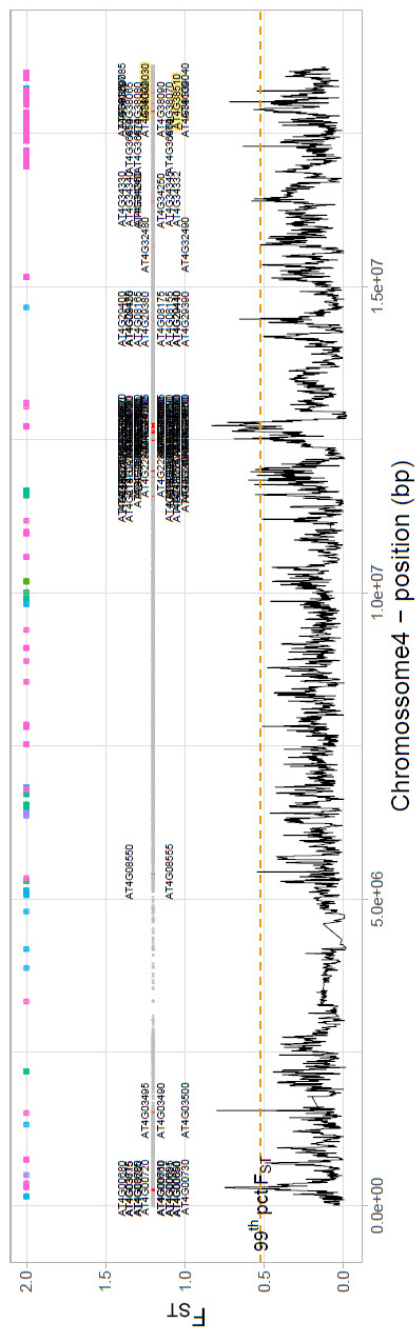
Supplementary Material



Chapter 1







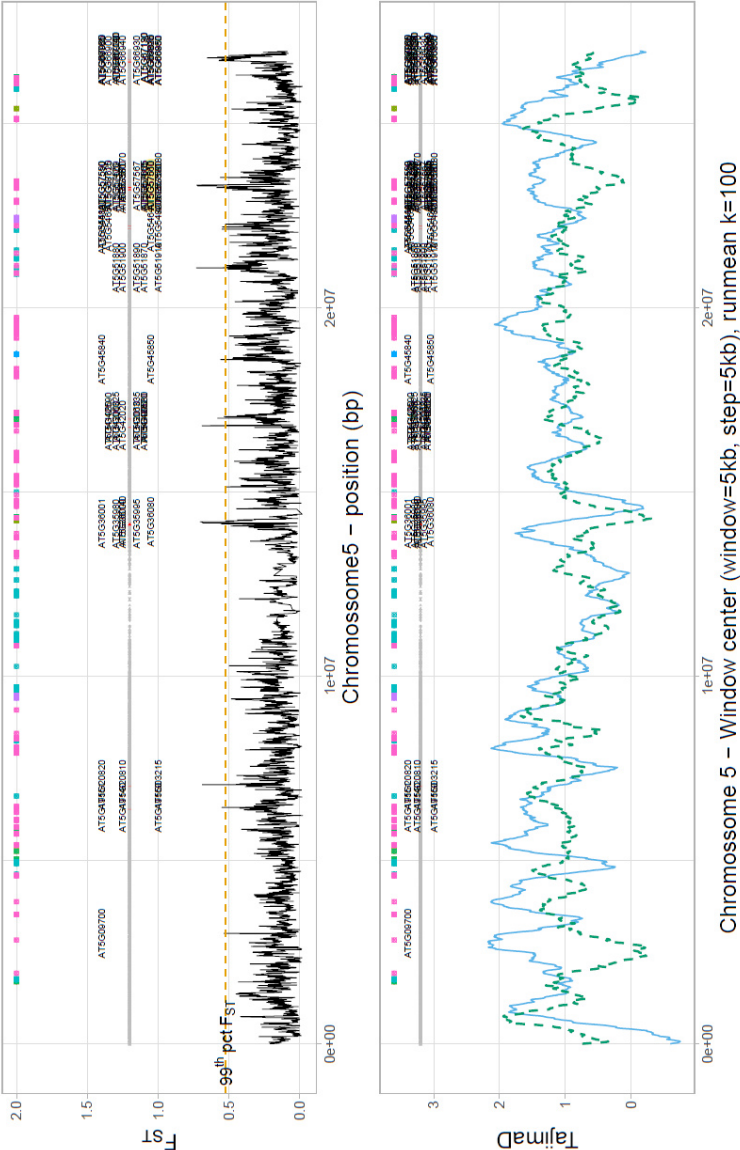
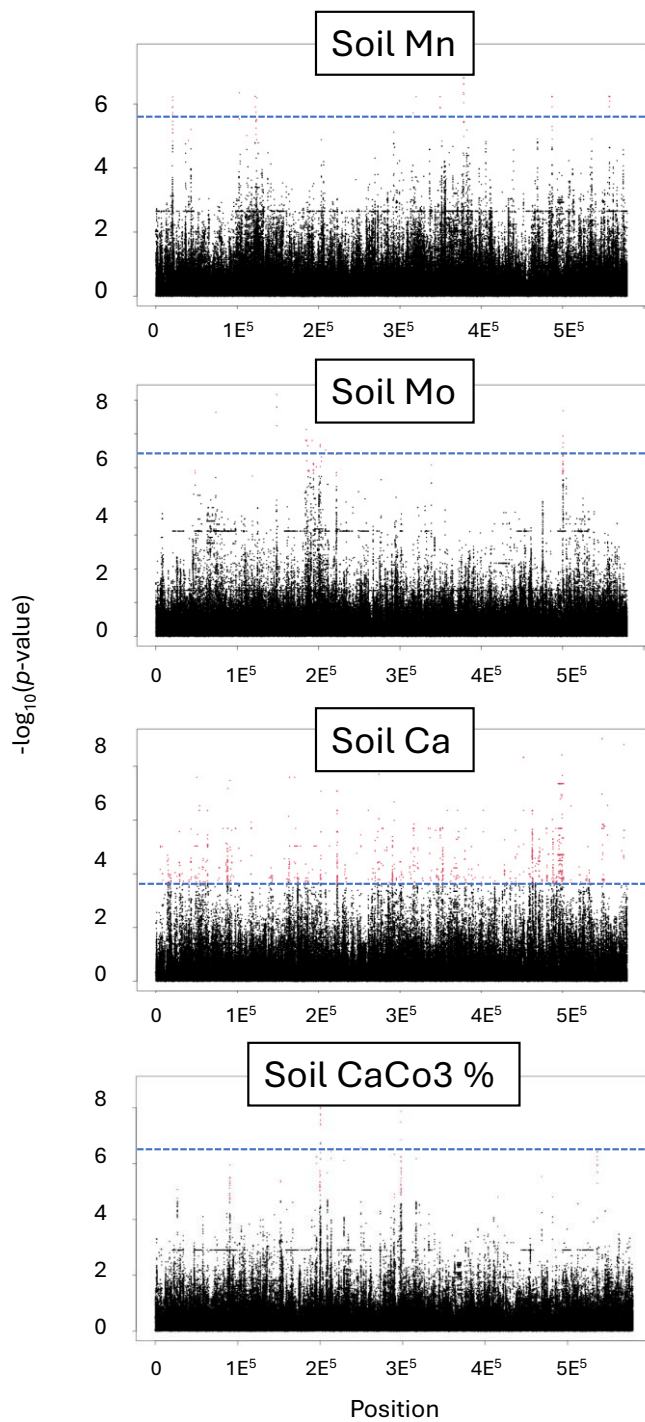


Figure S1.1. Divergence scans. Sliding window analysis of F_{ST} (top) and Tajima's D values (bottom) computed over 5 Kb windows and plotted along each chromosome between the early (blue) and late (dashed-green) flowering groups. Outlier F_{ST} threshold (99th percentile cutoff) is indicated with a dashed orange line.



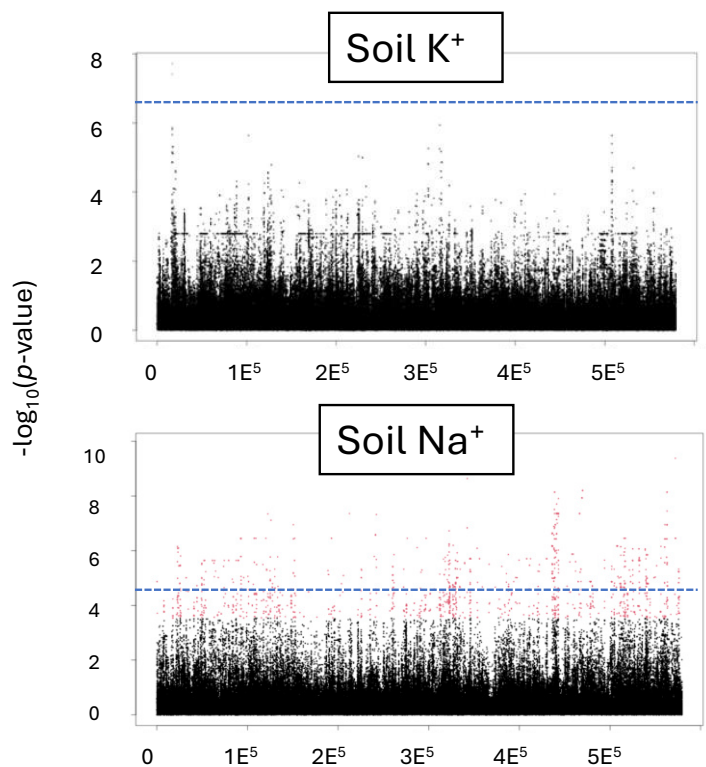


Figure S1.2. Genotype – Environment Association Study for soil traits (GEA). The plots represent the genome-wide distribution of significance values [x axis: $-\log_{10}(p\text{-value})$] obtained by LFMM for soil variables. Y axis: position (bp). Grey dashed line indicates significance threshold obtained by FDR p-value correction ($q\text{-value} < 0.01$).

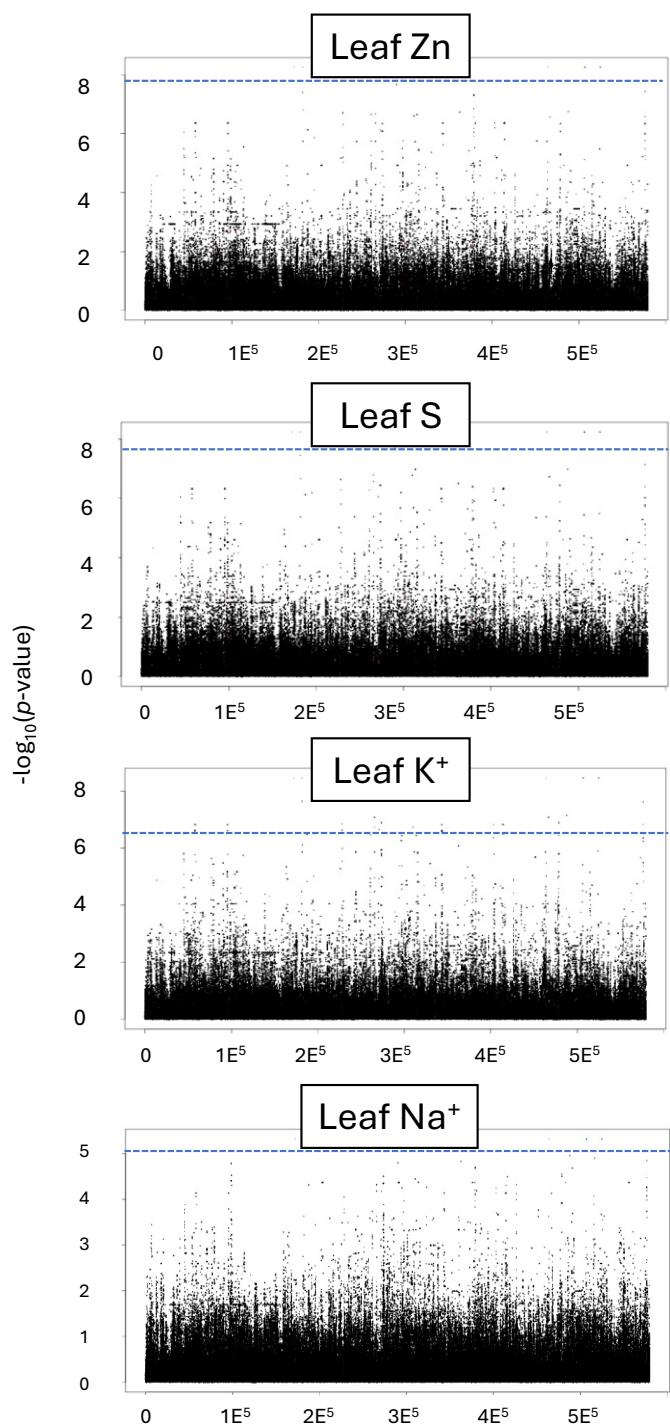


Figure S1.3. Genotype – Phenotype Association Study for leaf traits (GPA). The plots represent the genome-wide distribution of significance values [x axis: $-\log_{10}(p\text{-value})$] obtained by LFMM for soil variables. Y axis: position (bp). Grey dashed line indicates significance threshold obtained by FDR p-value correction (q-value < 0.01).

Chapter 2

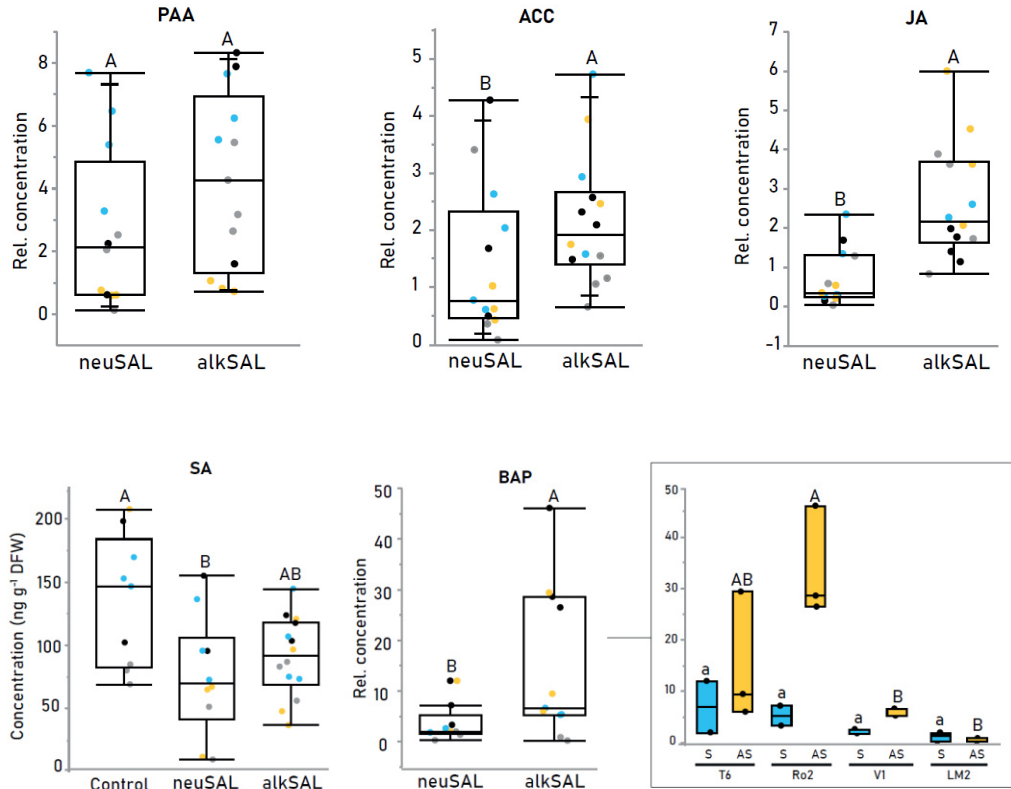
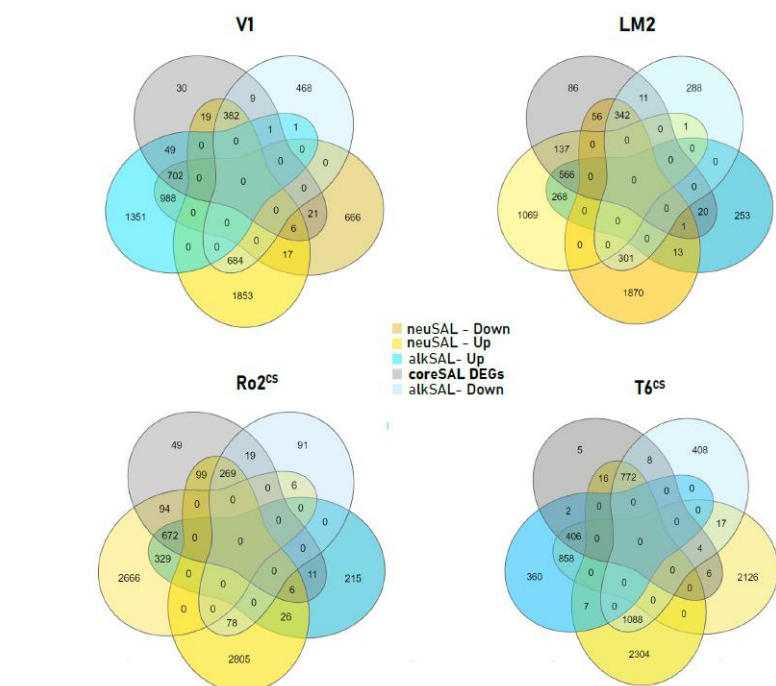


Figure S2.1. Complementary data on nutrition and endogenous phytohormone concentrations. Phenyl acetic acid (PAA), 1-aminocyclopropane-1-carboxylic acid (ACC), Jasmonic acid (JA), Salicylic acid (SA) and 6-benzylaminopurine (BAP) concentration in all demes under control and salinity treatments. Each dot represents a biological replicate ($n=3$), and demes are color-coded (see legend). Mean values with different letters indicate significant differences (Tukey's HSD, adj. *p*-value < 0.05). Plants were grown in potting mix soil and irrigated with C (0.5-Hoagland, pH 5.9), *neuSAL* (100 mM NaCl, pH 5.9) or *alkSAL* (85 mM NaCl, 15 mM NaHCO₃, pH 8.3) for 2 weeks.



Deme	Total	neu SAL	Trend	alk SAL	Trend	Shared
T6	1214	10	2 ↓ 8 ↑	22	6 ↑ 16 ↓	1182
Ro2	1170	30	19 ↓ 11 ↑	193	99 ↑ 94 ↓	947
LM2	1133	31	11 ↓ 20 ↑	193	56 ↑ 137 ↓	909
V1	1188	30	9 ↓ 21 ↑	65	19 ↑ 49 ↓	1090

Figure S2.2.
Contribution of each
deme to the
coreSAL DEGs set.

Trend			
446 ↑	772 ↓	4 sal ↓	alksal
269 ↑	672 ↓	6 sal ↓	alksal
342 ↑	566 ↓	1 sal ↓	alksal
382 ↑	702 ↓	1 sal ↓	alksal ; 6 sal ↑

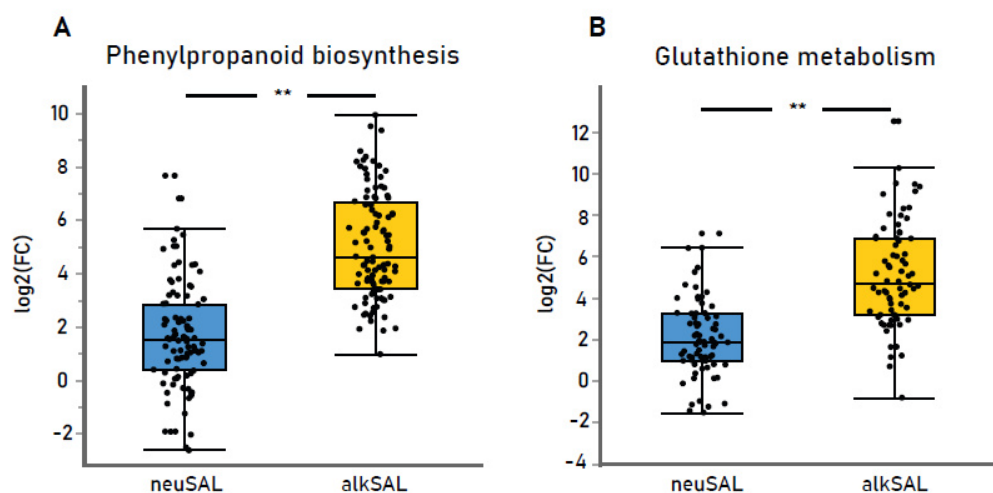
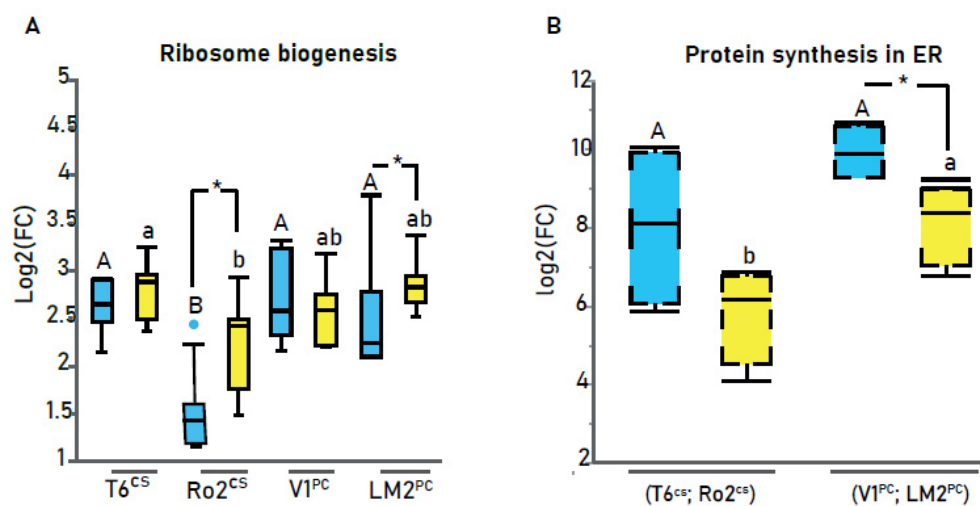


Figure S2.3. Dissection on significantly enriched pathways from *onlyALKSAL* upregulated DEGs.



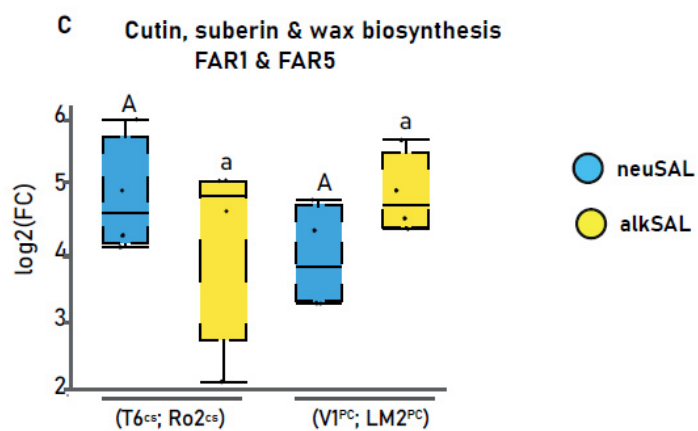


Figure S2.4. Dissection on significantly enriched pathways from *coreSAL* upregulated DEGs under neutral salinity (*neuSAL* in blue) and alkaline salinity (*alkSAL* in yellow) treatments.

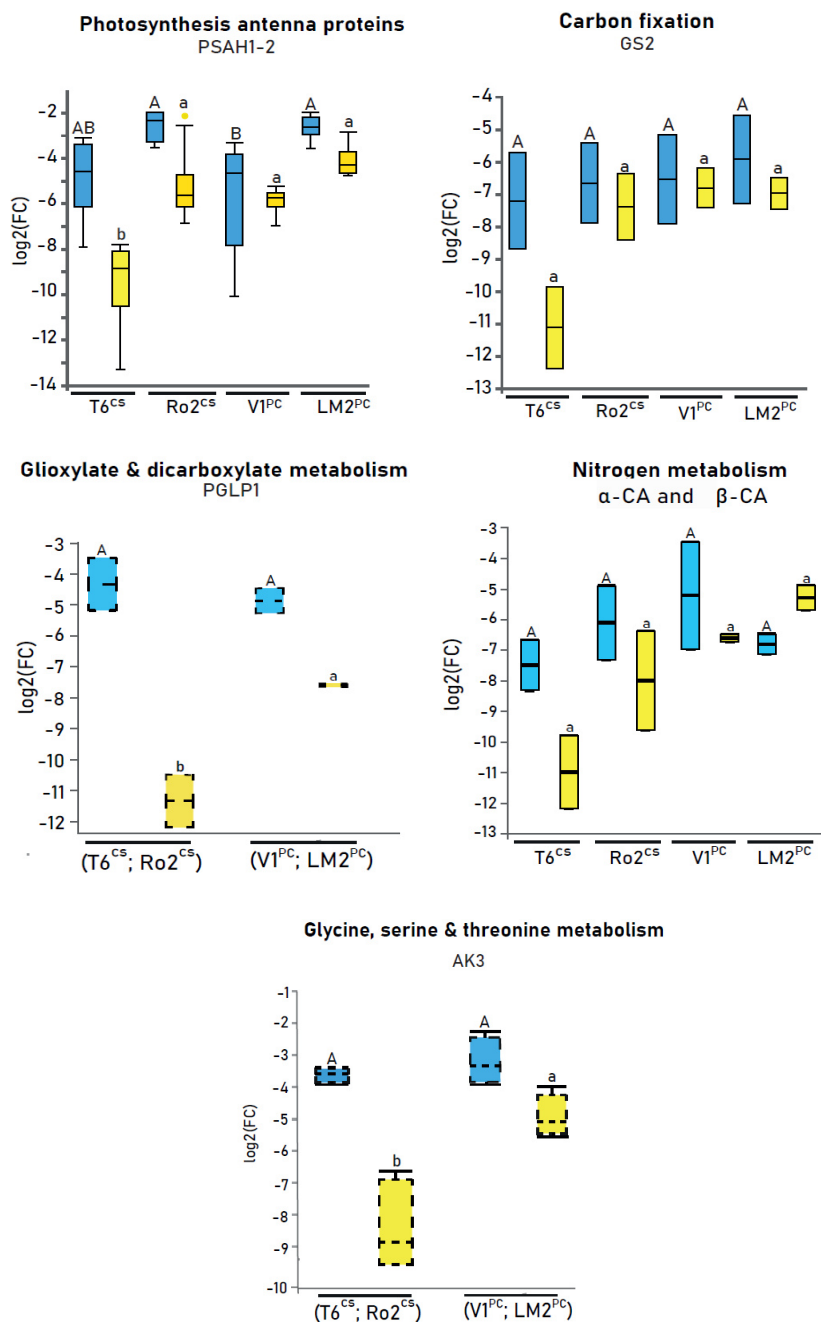


Figure S2.5. Dissection on significantly enriched pathways from *coreSAL* downregulated DEGs under neutral salinity (*neuSAL* in blue) and alkaline salinity (*alkSAL* in yellow) treatments.

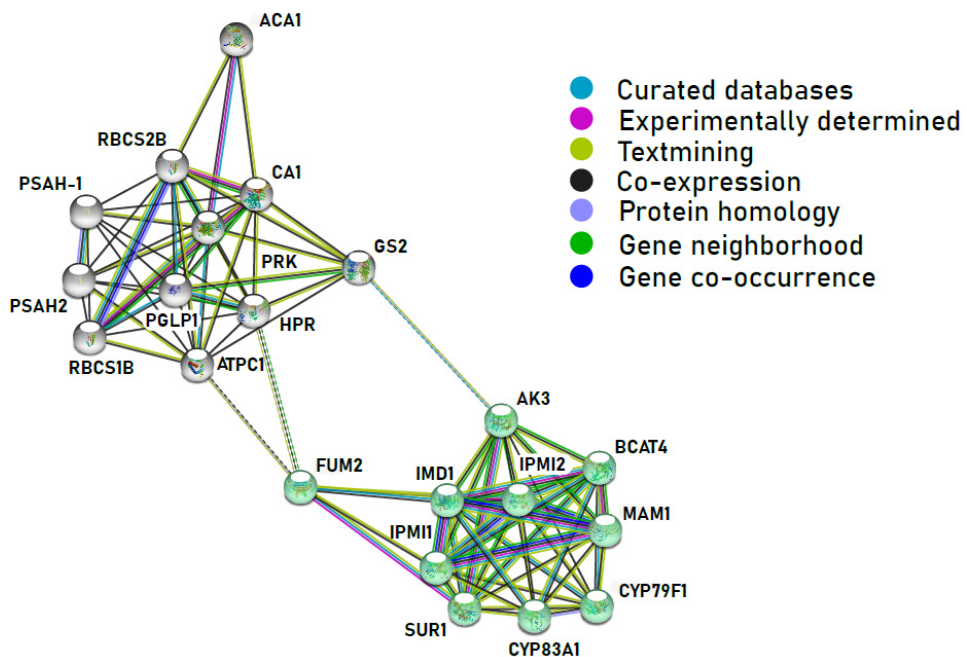


Figure S2.6. Key DEGs in the inhibition response of the studied demes.

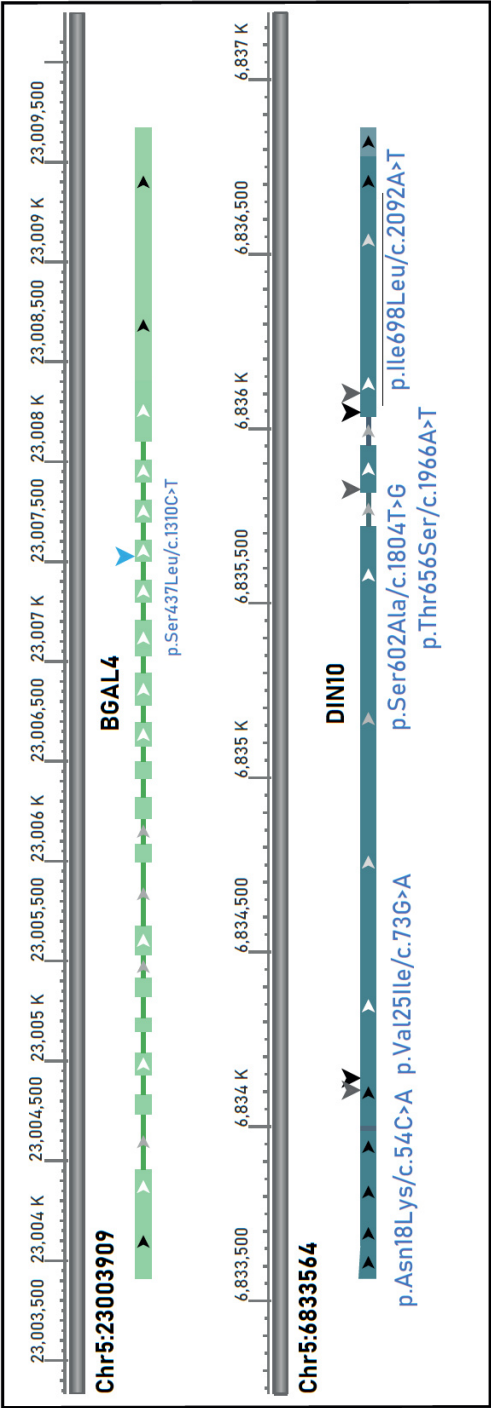


Figure S2.7. Gene models for BGAL4 and DIN10.

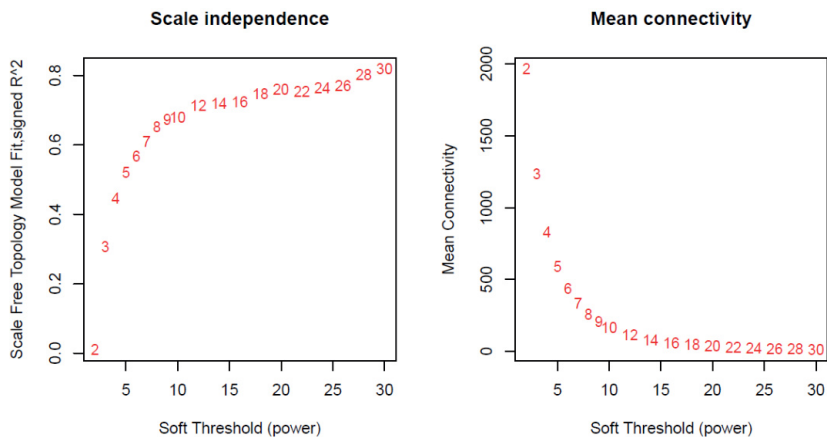


Figure S2.8. WGCNA analysis. Soft thresholding Network topology for different soft-thresholding powers (x axis).

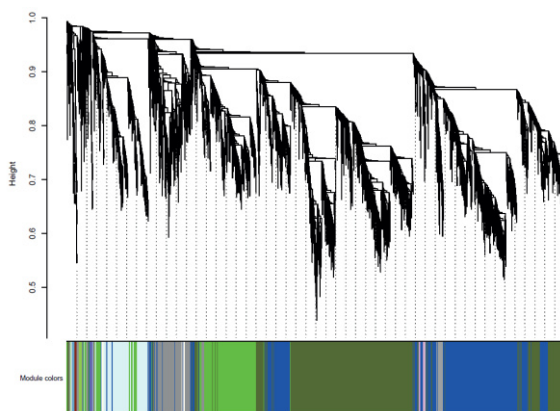


Figure S2.9. WGCNA analysis. Gene dendrogram obtained by clustering the dissimilarity based on consensus topological overlap with the corresponding module colors indicated by the color row. Each colored row represents a color-coded module which contains a group of highly connected genes.

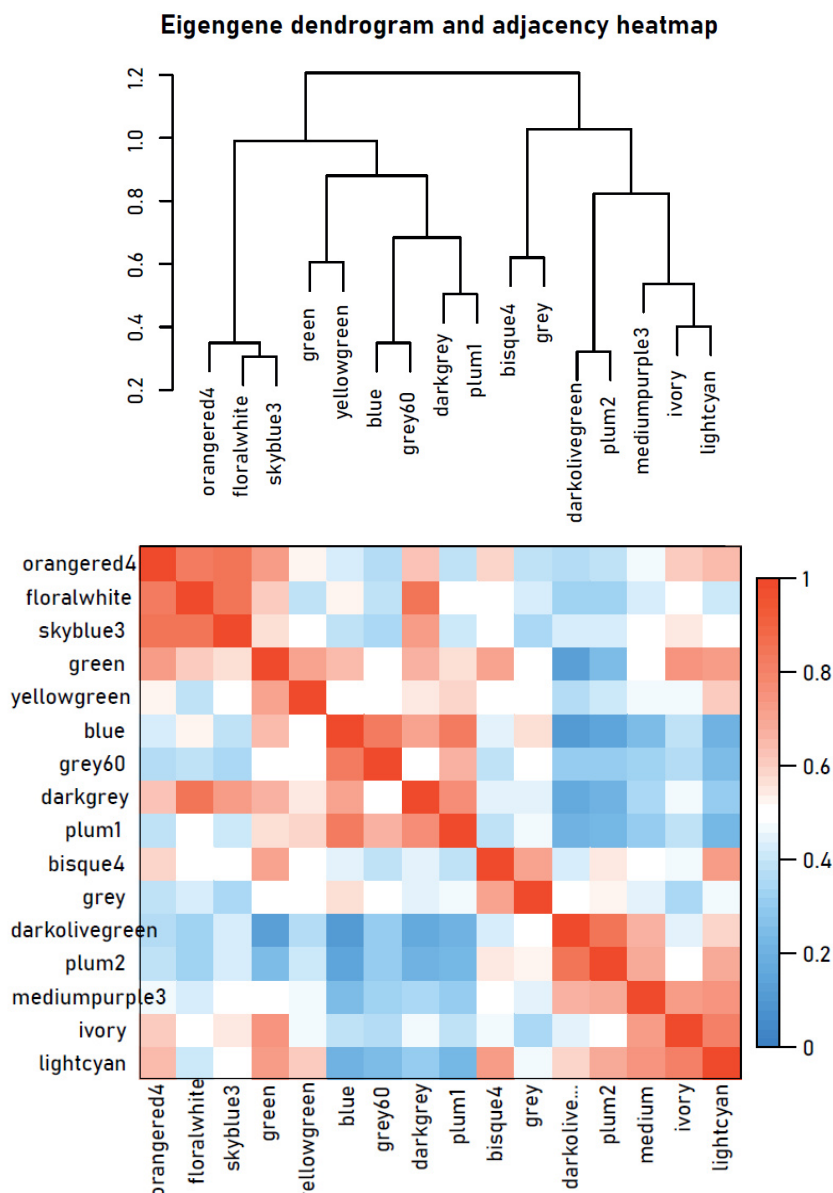


Figure S2.10. WGCNA analysis. Dendrogram of consensus module eigengenes obtained by WGCNA on the consensus correlation. Heatmap plotting adjacencies of modules. Red represents high adjacency (positive correlation) and blue represents low adjacency (negative correlation).

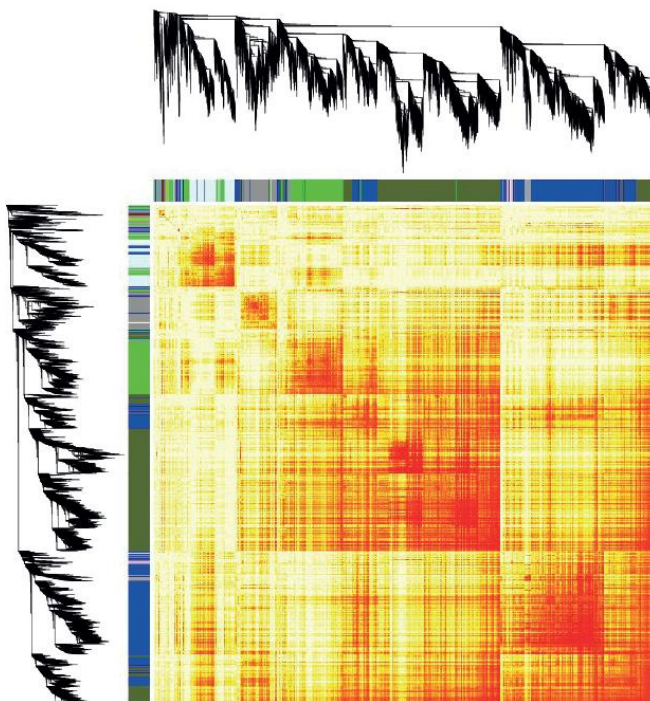
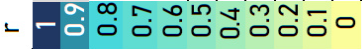


Figure S2.11. WGCNA analysis. Topological Overlap Matrix (TOM) showing the interaction of co-expression genes and the cluster dendrogram of 1,000 randomly selected genes. The intensity of the yellow inside the heatmap represents the degree of overlap (orange: high; yellow: low).

A

	Fe	Ca	Mg	K	Na	S	Mn	B	P	Zn	RD
Fe		0.535	0.324	0.802	-0.305	-0.520	0.896	-0.294	-0.463	-0.115	0.075
Ca	0.535		0.595	-0.281	0.000	-0.179	0.580	-0.136	-0.242	0.179	0.097
Mg	0.324	0.595		-0.068	0.189	0.090	0.501	0.007	-0.074	0.248	-0.002
K	-0.802	-0.281	-0.068		0.196	0.584	-0.649	0.252	0.536	0.248	0.034
Na	-0.305	0.000	0.189	0.196		0.310	-0.238	0.116	-0.027	0.191	-0.213
S	-0.520	-0.179	0.090	0.584	0.310		-0.330	0.136	0.388	0.272	-0.240
Mn	0.896	0.580	0.501	-0.649	-0.238	-0.330		-0.137	-0.333	0.063	0.007
B	-0.294	-0.136	0.007	0.252	0.116	0.136	-0.137		0.245	0.438	-0.103
P	-0.463	-0.242	-0.074	0.536	-0.027	0.388	-0.335	-0.245		0.080	0.011
Zn	-0.115	0.179	0.248	0.248	0.191	0.272	0.063	0.438	0.080		-0.165
RD	0.075	0.097	-0.002	0.034	-0.213	-0.240	0.007	-0.103	0.011	-0.165	



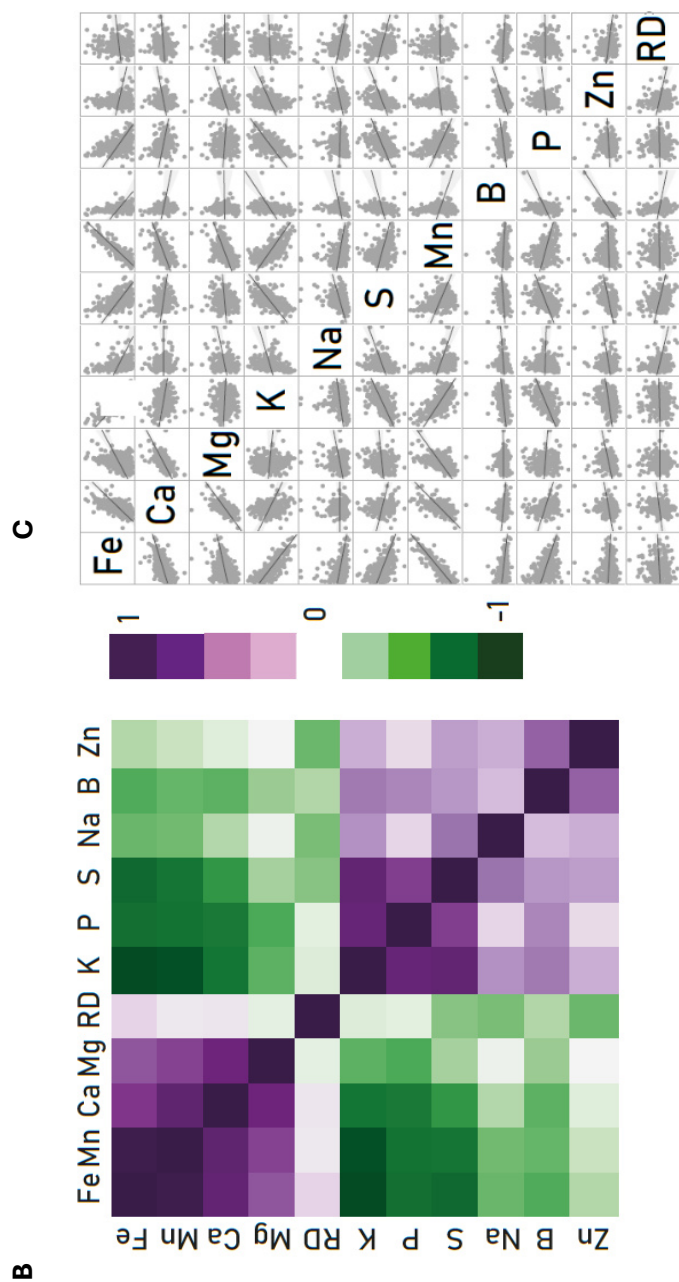


Figure S3.1. Correlogram (A), clustered heatmap (B) and scatter plot matrix (C) of leaf element concentrations across the studied *A. thaliana* accessions

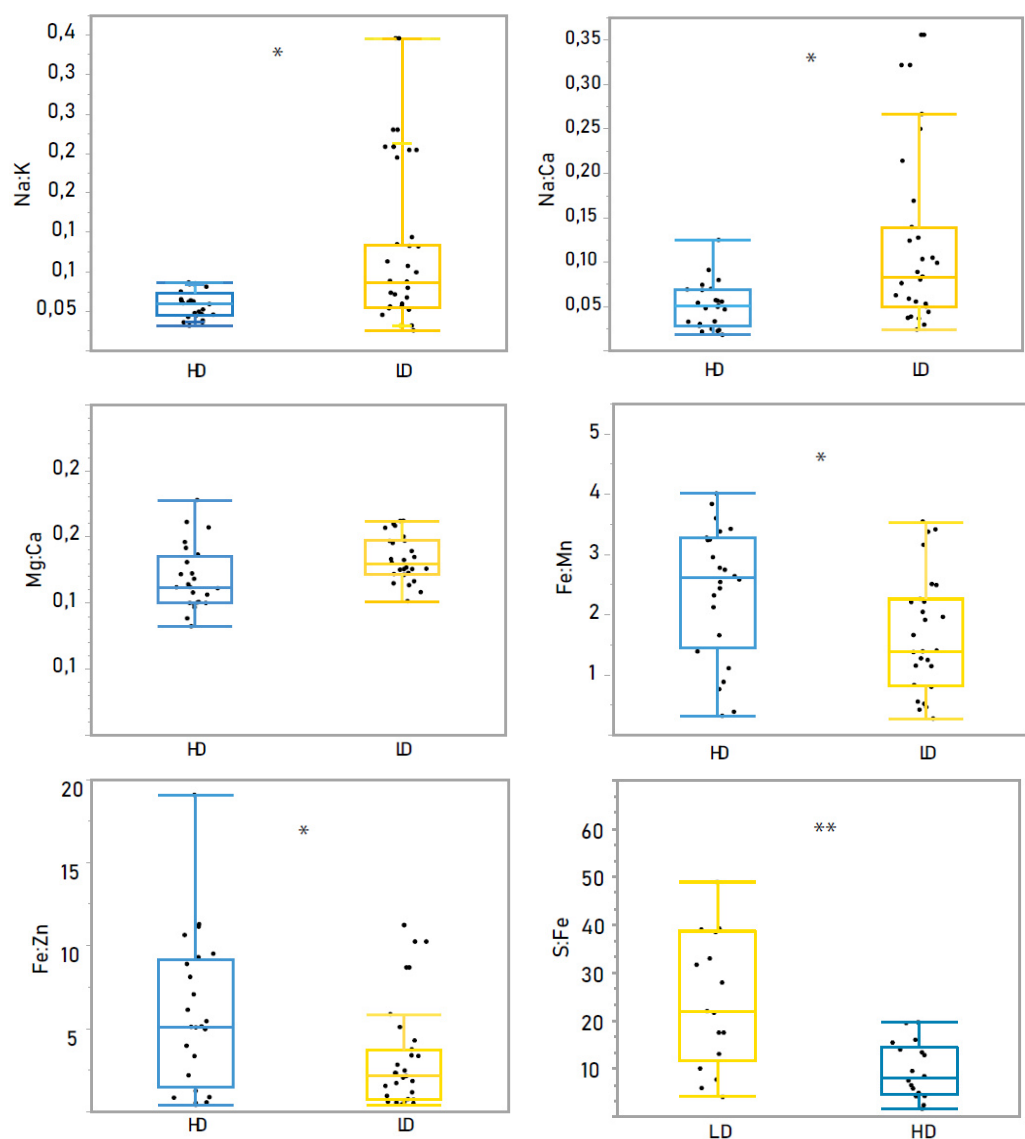
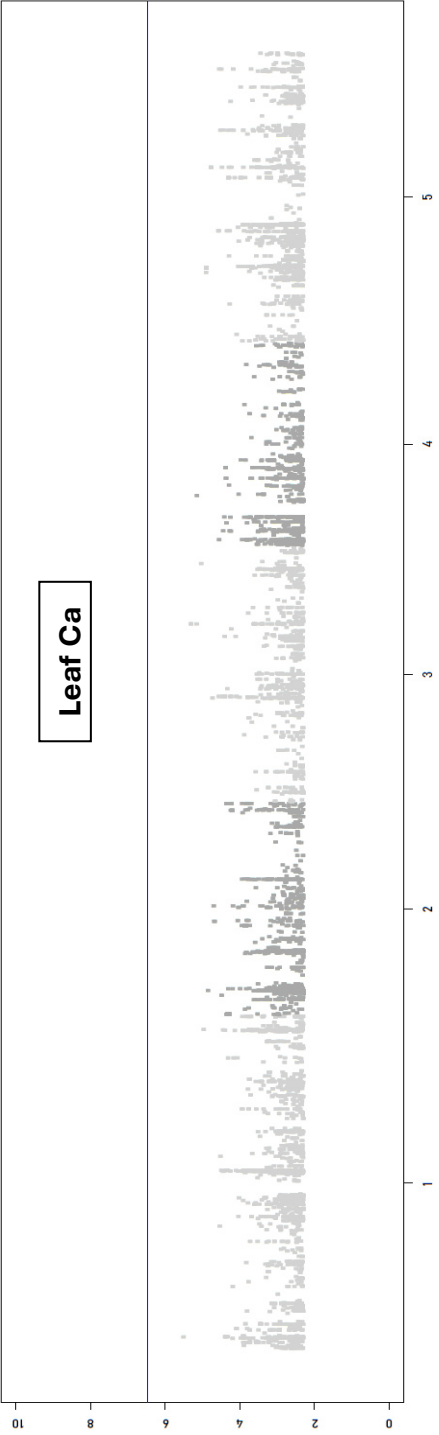
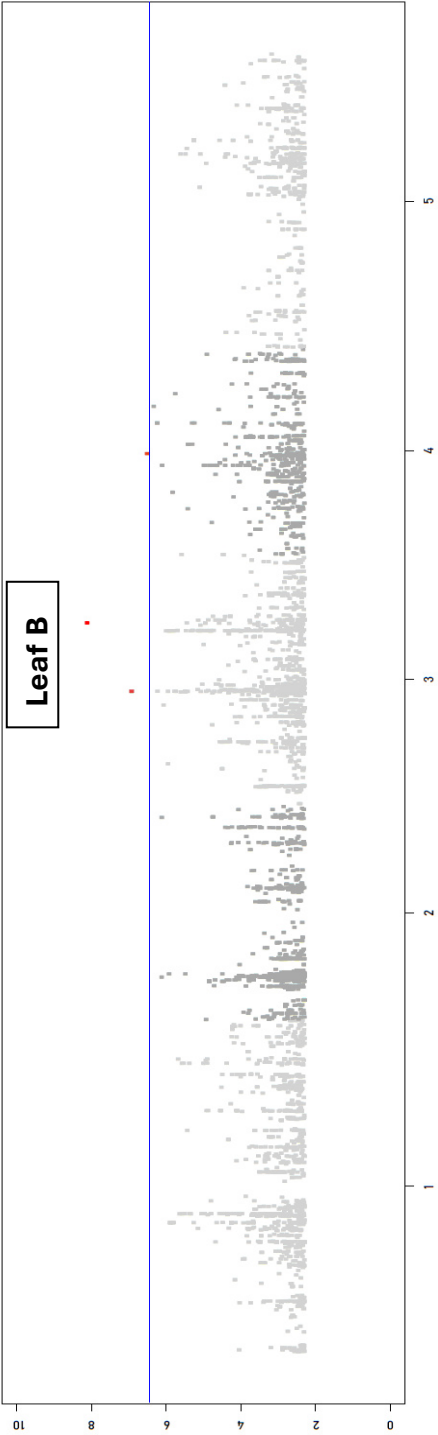
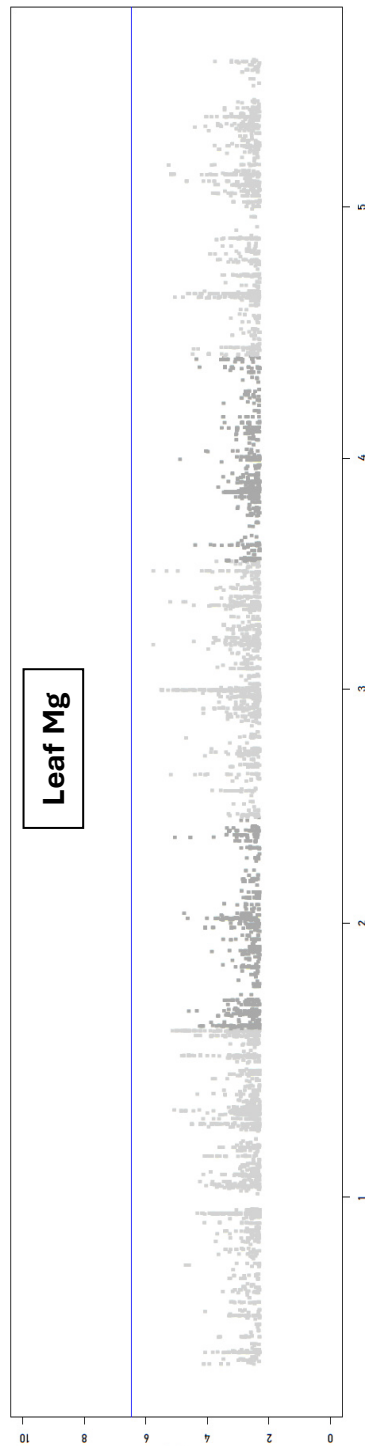
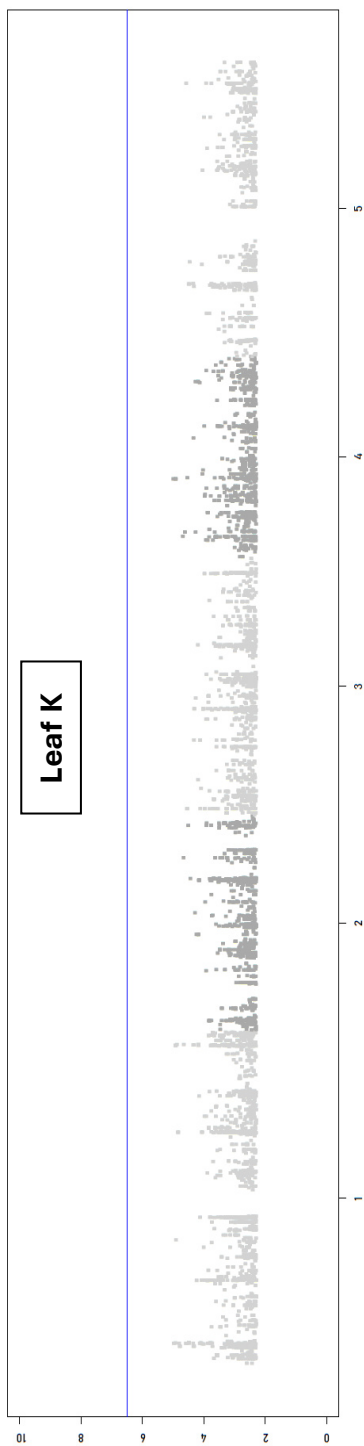
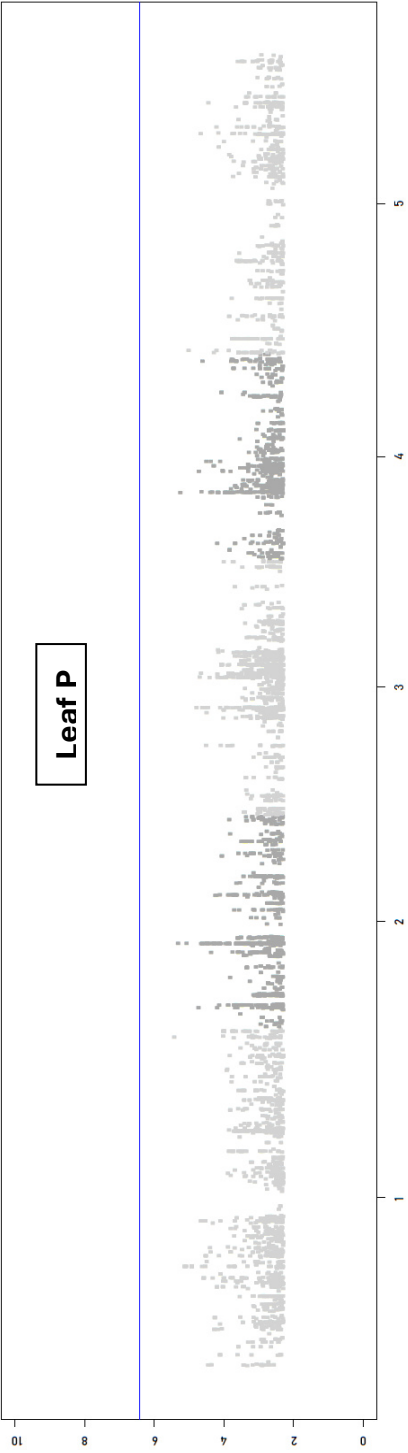
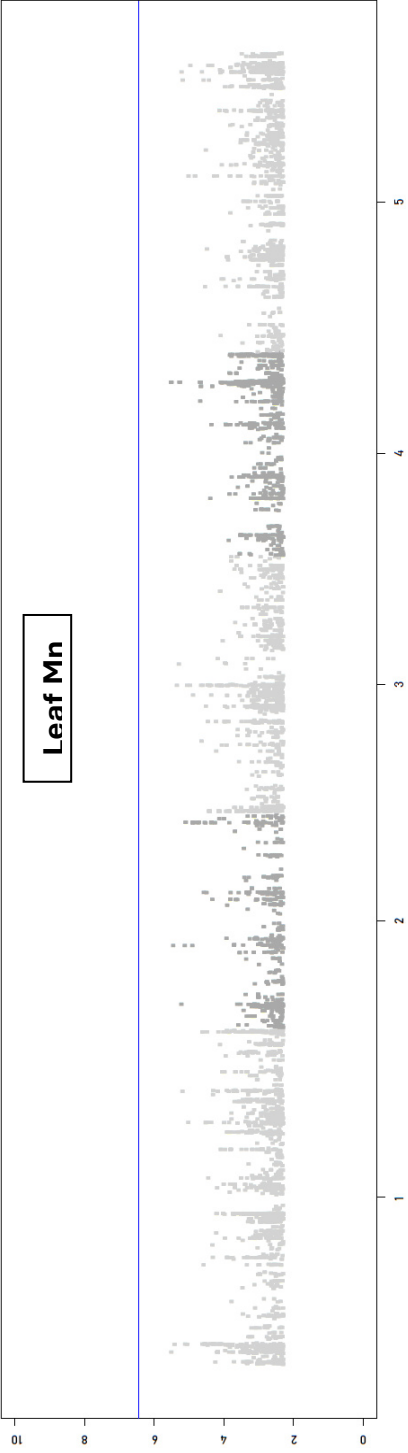


Figure S3.2. Nutrient ratios in leaves of the *A. thaliana* accessions used in the study.







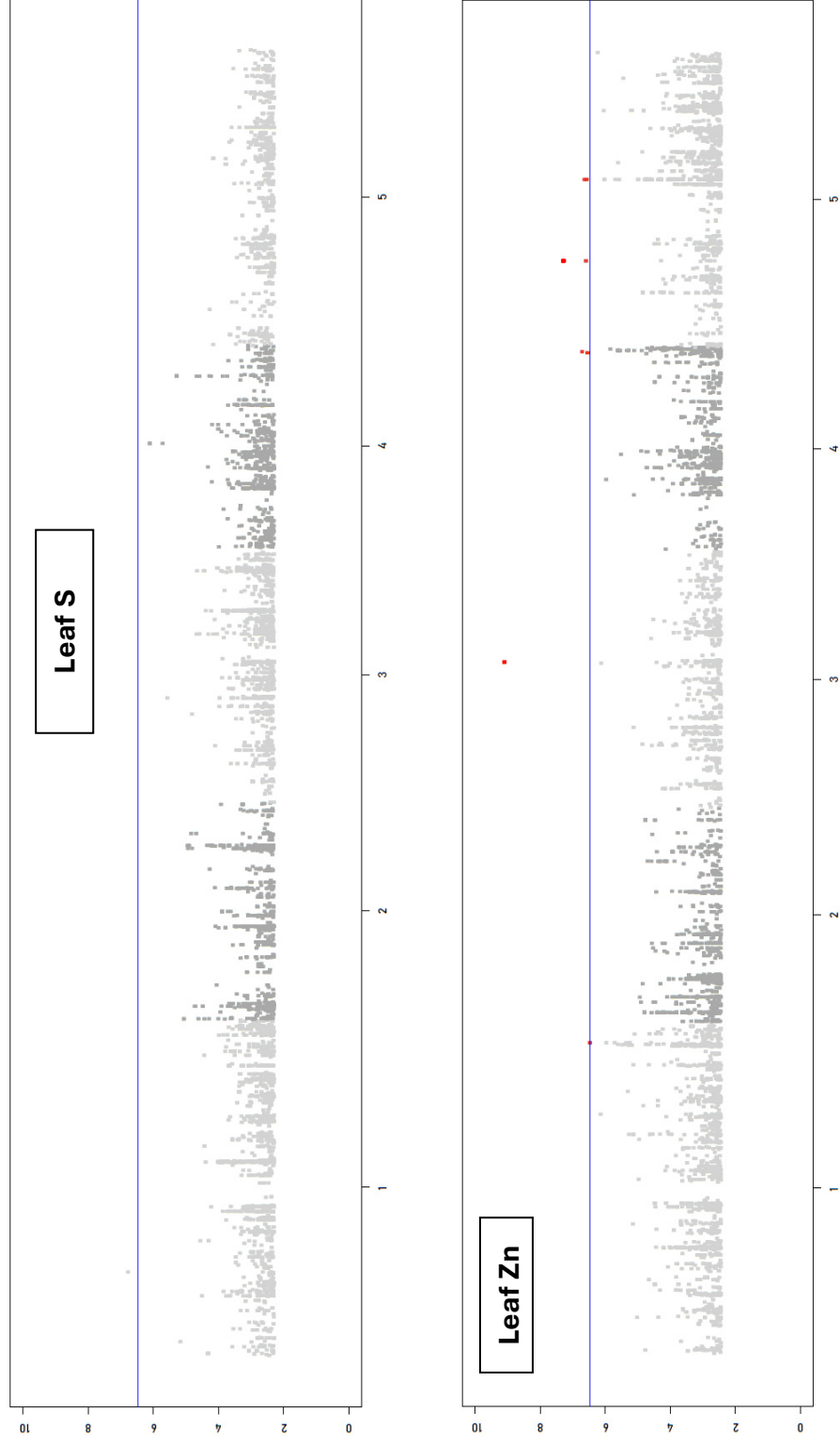


Figure S3.3. Genome wide association studies (GWAS) for leaf B, Ca, K, Mg, Mn, P, S, Zn ionome traits of HapMap accessions grown on SCS.

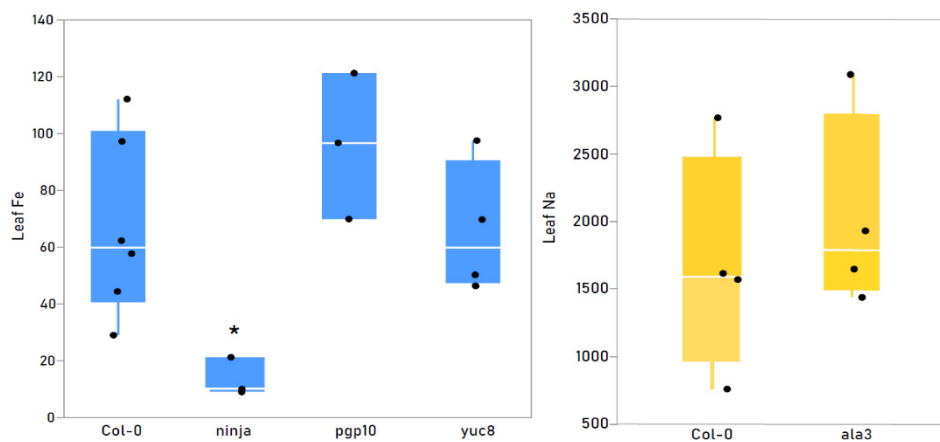


Figure S3.4. SNP specificity for the identified candidate locus. Leaf Fe and Na concentrations ($\mu\text{g g}^{-1}$) in T-DNA mutants for leaf Na and leaf Fe phenotypes, respectively.

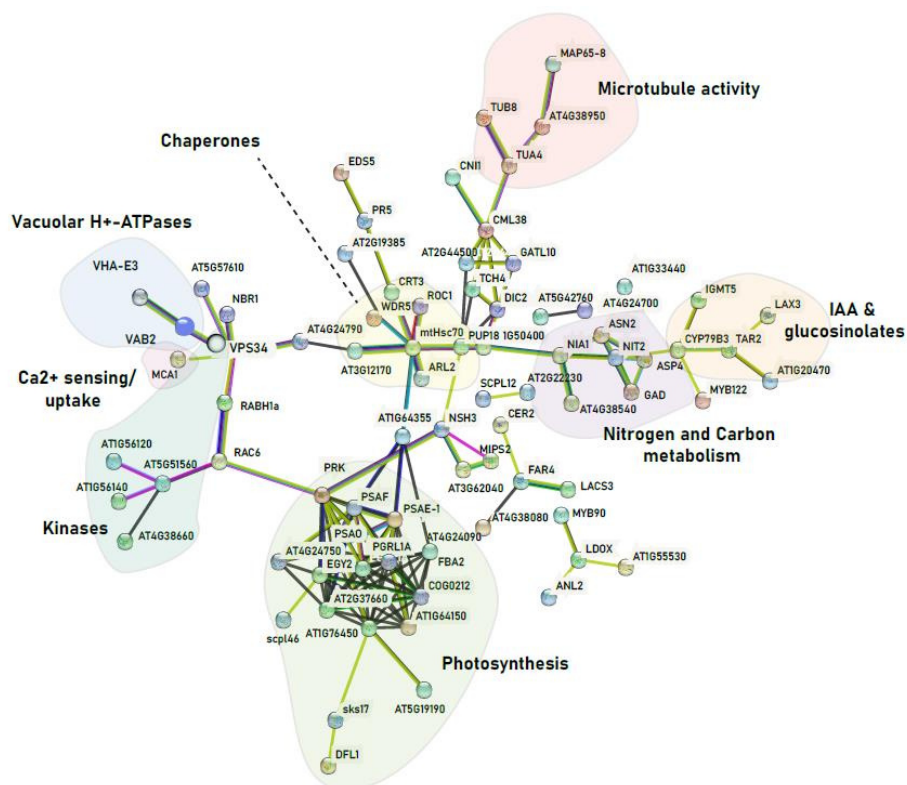
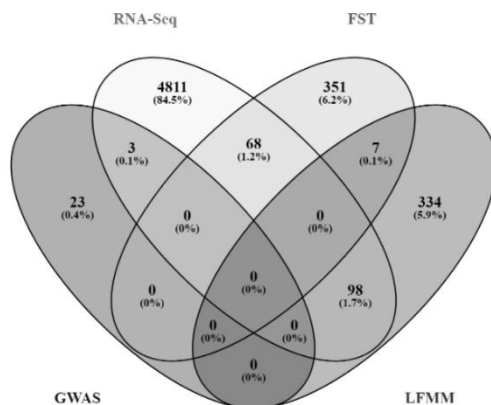


Figure S4.1. Candidates list for differential alkaline salinity tolerance in *Arabidopsis thaliana* natural populations.

PPI Network of candidates showing significant interaction and Venn Diagram showing overlapping gene sets. The candidate's list was obtained by integrating the lists of candidates from landscape genomics (chapter 1), RNA-Seq (chapter 2) and GWAS analyses (chapter 3) performed along this study.



SUPPLEMENTARY TABLES

Chapter 1

Table S1.1: Deme information. Deme ID, source, UTM coordinates, soil type classification according to soil Na concentration and soil CaCO₃%. BT: bolting time data. ICP: leaf nutrition data. RI: Rockwool irrigation experiment. RS: Soil reciprocal experiment. Crosses show in which experiments each deme was included. Demes were used according to stock availability.

Deme	Source	UTM (x)	UTM (y)	Soil-type	Avr soil Na (µg/g)	Avr soil CaCO ₃ (%)	BT		ICP		Re-seq
							RI	RS	RI	RS	
A1	S. Busoms	46,91	46,45	CN	32,25	12,13	x	x	x	x	x
A5	S. Busoms	47,04	46,44	CN	46,71	8,52	x		x	x	x
AM	S. Busoms	46,63	46,52	CN	43,67	8,69		x			
CALA	S. Busoms	49,56	46,20	SS	72,53	n.d.					x
JBB	K. Bomblies	48,39	46,14	SS	71,09	1,73	x	x	x	x	x
LG5	K. Bomblies	49,11	46,31	CS	65,85	7,50	x	x	x	x	x
LG7	K. Bomblies	49,08	46,31	CN	n.d.	6,08					x
LLO2	S. Busoms	48,63	46,17	SS	98,16	2,83	x	x	x	x	x
LM2	K. Bomblies	48,91	46,12	CN	49,64	12,34	x	x	x	x	x
O3	S. Busoms	46,77	46,45	CS	50,81	8,79	x	x	x	x	x
PA10	K. Bomblies	50,48	46,29	SS	168,73	1,26	x	x		x	x
PO1	Anthos	51,35	46,86	SS	67,25	2,22					x
RO2	Anthos	51,60	46,80	SS	73,12	1,30	x	x	x	x	x
SCF	S. Busoms	47,72	46,35	CN	42,94	6,25		x			x
SFG	S. Busoms	50,21	46,26	SS	87,69	1,71		x		x	x
T6	K. Bomblies	49,39	46,20	SS	103,32	0,81	x	x	x	x	x
T9	S. Busoms	49,38	46,18	SS	83,38	0,633		x		x	x
T11	S. Busoms	49,22	46,19	SS	80,57	1,37	x		x		x
T13	S. Busoms	49,41	46,19	SS	108,91	1,47	x	x	x	x	x
V1	Anthos	51,25	46,86	CS	70,98	5,00	x	x	x	x	x
V3	S. Busoms	51,18	46,86	CS	56,32	4,37		x		x	x

ID	Chr	Position	Description	Ref.	Alt.	Type_Substitution
1	4	268850	SNV C -> T	28%	72%	Upstream
2	4	268944	SNV T -> C	71%	29%	Upstream
3	4	269369	CT -> AT	77%	22%	frameshift_variant: cct/2p.Pro115fs/c.345delT2
4*	4	269462	codon change gAa/gGa2	5%	95%	Missense_AA change p.Glu146Gly/c.437A>G2
5*	4	269469	SNV A -> G	1%	99%	Missense_p.Ile148Met/c.444A>G
6*	4	269960	Insertion (16 bases): TCTTGTCCTAAGGTC	0%	100%	Frameshift_variant_p.Phe312_Gln313fs/c.936_937ins
7	4	270272	SNV A -> G	40%	60%	Intronic
8	4	270407	SNV A -> G	6%	94%	3_prime_UTR_variant
9	4	270724	SNV A -> G	74%	26%	3_prime_UTR_variant
10	4	270862	SNV A -> G	0%	100%	3_prime_UTR_variant
11	4	271105	SNV T -> C	7%	93%	3_prime_UTR_variant

Table S1.2. *FRI* genotyping. Variants detected in CatDeme sequences and haplotype summary. Asterisks show variants reported for *FRI* dominant alleles of the H51 accession.

	1	2	3	4	5	6	7	8	9	10	11
A1											
A5											
JBB											
LG5											
LLO2											
LM2											
O3											
PA10											
RO2											
SCF											
SFG											
T13											
T6											
T9											
V1											
V3											
T11											
PO1											
LG7											

Table S1.3. *FLC* variants detected in CatDeme sequences and haplotype summary. Asterisks show variants reported for *FLC*^A dominant haplogroups.

ID	Chr	Position	Description	Ref.	Alt.	Type_Substitution
1	5		Insertion AG	90%	10%	Downstream
2	5	3173462		0%	100%	Downstream
3	5	3173550	Deletion AT -> A	65%	35%	Downstream
4	5		Insertion (2 bases): TC	0%	100%	3' - UTR
5	5	3173943	SNV G -> T	12%	88%	Intronic
n.c.		3173996	Del-57*	20%	80%	Intronic
6	5	3174127	SNV C -> A	0%	100%	Intronic
7	5	3174538	SNV A --> T	0%	100%	Intronic
8	5	3174685	Deletion 18-bp	0%	100%	Intronic
9	5	3175210	G --> A	88%	12%	SYN_p.His123His/c.369C>T
10	5	3175290	Deletion CA -> C	50%	50%	Intronic
11	5	3176470	SNV C -> T	75%	25%	Intronic
12	5	3176549	SNV T -> G	76%	24%	Intronic
13	5	3176574	SNV A -> C (n.d.)	40%	60%	Intronic
14	5	3178308	Indel-1075*	40%	60%	Intronic
15	5	3177111	SNV T -> A	88%	12%	Intronic
16	5	3177838	SNV T -> C (n.d.)	77%	23%	Intronic
17	5	3178059	SNV T -> C	0%	100%	Intronic
18	5	3178825	SNV T -> G	50%	50%	Intronic
19	5	3178851	SNV T -> A	50%	50%	Intronic
20	5	3179123	SNV A -> T	0%	100%	Intronic
21	5	3179569	SNV T --> C	0%	100%	Upstream
22	5	3179648	SNV A -> T	0%	100%	Upstream

	1	9	2	4	6	7	8	16	17	20	21	22	5	11	12	13	18	Indel-1075	15	3	10	19	Del-57
O3			1	1	1	1	1	1	1	1	1	1	1	1	1	1	1						
LM2			1	1	1	1	1	1	1	1	1	1	1	1	1	1	1	1					1
T13			1	1	1	1	1	1	1	1	1	1	1	1	1	1	1						1
PO1			1	1	1	1	1	1	1	1	1	1	1	1	1	1	1						1
JBB			1	1	1	1	1	1	1	1	1	1	1										
RO2			1	1	1	1	1	1	1	1	1	1	1					1		1	1	1	
PA10			1	1	1	1	1	1	1	1	1	1	1					1		1	1	1	
SFG			1	1	1	1	1	1	1	1	1	1	1					1		1	1	1	
A1			1	1	1	1	1	1	1	1	1	1	1					1		1	1	1	
A5			1	1	1	1	1	1	1	1	1	1	1					1		1	1	1	
T9			1	1	1	1	1	1	1	1	1	1	1							1	1	1	
LG7			1	1	1	1	1	1	1	1	1	1	1					1		1	1	1	
V3			1	1	1	1	1	1	1	1	1	1	1	1	1	1		1		1	1	1	
LG5			1	1	1	1	1	1	1	1	1	1	1					1			1	1	
SCF			1	1	1	1	1	1	1	1	1	1	1					1			1	1	
LLO2			1	1	1	1	1	1	1	1	1	1	1				1						
V1			1	1	1	1	1	1	1	1	1	1	1	1	1	1	1	1				1	1
T6	1	1	1	1	1	1	1	1	1	1	1	1					1	1		1			
T11	1	1	1	1	1	1	1	1	1	1	1	1					1	1		1			

Table S1.4: Vernalization sensitivity. Mean \pm Standard error (*Std Err*), ANOVA (*F value*; *Prob > F*) and Student *t*-Test of Bolting Time (top) and *FLC* relative expression levels (bottom) in Col-0, Ro2 (*FLC_{Early}*) and T6 (*FLC_{Late}*) with and without 28-day vernalization. Mean expression level calculated as [(dCtgene-dCtACT2)]. Plants grown at 8:16h light/dark and 22/18°C day/night conditions for 15 days. After that, light was increased by 2h every 3 days until reaching 16:8h light/dark cycle.

Treatment	Accession	Mean BT	Std Err	N	F value	Prob > F	Student t-Test
NV	Col-0	30,63	0,32	8	71,87	<0,0001	A
V	Col-0	27,20	0,45	5			B
NV	Ro2	25,25	0,41	8	0,22	0,6483	A
V	Ro2	24,86	0,77	7			A
NV	T6	32,00	0,96	8	18,05	0,0038	A
V	T6	27,75	0,48	4			B

Treatment	Accession	Mean Exp	Std Err	N	F value	Prob > F	Student t-Test
NV	Col-0	0,830	0,130	8	13,87	0,0047	A
V	Col-0	0,009	0,004	4			B
NV	Ro2	1,440	0,270	8	27,76	0,0001	A
V	Ro2	0,001	0,000	8			B
NV	T6	0,660	0,260	4	6,15	0,0478	A
V	T6	0,007	0,005	4			B

Table S1.5: Element concentration in native soils of the studied demes. Mean \pm Standard error (*Std Err*), ANOVA (*F value*; *Prob > F*) and Tukey HSD of element concentration in each soil type. Soil types were established according to calcareous/siliceous (C: CaCO₃ content above 5%; S: CaCO₃ content below 5%) and to salinity (N: mg kg⁻¹ Na below 50; S: mg kg⁻¹ Na above 50).

Soil element							
mg kg	Soil type	Mean	Std Error	N	F value	Prob > F	Tukey
CaCO ₃ %	CN	8,01	0,68	20	87,73	< 0,0001	A
CaCO ₃ %	CS	7,06	0,62	16			A
CaCO ₃ %	SS	1,37	0,12	35			B
Na	CN	35,95	2,54	20	21,21	< 0,0001	C
Na	CS	68,12	2,85	16			B
Na	SS	97,61	7,46	39			A

K	CN	101,31	13,30	18	10,04	0,0001	B
K	CS	164,72	15,57	13			A
K	SS	119,40	11,73	39			AB
Ca	CN	696,00	11	15	3,94	0,024	AB
Ca	CS	698,00	14	10			A
Ca	SS	678,00	13	34			B
Mg	CN	94,77	5,97	20	9,45	0,0002	B
Mg	CS	145,56	10,80	16			A
Mg	SS	150,31	9,12	39			A
S	CN	n.a.	n.a.	n.a.	n.a.	n.a.	n.a.
S	CS	n.a.	n.a.	n.a.	n.a.	n.a.	n.a.
S	SS	n.a.	n.a.	n.a.	n.a.	n.a.	n.a.
P	CN	22,95	5,87	18	1,74	0,18	A
P	CS	9,7	2,8	10			A
P	SS	12	2	26			A
Fe	CN	20,63	2,15	17	3,52	0,036	AB
Fe	CS	27,15	3,56	12			A
Fe	SS	18,45	1,56	35			B
Mn	CN	36,77	4,35	20	3,72	0,029	AB
Mn	CS	46,10	6,64	16			AB
Mn	SS	30,74	2,40	39			B
Zn	CN	10,37	3,21	17	0,71	0,49	A
Zn	CS	11,43	2,85	14			A
Zn	SS	17,09	4,31	39			A
Mo	CN	0,02	0,002	20	14,96	<0,0001	B
Mo	CS	0,02	0,0007	16			B
Mo	SS	0,04	0,003	39			A
Li	CN	0,03	0,003	18	2,80	0,067	A
Li	CS	0,01	0,01	15			A
Li	SS	0,02	0,002	39			A
Ni	CN	0,1	0,04	15	1,36	0,26	A
Ni	CS	0,13	0,04	12			A
Ni	SS	0,12	0,03	34			A
Se	CN	1,03	0,13	20	2,96	0,058	A
Se	CS	0,88	0,10	16			A
Se	SS	1,23	0,08	38			A
Co	CN	0,23	0,04	18	1,40	0,25	A
Co	CS	0,27	0,02	14			A
Co	SS	0,19	0,03	39			A
As	CN	0,12	0,02	20	0,74	0,48	A
As	CS	0,09	0,01	16			A
As	SS	0,12	0,01	39			A
Cu	CN	10,68	0,59	20	25,37	< 0,0001	A
Cu	CS	8,28	1,13	13			A
Cu	SS	4,29	0,55	39			B

Table S1.6: Leaf element concentration in the studied demes grown on alkaline-saline soil (RS). Mean \pm Standard error (*Std Err*), ANOVA (*F value*; *Prob > F*) and Tukey HSD of element concentration in leaves of each deme group. Groups were established according to native soil type in calcareous/siliceous (C: CaCO_3 content above 5%; S: CaCO_3 content below 5%) and to salinity (N: mg kg^{-1} Na below 50; S: mg kg^{-1} Na above 50).

Leaf element							
μg^{-1}	Soil type	Mean	Std Error	N	F value	Prob > F	Tukey
Na	CN	59,03	13,07	6	5,13	0,0117	A
Na	CS	46,75	5,87	10			AB
Na	SS	31,22	3,74	18			B
K	CN	0,69	0,06	6	3,50	0,0421	AB
K	CS	0,76	0,02	10			A
K	SS	0,63	0,03	19			B
Ca	CN	0,54	0,06	6	2,32	0,1157	A
Ca	CS	0,63	0,06	10			A
Ca	SS	0,5	0,03	19			A
Mg	CN	0,79	0,06	6	3,87	0,0320	AB
Mg	CS	0,79	0,05	10			A
Mg	SS	0,68	0,03	19			B
S	CN	1,26	0,21	6	4,06	0,0271	A
S	CS	0,89	0,36	10			B
S	SS	0,91	0,06	19			B
P	CN	0,71	0,06	6	0,26	0,7723	A
P	CS	0,76	0,04	10			A
P	SS	0,72	0,03	19			A
$\mu\text{g g}^{-1}$	Soil type	Mean	Std Error	N	F value	Prob > F	Tukey
Fe	CN	0,48	0,02	6	1,70	0,1994	A
Fe	CS	0,89	0,15	10			A
Fe	SS	0,80	0,12	17			A
Mn	CN	0,81	0,10	6	1,62	0,2147	A
Mn	CS	0,91	0,08	10			A
Mn	SS	0,78	0,20	19			A
Zn	CN	0,92	0,15	6	2,69	0,0841	A
Zn	CS	0,92	0,05	10			A
Zn	SS	0,73	0,05	19			A
B	CN	1,00	0,37	6	2,74	0,0804	A
B	CS	1,13	0,09	10			A
B	SS	0,68	0,10	17			A

Table S1.7: Leaf element concentration in the studied demes grown on rockwool irrigated with alkaline salinity treatment (RI). Mean \pm Standard error (*Std Err*), ANOVA (*F value*; *Prob > F*) and Tukey HSD of element concentration in leaves of each deme group. Groups were established according to native soil type in calcareous/siliceous (C: CaCO₃ content above 5%; S: CaCO₃ content below 5%) and to salinity (N: mg kg⁻¹ Na below 50; S: mg kg⁻¹ Na above 50).

Leaf element								
μg^{-1}	Soil type	Mean	Std Error	N	F value	Prob > F	Tukey	
Na	CN	13152	903	15	5,06	0,0097	A	
Na	CS	8314	490	10			B	
Na	SS	13762	934	30			A	
K	CN	32086	1133	14	6,90	0,023	A	
K	CS	33503	1683	10			A	
K	SS	27570	990	28			B	
Ca	CN	44670	1333	14	2,00	0,15	A	
Ca	CS	42726	1351	10			A	
Ca	SS	45265	920	27			A	
Mg	CN	3451	387	18	0,14	0,87	A	
Mg	CS	3760	648	14			A	
Mg	SS	3624	202	29			A	
S	CN	8891	213	14	5,27	0,0085		
S	CS	7881	234	10				
S	SS	9488	329	27				
P	CN	4189	222	14	1,48	0,24	A	
P	CS	4272	216	10			A	
P	SS	2969	351	24			A	
$\mu\text{g g}^{-1}$	Soil type	Mean	Std Error	N	F value	Prob > F	Tukey	
Fe	CN	195	19	18	1,51	0,233	B	
Fe	CS	179	20	13			B	
Fe	SS	223	8	13			A	
Mn	CN	69	2	14	1,14	0,33	A	
Mn	CS	71	15	12			A	
Mn	SS	75	14	30			A	
Zn	CN	122	6	14	5,35	0,0079	AB	
Zn	CS	106	10	12			B	
Zn	SS	129	4	26			A	
B	CN	54	7	12	0,54	0,5867	A	
B	CS	51	5	10			A	
B	SS	62	7	29			A	

Table S1.8: Effects of neutral and alkaline salinity on the Bolting Time of CatDeme groups (RS). Mean \pm Standard error (*Std Err*), ANOVA (*F value*; *Prob > F*) and Tukey HSD or Student *t*-Test of bolting days (BT) of each deme group under neutral (Treatment 2) and alkaline saline soil (Treatment 3). Groups were established according to native soil type in calcareous/siliceous (C: CaCO₃ content above 5%; S: CaCO₃ content below 5%) and to salinity (N: mg kg⁻¹ Na below 50; S: mg kg⁻¹ Na above 50). Seedlings were vernalized at 4°C for 6 weeks under 8:16 light/dark photoperiod after 10 days of sowing. When transferred to growth conditions, a 10h light photoperiod and constant temperature of 21°C were established.

Soil type	Treatment	Mean BT	Std Err	N	F value	Prob > F	Student t- Test
CN	2	29,61	0,8	64	3,48	0,0644	A
CN	3	31,7	0,78	64			A
CS	2	34,3	1,17	30	1,42	0,2381	A
CS	3	32,53	0,95	38			A
SS	2	32,1	0,58	90	1,95	0,1639	A
SS	3	33,46	0,66	98			A

Treatment	Soil type	Mean BT	Std Err	N	F value	Prob > F	HSD Tukey
2	CN	29,61	0,8	64	7,07	0,0011	B
2	CS	34,3	1,17	30			A
2	SS	32,2	0,58	88			A
3	CN	31,7	0,78	64	1,51	0,2227	A
3	CS	32,53	0,95	38			A
3	SS	33,46	0,66	98			A

Table S1.9: Effects of neutral and alkaline salinity on the Bolting Time of each deme (RS). Mean \pm Standard error (*Std Err*), ANOVA (*F value*; *Prob > F*) and Student *t*-Test of bolting days (BT) of each deme under neutral (Treatment 2) and alkaline saline soil (Treatment 3). Groups were established according to native soil type in calcareous/siliceous (C: CaCO₃ content above 5%; S: CaCO₃ content below 5%) and to salinity (N: mg kg⁻¹ Na below 50; S: mg kg⁻¹ Na above 50). Seedlings were vernalized at 4°C for 6 weeks under 8:16 light/dark photoperiod after 10 days of sowing. When transferred to growth conditions, a 10h light photoperiod and constant temperature of 21°C were established.

Deme	Treatment	Mean BT	Std Err	N	t value	Prob > t	Student t-Test
A1	2	32,8	1,33	15	-0,07	0,9441	A
A1	3	32,9	1,23	14			A
A5	2	22,5	0,99	14	-0,40	0,6956	A
A5	3	23,1	1,14	8			A
AM	2	33,6	1,86	10	0,45	0,6541	A
AM	3	32,6	1,19	14			A
JBB	2	28,9	1,20	15	-2,42	0,0225	B
JBB	3	33,1	1,26	15			A
LG5	2	36,2	0,75	14	-0,48	0,6367	A
LG5	3	36,7	0,73	14			A
LLO2	2	29,4	1,69	12	2,03	0,0534	A
LLO2	3	25,3	1,19	15			A
LM2	2	28,0	1,72	9	0,11	0,9162	A
LM2	3	27,7	0,33	3			A
O3	2	25,3	0,65	8	-0,92	0,3702	A
O3	3	26,8	1,18	15			A
PA10	2	34,8	0,81	9	-3,57	0,0019	A
PA10	3	39,2	0,87	13			A
Ro2	2	23,7	3,33	3	-0,32	0,7655	A
Ro2	3	25,0	2,52	3			A
SCF	2	29,7	1,19	13	0,89	0,3814	A
SCF	3	28,2	1,13	13			A
T13	2	35,9	0,67	10	-1,37	0,1871	A
T13	3	37,8	1,16	12			A
T6	2	37,9	0,65	15	-1,24	0,2257	A
T6	3	39,0	0,64	15			A
T9	2	33,2	0,97	9	0,81	0,4301	A
T9	3	31,7	1,56	10			A
V1	2	40,0	1,28	8	2,83	0,0126	A
V1	3	35,6	0,94	9			B
V3	2	38,0	3,21	3	-0,81	0,4335	A
V3	3	39,7	0,73	12			A

Table S1.10: Effects of neutral and alkaline salinity on the Bolting Time of CatDeme groups (RI). Mean \pm Standard error (*Std Err*), ANOVA (*F value*; *Prob > F*) and Tukey HSD or Student *t*-Test of bolting days (BT) of each deme group under control (Treatment 1) neutral (Treatment 2) and alkaline salinity irrigation (Treatment 3). Groups were established according to native soil type in calcareous/siliceous (C: CaCO₃ content above 5%; S: CaCO₃ content below 5%) and to salinity (N: mg kg⁻¹ Na below 50; S: mg kg⁻¹ Na above 50). Seedlings were vernalized at 4°C for 6 weeks under 8:16 light/dark photoperiod after 10 days of sowing. When transferred to growth conditions, a 10h light photoperiod and constant temperature of 21°C were established.

Treatment	Soil type	Mean BT	Std Err	N	F value	Prob > F	HSD Tukey
1	CN	26,38	0,89	32	0,74	0,4791	A
1	CS	27,97	1,42	32			A
1	SS	28,23	0,91	74			A
2	CN	28,03	1,08	29	4,14	0,0178	AB
2	CS	31,79	1,43	42			A
2	SS	27,52	0,88	75			B
3	CN	28,12	0,87	43	0,84	0,4321	A
3	CS	30,12	1,25	43			A
3	SS	28,60	0,82	96			A

Soil type	Treatment	Mean BT	Std Err	N	F value	Prob > F	HSD Tukey
CN	1	26,38	0,89	32	1,06	0,3504	A
CN	2	28,03	1,08	29			A
CN	3	28,12	0,87	43			A
CS	1	27,97	1,42	32	1,81	0,1691	A
CS	2	31,79	1,43	42			A
CS	3	30,12	1,25	43			A
SS	1	28,23	0,91	74	0,88	0,4175	A
SS	2	26,96	0,88	75			A
SS	3	28,50	0,83	96			A

Table S1.11: Effects of neutral and alkaline salinity on the Bolting Time of each deme (RI). Mean \pm Standard error (*Std Err*), ANOVA (*F value*; *Prob > F*) and Student *t*-Test of bolting days (BT) of each deme under control (Treatment 1) neutral (Treatment 2) and alkaline salinity irrigation (Treatment 3). Groups were established according to native soil type in calcareous/siliceous (C: CaCO₃ content above 5%; S: CaCO₃ content below 5%) and to salinity (N: mg kg⁻¹ Na below 50; S: mg kg⁻¹ Na above 50). Seedlings were vernalized at 4°C for 6 weeks under 8:16 light/dark photoperiod after 10 days of sowing. When transferred to growth conditions, a 10h light photoperiod and constant temperature of 21°C were established.

Deme	Treatment	Mean BT	Std Err	N	F value	Prob > F	HSD Tukey
A1	1	32,82	0,50	11	4,51	0,0186	C
A1	2	33,90	0,46	10			B
A1	3	35,13	0,62	15			A
A5	1	23,27	0,44	15	2,46	0,0980	A
A5	2	26,00	1,45	13			A
A5	3	23,80	0,68	15			A
Col-0	1	22,20	0,35	15	1,43	0,2493	A
Col-0	2	21,67	0,44	15			A
Col-0	3	22,50	0,27	18			A
JBB	1	31,88	0,41	16	9,25	0,0004	B
JBB	2	31,27	0,57	15			B
JBB	3	33,78	0,34	18			A
LG5	1	34,50	0,60	12	9,21	0,0005	B
LG5	2	37,89	0,70	18			A
LG5	3	35,07	0,44	15			B
LLO2	1	17,42	0,15	12	1,84	0,1708	A
LLO2	2	18,26	0,20	19			A
LLO2	3	18,22	0,45	18			A
LM2	1	22,33	0,61	6	5,36	0,0127	B
LM2	2	22,67	0,95	6			B
LM2	3	25,00	0,52	13			A
O3	1	19,73	0,12	15	0,17	0,8435	A
O3	2	19,87	0,22	15			A
O3	3	19,94	0,35	16			A
Ro2	1	20,86	0,35	14	0,18	0,8368	A
Ro2	2	20,93	0,44	15			A
Ro2	3	21,15	0,33	20			A
T11	1	25,60	3,33	1	0,18	0,8395	A
T11	2	27,60	1,78	5			A
T11	3	26,75	1,60	5			A
T13	1	32,07	0,54	8	6,28	0,0042	B
T13	2	33,50	0,34	15			A
T13	3	33,31	0,38	10			A
T6	1	39,08	0,53	13	0,36	0,7033	A
T6	2	38,09	0,72	12			A
T6	3	38,42	0,83	11			A
Tsu	1	27,80	0,34	19	0,49	0,6161	A
Tsu	2	27,80	1,05	15			A
Tsu	3	26,63	0,98	15			A
V1	1	37,00	0,89	8	2,37	0,1160	A
V1	2	39,44	0,80	5			A
V1	3	37,50	0,71	12			A

Table S1.12: Effects of neutral and alkaline salinity on the Bolting Time of each deme (RI). ANOVA for soil type, treatment, and their interaction. Estimation, Standard error (*Std Err*), *t* value, *Prob > |t|* and Tukey HSD.

Level	Estimation	Std Err	t value	Prob > t	HSD Tukey
Model Fit	28,45	0,38	74,50	8,9E-258	
CN	-0,95	0,58	-1,63	1,0E-01	B
CS	1,50	0,56	2,68	7,5E-03	A
SS	-0,56	0,47	-1,17	2,4E-01	B
1	-0,93	0,56	-1,67	9,5E-02	A
2	0,47	0,55	0,86	3,9E-01	A
3	0,46	0,52	0,88	3,8E-01	A
1*CN	-0,20	0,84	-0,24	8,1E-01	AB
1*CS	-1,06	0,82	-1,29	2,0E-01	AB
1*SS	1,26	0,69	1,83	6,8E-02	AB
2*CN	0,05	0,84	0,06	9,5E-01	AB
2*CS	1,36	0,79	1,72	8,6E-02	A
2*SS	-1,41	0,68	-2,07	3,9E-02	B
3*CN	0,15	0,78	0,19	8,5E-01	AB
3*CS	-0,30	0,76	-0,39	7,0E-01	AB
3*SS	0,15	0,64	0,23	8,2E-01	AB

Chapter 2

Table S2.1: Relative Rosette Diameter. Mean \pm Standard error (*Std Err*), ANOVA (*F value*; *Prob > F*) and Tukey test from the studied demes irrigated with *alkSAL* and *neuSAL* treatments. Relative rosette diameter ($RD_{Control} / RD_{Treatment}$) is shown. *Control* treatment: Hoagland $\frac{1}{2}$ pH 5.9. *neuSAL* treatment: Hoagland $\frac{1}{2}$ NaCl 25-50-100 mM pH 5.9. *alkSAL* treatment: Hoagland $\frac{1}{2}$ NaCl 20 - 40- 85 mM + $NaHCO_3$ 5 - 10 - 15 mM pH 8.3.

Treatment	Deme	Mean	Std Err	N	F value	Prob > F	Tukey HSD
alkSAL	T6	0,55	0,007	3	5,557	0,0234	B
alkSAL	Ro2	0,57	0,053	3			B
alkSAL	V1	0,60	0,055	3			AB
alkSAL	LM2	0,80	0,059	3			A
neuSAL	T6	0,62	0,034	3	0,069	0,9747	A
neuSAL	Ro2	0,63	0,022	3			A
neuSAL	V1	0,61	0,058	3			A
neuSAL	LM2	0,64	0,070	3			A

Table 2.2: Maximal photochemical efficiency of PSII. Mean \pm Standard Error (*Std Err*), ANOVA (*F value*; *Prob > F*) and Tukey test from the studied demes irrigated with *alkSAL* and *neuSAL* treatments. F_v/F_m values (depicting maximum quantum efficiency of PSII photochemistry in the dark-adapted state) are shown. *Control* treatment: Hoagland $\frac{1}{2}$ pH 5.9. *neuSAL* treatment: Hoagland $\frac{1}{2}$ NaCl 25-50-100 mM pH 5.9. *alkSAL* treatment: Hoagland $\frac{1}{2}$ NaCl 20 - 40- 85 mM + $NaHCO_3$ 5 - 10 - 15 mM pH 8.3

Treatment	Deme	Mean F_v/F_m	StdErr	N	F value	Prob > F	Tukey HSD
C	T6	0,78	0,034	3	0,94	0,4656	A
C	Ro2	0,72	0,037	3			A
C	V1	0,79	0,003	3			A
C	LM2	0,75	0,049	3			A
alkSAL	T6	0,52	0,088	4	12,017	0,0002	C
alkSAL	Ro2	0,70	0,016	5			A
alkSAL	V1	0,77	0,012	3			A
alkSAL	LM2	0,82	0,016	6			A
neuSAL	T6	0,86	0,012	3	6,95	0,0058	A
neuSAL	Ro2	0,81	0,013	3			AB
neuSAL	V1	0,74	0,014	3			B
neuSAL	LM2	0,73	0,023	3			B

Line	Treatment	Tukey test
LM2	C	B
LM2	alkSAL	A
LM2	neuSAL	B
Ro2	C	A
Ro2	alkSAL	A
Ro2	neuSAL	A
T6	C	A
T6	alkSAL	B
T6	neuSAL	A
V1	C	A
V1	alkSAL	A
V1	neuSAL	B

Table 2.3. Leaf mineral nutrition. Mean \pm Standard Error (*Std Err*), ANOVA (*F value*; *Prob > F*) and Tukey test from the studied demes irrigated with *alkSAL* and *neuSAL* treatments. Standardized *z* values (value-mean)/(max-min) for each element are shown. *Control* treatment: Hoagland $\frac{1}{2}$ pH 5.9. *neuSAL* treatment: Hoagland $\frac{1}{2}$ NaCl 25-50-100 mM pH 5.9. *alkSAL* treatment: Hoagland $\frac{1}{2}$ NaCl 20 - 40- 85 mM + NaHCO₃ 5 - 10 - 15 mM pH 8.3.

Treatment	Element ($\mu\text{g g}^{-1}$ DW)	Deme	Mean	StdErr	N	F value	Prob > F	Tukey test
Control	Na	T6	0,32	0,07	7	32,74	0,000	A
		Ro2	0,04	0,02	7			B
		V1	-0,33	0,03	5			C
		LM2	-0,12	0,02	7			B
Control	K	T6	0,23	0,08	8	17,22	2,84E-06	A
		Ro2	0,12	0,01	7			A
		V1	-0,29	0,06	6			B
		LM2	-0,12	0,05	8			B
Control	Ca	T6	-0,02	0,04	5	3,28	0,039	AB
		Ro2	0,02	0,01	7			AB
		V1	-0,20	0,03	6			B
		LM2	0,15	0,13	8			A
Control	Mg	T6	0,11	0,08	7	19,03	0,000	A
		Ro2	0,05	0,02	7			A
		V1	-0,41	0,06	6			B
		LM2	0,19	0,06	7			A

Table 2.3. Continuation...

Control	K	T6	0,23	0,076	8	17,218	2,84E-06	A
		Ro2	0,12	0,012	7			A
		V1	-0,29	0,059	6			B
		LM2	-0,12	0,049	8			B
Control	Na	T6	0,32	0,075	7	32,744	0,000	A
		Ro2	0,04	0,023	7			B
		V1	-0,33	0,034	5			C
		LM2	-0,12	0,025	7			B
Control	S	T6	0,45	0,055	6	27,247	0,000	A
		Ro2	-0,25	0,040	6			B
		V1	-0,12	0,077	6			B
		LM2	-0,07	0,057	6			B
Control	Mn	T6	-0,05	0,078	4	2,163	0,126	A
		Ro2	0,16	0,049	6			A
		V1	-0,42	0,075	5			A
		LM2	0,03	0,218	7			A
Control	B	T6	-0,17	0,086	8	8,072	0,001	B
		Ro2	0,00	0,056	6			B
		V1	-0,18	0,145	6			B
		LM2	0,35	0,033	6			A
Control	P	T6	0,18	0,047	6	43,290	0,000	A
		Ro2	-0,36	0,035	7			B
		V1	-0,25	0,049	6			B
		LM2	0,33	0,063	7			A
alkSAL	Na	T6	0,19	0,17	5	1,80	0,205	A
		Ro2	-0,18	0,03	3			A
		V1	0,04	0,18	5			A
		LM2	-0,02	0,05	2			A
alkSAL	K	T6	-0,13	0,02	5	3,48	0,054	A
		Ro2	0,04	0,02	2			A
		V1	0,25	0,17	5			A
		LM2	-0,21	0,02	3			A
alkSAL	Ca	T6	0,15	0,07	5	9,23	0,002	AB
		Ro2	-0,33	0,16	2			BC
		V1	0,24	0,11	5			A
		LM2	-0,32	0,07	4			C
alkSAL	Mg	T6	0,05	0,03	5	5,30	0,015	AB
		Ro2	-0,23	0,01	2			AB
		V1	0,22	0,13	5			A
		LM2	-0,23	0,08	4			BC

Table 2.3. Continuation...

alkSAL	S	T6	0,07	0,09	5	1,25	0,336	A
		Ro2	0,21	0,27	2			A
		V1	0,04	0,18	5			A
		LM2	-0,24	0,10	4			A
alkSAL	P	T6	0,03	0,10	5	3,74	0,045	AB
		Ro2	0,15	0,16	3			AB
		V1	0,25	0,07	3			A
		LM2	-0,34	0,17	4			B
alkSAL	Fe	T6	-0,04	0,06	5	1,70	0,215	A
		Ro2	0,15	0,16	3			A
		V1	0,12	0,17	5			A
		LM2	-0,21	0,02	4			A
alkSAL	Mn	T6	-0,04	0,07	5	4,83	0,020	AB
		Ro2	-0,29	0,11	2			B
		V1	0,30	0,14	5			A
		LM2	-0,18	0,10	4			B
alkSAL	Zn	T6	0,01	0,03	5	3,27	0,059	A
		Ro2	-0,06	0,04	3			A
		V1	0,20	0,15	5			A
		LM2	-0,23	0,05	4			A
alkSAL	B	T6	0,05	0,17	5	0,70	0,574	A
		Ro2	-0,29	0,26	2			A
		V1	0,08	0,13	5			A
		LM2	-0,04	0,06	2			A
neuSAL	Na	T6	-0,46	0,02	5	11,75	1,40E-04	B
		Ro2	0,10	0,12	8			A
		V1	0,27	0,05	6			A
		LM2	-0,02	0,03	4			A
neuSAL	K	T6	0,00	0,07	8	3,56	0,031	AB
		Ro2	0,16	0,09	8			A
		V1	-0,09	0,05	5			AB
		LM2	-0,16	0,06	5			B
neuSAL	Ca	T6	-0,18	0,05	8	3,35	0,035	B
		Ro2	0,21	0,09	8			A
		V1	-0,03	0,11	7			AB
		LM2	-0,01	0,13	6			AB
neuSAL	Mg	T6	-0,15	0,05	8	4,71	0,009	B
		Ro2	0,20	0,08	8			A
		V1	-0,06	0,09	8			AB
		LM2	0,02	0,06	7			AB

Table 2.3. Continuation...

neuSAL	S	T6	0,20	0,06	8	5,62	0,004	A
		Ro2	0,09	0,10	8			A
		V1	-0,09	0,08	8			AB
		LM2	-0,26	0,08	6			B
neuSAL	P	T6	0,05	0,07	8	5,69	0,004	AB
		Ro2	-0,17	0,08	8			B
		V1	-0,12	0,11	8			B
		LM2	0,26	0,04	7			A
neuSAL	Fe	T6	0,01	0,08	8	2,17	0,118	A
		Ro2	0,15	0,12	8			A
		V1	-0,16	0,04	6			A
		LM2	-0,05	0,07	6			A
neuSAL	Mn	T6	-0,18	0,08	8	6,69	0,002	B
		Ro2	0,30	0,08	7			A
		V1	-0,10	0,07	8			B
		LM2	0,03	0,10	7			AB
neuSAL	Zn	T6	0,04	0,02	7	3,05	0,046	AB
		Ro2	0,11	0,07	8			A
		V1	-0,15	0,09	8			B
		LM2	0,00	0,02	7			AB
neuSAL	B	T6	0,05	0,06	7	1,86	0,162	A
		Ro2	0,06	0,12	8			A
		V1	-0,15	0,03	8			A
		LM2	0,06	0,03	6			A

Table S2.4. Leaf mineral nutrient ratios. Mean \pm Standard Error (Std Err), ANOVA (F value; Prob > F) and Tukey test from the studied demes irrigated with *alkSAL* and *neuSAL* treatments. Nutrient Ratios Na:K, Na:Ca and Fe:Mn are shown. *Control* treatment: Hoagland $\frac{1}{2}$ pH 5.9. *neuSAL* treatment: Hoagland $\frac{1}{2}$ NaCl 25-50-100 mM pH 5.9. *alkSAL* treatment: Hoagland $\frac{1}{2}$ NaCl 20 - 40- 85 mM + NaHCO₃ 5 - 10 - 15 mM pH 8.3.

Treatment	Nutrient Ratio	Deme	Mean	StdErr	N	F value	Prob > F	Tukey test
alkSAL	Na:K	T6	2,56	0,09	5	26,79	0,002	A
		V1	1,86	0,09	3			B
	Na:Ca	T6	1,97	0,12	5	0,78	0,407	A
		V1	2,13	0,15	4			A
	Fe:Mn	T6	0,47	0,04	5	2,17	0,184	A
		V1	0,34	0,09	4			A
neuSaL	Na:K	T6	1,52	0,09	5	75,42	< 0.0001	B
		V1	2,88	0,29	5			A
	Na:Ca	T6	1,49	0,04	5	50,17	< 0.0001	B
		V1	2,43	0,12	6			A
	Fe:Mn	T6	0,77	0,08	6	9,00	0,0095	A
		V1	0,40	0,10	6			B

Table S2.5. Endogenous phytohormone concentrations. Mean \pm Standard Error (Std Err), ANOVA (F value; Prob > F) and Tukey test from relative concentrations of each phytohormone under *neuSAL* and *alkSAL* treatments. Mean relative concentration values ([X] Sal/Mean [X] C; [X] AlkSal / Mean [X] C) are shown.

Phytohormone	Treatment	Mean Rel conc	StdErr	N	F value	Prob > F	Student t-Test
IAA	neuSAL	2,64	0,71	11	16,95	0,0005	B
	alkSAL	8,94	1,31	12			A
PAA	neuSAL	2,69	0,73	12	2,14	0,157	A
	alkSAL	4,25	0,78	13			A
ACC	neuSAL	0,97	0,24	11	9,28	0,0057	B
	alkSAL	1,99	0,23	14			A
ABA	neuSAL	3,01	0,38	13	1,66	0,209	A
	alkSAL	2,33	0,36	15			A
JA	neuSAL	0,72	0,20	13	18,91	0,0002	B
	alkSAL	2,67	0,39	14			A
BAP	neuSAL	3,62	1,23	9	4,79	0,0421	B
	alkSAL	14,93	4,54	11			A
KA	neuSAL	8,23	3,12	13	2,53	0,125	A
	alkSAL	3,00	1,03	13			A
SA	neuSAL	0,61	0,15	11	0,60	0,446	A
	alkSAL	0,75	0,12	16			A

Phytohormone	Treatment	Deme	Mean	StdErr	N	F value	Prob > F	Tukey's HSD
IAA	neuSAL	T6	5,046	2,1	3	2,112	0,187	A
		Ro2	2,618	0,1	3			A
		V1	1,81	0,3	3			A
		LM2	1,095	0,5	3			A
	alkSAL	T6	13,022	1,4	3	8,541	0,0071	A
		Ro2	12,363	2,4	3			AB
		V1	4,533	0,6	3			C
		LM2	5,844	0,8	3			BC
PAA	neuSAL	T6	0,647	0,1	3	9,881	0,0046	BC
		Ro2	1,422	0,8	2			BC
		V1	5,697	0,9	4			A
		LM2	1,558	0,7	3			BC
	alkSAL	T6	0,859	0,1	3	4,946	0,0268	BC
		Ro2	5,925	2,2	3			A
		V1	6,472	0,6	3			A
		LM2	3,876	0,6	4			AB
ACC	neuSAL	T6	0,647	0,1	3	1,572	0,2795	A
		Ro2	1,422	1,2	2			A
		V1	5,697	0,9	4			A
		LM2	1,314	1,7	2			A
	alkSAL	T6	1,339	0,5	4	3,788	0,0474	A
		Ro2	8,072	2,6	4			AB
		V1	4,91	1,0	3			AB
		LM2	3,876	0,6	4			B
ABA	neuSAL	T6	2,864	0,6	3	2,5890	0,1175	A
		Ro2	1,785	0,4	3			A
		V1	4,215	0,2	4			A
		LM2	2,751	1,2	3			A
	alkSAL	T6	1,253	0,3	4	17,636	0,00020	B
		Ro2	1,15	0,1	4			B
		V1	3,858	0,3	4			A
		LM2	3,296	0,6	3			A
JA	neuSAL	T6	0,364	0,1	3	0,502	0,6905	A
		Ro2	0,707	0,5	3			A
		V1	1,062	0,5	4			A
		LM2	0,633	0,4	3			A
	alkSAL	T6	4,051	0,8	4	2,784	0,09600	A
		Ro2	1,571	0,2	4			A
		V1	2,433	0,2	2			A
		LM2	3	0,7	4			A
BAP	neuSAL	T6	6,995	5,0	2	1,384	0,3495	A
		Ro2	5,246	1,9	2			A
		V1	2,225	0,4	2			A
		LM2	1,223	0,5	3			A
	alkSAL	T6	14,939	7,3	3	7,295	0,01470	AB
		Ro2	33,672	6,2	3			A
		V1	5,761	0,4	3			B
		LM2	1	0,3	2			B
KA	neuSAL	T6	18,347	8,0	3	5,396	0,0212	A
		Ro2	16,812	5,2	3			A
		V1	0,284	0,0	4			B
		LM2	0,135	0,0	3			B
	alkSAL	T6	5,954	1,8	3	2,779	0,1205	A
		Ro2	5,365	3,3	3			A
		V1	0,809	0,3	3			A
		LM2	1	0,2	4			A
SA	neuSAL	T6	0,168	0,1	3	1,246	0,3632	A
		Ro2	0,834	0,2	2			A
		V1	0,65	0,1	3			A
		LM2	0,858	0,5	3			A
	alkSAL	T6	0,264	0,1	4	6,186	0,0088	B
		Ro2	0,894	0,1	4			AB
		V1	0,64	0,1	4			AB
		LM2	1	0,3	4			A

Table S2.6. Principal Component Analysis (PCA) of 19 plant traits in the 4 studied demes under control, *neuSAL* and *alkSAL* conditions. The table shows the loadings and variance associated with each principal component with eigenvalues over 1.

PC	Value	Percentage	Acc. Percentage	Sq Ji	df	Prob > Sq Ji
1	4,75	24,99	24,99	303,06	169,07	1,13551E-09
2	4,35	22,88	47,87	228,89	159,08	0,000241077
3	2,33	12,24	60,11	137,18	148,43	0,736223118
4	1,71	8,99	69,10	87,78	134,55	0,999379068
5	1,24	6,52	75,62	49,03	120,53	0,999999999
6	0,99	5,23	80,86	20,96	106,42	1

Table S2.7. *onlySAL* (top) and *onlyALKSAL* (bottom) up-regulated transcripts enriched in ribosome biogenesis, anthocyanin biosynthesis and glutathione metabolism pathways. Mean \pm Standard Error (*Std Err*), ANOVA (*F value*; *Prob > F*) and Tukey test from DEGs normalized expression among demes. Mean normalized expression levels [$\log_2(\text{FC})$] of all DEGs belonging to each pathway as a pool are shown. *neuSAL*: Hoagland $\frac{1}{2}$ NaCl 25-50-100 mM pH 5.9. *alkSAL*: Hoagland $\frac{1}{2}$ NaCl 20 - 40- 85 mM + NaHCO_3 5 - 10 - 15 mM pH 8.3.

Pathway KEGG	Subset	Deme	Mean	StdErr	N	F value	Prob. > F	Tukey test
Ribosome Biogenesis	onlySAL	T6	2,23	0,09	6	6,15	0,0039	A
		Ro2	1,67	0,15	6			B
		V1	2,27	0,11	6			A
		LM2	2,42	0,17	6			A
Pathway KEGG	Subset	Deme	Mean	StdErr	N	F value	Prob. > F	Tukey test
Anthocyanin biosynthesis	onlySAL	T6	2,94	0,13	2	175,57	0,0001	B
		Ro2	2,11	0,15	2			C
		V1	2,69	0,09	2			BC
		LM2	5,53	0,06	2			A
Pathway KEGG	Treatment	Mean	StdErr	N	F value	Prob. > F	Student t -Test	
Glutathione metabolism	neuSAL	1,74	0,22	72	72,77	<0,0001	B	
	alkSAL	4,94	0,30	72			A	

Table S2.8. *onlySAL* down-regulated transcripts enriched in glucosinolate biosynthesis and phytohormone signaling pathways. Mean \pm Standard Error (*Std Err*), ANOVA (*F value*; *Prob > F*) and Tukey test from DEGs normalized expression among demes. Mean normalized expression levels [$\log_2(\text{FC})$] of all DEGs belonging to each pathway as a pool are shown. *Sal*: Hoagland $\frac{1}{2}$ NaCl 25-50-100 mM pH 5.9. *AlkSal* : Hoagland $\frac{1}{2}$ NaCl 20 - 40- 85 mM + NaHCO_3 5 - 10 - 15 mM pH 8.3.

Pathway KEGG	Subset	Deme	Mean	StdErr	N	F value	Prob. > F	Tukey test
Glucosinolates	<i>onlySAL</i>	T6	-3,05	0,18	3	12,42	0,0022	B
		Ro2	-3,95	0,26	3			B
		V1	-3,21	0,12	3			B
		LM2	0,11	0,97	3			A
Pathway KEGG	Subset	Deme	Mean	StdErr	N	F value	Prob. > F	Tukey test
Phytohormones	<i>onlySAL</i>	T6	-3,41	0,46	10	1,14	0,3452	A
		Ro2	-3,69	0,60	10			A
		V1	-2,39	0,53	10			A
		LM2	-3,23	0,49	10			A

Table S2.9. *onlyALKSAL* down-regulated transcripts enriched in photosynthesis, starch & sucrose metabolism, porphyrin & chlorophyll metabolism and amino acid biosynthesis pathways. Mean \pm Standard Error (*Std Err*), ANOVA (*F value*; *Prob > F*) and Tukey test from DEGs normalized expression among demes. Mean normalized expression levels [$\log_2(\text{FC})$] of all DEGs belonging to each pathway as a pool are shown. *neuSAL*: Hoagland 1/2 NaCl 25-50-100 mM pH 5.9. *alkSAL*: Hoagland 1/2 NaCl 20 - 40- 85 mM + NaHCO₃ 5 - 10 - 15 mM pH 8.3.

Pathway KEGG	Subset	Deme	Mean	StdErr	N	F value	Prob. > F	Tukey test
Photosynthesis	<i>onlyALKSAL</i>	T6	-3,70	0,19	11	13,95	<0,0001	C
		Ro2	-3,35	0,19	11			BC
		V1	-2,99	0,14	11			B
		LM2	-2,30	0,12	11			A
Pathway KEGG	Subset	Deme	Mean	StdErr	N	F value	Prob. > F	Tukey test
Starch & sucrose metabolism	<i>onlyALKSAL</i>	T6	-4,71	0,40	21	12,29	<0,0001	C
		Ro2	-4,09	0,26	21			BC
		V1	-3,34	0,16	21			AB
		LM2	-2,56	0,18	21			A
Pathway KEGG	Subset	Deme	Mean	StdErr	N	F value	Prob. > F	Tukey test
Porphyrin & chlorophyll metabolism	<i>onlyALKSAL</i>	T6	-3,94	0,21	10	14,27	<0,0001	C
		Ro2	-3,32	0,26	10			BC
		V1	-2,98	0,16	10			B
		LM2	-2,15	0,14	10			A
Pathway KEGG	Subset	Deme	Mean	StdErr	N	F value	Prob. > F	Tukey test
AA Biosynthesis	<i>onlyALKSAL</i>	T6	-4,00	0,22	27	15,26	<0,0001	B
		Ro2	-3,83	0,24	27			B
		V1	-2,74	0,11	27			A
		LM2	-2,42	0,21	27			A

Table S2.10. *coreSAL*, *onlySAL* and *onlyALKSAL* DEGs involved in the phytohormone signaling pathway. Mean \pm Standard Error (*Std Err*), ANOVA (*F value*; *Prob > F*) and Tukey test from DEGs normalized expression among demes and treatments. Mean normalized expression levels [$\log_2(\text{FC})$] of all DEGs belonging to each pathway as a pool are shown. *Sal*: Hoagland $\frac{1}{2}$ NaCl 25-50-100 mM pH 5.9. *AlkSal* : Hoagland $\frac{1}{2}$ NaCl 20 - 40- 85 mM + NaHCO_3 5 - 10 - 15 mM pH 8.3.

DEG subset	Treatment	Mean	StdErr	N	F value	Prob. > F	Student t-Test
SAURs	<i>neuSAL</i>	-4,01	0,19	70	39,45	< 0,0001	A
	<i>alkSAL</i>	-5,95	0,25	69			B
ERFs	<i>neuSAL</i>	-2,86	0,38	12	49,20	< 0,0001	A
	<i>alkSAL</i>	1,56	0,50	12			B
DREBs	<i>neuSAL</i>	3,87	0,45	24	17,86	0,0001	B
	<i>alkSAL</i>	7,53	0,74	24			A
PYL/PYRs	<i>neuSAL</i>	-0,57	0,73	13	5,92	0,0204	B
	<i>alkSAL</i>	1,76	0,59	23			A
ABIs	<i>neuSAL</i>	0,47	0,41	14	26,22	< 0,0001	B
	<i>alkSAL</i>	3,11	0,32	16			A
PP2Cs	<i>neuSAL</i>	0,21	0,31	8	38,53	< 0,0001	B
	<i>alkSAL</i>	4,19	0,56	8			A
LOXs & MYCs	<i>neuSAL</i>	-1,94	0,23	20	20,49	< 0,0001	A
	<i>alkSAL</i>	-3,76	0,33	20			B
JAZs	<i>neuSAL</i>	-1,56	1,07	8	13,07	0,0028	B
	<i>alkSAL</i>	2,81	0,56	8			A
CRFs & AHPs	<i>neuSAL</i>	1,51	0,18	23	20,44	< 0,0001	B
	<i>alkSAL</i>	2,96	0,27	22			A
WRKYs	<i>neuSAL</i>	0,91	0,24	86	126,07	< 0,0001	B
	<i>alkSAL</i>	4,84	0,26	88			A
DELLAs	<i>neuSAL</i>	-0,71	0,32	16	11,35	0,0021	A
	<i>alkSAL</i>	-2,22	0,32	16			B

Table S2.11. coreSAL up-regulated transcripts enriched in Ribosome Biogenesis.

Mean \pm Standard Error (Std Err), ANOVA (*F* value; *Prob* > *F*) and Tukey test from DEGs normalized expression among demes and treatments. Mean normalized expression levels [(log2FC)] of all DEGs belonging to each pathway as a pool are shown. *neuSAL*: Hoagland ½ NaCl 25-50-100 mM pH 5.9. *alkSAL*: Hoagland ½ NaCl 20 - 40- 85 mM + NaHCO₃ 5 - 10 - 15 mM pH 8.3.

KEGG Pathway	Treatment	Deme	Mean	StdErr	N	F value	Prob. > F	Tukey test
Ribosome Biogenesis	<i>neuSAL</i>	T6	2,63	0,11	7	14,89	< 0,0001	A
	<i>neuSAL</i>	Ro2	1,52	0,17	7			A
	<i>neuSAL</i>	V1	2,68	0,16	7			A
	<i>neuSAL</i>	LM2	2,29	0,11	6			B
	<i>alkSAL</i>	T6	2,79	0,11	7	3,46	0,033	A
	<i>alkSAL</i>	Ro2	2,25	0,18	7			B
	<i>alkSAL</i>	V1	2,57	0,13	7			AB
	<i>alkSAL</i>	LM2	2,76	0,06	6			AB

KEGG Pathway	Deme	Treatment	F value	Prob. > F	Student t -Test
Ribosome Biogenesis	T6	<i>neuSAL</i>	8,95	0,01	A
		<i>alkSAL</i>			A
	RO2	<i>neuSAL</i>	1,10	0,32	A
		<i>alkSAL</i>			B
	V1	<i>neuSAL</i>	0,27	0,61	A
		<i>alkSAL</i>			A
	LM2	<i>neuSAL</i>	13,55	0,00	A
		<i>alkSAL</i>			B

Table S2.12. *coreSAL* up-regulated transcripts enriched in Protein Synthesis in ER. Mean \pm Standard Error (*Std Err*), ANOVA (*F value*; *Prob > F*) and Tukey test from DEGs normalized expression among deme origin location and treatments. Mean normalized expression levels [$\log_2(\text{FC})$] of all DEGs belonging to each pathway as a pool are shown. *neuSAL*: Hoagland $\frac{1}{2}$ NaCl 25-50-100 mM pH 5.9. *alkSAL*: Hoagland $\frac{1}{2}$ NaCl 20 - 40- 85 mM + NaHCO_3 5 - 10 - 15 mM pH 8.3.

Pathway KEGG	Treatment	Origin	Mean	StdErr	N	F value	Prob. > F	Student t -Test
Protein Synthesis in ER	<i>neuSAL</i>	Coastal	8,17	1,29	4	3,04	0,13	A
	<i>neuSAL</i>	Inland	10,53	0,43	4			A
	<i>alkSAL</i>	Coastal	5,43	0,77	4	8,14	0,03	B
	<i>alkSAL</i>	Inland	8,31	0,65	4			A

Pathway KEGG	Origin	Treatment	F value	Prob. > F	Student t -Test
Protein Synthesis in ER	Coastal	<i>neuSAL</i>	3,32	0,12	A
		<i>alkSAL</i>			A
	Inland	<i>neuSAL</i>	8,08	0,03	B
		<i>alkSAL</i>			A

Table S2.13. *coreSAL* up-regulated transcripts enriched in Cutin, suberin & wax biosynthesis. Mean \pm Standard Error (*Std Err*), ANOVA (*F value*; *Prob > F*) and Tukey test from DEGs normalized expression among deme origin location and treatments. Mean normalized expression levels [$\log_2(\text{FC})$] of all DEGs belonging to each pathway as a pool are shown. *neuSAL*: Hoagland $\frac{1}{2}$ NaCl 25-50-100 mM pH 5.9. *alkSAL*: Hoagland $\frac{1}{2}$ NaCl 20 - 40- 85 mM + NaHCO_3 5 - 10 - 15 mM pH 8.3.

Pathway KEGG	Origin	Treatment	Mean	StdErr	N	F value	Prob. > F	Student t -Test
Cutin, suberin & wax biosynth.	<i>neuSAL</i>	Coastal	4,93	1,25	4	2,44	0,17	a
		Inland	4,02	0,89	4			a
	<i>alkSAL</i>	Coastal	4,33	1,76	4	0,72	0,43	A
		Inland	4,98	1,82	4			A

Table S2.14. coreSAL enriched pathways with down-regulated transcripts. Mean \pm Standard Error (Std Err), ANOVA (*F value*; *Prob > F*) and Tukey test from DEGs normalized expression among demes and treatments. Mean normalized expression levels [$\log_2(\text{FC})$] of all DEGs belonging to each pathway as a pool are shown. *neuSAL*: Hoagland $\frac{1}{2}$ NaCl 25-50-100 mM pH 5.9. *alkSAL*: Hoagland $\frac{1}{2}$ NaCl 20 - 40- 85 mM + NaHCO_3 5 - 10 - 15 mM pH 8.3.

Pathway KEGG	Treatment	Deme	Mean	StdErr	N	F value	Prob. > F	Tukey test
Photosynthesis	<i>neuSAL</i>	T6	-3,38	0,18	2	6,49	0,0503	B
	<i>neuSAL</i>	Ro2	-2,08	0,07	2			A
	<i>neuSAL</i>	V1	-2,94	0,29	2			AB
	<i>neuSAL</i>	LM2	-2,48	0,27	2			AB
	<i>alkSAL</i>	T6	-7,34	0,44	2	14,88	0,0123	B
	<i>alkSAL</i>	Ro2	-5,33	0,12	2			AB
	<i>alkSAL</i>	V1	-4,28	0,60	2			A
	<i>alkSAL</i>	LM2	-3,83	0,31	2			A

Pathway KEGG	Treatment	Deme	Mean	StdErr	N	F value	Prob. > F	Tukey test
Photosynthesis Antenna Proteins	<i>neuSAL</i>	T6	-4,88	0,71	6	5,76	0,0052	AB
	<i>neuSAL</i>	Ro2	-2,57	0,27	6			A
	<i>neuSAL</i>	V1	-6,56	1,03	6			B
	<i>neuSAL</i>	LM2	-2,65	0,22	6			A
	<i>alkSAL</i>	T6	-9,44	0,82	6	17,05	< 0.0001	B
	<i>alkSAL</i>	Ro2	-5,08	0,66	6			A
	<i>alkSAL</i>	V1	-5,88	0,24	6			A
	<i>alkSAL</i>	LM2	-4,15	0,29	6			A

Pathway KEGG	Treatment	Deme	Mean	StdErr	N	F value	Prob. > F	Tukey test
Glucosinolate biosynthesis	<i>neuSAL</i>	T6	-3,31	0,20	9	4,14	0,0138	B
	<i>neuSAL</i>	Ro2	-3,46	0,22	9			AB
	<i>neuSAL</i>	V1	-2,87	0,22	9			A
	<i>neuSAL</i>	LM2	-2,55	0,17	9			A
	<i>alkSAL</i>	T6	-7,50	0,96	9	10,01	< 0.0001	B
	<i>alkSAL</i>	Ro2	-8,13	0,77	9			B
	<i>alkSAL</i>	V1	-4,26	0,24	9			A
	<i>alkSAL</i>	LM2	-4,46	0,27	9			A

Table S2.14. Continuation...

Pathway KEGG	Treatment	Deme	Mean	StdErr	N	F value	Prob. > F	Tukey test
Carbon Fixation	<i>neuSAL</i>	T6	-7,21	1,48	2	0,10	0,9556	A
	<i>neuSAL</i>	Ro2	-7,40	1,01	2			A
	<i>neuSAL</i>	V1	-6,55	1,37	2			A
	<i>neuSAL</i>	LM2	-6,98	0,48	2			A
	<i>alkSAL</i>	T6	-11,13	1,27	2	4,15	0,1015	A
	<i>alkSAL</i>	Ro2	-6,66	1,24	2			A
	<i>alkSAL</i>	V1	-6,81	0,62	2			A
	<i>alkSAL</i>	LM2	-5,93	1,36	2			A

Pathway KEGG	Treatment	Deme	Mean	StdErr	N	F value	Prob. > F	Tukey test
Carbon Metabolism	<i>neuSAL</i>	T6	-3,30	0,27	3	2,43	0,1400	A
	<i>neuSAL</i>	Ro2	-2,53	0,33	3			A
	<i>neuSAL</i>	V1	-2,53	0,24	3			A
	<i>neuSAL</i>	LM2	-2,49	0,13	3			A
	<i>alkSAL</i>	T6	-5,31	0,12	3	8,27	0,0078	BC
	<i>alkSAL</i>	Ro2	-5,93	0,77	3			C
	<i>alkSAL</i>	V1	-3,32	0,34	3			A
	<i>alkSAL</i>	LM2	-3,75	0,13	3			AB

Pathway KEGG	Origin	Treatment	Mean	StdErr	N	F value	Prob. > F	Student t -Test
Glioxylylate & Decarboxylate Metabolism	<i>neuSAL</i>	Coastal	-3,10	0,31	6	0,03	0,87	A
		Inland	-3,02	0,38	6			A
	<i>alkSAL</i>	Coastal	-6,10	0,58	6	5,36	0,04	A
		Inland	-4,42	0,44	6			B

Pathway KEGG	Treatment	Deme	Mean	StdErr	N	F value	Prob. > F	Tukey test
Nitrogen Metabolism	<i>neuSAL</i>	T6	-7,70	0,82	2	1,00	0,48	A
	<i>neuSAL</i>	Ro2	-6,14	1,21	2			A
	<i>neuSAL</i>	V1	-5,23	1,75	2			A
	<i>neuSAL</i>	LM2	-5,29	0,39	2			A
	<i>alkSAL</i>	T6	-11,19	1,19	2	4,32	0,10	A
	<i>alkSAL</i>	Ro2	-8,03	1,62	2			A
	<i>alkSAL</i>	V1	-6,63	0,12	2			A
	<i>alkSAL</i>	LM2	-6,80	0,32	2			A

Table S2.15. List of SNPs in contrasted coreSAL DEGs. Gene symbol, TAIR Id, genomic region, variant type, codon or AA change, genomic position and studied deme containing each detected SNP. SNPs causing missense variants are highlighted in blue.

Gene	Id	Region	Type	Codon	AA change	Ps	Deme
BGAL4	AT5G56870	Intron				23005270	V1
BGAL4	AT5G56870	Intron				23005292	V1
BGAL4	AT5G56870	Intron				23005461	V1
BGAL4	AT5G56870	Intron				23005469	V1
BGAL4	AT5G56870	Intron				23005489	V1
BGAL4	AT5G56870	Intron				23005501	V1
BGAL4	AT5G56870	Exon	Synon	ccG/ccC	p.Pro196Pro/c.588G>C	23005576	V1
BGAL4	AT5G56870	Intron				23005962	LM2
BGAL4	AT5G56870	Exon	Synon	acC/acT	p.Thr353Thr/c.1059C>T	23006666	LM2
BGAL4	AT5G56870	Exon	Missense	tCa/tTa	p.Ser437Leu/c.1310C>T	23007091	LM2
BGAL4	AT5G56870	Intron				23007638	T6
BGAL4	AT5G56870	Intron					
BGAL4	AT5G56870	Intron					
BGAL4	AT5G56870	3' UTR	nd	nd	nd	23009626	V1
BGAL4	AT5G56870	3' UTR		427		23009076	LM2
BGAL4	AT5G56870	Promoter		288		23003907	T6, Ro2

Table S2.15. Continuation...

DIN10	AT5G20250	Exon	Missense	Tct/Gct	p.Ser602Ala/c.1804T>G	6835822	V1
DIN10	AT5G20250	Exon	Missense	Tct/Gct	p.Ser507Ala/c.1519T>G		
DIN10	AT5G20250	Exon	Missense	Tct/Gct	p.Ser507Ala/c.1519T>G		
DIN10	AT5G20250	Exon	Missense	Tct/Gct	p.Ser507Ala/c.1519T>G		
DIN10	AT5G20250	Exon	Missense	Act/Tct	p.Thr656Ser/c.1966A>T	6836066	Ro2
DIN10	AT5G20250	Exon	Missense	Act/Tct	p.Thr561Ser/c.1681A>T		
DIN10	AT5G20250	Exon	Missense	Act/Tct	p.Thr561Ser/c.1681A>T		
DIN10	AT5G20250	Exon	Missense	Act/Tct	p.Thr561Ser/c.1681A>T		
DIN10	AT5G20250	Exon	Missense	Ata/Tta	p.Ile698Leu/c.2092A>T	6836192	V1
DIN10	AT5G20250	Exon	Missense	Ata/Tta	p.Ile603Leu/c.1807A>T		
DIN10	AT5G20250	Exon	Missense	Ata/Tta	p.Ile603Leu/c.1807A>T		
DIN10	AT5G20250	Exon	Missense	Ata/Tta	p.Ile603Leu/c.1807A>T		
DIN10	AT5G20250	Exon	Synon	tgT/kgC	p.Cys712Cys/c.2136T>C	6836236	V1
DIN10	AT5G20250	Exon	Synon	tgT/kgC	p.Cys617Cys/c.1851T>C		
DIN10	AT5G20250	Exon	Synon	tgT/kgC	p.Cys617Cys/c.1851T>C		
DIN10	AT5G20250	Exon	Synon	tgT/kgC	p.Cys617Cys/c.1851T>C		
DIN10	AT5G20250	3' UTR		76	c.*76T>G	6836711	Ro2
DIN10	AT5G20250	3' UTR		76	c.*76T>G		
DIN10	AT5G20250	3' UTR		76	c.*76T>G		
DIN10	AT5G20250	3' UTR		76	c.*76T>G		
DIN10	AT5G20250	3' UTR		86	c.*86T>G	6836721	V1
DIN10	AT5G20250	3' UTR		86	c.*86T>G		
DIN10	AT5G20250	3' UTR		86	c.*86T>G		
DIN10	AT5G20250	3' UTR		86	c.*86T>G		
SEN1	AT4G35770	3' UTR		318	c.*318C>T	16946158	V1
SEN1	AT4G35770	3' UTR		194	c.*194C>T		
SEN1	AT4G35770	3' UTR		175	c.*175C>T		

Table S2.16. Overlapping between co-expression module genes and previous DEG subsets analyses. Module, KEGG enriched pathway, total DEGs comprised in each pathway and heatmap table of distribution of total DEGs per pathway into *coreSAL*, *onlySAL* or *onlyALKSAL* DEG subset. The two last columns classify total DEGs into categorized (Categorized = *coreSAL* + *onlySAL* + *onlyALKSAL* DEGs; Uncategorized = DEGs not previously identified). Color-scale shows overlapping degree between total module DEGs and each DEG subset (green: high; yellow: low).

Module	Pathway	Total DEGs	<i>coreSAL</i>	<i>onlySAL</i>	<i>onlyALKSAL</i>	Categorized	Uncategorized
Blue	Photosynthesis & Antenna	58	43	0	15	58	0
	Carbon fixation & metabolism	63	24	4	13	41	26
	Glyoxylate & dicarboxylate	27	17	1	5	23	5
	Porphyrin & chlorophyll	21	5	0	8	13	8
	Glycine & serine metabolism	20	10	0	2	12	8
	Other glycan metabolism	8	0	1	5	6	3
	Phytohormone signaling	46	13	3	14	30	19
	DNA replication	13	0	0	0	0	13
	Tyrosine metab	11	3	0	3	6	5
	Pentose phosphate	14	4	2	3	9	7
	Total	224	91	8	59	150	74
Darkgrey	Glucosinolates biosynthesis	13	8	0	4	12	1
	2-oxocarboxylic acid metabolism	13	9	0	3	12	1
	alpha-Linoleic acid metabolism	10	2	1	2	4	6
	Phytohormone signaling	21	3	2	3	6	15
	Carotenoid biosynthesis	6	1	0	2	3	3
	Total	63	23	3	14	37	26
plum1	Total	43	19	3	10	32	11

Table S2.17. PPI Network and Enrichment analysis. Enrichment of functional connections among the introduced set of DEGs from WGCNA, and statistical enrichments detected in the co-expression modules.

Module	Nodes	Edges	Avr node degree	Avr local cluster coef.	Expected edges	PPI Enrichment <i>p</i> -value
Blue	1218	8381	13,80	0,331	3013	< 1.0e-16
Darkgrey	645	1468	4,55	0,371	428	< 1.0e-16
plum1	43	7	0,33	0,256	1	0,000397

Chapter 3

Table S3.1. Student *t*-Test for growth and leaf mineral nutrition traits comparing HD (highest) and LD (lowest) growth groups in the study accessions. Leaf mineral nutrients are expressed as $\mu\text{g g}^{-1}$ DW.

Trait	Group	Mean	St Error	N	F Value	Prob > F
Diameter (cm)	HD	6,20	0,13	25	534,31	< .0001
	LD	1,90	0,13	27		
Fe	HD	188,70	38,65	25	8,17	0,0065
	LD	352,16	42,16	24		
Ca	HD	36690,36	1381,60	25	7,61	0,0083
	LD	31301,12	1381,60	27		
Mg	HD	4149,90	133,41	25	0,03	0,8721
	LD	4179,61	175,44	27		
K	HD	30869,78	1617,79	25	0,02	0,8959
	LD	30115,54	1947,36	27		
Na	HD	3504,90	560,44	25	6,69	0,0129
	LD	1835,80	210,51	27		
S	HD	6000,40	303,58	25	11,53	0,0014
	LD	4284,09	384,27	27		
Mn	HD	125,61	7,63	25	0,32	0,5799
	LD	134,37	8,52	27		

Table S3.1. Continuation...

P	HD	6289,17	486,02	25	0,067	0,04164
	LD	5717,63	316,30	27		
Zn	HD	73,14	6,48	25	4,25	0,0449
	LD	92,67	6,20	27		
Mo	HD	40,84	6,89	20	16,35	0,0003
	LD	81,93	7,47	21		
Na:K	HD	0,12	0,02	25	8,98	0,0042
	LD	0,06	0,00	27		
Na:Ca	HD	0,11	0,02	25	7,37	0,0091
	LD	0,06	0,01	27		
Mg:Ca	HD	0,12	0,00	23	10,67	0,002
	LD	0,13	0,01	27		
Fe:Mn	HD	1,69	0,19	25	6,85	0,0117
	LD	2,44	0,22	27		
Fe:Zn	HD	3,00	0,56	25	8,22	0,0061
	LD	6,02	0,91	27		
S:Fe	HD	56,79	11,32	25	5,13	0,028
	LD	33,07	10,10	27		

Table S3.2. Primer list for transcript quantification of target genes. Specific primers were designed for *A. thaliana* using NCBI Primer Blast tool.

Gene	Name	qPCR primers
<i>PGP10</i>	Forward-1	AGTCTCCCTCGAACCAACTC
	Reverse-1	GAGCCATCAGAACGCAATCG
<i>YUC8</i>	Forward-1	ACGGGAGAAAATGCGGAGAG
	Reverse-1	GACCATGGAAGGCTTAGCGA
<i>ALA3</i>	Forward-1	AACAAATACCCCTGCCTCGG
	Reverse-1	TGACGCTGAGCGATTCTTT
<i>NINJA</i>	Forward-1	GCACAAGATACACATGGACGA
	Reverse-1	CTAGAGCTTCTTCGCAGCGT
<i>HKT1</i>	Forward-1	CCTCGGTGGCGAAATCTTCA
	Reverse-1	TCTCAACGTCACAGCGATCC
<i>SOS1</i>	Forward-1	GCAACTCAGCATTTTCGGCA
	Reverse-1	CGAGACCTTGAGCTGGGTTT
<i>FRO2</i>	Forward-1	AGTGCGGCTATGTTGTGGAA
	Reverse-1	GAGATGGACGGTCGACGTTT
<i>IRT1</i>	Forward-1	TGGGTCTTGGCGGTTGTATC
	Reverse-1	TCCAGCGGAGCATGCATTTA
<i>ACT</i>	Forward-1	TCGCTGACCGTATGAGCAAA
	Reverse-1	TTGGAGATCCACATCTGCTG

Table S3.3. List for significant associations and corresponding QTLs detected by GWA mapping of Na and Fe concentration parameters of plants grown on saline-calcareous study soil. SNPs that were strongly associated [-log (p-value)> 6.42] with at least one trait and SNPs included in LD region are displayed in blue and black, respectively. QTL, quantitative trait locus; Chr, chromosome; Score, [-log (p-value)]; MAF, minor allele frequency.

Trait	QTL	Gene	Chr	Ps	Score	MAF	p-value	Symbol	Description
Na	1a	AT1G10680	1	3538341				PGP10	
	1a	AT1G10690	1	3549920				SMR8	
	1a	<i>Intergenic</i>	1	3552105	6,648	0,07	2,25E-07		
	1a	AT1G10700	1	3554104				PRS3	P-independent phosphoribosyl pyrophosphate (PRPP) synthase
Na	1b	AT1G10710	1	3558358					
	1b	<i>AT1G10720</i>	1	3562288	9,51	0,08	3,08E-10	PHS1	<i>BSD domain-containing protein</i>
	1b	AT1G10720	1	3562841				PHS1	
	1b	AT1G10730	1	3565257				AP1M1	Claithrin adaptor complexes medium subunit family protein
	1b	AT1G10740	1	3568112					Alpha/beta-Hydrolases superfamily protein
	1b	AT1G10750	1	3574807					Carboxyl-terminal peptidase
Na	2	AT4G28850	4	14244290				ATXTH26	Xyloglucan endotransglucosylase/hydrolase 26
	2	AT4G28860	4	14246260				CKL4	Member of CASEIN KINASE I-LIKE gene family (CKL-A group)
	2	AT4G28880	4	14251135				CKL3	Member of CASEIN KINASE I-LIKE gene family (CKL-A group)
	2	AT4G28890	4	14256243				ATL42	RING/U-box superfamily protein
	2	<i>AT4G28890</i>	4	14258447	7,56	0,095	2,77E-08	ATL42	<i>RING/U-box superfamily protein</i>
	2	AT4G28900	4	14259141					Transposable element
	2	AT4G28910	4	14264330				NINJA	Repressor in the jasmonic acid (JA) signalling

Table S3.3. Continuation...

	3	AT1G59800	1	22004964					Cullin family protein;(source:Araport11)
	3	AT1G59810	1	22008507					AGL50 MADS box gene
Fe	3	Intergenic	1	22010370	6,48	0,128	3,24E-07	AGL50	
	3	AT1G59820	1	22011305				ALA3	Phospholipid translocase. Involved in secretory vesicle formation from trans-Golgi at the root tip. Mutants have short primary roots and grow slower.
	3	AT1G59830	1	22020377				PP2A-1	Isoform of the catalytic subunit of protein phosphatase 2A
	4	AT4G28720	4	14192569				YUC8	Auxin biosynthetic gene
Na	4	AT4G28730	4	14199043				GRXC5	The monomeric apoprotein mediates the recycling of plastidial methionine sulfoxide reductase B1 and peroxiredoxin IIE; The dimeric holoprotein incorporates a [2Fe-2S] cluster
	4	AT4G28740	4	14200908					
	4	AT4G28750	4	14202758				PSAE-1	Photosystem I Reaction Centre Subunit IV Protein
	4	AT4G28750	4	14203417	5,56	0,061	2,78E-06	PSAE-1	

Table S3.4. List for candidate gene T-DNA insertion mutant lines for leaf Na (LNa) and leaf Fe (LFe) phenotyping. Leaf Na and Fe concentrations and rosette diameter (RD) from plants grown on saline-calcareous soil (SCS) for 8 weeks (n = up to 6 plants per genotype).

Phenotype	Locus	Name	$\mu\text{g Na g PF}^{-1}$	$\mu\text{g Fe g PF}^{-1}$	RD (cm)
LNa	AT1G10680	<i>pgp10</i>	4587,51	121,03	4,5
LNa		<i>pgp10</i>	n.d.	69,69	6,5
LNa		<i>pgp10</i>	4324,95	96,49	6,4
LNa		<i>pgp10</i>	4015,16	174,88	9,0
LNa		<i>prs3</i>	2443,02	70,50	6,5
LNa		<i>prs3</i>	n.d.	272,90	4,5
LNa		<i>prs3</i>	2403,52	68,64	4,0
LNa		<i>prs3</i>	2039,42	220,92	5,0
LNa	AT1G10710	<i>phs1</i>	n.d.	26,94	6,0
LNa		<i>phs1</i>	n.d.	16,30	9,5
LNa		<i>phs1</i>	1764,96	35,91	8,5
LNa		<i>SALK_202645</i>	3495,23	58,56	3,8
LNa		<i>SALK_202645</i>	1642,67	35,61	6,3
LNa		<i>yuc8</i>	4329,06	69,53	4,5
LNa		<i>yuc8</i>	n.d.	46,15	6,0
LNa		<i>yuc8</i>	3363,99	50,06	4,0
LNa	AT4G28720	<i>yuc8</i>	3846,99	97,30	5,0
LNa		<i>grxc5</i>	3007,00	27,52	5,0
LNa		<i>grxc5</i>	2915,00	41,84	5,0
LNa		<i>grxc5</i>	n.d.	n.d.	4,5
LNa		<i>SALK_124390C</i>	n.d.	45,17	2,3
LNa		<i>SALK_124390C</i>	2827,19	81,61	3,1
LNa		<i>SALK_124390C</i>	1910,43	136,65	4,3
LNa		<i>SALK_124390C</i>	3302,87	47,75	4,3
LNa	AT4G28860	<i>ckl4</i>	1956,30	37,22	5,6
LNa		<i>ckl4</i>	1640,73	20,58	6,7
LNa		<i>ninja</i>	3631,34	21,06	4,5
LNa		<i>ninja</i>	3418,28	9,84	3,5
LNa		<i>ninja</i>	6103,98	8,82	NA

Table S3.4. Continuation...

LFe		<i>SAIL_1281_F11</i>	1481,27	106,02	3,0
LFe	AT1G59800	<i>SAIL_1281_F11</i>	1962,94	142,83	4,1
LFe		<i>SAIL_1281_F11</i>	3063,76	38,12	5,2
LFe		<i>SAIL_1281_F11</i>	2445,63	63,91	5,5
LFe		<i>ala3</i>	2764,52	161,94	4,0
LFe	AT1G59820	<i>ala3</i>	1565,98	86,14	4,0
LFe		<i>ala3</i>	755,78	167,42	2,0
LFe		<i>ala3</i>	1612,15	134,60	4,0
LFe		<i>pp2A-1</i>	1563,82	77,69	3,0
LFe		<i>pp2A-1</i>	1582,00	86,06	2,8
LFe	AT1G59830	<i>pp2A-1</i>	2553,32	39,00	3,4
LFe		<i>pp2A-1</i>	837,20	19,93	5,5
LFe		<i>pp2A-1</i>	2520,93	80,39	6,3
LFe		<i>pp2A-1</i>	2419,62	101,82	NA
WT		Col-0	1434,35	44,22	9,5
WT		Col-0	1643,70	28,83	9,0
WT		Col-0	1926,56	62,09	10,0
WT		Col-0	n.d.	111,88	7,0
WT		Col-0	3085,04	57,51	10,0
WT		Col-0	n.d.	97,01	10,0
WT		Col-0	NA	NA	8,0
WT		Col-0	NA	NA	10,0

Table S3.5 Dunnet's test results for leaf Na and Fe quantification in T-DNA insertion mutants of the pinpointed candidate genes.

Element	Line	Mean	Std Err	N	Dunnet's p value
$\mu\text{g Na/gPF}$	<i>pgp10</i>	4309,20	16,93	4	0,005
	<i>prs3</i>	2295,32	14,92	4	1,000
	<i>phs1</i>	1764,96	n.d.	1	1,000
	SALK_069095.55.25	2303,31	27,00	3	1,000
	SALK_202645	2315,88	30,85	4	1,000
	<i>yuc8</i>	3846,68	21,97	4	0,036
	<i>grxc5</i>	2961,00	8,07	3	0,401
	SALK_124390C	2680,16	26,60	4	0,933
	<i>ckl4</i>	1798,51	14,94	2	1,000
	<i>ninja</i>	4384,53	38,64	3	0,003
	SAIL_1281_F11	2238,40	26,01	4	1,000
	Col-0	2022,41	27,14	3	Control
$\mu\text{g Fe/gPF}$	<i>ala3</i>	137,53	6,09	4	0,011
	<i>pp2A-1</i>	67,48	5,59	4	1,000
	Col-0	66,92	5,62	3	Control
RD (cm)	<i>pgp10</i>	6,60	1,36	4	0,0051
	<i>yuc8</i>	4,88	0,92	4	<,0001
	<i>ninja</i>	4,00	0,84	3	<,0001
	<i>ala3</i>	3,50	1,00	4	<,0001
	Col-0	9,10	1,08	6	Control

Table S3.6. Summary statistics for leaf Na (LNa) and leaf Fe (LFe) phenotyping of SNP specification in the candidate gene T-DNA insertion mutants. Difference, difference standard error (Dif Std Err), and Dunnet's test *p*-values are shown.

SNP	Trait	Line	Control	Difference	Dif St Err	Dunnet's p-value
LNa	Fe	<i>ninja</i>	Col-0	-536,86	17,71	0,0341
		<i>pgp10</i>	Col-0	288,11	17,71	0,3710
		<i>yuc8</i>	Col-0	-11,64	16,17	0,1020
LFe	Na	<i>ala3</i>	Col-0	-347,80	557,29	0,7745

Table S3.7. Effects of allelic variation at the locus of interest on growth and leaf nutrition. Summary statistics and ANOVA results of mean comparisons of rosette diameter (up), leaf Na (center) and leaf Fe (down) in pools of accessions bearing contrasted alleles. Table indicates pool of accessions (HLNa: high leaf Na content; LLNa: low leaf Na content; HLFe: high leaf Fe content; LLFe: low leaf Fe content), allelic variant at the candidate locus (rare: alternative variant; common: Col-0-like), standard deviation (Std Dev), standard error (Std Err), number of replicates (N) and ANOVA F value and *p*-values. Plants were grown for 2 weeks under control (0.5-strength Hoagland solution; pH 5.7) and treatment (0.5-strength Hoagland solution; 40 mM NaCl + 10 mM NaHCO₃, pH 8.3).

Line	Rep	RD	RL	LFW	RFW	Na allele	Rel Na	HKT1 allele	Fe Allele	Rel Fe	Score
CUR-3	R1	0,38	0,33	0,22	0,15			Col-0 -type	Col	0,68	3
CUR-3	R2	0,47	0,56	0,09	0,20			Col-0 -type	Col	0,53	3
CUR-3	R3	0,28	0,25	0,02	0,02			Col-0 -type	Col	NA	3
LI-OF-095	R1	0,65	0,65	0,82	0,72	Alt	145,26	Col-0 -type	Col	0,78	1
LI-OF-095	R2	0,63	0,62	0,38	0,42	Alt	104,47	Col-0 -type	Col	0,72	1
LI-OF-095	R3	0,68	0,56	0,59	0,30	Alt	152,71	Col-0 -type	Col	0,66	1
Hovdala-2	R1	0,70	0,44	0,50	0,26			Col-0 -type	Alt	0,90	1
Hovdala-2	R2	0,67	0,47	0,37	0,35			Col-0 -type	Alt	0,89	1
Hovdala-2	R3	0,59	0,47	0,35	0,30			Col-0 -type	Alt	0,64	1
T1130	R1	0,68	0,47	0,61	0,32			Col-0 -type	Alt	1,89	1
T1130	R2	0,60	0,45	0,41	0,48			Col-0 -type	Alt	0,73	1
T1130	R3	0,54	0,40	0,26	0,29			Col-0 -type	Alt	n.d.	1
Jm-1	R1	0,39	1,22	0,04	0,22	Alt	166,57	Col-0 -type	Col	1,54	3
Jm-1	R2	0,29	0,96	0,06	0,10	Alt	184,89	Col-0 -type	Col	0,76	3
Jm-1	R3	0,44	0,77	0,02	0,06	Alt	177,72	Col-0 -type	Col	0,66	3

Table S3.7. Continuation...

PHW-14	R1	0,46	0,49	0,34	0,45	Excluded	weak	3	
PHW-14	R2	0,38	NA	0,25	NA			3	
PHW-14	R3	0,37	NA	0,32	NA			3	
PHW-20	R1	0,44	0,50	0,08	0,08	Alt	105,95	Col-0 -type	3
PHW-20	R2	0,35	0,31	0,07	0,12	Alt	100,69	Col-0 -type	3
PHW-20	R3	0,51	0,46	0,40	0,38	Alt	87,97	Col-0 -type	3
Gd-1	R1	0,55	0,37	0,13	0,10	Col	NA	Col-0 -type	2
Gd-1	R2	0,51	0,41	0,02	0,04	Col	141,28	Col-0 -type	2
Gd-1	R3	0,40	0,39	0,02	0,03	Col	147,54	Col-0 -type	2
Ost-0	R1	0,54	0,46	0,33	0,23	Col	82,55	Col-0 -type	Alt 0,95
Ost-0	R2	0,75	0,43	0,77	0,90	Col	88,58	Col-0 -type	Alt 0,89
Ost-0	R3	0,66	0,43	0,73	0,65	Col	80,77	Col-0 -type	Alt 0,85
Lisse	R1	0,70	0,71	0,41	0,29	Col	NA	Col-0 -type	2
Lisse	R2	0,60	0,38	0,32	0,29	Col	50,33	Col-0 -type	2
Lisse	R3	0,57	0,58	0,00	0,00	Col	62,26	Col-0 -type	2
Col-0	R1	0,64	0,37	0,30	0,19				2
Col-0	R2	0,65	0,48	0,53	0,33				2
Col-0	R3	0,51	0,52	0,15	0,11				2

Table S3.8. Effects of allelic variation at the locus of interest on growth and leaf nutrition. Summary statistics and ANOVA results of mean comparisons of rosette diameter (RD; top), relative leaf Na⁺ (Rel Na; middle) and Fe concentrations (Rel Fe; bottom) in pools of accessions bearing contrasted alleles. Table indicates pool of accessions (HLNa: high leaf Na content; LLNa: low leaf Na content; HLFe: high leaf Fe content; LLFe: low leaf Fe content), allelic variant at the candidate locus (rare: alternative variant; common: Col-0-like), mean value, standard deviation (Std Dev) and standard error (Std Err), number of observations (N), ANOVA F value and adjusted *p*-values (Prob > F) for each trait. Plants were grown for 2 weeks under control (0.5-strength Hoagland solution; pH 5.7) and treatment (0.5-strength Hoagland solution; 40 mM NaCl + 10 mM NaHCO₃, pH 8.3).

Pool	Allele	Mean RD	Std Dev	Std Err	N	F value	Prob > F
HLNa	Rare	0,459	0,136	0,039	12	5,461	0,031
LLNa	Common	0,587	0,106	0,035	9		
HLFe	Rare	0,637	0,072	0,024	9	14,39	0,001
LLFe	Common	0,464	0,124	0,032	15		

Pool	Allele	Mean Rel Na	Std Dev	Std Err	N	F value	Prob > F
HLNa	Rare	136,800	33,393	10,068	10	6,63	0,0203
LLNa	Common	93,329	37,301	14,099	9		

Pool	Allele	Mean Rel Fe	Std Dev	Std Err	N	F value	Prob > F
HLFe	Rare	0,967	0,386	0,146	7	8,31	0,0137
LLFe	Common	0,791	0,311	0,117	7		

Table 3.9. Transcript expression analysis for *ALA3*, *NINJA*, *PGP10* and *YUC8* in leaves of selected *ExtP* accessions. On the left, table shows target transcript, pool of accessions (HLFe: High Leaf Fe, rare allele; LLFe: Low Leaf Fe, common allele; HLN_a: High Leaf Na, alternative allele; LLN_a: Low Leaf Na, reference allele), number of replicates per pool (N), mean expression level calculated as [(dCtgene-dCtACT2)/dCt Col-0]; Standard error (StdErr), ANOVA F value and adjusted *p*-value (Prob > F). Plants were grown for 2 weeks under control (0.5-strength Hoagland solution; pH 5.7) and treatment (0.5-strength Hoagland solution; 40 mM NaCl + 10 mM NaHCO₃, pH 8.3).

Leaf Relative Gene Expression					ANOVA					
Target	Allele	N	Mean	Std Error	Source	DF	Sum of Sq	Mean Sq	F Ratio	Prob > F
Ala3	HLFe	9	1,09	0,34	Allele	1	3,50	3,50	4,28	0,0552
	LLFe	12	0,18	0,27	Error	17	13,11	0,82		
					C. Total	18	16,61			
Ninja	HLNa	12	0,92	1,37	Allele	1	49,04	49,04	4,86	0,0461
	LLNa	12	4,45	1,21	Error	20	184,43	13,17		
					C. Total	21	233,48			
Pgp10	HLNa	9	0,74	0,21	Allele	1	0,02	0,02	0,05	0,8242
	LLNa	12	0,81	0,22	Error	17	5,91	0,39		
					C. Total	18	5,93			
Yuc8	HLNa	9	1,26	0,54	Allele	1	33,23	33,23	14,23	0,0031
	LLNa	12	4,55	0,68	Error	17	25,69	2,34		
						18	58,92			

Table S3.10.1. Transcript expression analysis for *ALA3*, *FRO2*, *HKT1*, *NINJA*, *SOS1* and *YUC8* in roots of the analyzed ExtP accessions. On the left, table shows target transcript, pool of accessions (HLNa: High Leaf Na accessions, rare allele; LLNa: Low Leaf Na accessions, common allele), number of replicates per pool (N), mean expression level calculated as (CtGene- CtActin1), standard error (Std Err), ANOVA F value and adjusted *p*-value (Prob > F).

Root Relative Gene Expression					ANOVA					
Target	Allele	N	Mean	Std Error	Source	DF	Sum of Sq	Mean Sq	F Ratio	Prob > F
ALA3	HLFe	12	2,17	0,68	Allele	1	124,23	124,23	16,82	0,0003
	LLFe	12	6,34	0,75	Error	23	199,38	7,38		
					C. Total	24	323,61			
FRO2	HLFe	9	8,06	2,72	Allele	1	159,20	159,20	1,66	0,2116
	LLFe	9	2,75	3,10	Error	17	2013,73	95,89		
					C. Total	18	2172,93			
HKT1	LLNa	18	1,41	1,86	Allele	1	674,29	674,29	13,92	0,0015
	HLNa	9	14,08	2,84	Error	26	872,16	48,45		
					C. Total	27	1546,45			
IRT1	HLFe	15	3,46	1,20	Allele	1	0,09	0,09	0,01	0,9316
	LLFe	9	3,61	1,20	Error	14	160,22	11,44		
					C. Total	15	160,31			
NINJA	LLNa	18	2,33	1,33	Allele	1	1590,56	1590,56	37,44	<,0001
	HLNa	9	20,53	2,66	Error	26	1189,55	42,48		
					C. Total	27	2780,11			
SOS1	LLNa	18	4,34	0,83	Allele	1	22,09	22,09	1,10	0,3026
	HLNa	9	2,23	1,83	Error	26	664,48	20,14		
					C. Total	27	686,57			
YUC8	LLNa	18	5,57	2,40	Allele	1	90,74	90,74	0,65	0,4257
	HLNa	9	0,89	5,27	Error	27	3744,35	138,68		
					C. Total	28	3835,09			

Table S3.10.2. Transcript expression analysis for *ALA3*, *FRO2*, *HKT1*, *NINJA*, *SOS1* and *YUC8* in roots of the analyzed ExtP accessions. On the left, table shows target transcript, accession, number of replicates per pool (N), mean expression level calculated as (CtGene- CtActin1), standard error (Std Err), ANOVA F value and adjusted p-value (Prob > F).

Root Relative Gene Expression				
Target gene	Accession	N	Mean	Std Error
ALA3	CUR-3	3	0,8871	1,821
	Hovdala-2	3	8,8396	1,487
	Jm-1	3	0,398	1,821
	Lisse	3	4,5757	1,288
	Nw-0	3	1,7682	1,052
	Ost-0	3	5,1345	1,288
	PHW-20	3	1,6511	1,821
	T1130	3	5,8848	1,052
FRO2	CUR-3	3	0,0495	4,374
	Lisse	3	0,2345	3,093
	Nw-0	3	20,5699	2,766
	Ost-0	3	6,4406	3,093
	PHW-20	3	0,423	4,374
	T1130	3	0,2882	2,525
HKT1	6039	2	21,5427	2,3107
	6039-2	2	10,8057	2,3107
	6102-1	2	5,0191	2,3107
	6102-2	1	2,7556	3,2678
	6102-3	2	1,7262	2,3107
	07-ene	2	29,0142	2,3107
	7258	6	1,1329	1,3341
	7490	2	2,8924	2,3107
	81-1	2	10,3464	2,3107
	8351	4	0,4995	1,6339
	8430	4	2,36	1,6339
	Col1	2	0,6172	2,3107
	Col2	2	1,16	2,3107

Table S3.10.2. Continuation...

IRT1	CUR-3	3	8,9463	7,945
	Hovdala-2	3	5,4246	5,618
	Jm-1	3	3,5812	7,945
	Lisse	3	13,0186	5,618
	Nw-0	3	31,4786	4,587
	Ost-0	3	1,789	5,618
	PHW-20	3	0,0174	7,945
	T1130	3	9,7131	11,235
NINJA	Col-0	3	1,9444	2,239
	CUR-3	3	30,7554	3,1664
	Hovdala-2	3	2,0789	2,239
	Jm-1	3	25,9956	3,1664
	Lisse	3	2,9278	4,4779
	Nw-0	3	2,3935	2,0026
	Ost-0	3	3,4369	2,239
	PHW-20	3	4,8436	3,1664
SOS1	T1130	3	1,8563	1,8281
	Col-0	3	2,6413	2,067
	CUR-3	3	2,7163	2,923
	Hovdala-2	3	9,3493	1,688
	Jm-1	3	1,2963	2,923
	Lisse	3	2,9356	2,387
	Nw-0	3	1,5112	1,688
	Ost-0	3	4,5147	2,067
YUC8	PHW-20	3	2,6771	2,923
	T1130	3	3,8665	1,688
	Col-0	3	1,0451	5,816
	CUR-3	3	0,0344	10,073
	Hovdala-2	3	2,8693	4,112
	Jm-1	3	1,0154	7,123
	Lisse	3	0,527	7,123
	Nw-0	3	0,5193	4,112
	Ost-0	3	4,022	5,816
	PHW-20	3	1,1813	7,123
	T1130	3	24,2631	5,037

Table S3.11. Potentially causal SNPs for allelic variation of the identified candidate genes. Table shows Phenotype of SNP association (Leaf Na: LNa; leaf Fe: LFe), Gene, Gene Id, splice variant when described, Position, variant length (bp), variant description (base substitution); Reference (Ref) and Alternative (Alt) allele versions and type of variant according to the affected region.

Phenotype	Gene	Id	Splice variant	Position	Length (bp)	Description	Ref	Alt	Region
LNa	YUC8	AT4G28720		14189571	1	SNV A -> G	A	G	Upstream gene
	YUC8	AT4G28720		14192777	1	SNV T -> A	T	A	Exon
LNa	YUC8	AT4G28720		14195241	1	SNV G -> A	G	A	Downstream gene
LNa	NINJA	AT4G28910	1, 2, 3	14264228	1	SNV C -> G	C	G	3' UTR
LNa	NINJA	AT4G28910	1	14266068	1	SNV A -> T	A	T	Intron
LNa	NINJA	AT4G28910	2, 3	14266068	1	SNV A -> T	A	T	5' UTR
LNa	NINJA	AT4G28910	1, 2	14266152	1	SNV C -> A	C	A	Intron
LNa	NINJA	AT4G28910	3	14266152	1	SNV C -> A	C	A	Splice region
LNa	NINJA	AT4G28910	1, 2, 3	14266181	1	SNV A -> G	A	G	Intron
LNa	NINJA	AT4G28910	1, 2, 3	14266265	1	SNV A -> T	A	T	Intron
LFe	ALA3	AT4G28910		22010380	1	SNV C -> T	C	T	Upstream gene
LFe	ALA3	AT4G28910		22010711	1	SNV C -> T	C	T	Promoter
LFe	ALA3	AT4G28910		22010821	1	SNV T -> C	T	C	Promoter
LFe	ALA3	AT4G28910		22012346	1	SNV G -> A	G	A	Downstream gene

Supplementary Datasets

The supplementary Datasets of this doctoral thesis, comprising genomic and transcriptomic data from chapters 1 and 3, respectively, were uploaded in Zenodo online repository <https://doi.org/10.5281/zenodo.7806360>



Chapter 1

Dataset S1.1. Sliding window divergence scans. Top 1% F_{ST} outlier list.

Dataset S1.2. Environmental Association Analysis (GEA). Soil nutrition data.

Dataset S1.3. Phenotype Association Analysis (GPA). Leaf nutrition and bolting time data (RS).

Dataset S1.4. Irrigation experiment. Leaf nutrition and bolting time data (RI).

Dataset S1.5. LFMM candidates. GEA and GPA candidates list and annotation.

Dataset S1.6. LFMM candidates. LFMM SNPs list.

Chapter 2

Dataset S2.1. Differentially expressed genes (DEGs) analysis. Genes differentially expressed exclusively under neutral salinity (*onlySAL*).

Dataset S2.2. Differentially expressed genes (DEGs) analysis. Genes differentially expressed exclusively under alkaline salinity (*alkSAL*).

Dataset S2.3. Differentially expressed genes (DEGs) analysis. Genes differentially expressed in the shared core of neutral and alkaline salinity (*coreSAL*).

Dataset S2.4.1. KEGG Enrichment. *onlySAL* and *onlyALKSAL* DEGs detected in KEGG Enrichment analysis.

Dataset S2.4.2. Differentially expressed genes (DEGs) analysis. Genes involved in phytohormone signaling differentially expressed regardless of treatment. From left to right: gene Id, gene name, gene symbol, fold change in each deme under *neuSAL* and *alkSAL* and DEG subset in which each gene classifies.

Dataset S2.4.3. *coreSAL* DEGs detected in KEGG Enrichment analysis. UPREG: Up-regulated; DOWNREG: Down-regulated. Kegg Pathway, Gene Id, log2(FC), treatment and deme are specified.

Chapter 3

Dataset S3.1. List of accessions used in this study.

Dataset S3.2. Raw data on leaf nutrition, growth, and native soil characterization of the studied accessions.



UAB

Universitat Autònoma de Barcelona